GEOLOGICAL SURVEY OF DENMARK AND GREENLAND BULLETIN 31 • 2014

Review of Survey activities 2013

Edited by
Ole Bennike, Adam A. Garde and W. Stuart Watt

GEOLOGICAL SURVEY OF DENMARK AND GREENLAND
MINISTRY OF CLIMATE, ENERGY AND BUILDING

Geological Survey of Denmark and Greenland Bulletin 31

Keywords
Geological Survey of Denmark and Greenland, survey organisations, current research, Denmark, Greenland.

Cover photographs from left to right
1. A Hercules aircraft from the US Air Force on the Greenland ice sheet. Photograph: Dirk van As.
2. Perhaps a future geologist searching for fossils in the Faxe quarry. Photograph: Ole Bennike.
3. In 2013 GEUS celebrated its 125th anniversary. Photograph: Jakob Lautrup.
4. Learning about geothermal energy by testing the temperature of the water. Photograph: Jakob Lautrup

Frontispiece: facing page
In 2012 and 2013 GEUS carried out field work in North Greenland (see paper by Bojesen-Koefoed *et al*. in this issue). The overturned sedimentary rocks exposed along the margin of the glacier belong to a Cretaceous succession in the Harder Fjord fault zone, Wandel Sea basin, northern Peary Land. Photograph: Jørgen A. Bojesen-Koefoed.

Printer: Rosendahls-Schultz Grafisk A/S, Albertslund, Denmark
Manuscripts received: 17 January 2014 – 28 March 2014
Final versions approved: 26 February 2014 – 9 May 2014
Printed: 25 June 2014

ISSN 1603-9769 (Review of Survey activities)
ISSN 1604-8156 (Geological Survey of Denmark and Greenland Bulletin)
ISBN 978-87-7871-383-4

Citation of the name of this series
It is recommended that the name of this series is cited in full, viz. *Geological Survey of Denmark and Greenland Bulletin*.
If abbreviation of this volume is necessary, the following form is suggested: *Geol. Surv. Den. Green. Bull*. 31, 98 pp.

Available from
Geological Survey of Denmark and Greenland (GEUS)
Øster Voldgade 10, DK-1350 Copenhagen K, Denmark
Phone: +45 38 14 20 00, fax: +45 38 14 20 50, e-mail: *geus@geus.dk*

and at *www.geus.dk/publications/bull*

GEUS working areas 2013 shown in **grey**.
Orange areas are covered in this volume.

Review of Survey activities 2013

Flemming G. Christiansen
Deputy Director

2013 was a very special year for the Geological Survey of Denmark and Greenland (GEUS), which acquired its present name in 1995 when the Geological Survey of Denmark, established in 1888, and the younger Geological Survey of Greenland were merged. On 4 April 2013 GEUS celebrated its 125th anniversary with a series of presentations by prominent guests and GEUS scientists followed by a reception and a gala evening. GEUS' 125-year long history has provided an overwhelming body of results and experience, and today GEUS is broader, stronger and more international and collaborative than ever, covering all aspects of which a geological survey can be of use for society.

The anniversary is also reflected in this issue of *Review of Survey activities* that contains a total of 22 four-page papers, 11 on Denmark, nine on Greenland and three on broader themes: CO_2 capture and storage, the recently established Center for Minerals and Materials (MiMa) housed within the Survey – and, of course, a paper dedicated to the 125th anniversary.

This first paper highlights the anniversary and introduces the newly published book on the history of GEUS 'We – the people down to earth' (in Danish: *Vi de jordbundne*); a book that gives glimpses and highlights of the story of GEUS spiced with anecdotes on colourful characters, culture and politics.

Activities in Denmark

The activities and research in Denmark by GEUS cover many topics within our main programme areas: data, water, energy, mineral resources as well as nature and climate.

The island of Bornholm has a different geological history from the rest of Denmark; a dominance of outcropping basement rocks and Palaeozoic sedimentary rocks gives special challenges and possibilities. One paper describes the use of geophysical wire-line borehole logs from the Precambrian basement and the mapping of fracture patterns affecting groundwater flow.

Previous coring results from Bornholm have provided important geological input for assessing the unconventional gas resources in the Lower Palaeozoic shales of Denmark. Based on several years of collaboration with GEUS, the U.S. Geological Survey presented their shale gas estimate in November 2013 suggesting that significant technically recoverable resources may be present in several prospective areas.

Chalk is a very important rock for Denmark as it hosts more than 90% of the Danish petroleum reserves in the North Sea but it also has many other important uses. One paper is from a pilot project in south-west Denmark where seismic stratigraphy and sedimentary architecture of the chalk group has been used in a geothermal evaluation. Another paper describes a new technique for important CO_2 flooding experiments of chalk at reservoir conditions; if these experiments can be up-scaled, their results are potentially crucial to enhanced oil recovery.

Large infrastructure projects such as tunnels and bridges require detailed geotechnical knowledge of the subsurface, and based on material from new core holes, a more detailed understanding of understudied stratigraphic intervals may be reached. Based on cores from the Femern Bælt, one paper describes a study of the calcareous microfossil and foraminiferal biostratigraphy of the Campanian–Maastricthian chalk, and another paper focuses on the palynological and microfossil biostratigraphy and palaeoecology of the Paleocene–Eocene transition.

GEUS is involved in many studies of Quaternary and recent geological processes. One paper describes ribbed moraines from eastern Himmerland in Jylland formed during the retreat of the Scandinavian ice sheet. Another paper focuses on plant remains from cores in the North Sea, and demonstrates that parts of this area constituted an open, treeless, tundra-like environment in the Weichselian. A third paper is on stormwater management, where a test site in Høje Taastrup has been used to evaluate the infiltration capacity of clayey till. Based on field experiments, the paper discusses how different methods can be used to measure the infiltration capacity of the sediments.

Geothermal energy and ground-source heating may be of great importance in many areas in Denmark in order to live up to the ambition that by 2050 energy and transport shall be 100% based on renewable energy. Over many years, GEUS has been involved in an increasing number of projects covering different aspects of geothermal energy and ground-source heating. One paper describes a multidisciplinary approach to geothermal reservoir characterisation in Thisted,

where Denmark's first plant was established already in 1984. The plant now needs to increase its capacity with a new borehole. Another paper goes into detail about one of the critical key parameters – thermal conductivity of soils.

Activities in Greenland

Once again there was a high level of field activities in Greenland in 2013 with large field programmes in North Greenland and in the Gardar Province in South Greenland. Many other field studies were also carried out. Results from these large and small projects that are very important for evaluating and marketing the resource potential in Greenland and for monitoring climate changes will be presented in the coming years.

In this issue, results are presented from other completed and on-going projects. A first paper gives a review of six years of petroleum geological activities in North-East Greenland with focus on completed projects, and takes a look at the future. The activities were carried out prior to the preparation of recently completed offshore licensing rounds, and the studies are very important for evaluating key geological risks such as occurrence and quality of petroleum source rocks, understanding critical reservoir intervals and the uplift history. They are therefore crucial for planning of future exploration activities by both the authorities and industry.

Several papers focus on mapping and evaluation of the mineral potential in Greenland. One paper gives details of an aeromagnetic survey that was carried out in southern East Greenland in 2013, a region where GEUS has been active over several years with large completed and planned field programmes. The paper outlines how data can be applied to map regional geological and tectonic features. The project Aeromag 2013 has recently been released by the Greenland authorities. Another paper describes how exploration and multivariate techniques were used to detect a gold occurrence in southern West Greenland. A third paper demonstrates how integration of 3D photogeology, aeromagnetic and other geophysical data can be used as a promising tool for base-metal exploration in the remote region of East Greenland.

Earthquake swarms in Greenland are a very interesting subject that can now be analysed in greater detail than previously thanks to an increased number of seismic stations. Data from older detected swarms have been revisited and two new earthquake swarms have been identified on Disko and off South-East Greenland.

Shrinking of the ice sheet and local glaciers in Greenland provide a significant contribution to global sea-level rise. Understanding the dynamics and calculation of mass loss requires a detailed understanding of climate, glacier configuration and fjord bathymetry. One paper describes a case study from the Upernavik Isstrøm and Upernavik Isfjord in North-West Greenland.

The important monitoring programme of the Greenland Ice Sheet (PROMICE) that was initiated in 2007 continuously supplies crucial data that are used in a number of subsequent projects and in key publications. Three papers in this issue use such data from PROMICE. One is on katabatic winds and explanation of piteraq storms and is based on observations from the Greenland ice sheet. A second is on mass loss on a basinal scale with its focus on a large area in West Greenland. A third paper discusses the possibility of using surface albedo as a proxy for Greenland ice mass balance. This is particularly important at the moment to help fill data gaps in gravimetric data from satellites.

Broader international activities

Internationally GEUS works in many different countries with a variety of projects and is also involved in broader thematic studies. The last paper addresses scarcity of mineral raw materials, a theme that has recently been placed high on the political agenda in the US, EU, including in Denmark, as well as in Asia. As a consequence of this, GEUS has established the Center for Minerals and Materials (MiMa) in order to identify and study important raw material chains from source to use. One of the first tasks of MiMa is to enhance our knowledge of the risk of resource scarcity and the ensuing vulnerability of Danish society.

125 years of geological research for society

Johnny Fredericia and Peter Gravesen

In 1888 the first geological survey in the Kingdom of Denmark was born as the Geological Survey of Denmark (DGU, Danmarks Geologiske Undersøgelse) and in 1946 the Geological Survey of Greenland (GGU, Grønlands Geologiske Undersøgelse) was established. Both surveys were located in Copenhagen and were amalgamated in 1995 to form the Geological Survey of Denmark and Greenland (GEUS).

This was a happy amalgamation for both surveys. Even though DGU and GGU had different backgrounds and different working areas the employees had a lot in common, and today GEUS continues DGU's and GGU's work, but in an integrated way with new synergies – so a stronger Survey has evolved. This was the reason for celebrating GEUS' 125th anniversary on 4 April 2013 and it also explains the logo with the years 1888 and 1946 to the left and 2013 to the right (Fig. 1). The event was celebrated with a series of lectures held by national and international geoscientists, a reception for invited guests and a gala night for GEUS staff and board.

The Geological Survey of Denmark 1888–1995: geology for society

The document shown in Fig. 2 is considered the birth certificate of the first geological survey in the Kingdom of Denmark: the Geological Survey of Denmark (DGU). The letter, dated 4 April 1888, grants the first Danish professor of geology J.F. Johnstrup from the Mineralogical Museum government funds to organise and start the geological mapping of Denmark. It was estimated to take 20 years and cost 20 000 Danish kroner per year – corresponding to a little less than 1 million Euro per year in today's money.

Establishing a national geological survey was not an entirely new idea. Denmark lagged far behind its neighbours, who had started more than 25 years earlier – and it was one of the convincing arguments in Parliament at the time. The Geological Surveys of Norway and of Sweden were both established in 1858 (Fig. 3). The survey programmes in the

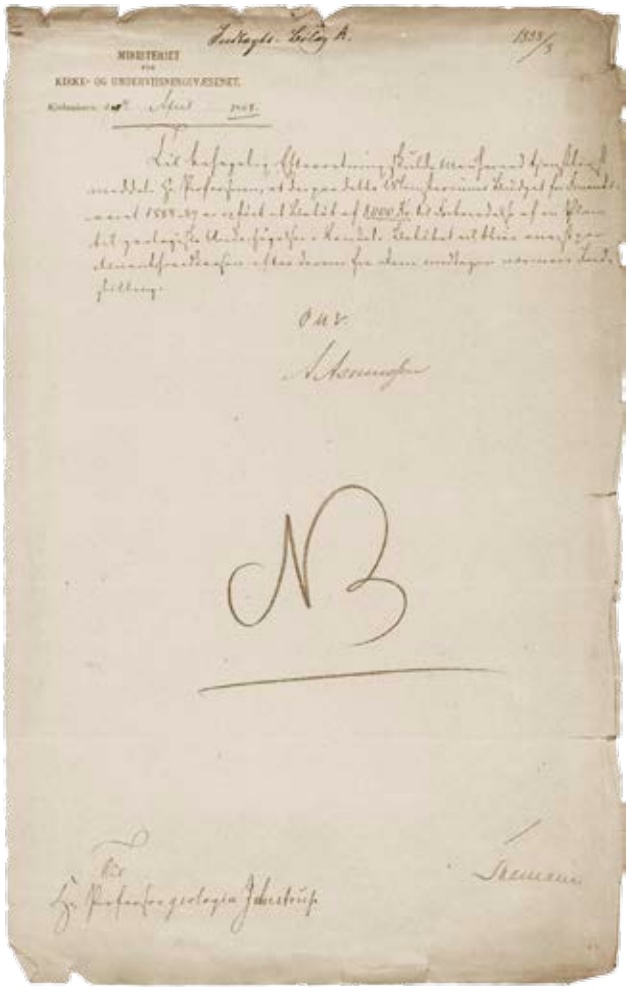

Fig. 2. The birth certificate of the Geological Survey of Denmark from 1888 granting funds to start geological mapping of Denmark.

Fig. 1. GEUS' 125th anniversary logo.

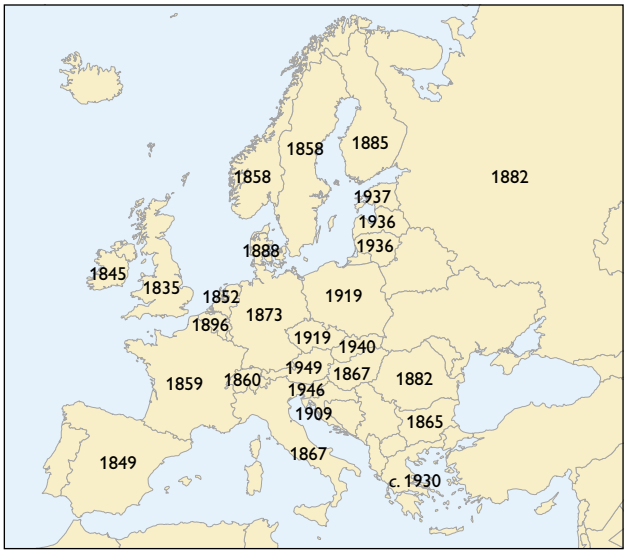

Fig. 3. The years of establishment of the European geological surveys (Påsse & Kim-Andersson 2008).

other Nordic countries were also much more extensive than the modest beginnings in Denmark.

The purpose of the new Survey was to map the superficial deposits of the country to obtain knowledge about the important geological resources. At that time it was largely gravel, sand, clay, peat, brown coal and limestone, but also hydrogeology and the quality of agricultural soils were important. Knowledge of the superficial deposits was also of strategic importance for military operations. Figure 4 shows the first published map and one of the most recent. The same mapping units have been used throughout the years, which means that it is now possible to produce seamless digital maps. Mapping and investigating the Quaternary deposits in Denmark were core tasks for the Survey for more than a century, but over the years the systematic mapping of the superficial deposits has been overshadowed by large numbers of other tasks and commitments. A few examples are mentioned below.

Danish brown coal was previously widely used for heating, and exploration of brown-coal deposists in Jylland during World War I and up to World War II was a major task for DGU. The mapping of marl deposits was another important task for the young Survey; local marl was used to improve the agricultural soils in Denmark. Investigation of palaeoclimate and vegetation history based on macrofossils and pol-

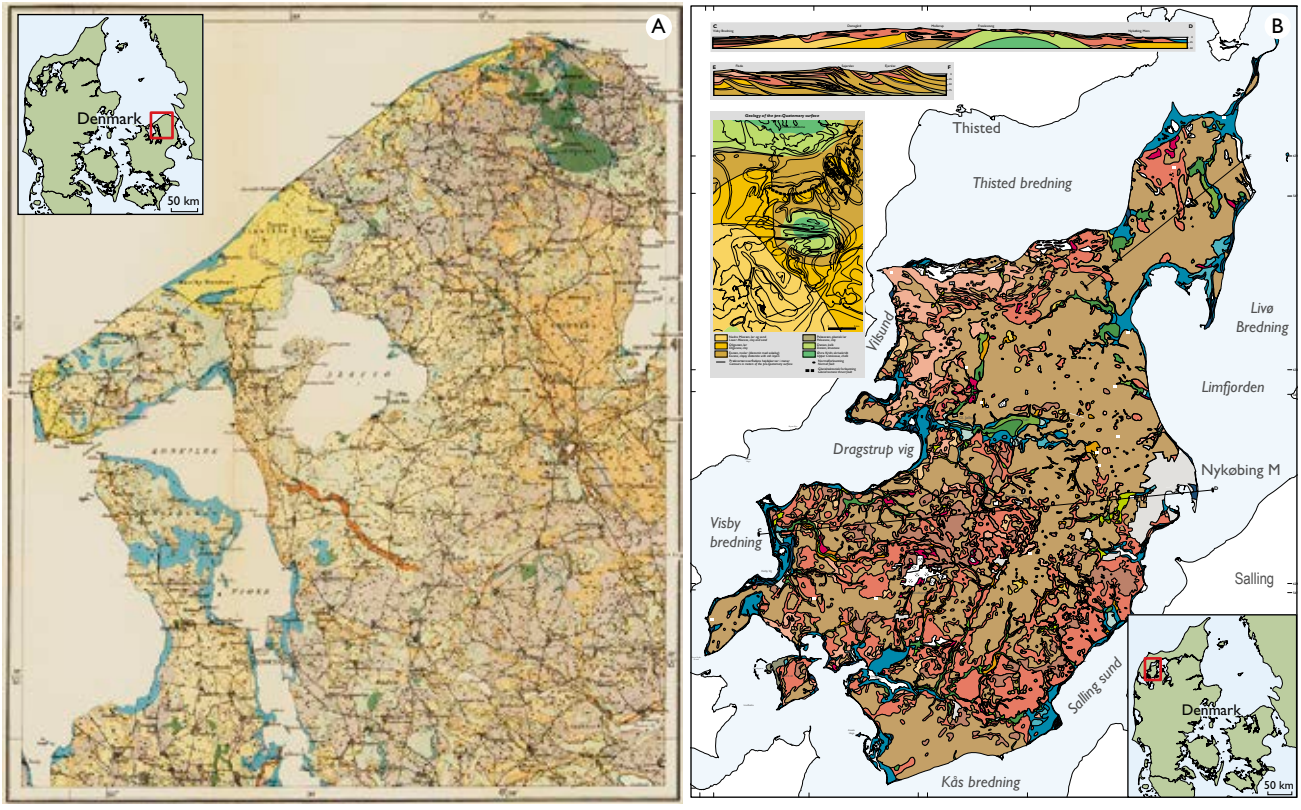

Fig. 4. Old and recent published maps of deposits at the terrain surface. The deposits are mainly of Quaternary age. **A**: Map covering parts of north-east Sjælland, published on a scale of 1:40 000 (Rørdam 1893). **B**: One of the latest maps covers the island of Mors in north-west Jylland, published on a scale of 1:50 000 (Pedersen & Jakobsen 2012).

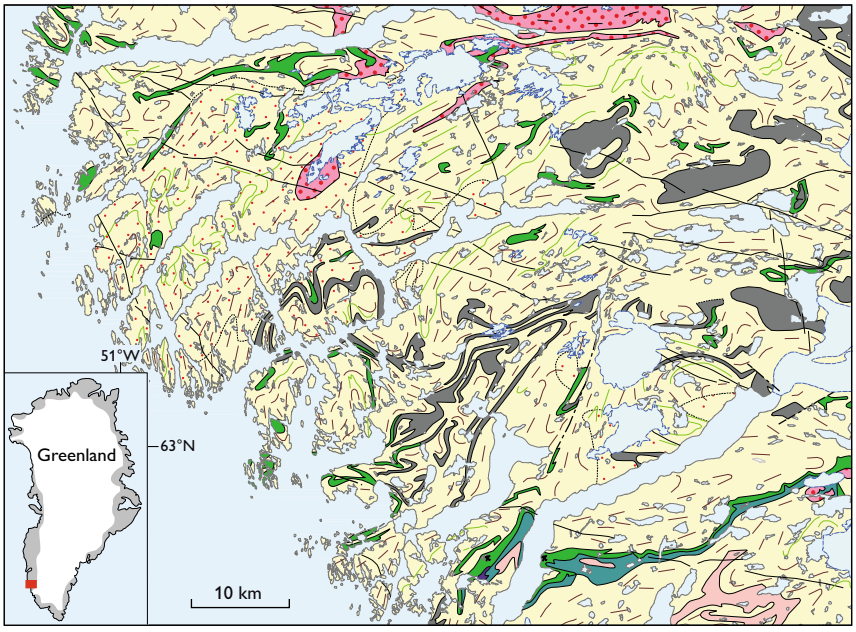

Fig. 5. Excerpt from the seamless geological map of Greenland, published on a scale of 1:500 000.

len from bog and lake sediments was another research area that started early at DGU. Danish water supply has been increasingly based on groundwater, and at an early stage DGU became engaged in solving quantity and quality problems for the public. In the 1970s and the 1980s the Survey was involved in groundwater mapping, and during this period the first large digital database in Denmark was established with borehole and groundwater data. Several projects concerning pollution of the groundwater with nitrate and pesticides were initiated in the 1980s and 1990s. Special attention was put into locating areas in Denmark which were sensitive to pesticide pollution and the Danish Pesticide Leaching Assessment Programme was established. Further nation-wide groundwater mapping was carried out in the early 2000s.

Interest in oil and gas exploration in Denmark began in 1935, and DGU became involved in aspects of this work, analysing borehole samples and interpreting seismic data. This work also resulted in the production of a series of thematic geological maps. The Samba database was established to store borehole data, geophysical surveys and reports. In the 1970s when it was suggested that radioactive waste from potential nuclear power plants in Denmark would be stored in Permian salt deposits, DGU demonstrated that salt diapirs were not suitable repositories. This was one of the reasons why Denmark decided in 1985 not to build nuclear power plants to produce electricity.

From 1888 to 1987 DGU was also the geological survey of the Faeroe Islands and mapped the volcanic rocks and superficial deposits of the islands. In addition, DGU carried out initial investigations to map potential oil reservoirs and conducted the first exploration boreholes.

The Geological Survey of Greenland 1946–1995: a survey at the frontier

After K.L. Giesecke's initial studies during the Napoleonic wars, other geological investigations and mineral exploration in Greenland began around 1850. From 1879 the expeditions were organised under the auspices of the Commission for Scientific Investigations in Greenland, often covering a wide range of natural science topics.

Geological investigations later became a key element in a number of expeditions to East Greenland under the leadership of Lauge Koch, funded by the Danish State. The expeditions began in 1926 and continued until the outbreak of World War II. They were resumed after the war and lasted until 1958.

In West Greenland geological mapping began in 1946 following the establishment of the Geological Survey of Greenland (GGU). The systematic mapping of Greenland was a tremendous task; Greenland is characterised by very limited infrastructure, and the size of the ice-free area is *c.* 410 000 km^2, nearly the size of Sweden.

As the knowledge of Greenland geology was initially very limited, the first years were spent on a reconnaissance study of the west coast to gain an impression of the geology involved. Systematic mapping on a scale of 1:100 000 began in the Ivittuut area in 1956. Ten years later it was realised that on that scale it would take a lifetime to cover Greenland, so the mapping was augmented with a series on 1:500 000 scale, first in West Greenland, then in East Greenland and in North Greenland from the 1970s (Figs 5, 6). The systematic

Fig. 6. Base camp in Warming Land in North Greenland in 1985. An Islandic Twin Otter aircraft and two Swiss helicopters are parked at the tent camp. The 600 m high cliffs in the background consist of Palaeozoic platform carbonates. Photograph: Jakob Lautrup.

mapping on 1:500 000 scale was completed in 40 years from 1964 to 2004.

Study and evaluation of mineral deposits of potential economic interest also took place along with the geological mapping. This was augmented in later years with airborne geophysical surveys with focus on mineral deposits. These studies, including geophysical investigations of offshore sedimentary basins, still continue, most recently in 2013 in South-East Greenland. In the 1960s, when Denmark was considering use of nuclear power, survey emphasis was placed on the discovery of radioactive minerals, as the Danish State had excluded radioactive minerals from commercial prospecting licences. Kvanefjeld in South Greenland was identified as a target in the 1960s and was extensively drilled (Fig. 7). Later stream sediment surveys throughout Greenland

Fig. 7. Ten kilometres of core were drilled between 1958 and 1981 at Kvanefjeld in South Greenland to investigate the uranium contents. The drilling teams and geologists were camped. Photograph: Jan Bondam.

Fig. 8. Setting up an automatic weather station near the margin of the Greenland ice sheet. Photograph: Claus Heinberg.

have helped to locate gold and diamond provinces and indicate potential environments for base metals, platinum-group elements and rare-earth elements.

Following the discovery of oil in Alaska there was interest in the sedimentary basins offshore West Greenland and six licence blocks were issued in 1974. This entailed extensive detailed studies by the Survey of the adjacent onshore sedimentary areas. It was followed by active airborne and seaborne geophysical surveys and further study of onshore sedimentary basins in both West and East Greenland.

Greenland is dominated by a large ice sheet that influences the climate of the northern hemisphere. The run-off from this ice sheet was investigated in West Greenland prior to the building of hydroelectric plants, and the advances and retreats of its outlet glaciers have been followed and reconstructed backwards for decades. With the advent of climatic change the study of mass-balance models for the whole ice sheet has intensified, and in recent years GEUS has established a network of automatic weather stations which allows detailed monitoring of changes in the mass balance of the ice sheet (PROMICE; Fig. 8).

The Geological Survey of Denmark and Greenland – the first challenges

A reorganisation of the raw materials administration between Denmark and Greenland took place in 1995. As part of this reorganisation the future of GGU was discussed. The two directors, Martin Ghisler from GGU and Ole Winther Christensen from DGU, had the same vision and worked to amalgamate GGU and DGU and make a larger and stronger geological Survey (Fig. 9). Cooperation with geologists form the University of Copenhagen was strengthened by the estab-

Fig. 9. DGU and GGU amalgamated in 1995. **Left**: The headquarters of GEUS at Øster Voldgade 10 in Copenhagen. **Right**: From the left, the former directors Martin Ghisler and Ole Winther Christensen in discussion with Niels Henriksen and Jens Morten Hansen on a field trip to North-East Greenland in 1995. Photographs: Jakob Lautrup.

lishment of Geocenter Copenhagen that comprised GEUS, the Geological Institute, the Geographical Institute and the Geological Museum of the University of Copenhagen. In 2007 an act for GEUS was passed by the Danish Parliament, and Geocenter Denmark was created, with a formalised collaboration between GEUS, the University of Copenhagen and the University of Aarhus. When GEUS celebrated its 125th anniversary, it was a celebration both for the Survey and for a strong alliance with the integrated Danish geoscience community. DGU and GGU had different beginnings and initially different schedules like trains meeting at a station, but we have stayed together and share the full story. Therefore it was logical to celebrate 125 years.

A book describing the history of GEUS: 'We – the people down-to-earth' (Vi de jordbundne) was published by GEUS in connection with the anniversary (Hansen & Thomsen 2013). Its subtitle: 'Glimpses of GEUS over 125 years' (Glimt af GEUS gennem 125 år). The book focuses on GEUS' role in society through the years and is partly based on earlier publications (Rasmussen 1988; Ellitsgaard-Rasmussen 1996; Fig. 10). The book does not give the complete story of GEUS, but provides an overview and glimpses of its history. It comprises special highlights, important changes of the institution and tells about people at GEUS in the past and at present. The book also includes a number of anecdotes that capture the work and social culture at GEUS.

GEUS today

GEUS is striving to be an international research organisation with the purpose of advising its users, the surrounding society in a broad sense. GEUS also develops and maintains national databanks with geological information on water, energy and mineral deposits and to some degree the climate, and is thus the geological memory of Danish society.

Being increasingly internationally orientated, GEUS has many partners in the Nordic countries, in the rest of Europe and farther afield. In particular, GEUS shares the vision of a much closer collaboration between the geological surveys of Europe, e.g. EuroGeoSurveys. A new regional cooperation between the surveys around the North Atlantic (NAG, Northeast Atlantic Geosciences) and increased cooperation between the Nordic countries have created important new avenues to develop our common role as surveys for a broader public.

However, other research organisations are also important partners for GEUS. For instance, GEUS has been partner in more than 75 European Union projects. GEUS also has a number of Memoranda of Understanding with countries outside the EU, and has been working in more than 30 countries outside Europe over the past 10 years. For example, GEUS has worked together with Vietnam for 17 years to build the country's capacity to develop their oil, gas and water resources.

GEUS also forms partnerships with other users of our knowledge, where we can contribute to growth in Denmark and Greenland. Water technology as a new business adventure is currently high on the political agenda, and GEUS strongly supports this effort. It is the intention to strenghten GEUS' unique cooperation with Copenhagen and Aarhus Universities in Geocenter Denmark, since it is a cornerstone in the future development of GEUS.

GEUS in the future

GEUS' goals for the future are expressed in the institution's strategy: GEUS strategi 2012. It stresses that GEUS

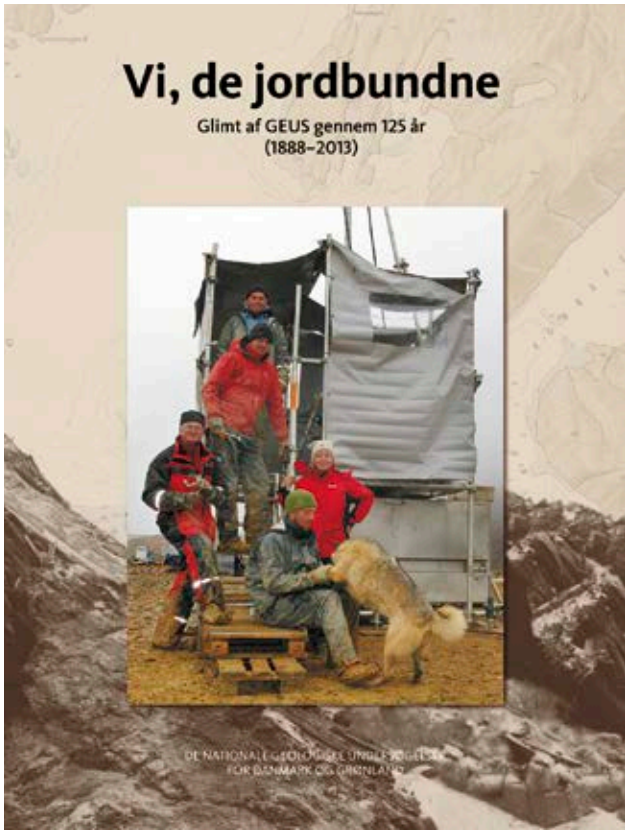

Fig. 10. The front cover of the anniversary book (Hansen & Thomsen 2013) shows a GEUS drilling team in North-East Greenland. Photograph: Jørgen Bojesen-Koefoed.

Fig. 11. The nine strategic topics from 'GEUS Strategy 2012 – basis for performance contract 2012–2015' coincide with several of the grand challenges of this century: minerals, environment and climate change, water resources and energy supply, and energy storage (GEUS 2012).

will focus on increased cooperation and partnership – here and abroad, based on GEUS' nine strategic topics shown in Fig. 11. The strategic topics coincide with several of the grand challenges of this century: minerals, environment and climate change, water resources, energy supply and energy storage. These challenges match GEUS' own ambitions, and GEUS is ready to deal with the challenges where geoscience plays an important role. This reflects that GEUS is responsible and constantly trying to adjust itself to the changing needs of our society, which is becoming more and more internationally integrated.

Geological knowledge is of crucial importance to society in the 21st century. GEUS will follow the changing demands from society and focus on the geological knowledge required so this can be developed to the benefit of Danish and international societies.

References

Ellitsgaard-Rasmussen, K. 1996: En stjerne fødes. Beretning om GGU's tilblivelse, 76 pp. Danmarks og Grønlands Geologiske Undersøgelse Rapport **1996/102**, 76 pp.

GEUS 2012: GEUS strategy 2012, basis for performance conctract 2012–2015, 28 pp. Copenhagen: Geological Survey of Denmark and Greenland.

Hansen, J.M. & Thomsen, H.H. (eds) 2013: Vi, de jordbundne. Glimt af GEUS gennem 125 år (1888–2013), 160 pp. Copenhagen: Geological Survey of Denmark and Greenland.

Pedersen, S.A.S. & Jakobsen, P.R. 2012: Geological map of Denmark 1:50 000, Mors. Copenhagen: Geological Survey of Denmark and Greenland.

Påsse, T. & Kim-Andersson, A. (eds) 2008: Sveriges Geologiska Undersökning. 150 år i samhällets tjänst, 185 pp. Uppsala: Sveriges Geologiska Undersökning.

Rasmussen, L.B. 1988: En jordisk krønike. Træk af DGU's historie 1888–1998, 114 pp. Copenhagen: Danmarks Geologiske Undersøgelse.

Rørdam, K. 1893: Kortbladene Helsingør og Hillerød. Danmarks Geologiske Undersøgelse I. Række **1**, 110 pp.

Authors' address

Geological Survey of Denmark and Greenland, Øster Voldgade 10, DK-1350 Copenhagen K, Denmark. E-mail: *pg@geus.dk*

Borehole logs from the Precambrian basement on Bornholm, eastern Denmark: geology and groundwater flow

Peter Gravesen, Bertel Nilsson, Per Rasmussen and Stig A. Schack Pedersen

Bornholm is situated in the Sorgenfrei–Tornquist Zone that separates the North-West European Craton from the Baltic Shield and the East European Platform (Fig.1). The Precambrian basement of northern and eastern Bornholm consists of different granitic and gneissic Mesoproterozoic rocks that are dated to *c.* 1455 Ma (Waight *et al.* 2012). It appears from the age data that granitic magmatism, deformation and metamorphism occurred over a relatively short time period. The rocks contain abundant pegmatite and aplite bodies. More than 250 mafic dykes occur. The dykes were intruded during three Precambrian events at *c.* 1326 Ma, 1220 Ma, 950 Ma and during a Permian event at *c.* 300 Ma (Holm *et al.* 2010).

The present study focuses on the Østermarie–Paradisbakke area north of Paradisbakkerne and deals with the Paradisbakke migmatite and part of the Bornholm gneiss. The aim of the study was to map the distribution of fractures in the rocks and determine the groundwater flow in these low-permeability rocks using outcrop data and borehole logs.

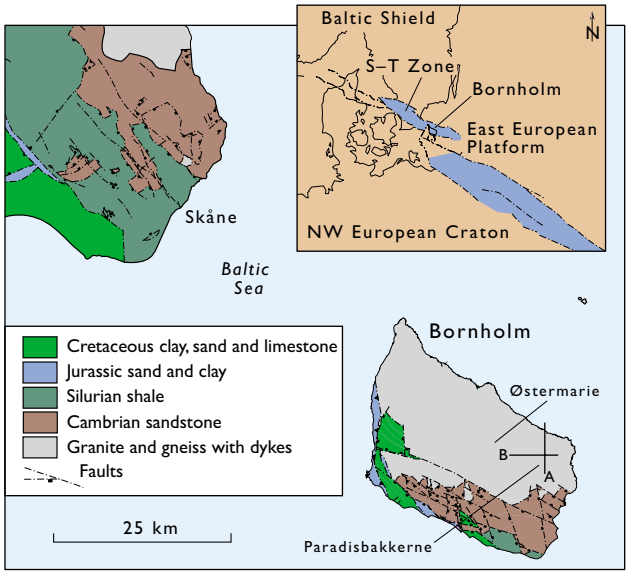

Fig. 1. Geological map of Bornholm and Skåne in southern Scandinavia. The location of the two cross-sections shown in Fig. 4 is indicated. Inset: Bornholm's location in the Sorgenfri–Tornquist Zone (S–T Zone; from Graversen 2009).

The survey was part of an investigation of potential areas for disposal of radioactive waste from the Research Centre Risø area (Gravesen *et al.* 2011a, b, 2012, 2013).

Rocks, fractures and groundwater

The two types of crystalline basement rocks in the study area show similar mineralogy and are dominated by K-feldspar (35–38%), quartz (23–30%), plagioclase (22–25%) and hornblende (11–17%); biotite and other minerals also occur (Micheelsen 1961). The Bornholm gneiss is medium-grained and grey or reddish grey. The fine- to medium-grained Paradisbakke migmatite consists of almost parallel, light grey

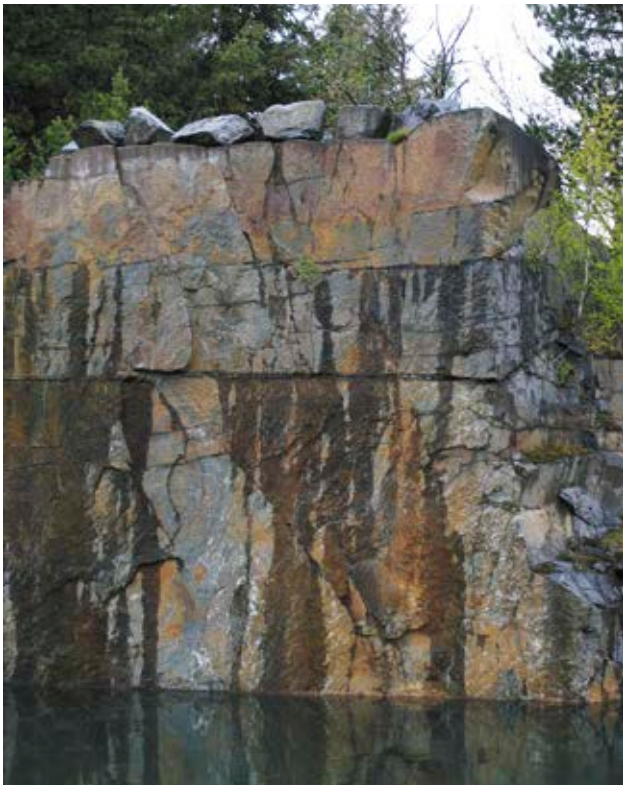

Fig. 2. Paradisbakke migmatite in Præstebo quarry at the northern rim of Paradisbakkerne. Horizontal and vertical fractures are common whereas oblique fractures are rare. The height of the outcrop is *c.* 12 m.

granitic quartz-feldspar veins in a darker matrix. Both rocks contain pegmatite bodies and are cut by thin NNE–SSW-oriented dykes that were intruded *c.* 1220 Ma ago. Minor bodies of reddish grey granite are also present.

The rocks are cut by four fracture systems, which can be observed in quarries with Paradisbakke migmatite along the northern rim of Paradisbakkerne (von Bubnoff 1942; Fig. 2). After deformation and cooling in the Precambrian, large tectonic faults and fractures and minor vertical fractures were formed.

The main fracture system in the area has an NNE–SSW orientation, corresponding to the direction of the mafic dykes (Micheelsen 1961). Large linear, fault-controlled valleys are found in Paradisbakkerne and in the western part of the Precambrian basement on Bornholm, but such valleys are absent in the study area. However, small vertical fractures with the same orientation are seen in outcrops.

A second ESE–WNW-oriented verical tectonic fracture system that shows the same orientation as Palaeozoic faults was probably formed during a main phase of wrench faulting in the Sorgenfrei–Tornquist zone in the Late Palaeozoic or later (Graversen 2009). Zones of 4.5 m thickness contain thin fractures with centimetre-sized spacing, while single fractures can have up to 5 m spacing. Small faults with slickensides are present and show that some horizontal movement has occurred. In addition to the vertical or subvertical fractures, rare occurrences of oblique fractures and conjugate fracture sets are also found.

A third system of horizontal fractures (sheet jointing) at levels from 25 m to 100 m depth was probably formed by load release when an overburden of supposed younger deposits, probably of Cambrian to Quaternary age, was eroded and removed (Spencer 1969). We assume that the spacing

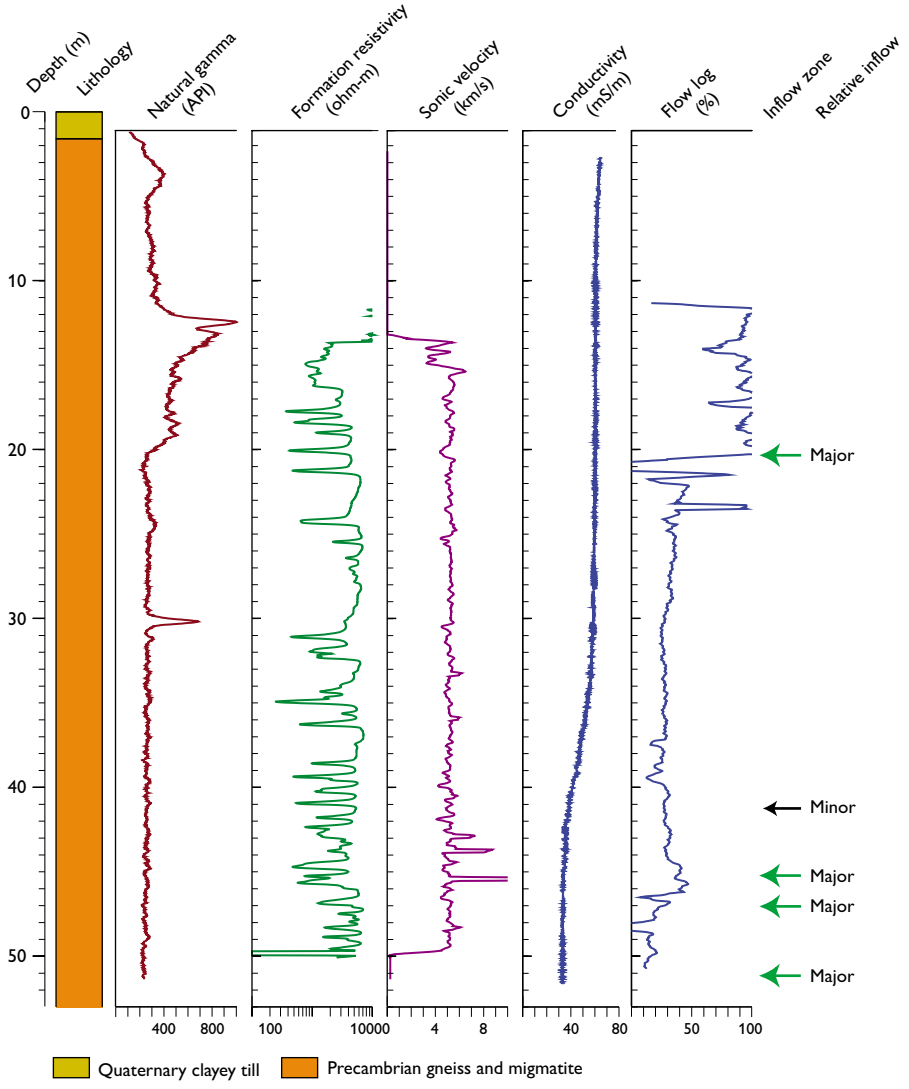

Fig. 3. Lithology and logs in borehole DGU no. 247.458. The flow-log data were acquired at a pumping rate of 1.3 $m^3 h^{-1}$. **API**: American Petroleum Institute units.

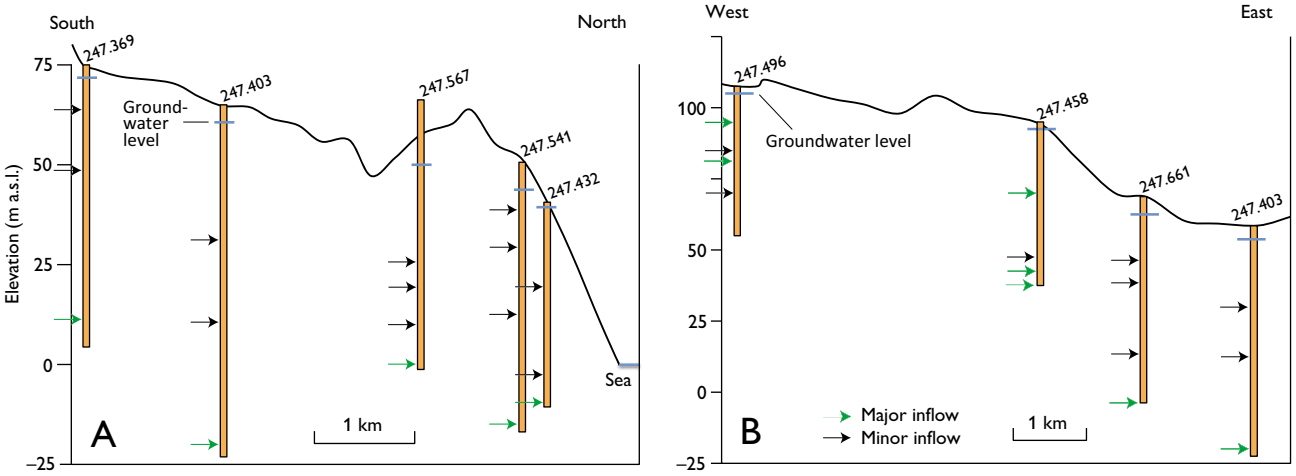

Fig. 4. Two cross sections through the logged boreholes. For location see Fig. 1. Note different horizontal and vertical scales.

between the fractures increases downwards, because this is seen in quarries.

A fourth fracture system consists of horizontal fractures near the ground surface with a spacing of 1–2 m, which also increases downwards. Crushed rocks with blocky structures also occur. This system may have been formed by glaciers during the Quaternary.

The lower limit of the fractures is unknown but some horizontal fractures are found at 90 m below the ground surface. This means that water flow in vertical fractures that cross-cut the deep horizontal fractures can supply the deep fracture system with groundwater from above.

The rocks in the area are slightly weathered and Fe-containing minerals are oxidised to yellow- brown clayey, Fe-rich deposits on some fracture surfaces. Such deposits may prevent water flow in some of the fractures. Most of the area is covered by a clayey till up to 6 m thick.

The groundwater reservoir is characterised by a network of vertical to subvertical and horizontal to subhorizontal fractures. Surface water is mainly transported to the groundwater zone in the vertical fractures and the groundwater can be transported over long distances in the horizontal fractures. It is difficult to map the subsurface fractures but data from borehole logs can contribute to our understanding of the network. Normally the groundwater table is found a few metres below the ground surface but pumping will often lower the groundwater table because the storage capacity in the reservoir is small. The yield of boreholes in basement rocks on Bornholm is commonly low, but boreholes supplying Østermarie waterworks show high yields because of fracture systems in the rocks in this area.

Borehole logs

Eight private water boreholes in the study area were investigated by geophysical wireline logging. The water pump was removed in the morning and re-installed in the late afternoon after logging. The following geophysical parametres were measured: natural gamma radiation, formation resistivity, sonic velocity, conductivity and impeller flow. Conductivity and flow log data were acquired during groundwater pumping from the borehole. Natural gamma, resistivity and sonic velocity logs provide information on lithological variation in the borehole. The conductivity log gives information about groundwater chemistry and under certain conditions also provides information on groundwater inflow zones. The flow log measures the vertical flow velocity in the borehole. Changes in flow velocity during pumping indicate groundwater inflow zones at specific depths or depth intervals in the borehole.

Results

The results from the logging of borehole DGU no. 247.458 are shown in Fig. 3 and two constructed geological sections through the study area are shown in Fig. 4. In the *c.* 5 km long north–south section, the fracture inflow into four boreholes is shown (Fig. 4A). The depths of water flow in the basement rocks indicate the location of fractures and the inflow is evaluated semi-quantitatively as 'major' or 'minor' in each borehole. 'Major' indicates that the fracture inflow contributes a large part of the total inflow whereas 'minor' indicates only a minor contribution. 'Major' inflows are interpreted from the flow log where an increase in the flow log (%) occurs, measured from the bottom towards the top of the borehole. 'Minor' inflows are interpreted from the conductivity log where

changes in conductivity appear. The conductivity log can be more sensitive to minor influx zones than the flow log. It is relevant to compare the boreholes because they have the same low specific yield (0.05–0.22 m^3/h^{-1}). Figure 4 shows fracture inflow at four different depth intervals. Major inflow is registered near the bottom of the boreholes and minor fracture inflow is seen closer to the surface. The groundwater table is situated a few metres below the surface in all boreholes.

It is not possible to directly determine the orientation of the fractures, but fractures that are found at the same level, at *c.* 10 to 12 m a.s.l., are likely to be horizontal or subhorizontal and hydraulically connected.

In the *c.* 8 km long west–east section, fracture inflow is registered between *c.* 100 m a.s.l. and 25 m b.s.l. (Fig. 4B). Borehole DGU no. 247.496 at Østermarie waterworks is included in this section (Rasmussen *et al.* 2007). Inflow is seen in all boreholes but the largest inflow is found at the bottom of borehole DGU no. 247.403. Several important water-bearing fracture zones are found in the waterworks borehole. The fractures occur at shallower depths at at least four levels.

The results from the logging survey appear to confirm the occurrence of important fracture systems at depth. Fractures are located at different levels. Horizontal fracture systems seen over a large area are found at 10–12 m a.s.l. and a similar system occurs at *c.* 20 m b.s.l. Several smaller fracture systems without large water flow also occur. The most important and largest fracture system is found at 90 m below the surface, usually at the bottom of the boreholes. As mentioned above we cannot determine the orientation of the fractures from the borehole log survey, but the structural model indicates major elements of the fracture systems. The horizontal fracture spacing apparently increases with depth, but it is still posssible to find fracture systems with major water flow if they are connected to other vertical and horizontal fractures.

Conclusions

The conclusions of the investigations are as follows:

1. The logging of the boreholes shows that fracture systems occur in all of them.
2. The fractures occur down to at least 90 m below the surface, and flow logging documents the occurrence of groundwater flow down to this depth. The downward transport of surface water to the horizontal fractures may be via vertical fractures to at least the same depth.
3. Horizontal fractures are found at 10–12 m a.s.l. and at 20 m b.s.l. The fractures appear to be connected over kilometre-long distances.

Acknowledgements

The Danish Parliament is thanked for financial support. We are grateful to local landowners that gave us permission to log their private boreholes.

References

Graversen, O. 2009: Structural analysis of superposed fault systems of the Bornholm horst block, Tornquist Zone, Denmark. Bulletin of the Geological Society of Denmark **57**, 25–49.

Gravesen, P., Nilsson, B., Pedersen, S.A.S. & Binderup, M. 2011a: Low- and intermediate level radioactive waste from Risø, Denmark. Location studies for potential disposal areas. Report no. 4. Characterisation and description of areas Bornholm. Danmarks og Grønlands Geologiske Undersøgelse Rapport **2011/44**, 85 pp.

Gravesen, P., Binderup, M., Nilsson, B. & Pedersen, S.A.S. 2011b: Geological characterisation of potential disposal areas for radioactive waste from Risø, Denmark. Geological Survey of Denmark and Greenland Bulletin **23**, 21–24.

Gravesen, P., Nilsson, B., Binderup, M. Larsen, T. & Pedersen, S.A.S. 2012: Lav- og mellem radioaktivt affald fra Risø, Danmark. Omegnsstudier. Rapport nr. 1. Område Østermarie-Paradisbakkerne, Bornholms Regionskommune. Danmarks og Grønlands Geologiske Undersøgelse Rapport **2012/123**, 100 pp.

Gravesen, P., Nilsson, B., Binderup, M., Larsen, T.B. & Pedersen, S.A.S. 2013: Geology, seismic activity and groundwater conditions at six potential disposal sites for radioactive waste from Risø, Denmark. Geological Survey of Danmark and Greenland Bulletin **28**, 13–16.

Holm, P.M., Pedersen, L.E. & Højsteen, B. 2010: Geochemistry and petrology of mafic Proterozoic and Permian dykes on Bornholm, Denmark: four episodes of magmatism on the margin of the Baltic Shield. Bulletin of the Geological Society of Denmark **58**, 35–65.

Micheelsen, H. 1961: Bornholms grundfjæld. Meddelelser fra Dansk Geologisk Forening **14**, 308–349.

Rasmussen, P., Klitten, K., Nielsen, S. & Jensen, P. 2007: Bornholms Regionskommune. Logging og vandkemi i vandforsyningsboringer, 2006. Danmarks og Grønlands Geologiske Undersøgelse Rapport **2007/36**, 91 pp.

Spencer, E.W. 1969: Introduction to the structure of the Earth, 597 pp. New York: McGraw-Hill.

von Bubnoff, S. 1942: Beiträge zur Tektonik des skandinavischen Südrandes. 2. Die älteren Granite Bornholms im Rahmen der svekofennidischen Tektogenese. Neues Jahrbuch für Mineralogie, Geologie und Paläontologie, Beilagen-Band **87**, 277–396.

Waight, T., Frei, D. & Storey, M. 2012: Geochronological constraints on granitic magmatism, deformation, cooling and uplift on Bornholm, Denmark. Bulletin of the Geological Society of Denmark **60**, 23–46.

Authors' address

Geological Survey of Denmark and Greenland, Øster Voldgade 10, DK-1350 Copenhagen K, Denmark. E-mail: *pg@geus.dk*

The Lower Palaeozoic shale gas play in Denmark

Niels H. Schovsbo, Arne T. Nielsen and Donald L. Gautier

The unconventional gas resources in the Lower Palaeozoic shale of Denmark were recently assessed by the United States Geological Survey (USGS; Gautier *et al.* 2013). Assuming unrestricted application of best practice current technology, recoverable gas resources of 0 to 130 × 10^9 Nm^3 gas were estimated onshore (mean = 67 × 10^9 Nm^3 gas) and 0 to 228 × 10^9 Nm^3 gas were estimated offshore (mean = 119 × 10^9 Nm^3 gas), i.e. a total estimated mean of 186 × 10^9 Nm^3 gas (Nm^3: normal cubic metre, unit used for natural gas at 0°C and 101.325 kPa). Nearly all of this potential resource is assumed to be contained in the Cambro-Ordovician Alum Shale. The wide range of estimates reflects the sparse data and the geological uncertainty inherent in the still untested play. The estimated mean quantity of gas resource is comparable to the total volume of gas produced from the Danish part of the North Sea during 1972–2011 and twice the amount of the estimated remaining reserves of conventional gas in the Danish part of the North Sea.

The assessment is the result of collaboration between The Geological Survey of Denmark and Greenland (GEUS) and USGS. GEUS and the University of Copenhagen contributed with the geological input data and models and USGS provided assessment methodology and North American resource analogues. In this paper the geological model that underlies the assessment is presented along with some additional considerations on the nature of the play. Details and methodology of the assessment itself were summarised by Gautier *et al.* (2013).

The Danish shale gas play

Shale gas is an unconventional energy resource in which gas is produced directly from a shale source rock. Highly productive formations in North America are regionally extensive, tens of metres thick, highly organic-rich, and have been buried sufficiently to reach the temperatures necessary for thermal gas generation. The technique of using horizontal drilling and hydraulic fracturing to extract gas from shale was developed in North America, where it has had a significant impact on gas markets. Application of this technology has not yet led to shale gas production in Europe. The first shale gas exploration borehole in Denmark, the Vendsyssel-1, is due to be drilled in northern Jylland in 2015 by the company Total E&P (Fig. 1).

Since 2009, GEUS has conducted a wide range of shale gas evaluation programmes including screening of onshore Denmark for potential shale gas units. The evaluation is partly based on extensive shallow coring on Bornholm where the shale is accessible immediately beneath a thin Quaternary cover (Schovsbo *et al.* 2011). The main target for exploration in Denmark is the Alum Shale Formation, which is up to 180 m thick and unusually rich in organic matter, typically with 5–10% total organic carbon (TOC; Schovsbo *et al.* 2011). Organic-rich shales also occur in younger Ordovician–Silurian successions. These black shales are thinner and less TOC-rich than the Alum Shale, but may still be interesting for shale gas exploration.

Thermal modelling

The Terne-1 borehole, drilled in Kattegat in 1985 (Fig. 1), penetrated a 180 m thick Alum Shale Formation and is a

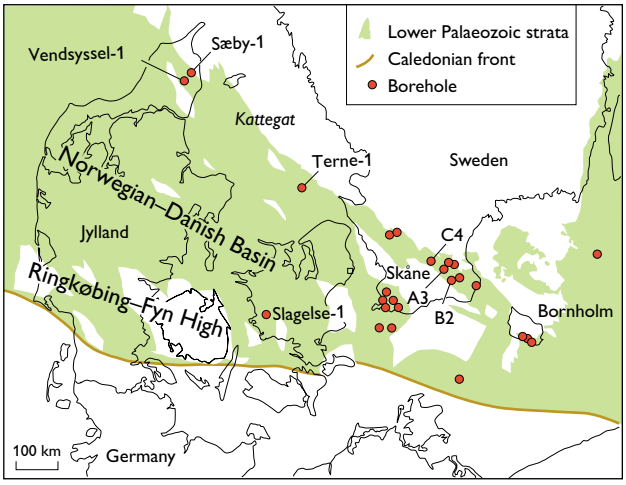

Fig. 1. Map showing simplified distribution of Lower Palaeozoic strata in Denmark and the location of scientific and exploration boreholes used for the geological assessment. The position of the planned Vendsyssel-1 borehole is also shown. In all boreholes made so far in Denmark and Skåne, the Alum Shale is mature to gas rank and positioned beneath a Palaeozoic sequence less than 1 km thick; at these sites the shale did not contain significant amounts of gas. The distribution of Lower Palaeozoic strata is from Nielsen & Schovsbo (2011).

key borehole for shale gas exploration in Denmark. Thermal modelling of Terne-1 was carried out to calibrate the burial history and maturation profiles. The Alum Shale contains a marine type II kerogen that yields lighter hydrocarbons on maturation than typical type II kerogen. Maturity gradients were constructed by converting the reflectance values of vitrinite-like particles to vitrinite-equivalent values following Petersen *et al.* (2013) since vitrinite-like particles in the Alum Shale mature at lower temperatures than true vitrinite.

The modelling showed that the Lower Palaeozoic shales were buried within a Caledonian foreland basin and that large volumes of oil were probably generated during the Silurian (Gautier *et al.* 2013). In most areas, kerogen subsequently attained a maturation rank of dry gas, cracking the previously formed oil. In the Carboniferous and early Permian, the Palaeozoic succession was faulted, tilted and subjected to intensive erosion (Fig. 2). Local Permo-Carbonifereous igneous intrusive rocks occur in the Terne-1 borehole and elsewhere. However, these did not affect the regional maturity related to burial.

In the area of the Terne-1 borehole, subsidence resumed in the Permo-Triassic and maximum reburial probably occurred in Cretaceous to early Palaeogene time as is the general scenario in Denmark (Fig. 2). Modelling suggests that the thermal rank reached during the Palaeozoic was not exceeded during the reburial of the Terne-1 area. Nevertheless, because of sparse data and modelling uncertainty, we cannot exclude that some shale could have retained hydrocarbon-generation potential throughout the Palaeozoic, and additional hydrocarbons may have formed during the Mesozoic and Cenozoic in some areas.

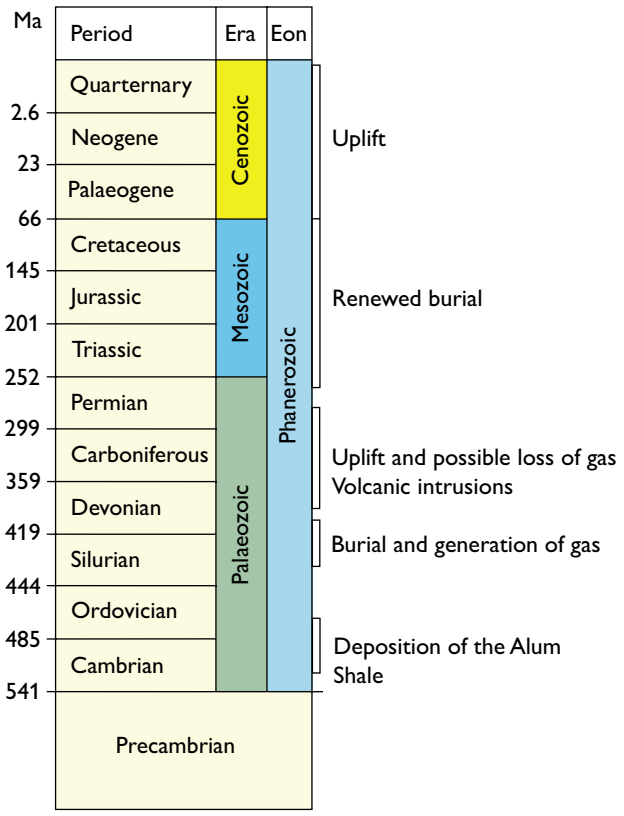

Fig. 2. Timing of main events affecting the gas potential in the Alum Shale in southern Scandinavia.

The geological model for the assessment

In Denmark only two boreholes outside the Skåne–Bornholm area penetrate the Alum Shale (Slagelse-1 and Terne-1; Fig. 1), hence the prospective area of the Alum Shale was delimited largely without borehole data. The analysis was based on maps of (1) the depth to the base of the Palaeozoic (Lassen & Thybo 2012), (2) the distribution of Palaeozoic strata (Vejbæk & Britze 1994) and (3) the regional thickness of the Alum Shale Formation and its subdivisions (updated and somewhat modified from Buchardt *et al.* 1997). These maps were used to identify areas where the Alum Shale is thicker than 20 m, gas mature and within a current depth interval of 1.5–7 km, which are relevant parameters for gas exploration.

The prospective areas (Fig. 3A) largely follow the margins of the Norwegian–Danish Basin. Alum Shale is most likely also present in the central part of the basin, but the shale is here buried too deeply for exploration. The Alum Shale thins out or is missing on the Ringkøbing–Fyn High and southwards towards the Caledonian front (Fig. 1).

Sweet-spot mapping within the prospective area

Exploration undertaken by Shell in Skåne, southern Sweden (boreholes A3, B2 and C3 in Fig. 1), indicates that the Alum Shale Formation, which is now located at 700–800 m depth, does not contain gas in economically producible quantities and that gas leakage from the shale has increased the risk for a viable gas play (Pool *et al.* 2012). Reservoir pressure reduction caused by uplift and loss of reservoir integrity due to faulting and fracturing are the likely mechanisms of gas loss. In Skåne the gas may have leaked out through millions of years of uplift and progressive erosion since it formed more than 400 million years ago. In Denmark, in contrast to Skåne, the Palaeozoic shale was reburied in the Mesozoic and thus may retain gas to a greater degree.

Two types of areas with different risks of gas leakage were defined in the geological model, based on the thickness of Palaeozoic strata mapped by Lassen & Thybo (2012). Preserved thickness is taken as the best indicator for the magnitude of uplift and thus for the risk of reservoir depressurisa-

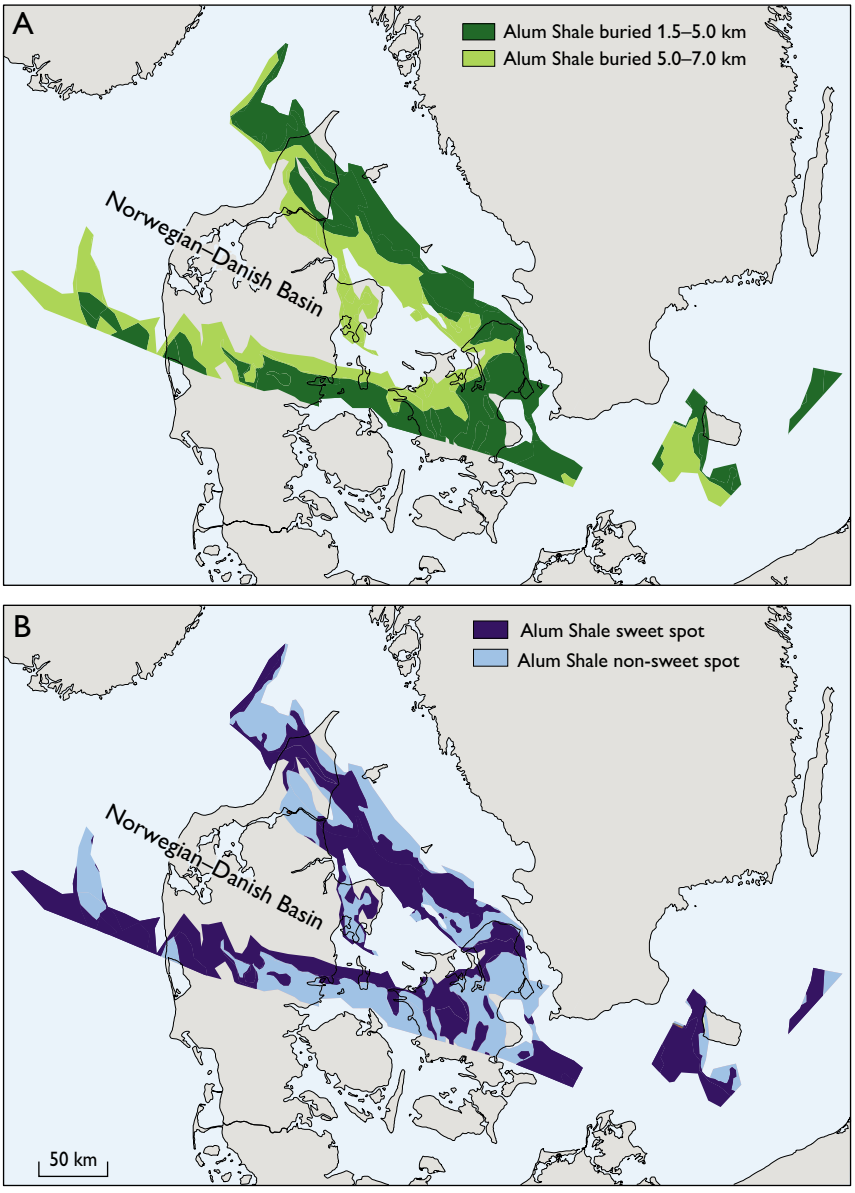

Fig. 3. **A**: Prospective areas in Denmark for gas in the Alum Shale. **B**: Distribution of sweet spots versus non-sweet spots within the prospective area of Denmark (the term sweet spot is defined in the text). Alum Shale is likely also present in the deeper parts of the Norwegian–Danish Basin, but here it is buried more than 7 km, i.e. too deeply for shale gas exploration with the current costs of drilling.

tion in Late Palaeozoic time (Fig. 3B). Accordingly, within the prospective area, 'sweet spots' were defined as fault blocks that contain Alum Shale overlain by more than 1 km of Palaeozoic strata (e.g. below the blue line in Fig. 4), indicating less intensive Late Palaeozoic uplift and erosion and, hence, greater probability of gas retention (Fig. 4). Where the Alum Shale is overlain by less than 1 km of Lower Palaeozoic strata, the formation is inferred to have been uplifted to less than 1 km during the Late Palaeozoic, and those areas are therefore classified as non-sweet spot areas in the assessment.

All the boreholes drilled so far in the Alum Shale in Denmark and Skåne play have been in non-sweet spots as defined here, with the highest reported gas saturation of 20% (Pool *et al.* 2012). Hence the quality of sweet spots remains to be tested. The difference in uplift history, and thus potentially in the gas content, is accounted for in the assessment model of Gautier *et al.* (2013) by adopting different estimated ultimate recovery (EUR) and success ratios for boreholes drilled in sweet spots (average EUR 13.1 × 10^6 Nm^3 gas) versus non-sweet spots (average EUR 6.7 × 10^6 Nm^3).

Development strategies

The USGS assessment methodology assumes unrestricted application of best practice current technology, which in the present case is expected to be horizontal drilling with multistage hydrofracturing. In Denmark the Ordovician–Silurian shale overlying the Alum Shale may constitute a rather thick (*c.* 300 m) additional interval in which other development strategies may be relevant. This inference is based on

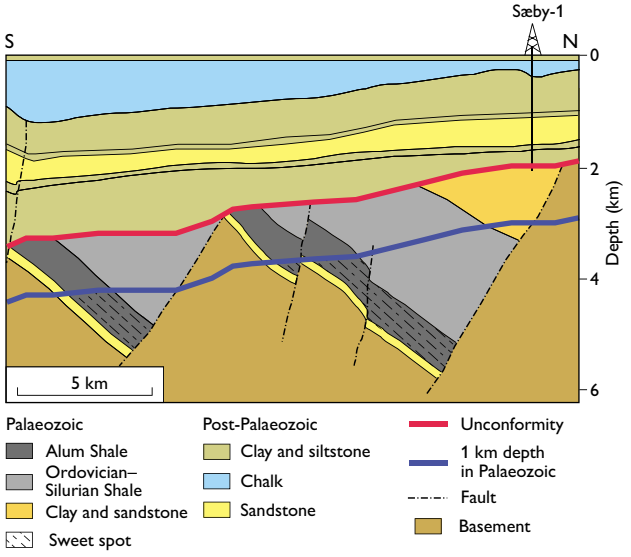

Fig. 4. Conceptual cross section showing the subsurface geology in northern Jylland. The Alum Shale is present in tilted fault blocks below the Caledonian unconformity. Sweet spots are the areas with lowest risk of gas leakage during Late Palaeozoic uplift and are defined as regions where the Alum Shale is overlain by more than 1 km of Lower Palaeozoic strata. Modified and generalised from Mogensen & Korstgård (2003).

the Terne-1 borehole where a 250 m thick shale interval with TOC values of 1–3% overlies the Alum Shale. These stratigraphic intervals are the targets for exploration in Poland, Lithuania and other countries in the eastern sector of the basin and may constitute an important additional reservoir in Denmark. In addition, a tight gas play in Upper Silurian or Lower Permian sections may also be present in the subsurface of Denmark and might add to the unconventional resource estimate.

Conclusions

The estimated technically recoverable shale gas resource is comparable to the total volume of gas produced from the Danish part of the North Sea in the period 1972–2011 and twice the amount of remaining reserves of conventional gas in the Danish sector of the North Sea. However, in contrast to the resource estimates for the North Sea, the estimated shale gas resource does not take economic viability into account.

Shale gas exploration in Denmark is in its early stages. This is reflected in the large range of the estimate. It is thus crucial to obtain information from new boreholes, notably from sweet-spot areas, in order to calibrate and constrain the resource estimation model.

The impact on the resource estimate from other development strategies or from additional play intervals and plays is not taken into consideration in the gas resource estimate by Gautier *et al.* (2013). Whether this is relevant awaits the evaluation of the first Danish exploration borehole to be drilled in the Lower Palaeozoic in northern Jylland.

References

Buchardt, B., Nielsen, A.T. & Schovsbo, N.H. 1997: Alun Skiferen i Skandinavien. Geologisk Tidsskrift **1997**(3), 1–30.

Gautier, D.L., Charpentier R.R., Gaswirth, S.B., Klett, T.R., Pitman, J.K., Schenk, C.J., Tennyson, M.E. & Whidden, K.J. 2013: Undiscovered gas resources in the Alum Shale, Denmark. U.S. Geological Survey Fact Sheet **2013–3103**, 4 pp.

Lassen, A. & Thybo, H. 2012: Neoproterozoic and Palaeozoic evolution of SW Scandinavia based on integrated seismic interpretation. Precambrian Research **204–205**, 75–104.

Mogensen, T.E. & Korstgård, J.A. 2003: Triassic and Jurassic transtension along part of the Sorgenfrei–Tornquist Zone, in the Danish Kattegat. In: Ineson, J.R. & Surlyk, F. (eds): The Jurassic of Denmark and Greenland. Geological Survey of Denmark and Greenland Bulletin **1**, 439–458.

Nielsen, A.T. & Schovsbo, N.H. 2011: The Lower Cambrian of Scandinavia: depositional environment, sequence stratigraphy and palaeogeography. Earth Science Reviews **107**, 207–310.

Petersen, H.I., Schovsbo, N.H. & Nielsen, A.T. 2013: Reflectance measurements of zooclasts and solid bitumen in Lower Palaeozoic shales, southern Scandinavia: correlation to vitrinite reflectance. International Journal of Coal Petrology **114**, 1–18.

Pool, W., Geluk, M., Abels, J. & Tiley, G. 2012: Assessment of an unusual European shale gas play: the Cambro-Ordovician Alum Shale, southern Sweden. Proceedings of the Society of Petroleum Engineers/European Association of Geoscientists and Engineers Unconventional Resources Conference, 20–22 March, 2012, Vienna, 152339.

Schovsbo, N.H., Nielsen, A.T., Klitten, K., Mathiesen, A. & Rasmussen, P. 2011: Shale gas investigations in Denmark: Lower Palaeozoic shales on Bornholm. Geological Survey of Denmark and Greenland Bulletin **23**, 9–12.

Vejbæk, O.V. & Britze, P. (compilers) 1994: Geological map of Denmark 1:750 000. Top pre-Zechstein (two-way traveltime and depth). Danmarks geologiske Undersøgelse Kortserie **45**, 8 pp., 3 maps.

Authors' addresses

N.H.S, *Geological Survey of Denmark and Greenland,* Øster *Voldgade 10, DK-1350 Copenhagen K, Denmark.* E-mail: *nsc@geus.dk*

A.T.N., *Natural History Museum of Denmark,* Øster *Voldgade 5–7, DK-1350 Copenhagen K, Denmark.*

D.L.G., *Consulting Geologist, 3954 Nelson Court, Palo Alto, California 94306, USA.*

Seismic stratigraphy and sedimentary architecture of the Chalk Group in south-west Denmark

Connie Larsen, Jon Ineson and Lars Ole Boldreel

The Chalk Group is ubiquitous in the subsurface of the Danish Basin and its upper levels are exposed locally onshore, most notably in eastern Denmark. Although many subsurface studies have been made of the group in the Danish Basin, most of these have been in the eastern part of Denmark (e.g. Esmerode *et al*. 2007; Surlyk & Lykke-Andersen 2007) whereas the stratigraphy and character of the Chalk Group in the western onshore region is less well-known. The work described here was undertaken as a BSc project at the Department of Geosciences and Natural Resource Mangement at the University of Copenhagen by the first author as part of regional seismic mapping work contributing to an evaluation of the geothermal energy potential in Denmark. The aim of this paper is to present a summary of the key results of the study. We have subdivided and mapped the distribution of the Chalk Group in the northern North German Basin and the south-western Danish Basin based on digital reflection seismic profiles. We also highlight seismic architectural features that testify to periods of active bottom currents.

Geological setting

Following rifting in Late Carboniferous – Early Permian times, the Mesozoic history of the Danish Basin was dominated by thermal subsidence, albeit with an important mid-Jurassic uplift event and phases of localised inversion in the Late Cretaceous – Palaeogene (Liboriussen *et al.* 1987). The combination of high sea-levels, a peneplaned hinterland and aridity in northern Europe in the Late Cretaceous led to a reduced influx of siliciclastic sediment to the sea and favoured the accumulation of pure pelagic chalk composed primarily of skeletal fragments from coccolithophorid algae. The pelagic chalk deposits were subject to redistribution by various processes including downslope mass-flow movements from

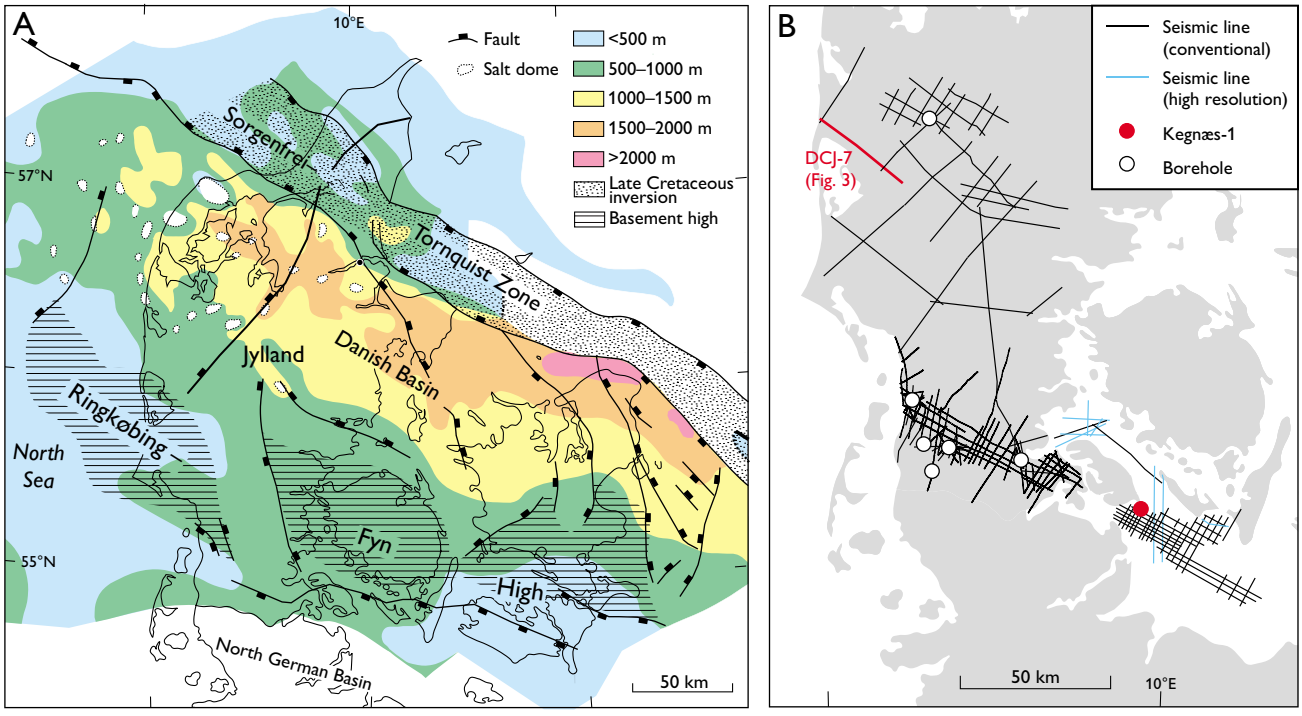

Fig. 1. Structural map of the Danish Basin (**A**) showing the thickness of the Upper Cretaceous – Danian Chalk Group (modified after Rasmussen & Surlyk 2012); note that the study area (shown in detail in **B**) straddles a major structural high, the Ringkøbing–Fyn High. The enlarged map (**B**) displays the seismic lines and deep boreholes used in this study; highlighted in red are the Kegnæs-1 borehole (see Fig. 2) and the seismic line illustrated in Fig. 3.

slope instability caused by syndepositional tectonics as well as along-slope bottom currents that sculpted the sea floor into valleys, channels, drifts, ridges and mounds (e.g. Surlyk & Lykke-Andersen 2007).

Results

The subdivision of the Chalk Group is based on seismic facies analysis and seismic structural analysis, and the resultant seismic units are correlated to wireline-logs and stratigraphic units from seven deep boreholes (Fig. 1). The study used 2D digital and scanned seismic profiles from nine surveys on- and offshore; the digital high-resolution and conventional offshore data are of high quality whereas onshore the digital data are of good quality and the few older scanned data are of low quality. The interval between the base and top of the Chalk Group on the seismic profiles is divided into seismic units based on the recognition and mapping of relatively strong, bounding reflectors. The brief descriptions of the units given below are based on the interpretation of all the seismic profiles in the study area. In the northern part of the study area, the Chalk Group is subdivided into 10 seismic units but the uppermost unit is absent south of the Ringkøbing–Fyn High, i.e. only nine units are recognised in this area (Figs 1, 2). The inferred ages of these units are based on correlation to dated borehole sections.

Seismic units 1–3 show parallel, continuous or discontinuous reflector patterns with low amplitude. Boundaries of unit 1 are clearly defined on gamma-ray logs (Fig. 2) whereas the boundaries of unit 3 are typically marked by minor log fluctuations. Units 1–3 are recognised throughout the study area and are broadly of Cenomanian, Turonian and Coniacian ages respectively.

Seismic units 4–6 display discontinuous, semi-parallel internal reflector patterns which are locally chaotic. Boundaries can be correlated with minor gamma-ray log fluctuations in most boreholes; the base of unit 6 is marked by a prominent sonic peak log in the Kegnæs-1 borehole (Fig. 2). Units 4–6 are recognised throughout the study area and are of probable Santonian, early Campanian and late Campanian ages respectively.

Seismic units 7 and 8 show discontinuous, semi-parallel internal reflector patterns that become chaotic locally. Correlation to log data in boreholes can be difficult but a clear response is observed on the gamma-ray logs in some of the boreholes; the unit is recognised throughout the study area and probably of early to mid-Maastrichtian age.

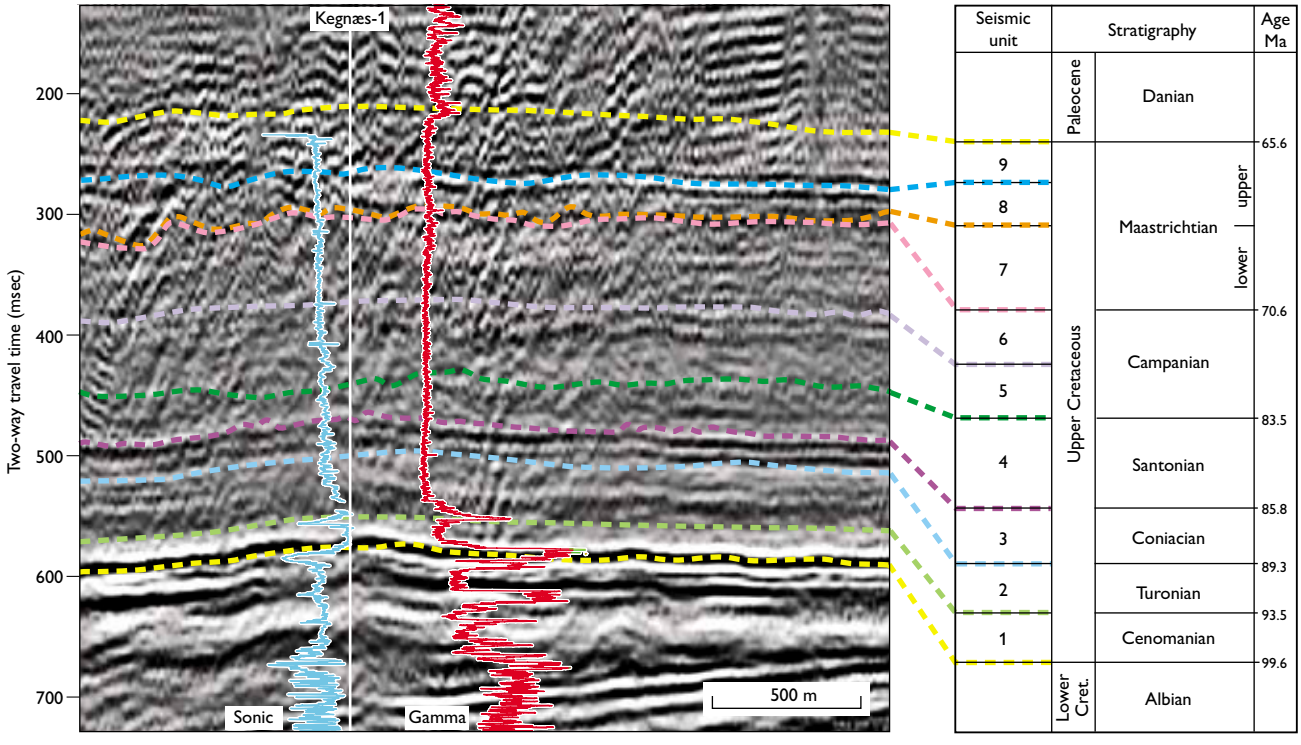

Fig. 2. Seismic profile (in two-way travel-time, TWT) intersecting the Kegnæs-1 borehole, illustrated by the sonic log (blue) and gamma-ray log (red), and showing the correlation between the seismic units and the chronostratigraphy, based on data from Gearhart (1986).

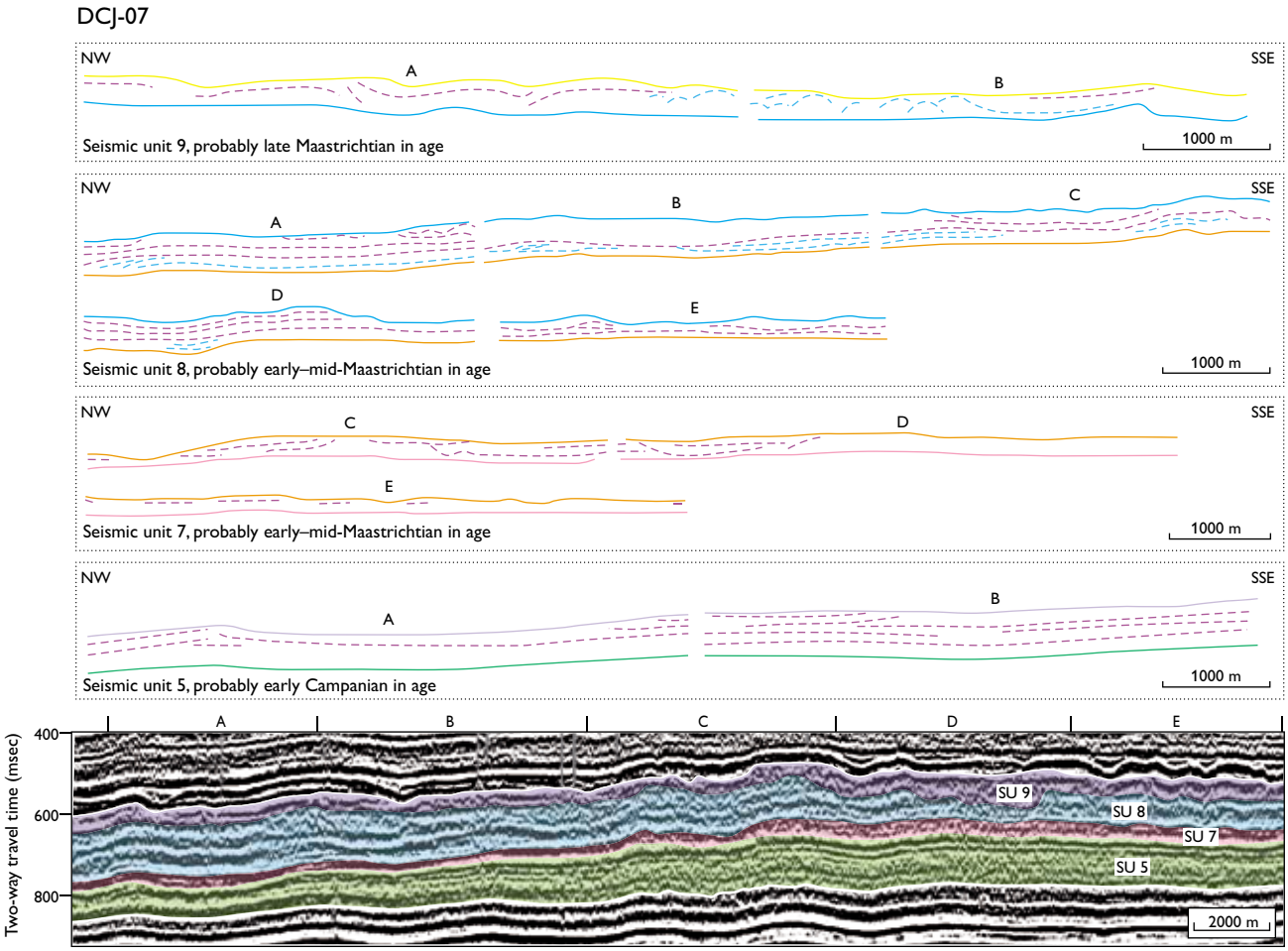

Fig. 3. Internal architecture of selected seismic units in the seismic profile DCJ-07 (for location, see Fig. 1): unit 5 (green), unit 7 (pink), unit 8 (blue) and unit 9 (purple). The accompanying sketches illustrate the internal architecture of these units; the bounding surfaces indicated in colour are defined on Fig. 2 .

Seismic unit 9 commonly shows localised disturbance of the internal reflector pattern but elsewhere exhibits a parallel, continuous to discontinuous pattern. The unit boundaries are readily correlated to gamma-ray logs and are recognised throughout the study area. Unit 9 is of probable late Maastrichtian age.

Seismic unit 10 is only present in the western part of the study area, north of the Ringkøbing–Fyn High, and wedges out to the south near the Ringkøbing–Fyn High. It shows a parallel, continuous or discontinuous internal reflector pattern with high amplitude. It is recognisable on some of the gamma-ray logs and is probably of early Danian age.

Based on seismic facies analysis, seismic units 1–3 and 9 (Cenomanian, Turonian, Coniacian and upper Maastrichtian ages respectively) typically display parallel and low-angle, mounded internal geometries, whereas seismic units 4–8 (Santonian, Campanian, lower Maastrichtian) show low-angle, mounded, sigmoidal, oblique and hummocky forms (Fig. 3). Evidence of seismic truncation, linked in some cases to log or biostratigraphic data, indicates the presence of three unconformities in the upper Chalk Group at 'mid-Campanian' (base unit 6), 'Base Maastrichtian' (base unit 7) and 'Top Maastrichtian' (top unit 9, base unit 10 where present); these surfaces seem to be associated with complex systems of major drift, minor mounded drift and channel-like features (Fig. 3).

Discussion

Mapping the distribution and thickness of the Chalk Group seismic units in the study area illustrates both regional trends, related to active inversion of the Sorgenfrei–Tornquist Zone during deposition of the Chalk Group, and local trends related to the influence of the Ringkøbing–Fyn High. The structural control exerted by Late Cretaceous inversion along the Sorgenfrei–Tornquist Zone is reflected by the over-

all geometry of the Chalk Group and the gentle northward tilt of the base of the Chalk Group (see also Lykke-Andersen & Surlyk 2004).

The influence of the Ringkøbing–Fyn High, at least episodically, is indicated by both the distribution of the Danian strata and by the evidence of active bottom current activity. The Danian chalk succession (seismic unit 10) is limited to the area north of the Ringkøbing–Fyn High and locally these deposits are preserved in trough-like, channel features. This distribution is consistent with the work of Thomsen (1995) who reported that the Danian succession wedges out in the south-western part of Jylland, crossing the Ringkøbing–Fyn High. Major drifts, minor mounded drifts and channel-like features are identified north of the Ringkøbing–Fyn High and represent a complex depositional system that is mainly recognised in the Campanian–Maastrichtian interval; such features were not identified south of the Ringkøbing–Fyn High. Most of the structures are recognised on NW–SE- and NNW–SSE-oriented seismic lines indicating, together with internal architecture, drift migration towards the NW or NNW. A comparable, complex system has been described in the Øresund area (Esmerode *et al*. 2007; Surlyk & Lykke-Andersen 2007) where it is seen in middle Santonian – Campanian and upper Maastrichtian intervals, and is considered to be analogous to modern deep-water contourite systems; i.e. that the deposits were moulded by bottom currents that flowed parallel to bathymetric contours. Such processes do not seem to have influenced the Santonian succession in the study area of south-west Denmark, possibly because there was no significant bathymetric relief in this part of the basin at that time.

In addition to the upper surface of the Chalk Group south of the Ringkøbing–Fyn High, two intra-Chalk unconformities are recognised seismically over the entire study area, the inferred mid-Campanian hiatus and the 'Base Maastrichtian' surface; note that the former is correlated to a pronounced cemented layer (hardground?) and a biostratigraphically defined middle Campanian hiatus in the Kegnæs-1 borehole (Gearhart 1986). According to Abramovitz *et al*. (2010), two major unconformities are recognised within the Chalk Group in the southern part of the Danish Central Graben: one within the Turonian–Campanian Hod Formation and one at the base of the overlying Maastrichtian Tor Formation boundary. Although it is possible that the 'intra-Hod' unconformity may correspond in part to the mid-Campanian hiatus in Jylland, this event in the Danish Central Graben has typically been attributed a Santonian age (e.g. Abramovitz *et al*. 2010). It is noteworthy, however that a mid-Campanian inversion event is well-known from the Central Graben in the Netherlands sector (van der Molen *et al*. 2005). The 'base-Tor' unconformity of the Danish Central Graben may correspond to the Base Maastrichtian unconformity recognised in this study. Future work will focus on tying the Jylland data set with that of the better-studied Chalk Group of eastern Denmark.

Acknowledgements

The regional investigations to assess the geothermal energy potential in Denmark are supported by the Danish Agency for Science, Technology and Innovation, and INTERREG4A (European Regional Development Fund).

References

Abramovitz, T., Andersen, C., Jacobsen, F.C., Kristensen, L. & Sheldon, E. 2010: 3D seismic mapping and porosity variation of intra-chalk units in the southern Danish North Sea. In: Vining, B.A. & Pickering, S.C. (eds): Petroleum geology: from mature basins to new frontiers **1**, 537–548. London: Geological Society.

Esmerode, E.V., Lykke-Andersen, H. & Surlyk, F. 2007: Ridge and valley systems in the Upper Cretaceous chalk of the Danish Basin: contourites in an epeiric sea. In: Viana, A.R. & Rebesco, M. (eds): Economic and palaeoceanographic significance of contourite deposits. Geological Society Special Publication (London) **276**, 265–282.

Gearhart 1986: Biostratigraphy report. Texaco 5410/5-1 Danish well [Kegnæs-1], 33 pp. Unpublished report, Gearhart Geo Consultants Ltd. (In archives of GEUS – File 9689).

Liboriussen, J., Ashton, P. & Tygesen, T. 1987: The tectonic evolution of the Fennoscandian border zone in Denmark. Tectonophysics **137**, 21–29.

Lykke-Andersen, H., & Surlyk, F. 2004: The Cretaceous–Palaeogene boundary at Stevns Klint, Denmark: inversion tectonics or sea-floor topography? Journal of the Geological Society (London) **161**, 343–352.

Rasmussen, S.L. & Surlyk, F. 2012: Facies and ichnology of an Upper Cretaceous chalk contourite drift complex, eastern Denmark, and the validity of contourite facies models. Journal of the Geological Society (London) **169**, 435–447.

Surlyk, F. & Lykke-Andersen, H. 2007: Contourite drifts, moats and channels in the Upper Cretaceous chalk of the Danish Basin. Sedimentology **54**, 405–422.

Thomsen, E. 1995: Kalk og kridt i den danske undergrund. In: Nielsen, O.B. (ed.): Danmarks geologi fra kridt til i dag, 31–67. Århus: Geologisk Institut, Aarhus Universitet.

Van der Molen, A.S., Dudok van Heel, H.W. & Wong, T.E. 2005: The influence of tectonic regime on chalk deposition: examples of the sedimentary development and 3D-seismic stratigraphy of the Chalk Group in the Netherlands offshore. Basin Research **17**, 63–81.

Authors' addresses

C.L. & L.O.B., *Department of Geosciences and Natural Resource Mangement, University of Copenhagen, Øster Voldgade 10, DK-1350 Copenhagen K, Denmark*. E-mail: *gnk171@alumni.ku.dk*

J.I., *Geological Survey of Denmark and Greenland,* Øster *Voldgade 10, DK-1350 Copenhagen K, Denmark*.

A novel technique for obtaining representative water samples during CO_2 core-flooding experiments on chalk at reservoir conditions

Claus Kjøller and John Zuta

There is a huge potential for using CO_2 gas to recover additional oil after water flooding in reservoir chalk. However, the injection of CO_2 into chalk reservoirs will disturb the chemical equilibrium between formation water, injection water and chalk. A proper understanding of these CO_2-induced interactions and the resulting changes in the physical properties at representative reservoir conditions is required. Unfortunately, reliable chemical data are rare because data cannot be acquired directly at reservoir conditions with present-day techniques. In published experiments, water samples are in many cases obtained at atmospheric conditions with the aid of a back-pressure regulator. Thus, water samples are not representative of *in situ* reservoir conditions and if proper care is not taken, the collected data cannot be used to judge the magnitude of the chemical reactions taking place at reservoir conditions. However, in some cases water obtained at laboratory conditions can give information on *in situ* reservoir conditions by using geochemical speciation models to account for dissolved gases that are lost from the effluents during sampling (Bachu & Adams 2003).

The objective of this study was to develop and test a new technique for obtaining water samples during CO_2-brine–rock interactions in reservoir chalk under representative reservoir conditions and gain a better understanding of the chemical interactions which occur during the injection of CO_2. The experiments were performed by injecting CO_2-saturated seawater at supercritical CO_2 conditions, at a pressure of 17.24 MPa (2500 psig; pounds per square inch of gauge pressure) and a temperature of 75°C. These values are typical of a region in a chalk field where the rock is exposed to long term reactions with flow of CO_2-bearing water. In addition, the numerical code PHREEQC-3 (Parkhurst & Appelo 2013) was used to reproduce the experiments by assuming equilibrium between calcite and injected fluids. In this way, we can validate the sampling procedure and investigate how the measured parameters (pH, CO_2 pressure, calcium (Ca) and bicarbonate (HCO_3^-) concentrations) compared with the calculated parameters.

Reservoir chalk samples

Chalk plugs for the experiment were sampled from the Maastrichtian Tor Formation in the central North Sea and were first cleaned of salt and oil with methanol and toluene. Following initial determination of porosity and permeability, the samples were saturated with synthetic formation water (FW). All plugs had a diameter of 3.81 cm and a length of approximately 7.5 cm; plugs with similar petrophysical properties (Table 1) were used to check the reproducibility of the studied sampling procedure. The compositions of synthetic formation water, synthetic seawater and CO_2 synthetic saturated seawater are listed in Table 2.

Experimental setup

The setup/rig for the experiments is shown in Fig. 1. It includes three cylinders with pistons placed in an oven to maintain constant temperature. Two of the cylinders were used

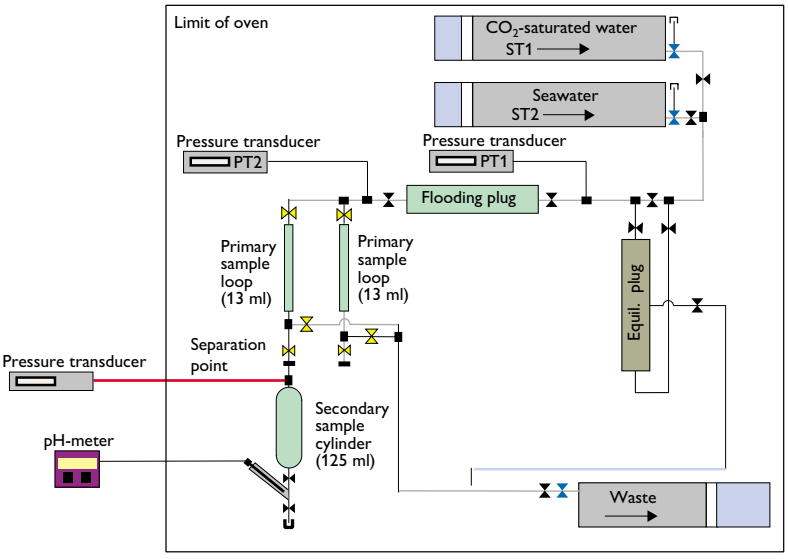

Fig. 1. Experimental setup/rig within the oven. The rig has two primary sample loops.

Table 1. Petrophyscial properties of plugs prior to the injection of CO_2-saturated water at 17.24 MPa (2500 psig) and 75°C

Plug ID	Porosity (%)	Pore volume (ml)	Permeability (mD)
17A	32.60	26.94	1.36
19A	30.60	25.59	1.49

for the delivery of CO_2-saturated seawater and seawater. The third cylinder was used as a waste tank and for maintaining fluid pressure. All the fluids were injected at a constant rate of 6.5 ml/h with the plug in a horizontal position. The injection of CO_2-saturated seawater was preceded by injecting close to 3.5 pore volume (PV) of seawater to mimic the present-day water flooding. At the end of the injection of CO_2-saturated seawater, seawater was again injected through the plug. At this point, equilibrium with calcium carbonate was obtained in the injection fluid by first passing the seawater through the equilibrium plug (Fig. 1). This was done in order to avoid any further dissolution of chalk in the plug under study. The final seawater flooding was performed to displace any residual CO_2 gas and bring the concentrations back to initial levels.

Water sampling technique

The system for obtaining water samples was located at the downstream end of the rig (Fig. 1). It consists of two primary sample loops each with a volume of *c.* 13 ml. This enabled continuous collection of water samples for every 13 ml (*c.* 0.5 pore volume) of plug flooded. The sampling was done by alternating the flow process between the two primary loops with the aid of computer-controlled valves (CV-210 valves) without disrupting the injection process. The primary sample loops were connected to a secondary sample cylinder with a volume of 125 ml by a separation point. Water samples were transferred from the primary sample loop to the secondary sample cylinder by a de-pressurisation step. This made it possible to collect water samples for a set of chemical parameters (Ca and HCO_3^- concentrations) at predefined sampling intervals. The pH and CO_2 pressures of the de-pressurised

Table 2. Composition (in mg/l) of synthetic formation water (FW), seawater (SW), and CO_2-saturated seawater (CSW)

Ions	(FW)	(SW)	(CSW)
Na	22866	11090	11090
K	175	408	408
Mg	226	1370	1370
Ca	1244	434	434
Sr	142	6.8	6.8
Cl^-	38383	20173	20173
HCO_3^-	22	30	70
SO_4^{2-}	–	2780	2780

Table 3. Composition of resulting solutions at the two different equilibrium steps followed by the de-pressurisation step based on calculations with phreeqc.dat database in PHREEQC-3

Chemical parameter	Step 1	Step 2	Step 3
pH	3.2	4.8	6.3
Ca (mg/l)	438	1970	1970
Alkalinity, HCO_3^- (mg/l)	82	3274	3308
Saturation index (calcite)	−3.78	0	1.43

effluents were measured on-line in the secondary sample cylinder after the de-pressurisation step. The sampling from the secondary sample cylinder was subsequently done as fast as possible, in less than 5 min., thereby providing a consistent chemical dataset for the conditions prevailing in the secondary sample cylinder. In this way it was possible to validate the subsequent numerical calculations used to estimate the *in situ* chemical conditions. A detailed description of the sampling procedure as well as documentation for the consistency of the collected dataset was published by Kjøller & Zuta (2012).

Batch modelling with PHREEQC-3

The modelling was performed at the same conditions – pressure and temperature of 17.24 MPa (2500 psig) and 75°C as the experiments, in order to estimate the true *in situ* reservoir condition chemistry. Three equilibrium steps in a closed system were investigated: (1) equilibrium between CO_2 and seawater corresponding to the injected solution, (2) equilibrium between CO_2-saturated seawater and calcite, representing reservoir conditions, and (3) composition of the solution after de-pressurisation in the secondary sample cylinder. A good fit between experimental and numerical data after step

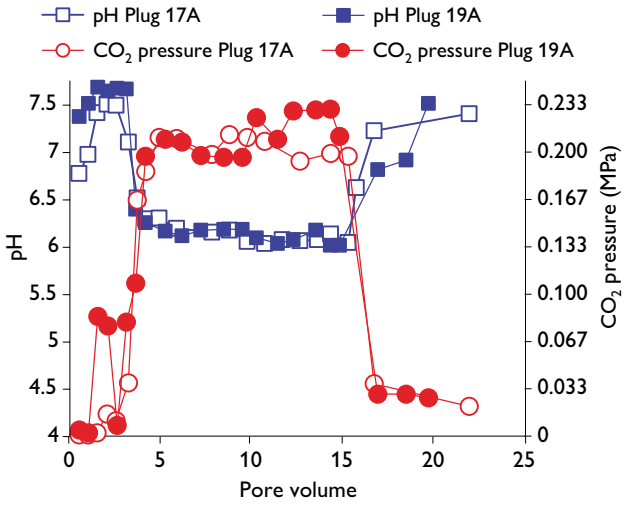

Fig. 2. Measured pH and CO_2 pressure for plug 17A and parallel plug 19A versus cumulative, injected pore volume.

Table 4. Properties of the gas phase generated after the de-pressurisation stage in the 125 ml secondary sample cylinder with the phreeqc.dat database in PHREEQC-3

Total pressure	2.00 MPa (28.9 psig)
Gas volume	1.25e-001 litres
Molar volume	1.38e+001 litres/mole
P×Vm/RT	0.99228 (compressibility factor Z)

3 is considered as a validation of the numerical estimate of reservoir conditions in step 2 (Kjøller & Zuta 2012).

Results

Figures 2–4 show pH, CO_2 pressure, Ca, and HCO_3^- concentrations measured as a function of injected cumulative pore volumes. The compositions of the resulting solutions calculated at the three steps with PHREEQC-3 are shown in Table 3. Equilibrium of CO_2 and seawater results in an initial CO_2-saturated seawater solution with a pH of 3.2 and a saturation index of calcite of –3.78 (Table 3, step 1), an indication of a strong dissolution potential for chalk. Thus, CO_2 is dissolved and reacts with water to form carbonic acid (H_2CO_3). It is part of this acidity that is removed as the dissolution process advances into the plugs. The dissolution of calcium carbonate in the plugs takes place according to the overall chemical reaction:

$$H_2CO_3 + CaCO_3 \rightarrow Ca^{2+} + 2HCO_3^-$$

During the injection of seawater within the first 3.5 pore volume, the pH increases to between 7.5 and 7.7 and subsequently decreases to an average of 6.1 during the injection of CO_2-saturated seawater (Fig. 2). At the final stage of the experiment, the pH increases again to the initial seawater pH level, an indication that all the residual CO_2 was removed from the plugs during the injection of seawater in equilibrium with chalk. The calculated decrease in pH at reservoir conditions (Table 3, step 2) corresponds with the measured decrease in pH after 3.5 pore volume, where breakthrough of the CO_2-saturated seawater is observed. However, the calculated reservoir condition pH of 4.8 is much lower than the average measured pH during the injection of CO_2-saturated seawater. This was expected since the pH was measured after the de-pressurisation step where CO_2 gas had already degassed from the solution. Thus, taking the pH (6.3) of the degassed solution into account in the numerical simulation provides an excellent fit to the average measured pH of 6.1 (Table 3, step 3). The CO_2 pressure in the secondary sample cylinder varied between 0.17 MPa (25 psig) and 0.24 MPa (35 psig) at the de-pressurisation stage during the injection of CO_2-saturated seawater (Fig. 2). This matches with the calculated CO_2 pressure of 0.20 MPa (28.9 psig) in the gas phase of the secondary sample cylinder (Table 4), and further validates the numerical calculations.

According to the equation, degassing of CO_2 from the water samples, caused by the transfer of water samples from the primary sample loop to the secondary sample cylinder, was expected to result in precipitation of $CaCO_3$. Comparison of Ca and HCO_3^- concentrations measured in both filtered and unfiltered water samples showed no evidence of mobilisation or precipitation of fine particles during the de-pressurisation stage, neither in plug 17A nor in plug 19A (Fig. 3A, B). The Ca concentration decreases during the first 3.5 pore volume to the Ca-concentration level in seawater

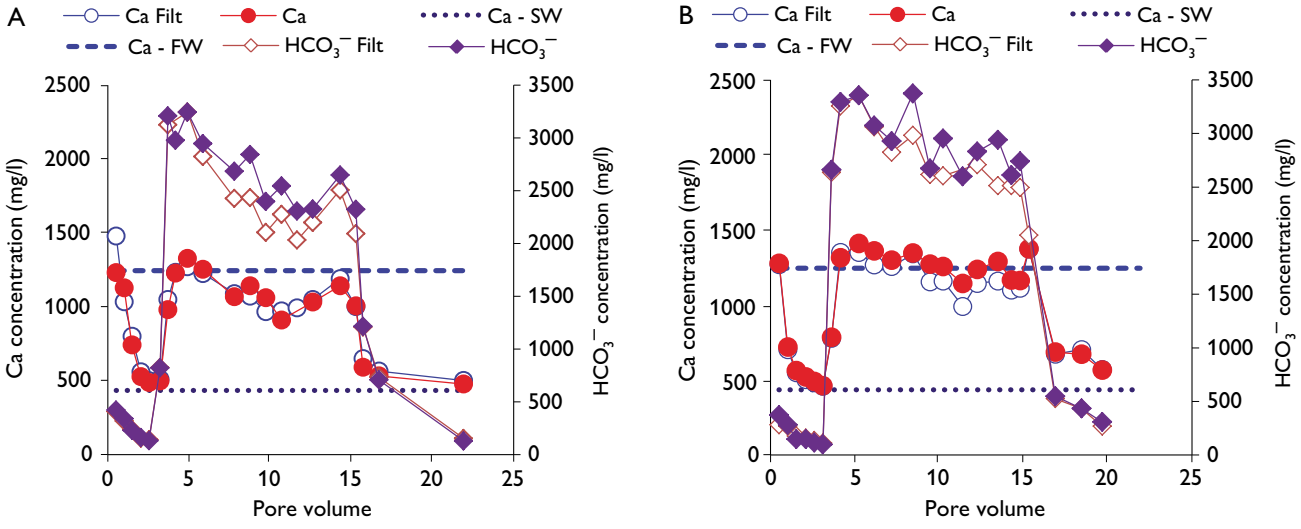

Fig. 3. Measured Ca and HCO_3^- concentrations for filtered and unfiltered water samples in plugs 17A (**A**) and 19A (**B**) versus cumulative, injected pore volume. **Filt**: filtered. **SW**: synthetic seawater. **FW**: synthetic formation water.

of *c.* 450 mg/l. Subsequently, the measured Ca concentration increases to an average of 1200–1300 mg/l during the injection of CO_2-saturated seawater, which is due to dissolution of calcium carbonate in the plugs. At the final steps of the experiment, the Ca concentration again decreases to the seawater level during injection of seawater to remove residual CO_2 from the plugs. In the geochemical model, the calculated Ca concentration of 1970 mg/l at reservoir conditions (Table 3, step 2) is simulated by dissolution of calcite at reservoir conditions, and does not take into account the possible precipitation of calcium carbonate during sampling. Therefore, the calculated reservoir-condition Ca concentration is higher than the concentrations measured in the experiments during the period with CO_2-saturated seawater flooding. Since no mobilisation or deposition of suspended fine particles in the water samples were observed, the difference in Ca concentration must be attributed to deposition of fine calcium carbonate particles on the inner surface walls of the secondary sample cylinder during the pressure-reduction stages. In line with this, the simulated saturation index (SI) with respect to calcite of 1.43 after de-pressurisation (Table 3, step 3) is higher than the saturation indices between 0.6 and 1.2 that can be calculated based on the measured water chemistry.

If the saturation index with respect to calcite is constrained to be between 0.6 and 1.2 in the numerical calculations in step 3, the calculated Ca concentration at the sampling conditions varies between *c.*1150–1650 mg/l, which is in much better agreement with the actually measured Ca concentrations (Fig. 3). Similar considerations and conclusions can be made for the HCO_3^--concentration trend during the experiment. Thus, the measured HCO_3^- concentration averages 2350–2550 mg/l during the injection of CO_2 saturated seawater, while the calculated HCO_3^- concentration after de-pressurisation is 3308 mg/l when no constraints on the saturation index with respect to calcite are applied (Table 3, step 3). However, accounting for some calcium carbonate precipitation during de-pressurisation will diminish the difference between calculated and measured concentrations, and overall it is suggested that the calculated reservoir condition concentrations shown in Table 3, step 2 represent the true *in situ* reservoir conditions prevailing in the plugs during experiments.

The general decrease in measured Ca and HCO_3^- concentrations during the injection of CO_2-saturated seawater from 3.5 to 15 pore volume (Fig. 3), suggests that, with time, there is an increasing amount of calcium carbonate precipitating in the secondary sample cylinder during sampling. For future studies, this gradual change in calcium carbonate precipitation should be avoided in order to minimise the uncertainty in the measured data, and thereby also the uncertainty of the numerical estimate of the reservoir condition chemistry (Table 3, step 2).

Conclusions

- A new sampling technique was developed and used to study CO_2-brine–rock interactions in reservoir chalk at reservoir conditions.
- The similar results obtained in the parallel plugs validate the sampling procedure and show a high degree of reproducibility.
- The results from the experiment and the modeling show increased levels of calcium and alkalinity (HCO_3^-) with decreasing pH during the injection of CO_2-saturated water at reservoir conditions. There were, however, differences between the measured and calculated calcium concentration and HCO_3^- concentration which is probably due to accumulation of fine calcium carbonate particles on the inner walls of the secondary sample cylinder during the de-pressurisation stage.
- Further refinement of the method may include modification of the secondary sample cylinder, in order to minimise the accumulation of fine calcium carbonate particles on its inner surface walls.

Acknowledgements

We are grateful to Dansk Undergrunds Consortium (DUC) – a co-operation between A.P. Møller Maersk, Shell, Chevron and Nordsøfonden (the Danish North Sea Fund) – for sponsoring the work.

References

Bachu, S. & Adams, J.J. 2003: Sequestration of CO_2 in geological media in response to climate change: capacity of deep saline aquifers to sequester CO_2 in solution. Energy Conversion and Management **44**, 3151–3175.

Kjøller, C. & Zuta, J. 2012: CO_2-brine–rock interactions in reservoir chalk rock – a coupled experimental and numerical approach for obtaining hydrochemical results at reservoir conditions. Paper SCA2012-04 presented at International Symposium of the Society of Core Analysts, Aberdeen, Scotland, UK, 27–30 August, 2012, 12 pp.

Parkhurst, D.L. & Appelo, C.A.J. 2013: Description of input and examples for PHREEQC version 3 – a computer program for speciation, batch-reaction, one-dimensional transport, and inverse geochemical calculations. U.S. Geological Survey Techniques and Methods, *http://pubs.usgs.gov/tm/06/a43/.*

Authors' address:

Geological Survey of Denmark and Greenland, Øster *Voldgade 10, DK-1350 Copenhagen K, Denmark.* E-mail: *clkj@geus.dk*

Calcareous nannofossil and foraminifer biostratigraphy of the Campanian–Maastrichtian chalk of the Femern Bælt (Denmark–Germany)

Emma Sheldon, Caterina Morigi and Sarah D. Møller

A new study based on calcareous nannofossil and benthic and planktonic foraminifer biostratigraphy is presented for the upper Campanian – Maastrichtian chalk of the Femern Bælt (Denmark and Germany; Fig.1). The results are consistent with recent studies of the Danish chalk for this interval, allowing correlation across the Danish Basin and forming the basis for correlation further afield within the Boreal Realm. Numerous studies have been carried out recently on the upper Campanian – Maastrichtian chalk of the Danish Basin, covering aspects such as sedimentology, depositional environment, macrofossil biostratigraphy, carbon isotope stratigraphy as well as nannofossil and dinoflagellate biostratigraphy. However, very few published studies on foraminifers exist across this interval in this area. The 09.A.006, 09.A.007 and 09.A.008 boreholes (Fig. 2) were drilled in 2009 in preparation for construction of a fixed link across the Femern Bælt, which will connect Denmark to Germany (Rambøll Arup JV 2011). The boreholes penetrated glacial till, Paleocene–Eocene clay and chalk (Sheldon *et al.* 2012). Here, for the first time, the Boreal foraminifer biostratigraphy of the late Campanian – Maastrichtian interval is investigated and presented alongside nannofossil biostratigraphy.

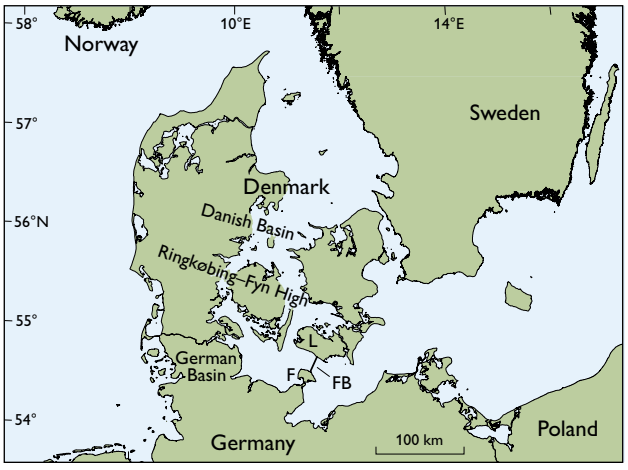

Fig.1. Map of Denmark and northern Germany showing the location of the planned fixed road and rail link across Femern Bælt. **L**: Lolland, **F**: Fehmarn, **FB**: Femern Bælt.

Geological setting and palaeogeography

The Femern Bælt area is located to the south of the Ringkøbing–Fyn High and is part of the German Basin (Fig. 1). During the Late Cretaceous the Danish area was part of the extensive epicontinental sea where cool-water carbonate deposition dominated. The Maastrichtian chalk was deposited at depths of 100–250 m (Surlyk 1997). Chalk distribution patterns are affected in the Danish area by folding, salt diapirism, non-deposition and erosion, especially in the southern region (Lieberkind *et al.* 1982). In the Maastrichtian to Danian, the area was situated at 44°–46°N (Smith *et al.* 1994). In the upper Maastrichtian of this part of the Danish area, two main facies types dominate: (1) relatively deep water basinal sediments comprising coccolith and foraminifera-rich pelagic chalk, and (2) shallow marine chalk with high diversity faunas dominated by bryozoans, echinoids, bivalves and brachiopods (Surlyk 1997; Hart *et al.* 2004).

The upper Campanian – Maastrichtian chalk of onshore Denmark was until recently referred to the Tor Formation equivalent. The Tor Formation was established by Deegan & Scull (1977) as a Maastrichtian (locally upper Campanian) chalk unit in the Norwegian and Danish sectors of the North Sea. A new holostratigraphic analysis of the upper Cretaceous chalk of eastern Denmark resulted in a lithostratigraphic subdivision of the onshore chalk (Surlyk *et al.* 2013). However due to local facies variations this new subdivision cannot be applied to the chalk of the Femern Belt area with-

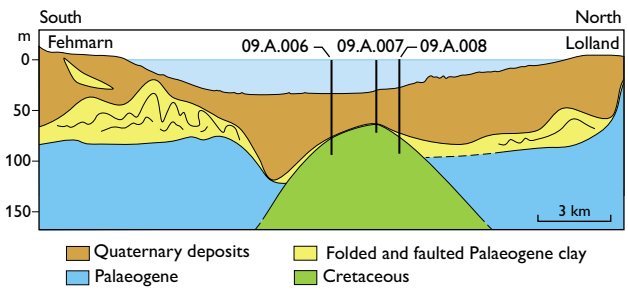

Fig. 2. Sketch south–north cross-section of the Femern Bælt area and the location of the boreholes (from Sheldon *et al.* 2012).

out sedimentological analysis and the term 'Tor Formation equivalent' is retained here.

Biostratigraphy

From the 09.A.008 and 09.A.006 boreholes nannofossils and foraminifers from the Campanian–Maastrichtian were analysed; from the 09.A.007 borehole nannofossils from the upper Maastrichtian were examined. The southern North Sea foraminifer zonation of King *et al.* (1989) and the Boreal nannofossil scheme of Burnett (1998) were applied (Fig. 3). Marker species are shown in Fig. 4 and biostratigraphic results on Fig. 5.

Nannofossil zones – The co-occurrence of *Orastrum campanensis* and *Eiffelithus eximius* indicates the presence of UC15d^{BP} at the base of core 09.A.008. Subzone UC15e^{BP} is absent. UC16^{BP} was defined by Burnett (1998) but recent studies of Danish Campanian–Maastrichtian chalks (Sheldon 2008; Thibault *et al.* 2012) question the reliability of the UC16^{BP} marker species in the Danish area. The top of UC16a^{BP} is defined by the last occurrence (LO) of *Heteromarginatus bugensis*. In the present study and in the Stevns-1 borehole, eastern Denmark, the LO of *H. bugensis* is below the LO of *Tortolithus caistorensis* (marker for top UC16b^{BP}). Other studies (e.g. Fritsen *et al.* 1999) assign the LO of *H. bugensis* to the top of UC16c^{BP}. The top of UC16b^{BP} is defined by the LO of *T. caistorensis*, which is very rare in the Danish area. UC16a^{BP} and b are not easily subdivided in the Danish area and alternative markers are suggested for the top of UC16b^{BP}: the LO's of *Tortolithus hallii* and *Tortolithus pagei* were successfully applied in the present study, positioned prior to the LOs of *Broinsonia parca parca* and *Zeugrhabdotus praesigmoides* (markers for the overlying UC16c^{BP}). The top of UC16c^{BP} is defined by the LO of *Monomarginatus quaternarius*. The LO of *B. parca parca* as a top UC16c^{BP} marker is a more reliable marker in this study. The LO of *Z. praesigmoides* as an additional top UC16c^{BP} marker is confirmed in this study. The top of subzone UC16d^{BP} is defined by the LO of *Broinsonia parca constricta*. The first occurrence (FO) of *Prediscosphaera mgayae* as an additional marker

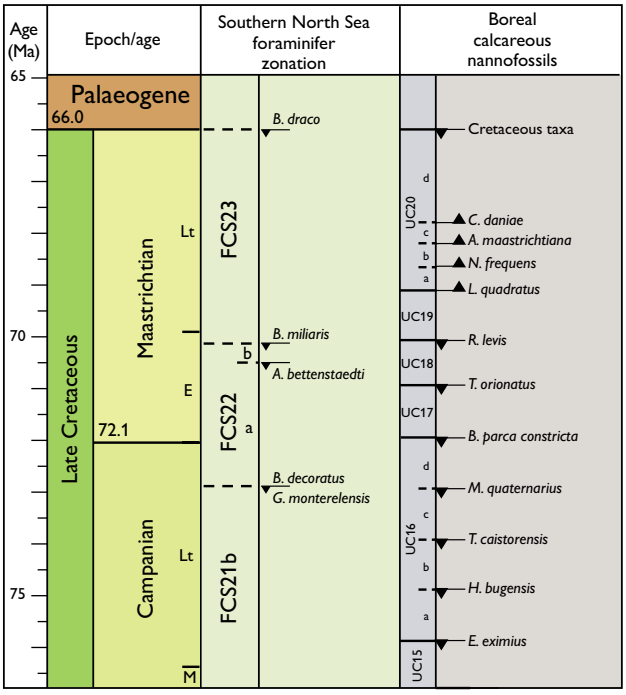

Fig. 3. Nannofossil and foraminifer zonations. The timescale is according to Gradstein *et al.* (2012). **UC**^{BP}: Upper Cretaceous Boreal Province nannofossil zones of Burnett (1998), **FCS**: Cretaceous southern North Sea Foraminfers, shelf facies, including chalk, zones of King *et al.* (1989). Nannofossil and foraminifer zonations correlated using Fritsen (1999).

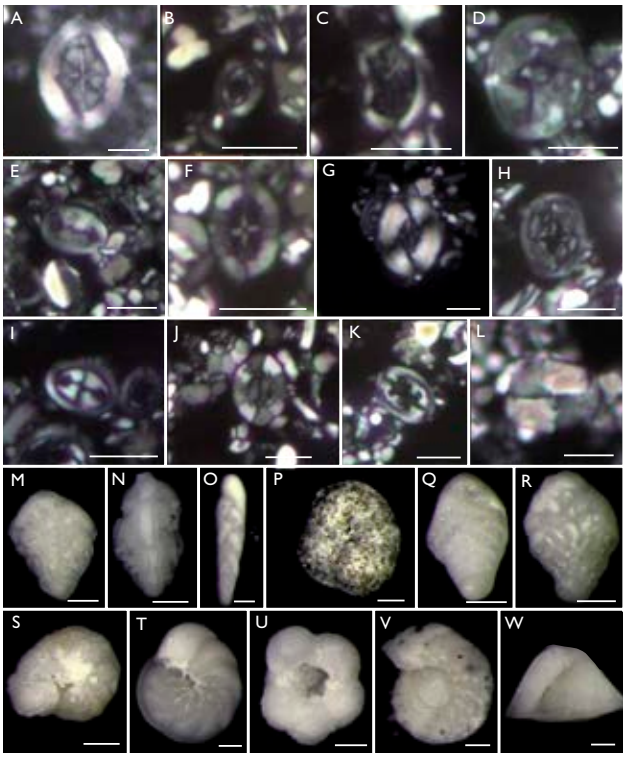

Fig. 4. Sselected nannofossils and foraminifers from the Femern Bælt. **A**: *Arkhangelskiella maastrichtiana*. **B**: *Prediscosphaera stoveri*. **C**: *Nephrolithus frequens*. **D**: *Reinhardtites levis*. **E**: *Tranolithus orionatus*. **F**: *Prediscosphaera mgayae*. **G**: *Broinsonia parca constricta*. **H**: *Monomarginatus quaternarius*. **I**: *Zeugrhabdotus praesigmoides*. **J**: *Tortolithus caistorensis*. **K**: *Heteromarginatus bugensis*. **L**: *Orastrum campanensis*. **M**: *Bolivinoides draco*. **N**: *Pseudouvigerina cristata*. **O**: *Brizalina incrassata*. **P**: *Hagenowella paleocenica*. **Q**: *Bolivinoides draco giganteus*. **R**: *Bolivinoides decoratus*. **S**: *Stensioeina pommerana*. **T**: *Angulogavelinella bettenstaedti*. **U**: *Globotruncana arca*. **V**: *Gavelinella monterelensis*. **W**: *Globorotalites micheliana*. Scale bars, nannofossils: 5 μm, foraminifers: 0.1 mm.

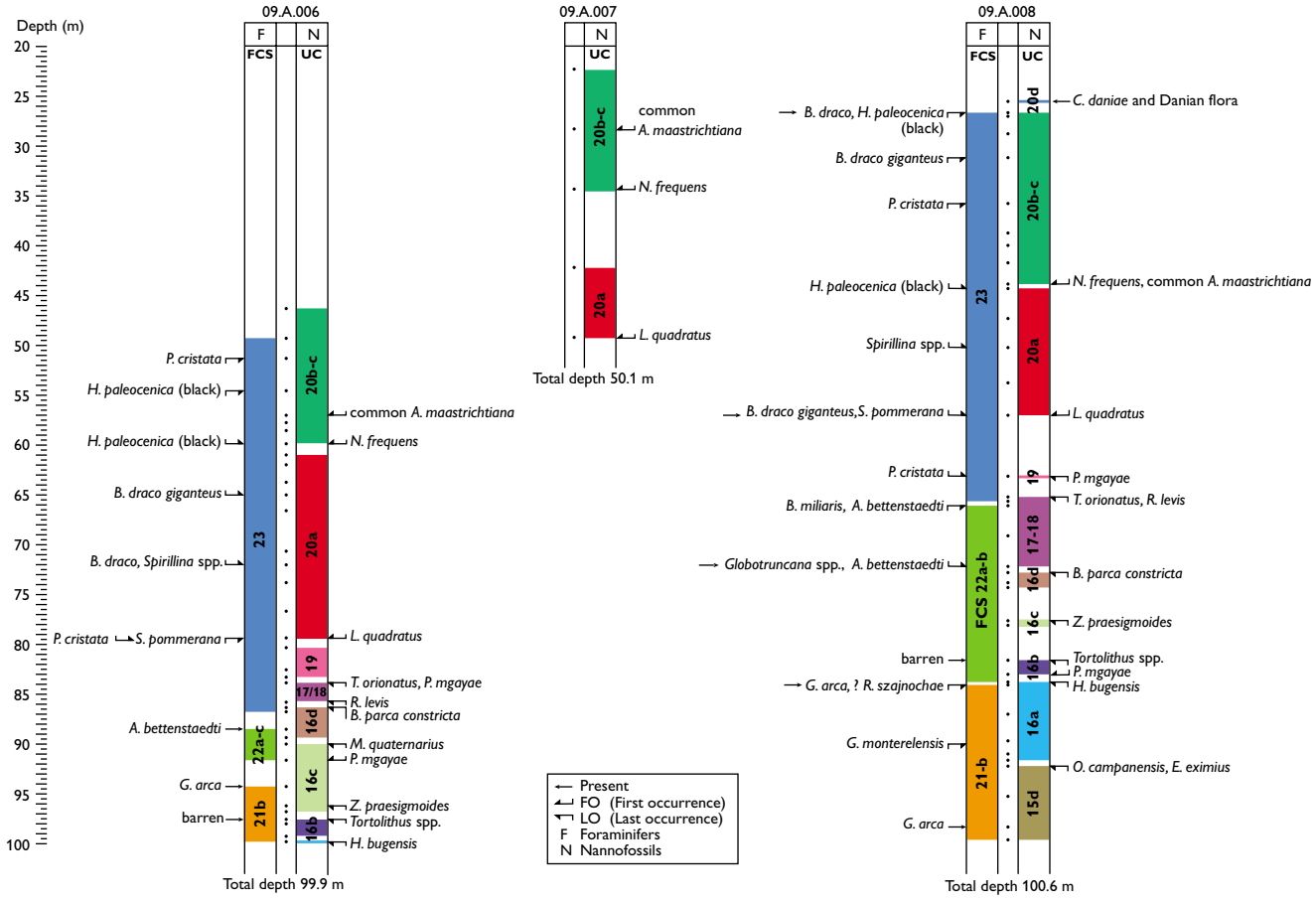

Fig. 5. Nannofossil and foraminifer biostratigraphic correlations of the three boreholes at the Femern Bælt.

in the middle of UC16d ^{BP} (Thibaut *et al.* 2012) is confirmed in this study. The LO of *Tranolithus orionatus* marks the top of UC17 ^{BP}. In the present study, the LO of this species occurred after the LO of *Reinhardtites levis* (the LO of which marks the top of the overlying UC18 ^{BP}). In Stevns-1 these species also occur in the 'reverse' order. The LO of *R. levis* marks the top of UC18^{BP}, but in this study its LO is before that of *T. orionatus*. It is suggested that in the Danish area, UC17^{BP} and UC18^{BP} should be combined, using either the LO of *T. orionatus* or the LO of *R. levis* to mark the zone top. The LO of *P. mgayae* has been suggested as an additional marker for the top of this zone (Thibaut *et al.* 2012); this is confirmed in this study. UC19^{BP} comprises the interval from the LO of *Reinhardtites levis* to the FO of *Lithraphidites quadratus*. The FO of *L. quadratus* defines the base of UC20a^{BP}. The base of UC20b^{BP} is defined by the FO of *Nephrolithus frequens*. The base of UC20c^{BP} is defined by the FO of *Arkhangelskiella maastrichtiana*. The uncertainties surrounding the use of the FO of *A. maastrichtiana* as a marker are well-documented (e.g. Thibault 2010) and the two subzones are merged here. The first common occurrence of *A. maastrichtiana* is used to mark the base of UC20b-c^{BP} in this study. The base of the *Prediscosphaera stoveri* acme within this combined subzone is also applied successfully in this study. The LO of *Helicolithus trabeculatus* was suggested as a supplementary marker for this level (Sheldon 2008) and is confirmed here. The FO of *Cribrosphaerella daniae* marks the base of UC20d^{BP}, the uppermost subzone of the Maastrichtian. The co-occurrence of *Chiasmolithus edentulus*, *Coccolithus pelagicus*, *Cyclagelosphaera alta* and *Neochiastozygus saepes* assigns the base of the overlying Danian in borehole 09.A.008 to the upper Danian subzone NNTp4F (Varol 1998). Lower – upper Danian subzones NNTp1A-4F are missing or were not sampled. Danian chalk in the Femern area was documented for the first time recently (Sheldon *et al.* 2012). Previously the southern limits of Danian deposits were thought to be farther to the north (Håkansson & Pedersen 1992).

Foraminifer zones – The top of FCS23 is defined by the LO of *Pseudotextularia elegans*. *Bolivinoides draco* (s.s.) is an index species. The top of subzone FCS23a is defined by the FO of *P. elegans*. *P. elegans* is not seen in the present study, but rare occurrences of *Bolivinoides draco* were noted, indicating the

presence of FCS23. In upper FCS23 the range of *Hagenowella paleocenica* and the FO of *Spirillina* spp. are additional markers in the present study. The LO of *Stensioeina pommerana* occurring towards the bottom of FCS23 (corresponding to the base of nannofossil subzone UC20a^{BP}) in this study may also prove useful. The range of *Pseudouvigernina cristata* within FCS23 may prove to be another useful marker. The absence of *P. elegans* means that it is not possible to subdivide FCS23 in this study. The top of FCS22 is defined by the LO of *Bolivinoides miliaris*. FCS22 is divided into FCS22b, the top of which is defined by the LO of *B. miliaris,* and FCS22a, the top of which is defined by the LO of *Angulogavelinella bettenstaedti*. The LOs of *A. bettenstaedti* and *B. miliaris* occurred in the same sample suggesting the presence of only FCS22a, but the range of *A. bettenstaedti* within FCS22 could be useful. The top of FCS21 is defined by the LO (often a flood occurrence) of *Reussella szajnochae.* FCS21 is divided into FCS21b, the top of which is defined by the LO of *R. szajnochae*, and FCS21a, the top of which is defined by the LO of *Gavelinella usakensis. G. usakensis* was not found in the present study, indicating the presence only of FCS21b. The LO of *Globotruncana arca* at the top of FCS21 is an additional marker, as are the LOs of *Gavelinella monterelensis* and *Globorotalites micheliana* and FO of *Brizalina incrassata* at a slightly lower stratigraphic level.

Conclusions

The Campanian–Maastrichtian chalk of the Danish area has recently been studied intensively using calcareous nannofossils, applying the UC^{BP} scheme. The studies underline the need for an amendment of the UC scheme for the Danish area. The present study highlights the need to reconsider the subdivision of UC20b^{BP} and UC20c^{BP} based on the FO of *Arkhangelskiella maastrichtiana*. It is recommended for the Danish area to use the FO of common *A. maastrichtiana* to mark the base of UC20C^{BP}. It may also be practical to merge UC17^{BP} and UC18^{BP}. Additionally the subdivision of UC16^{BP} cannot be reliably applied in the Danish area. The Danian nannofossil assemblage in borehole 09.A.008 provides further evidence for the southerly encroachment of the Danian sea.

The foraminifer zonation of the Late Campanian – Maastrichtian is for the first time correlated with the nannofossil zonation based on the 09.A.006 and 09.A.008 cores (Fig. 5). In the absence of certain established FCS marker foraminifera for the North Sea chalk, new zonal markers, e.g. *Hagenowella paleocenica, Pseudouvigerina cristata, Globotruncana arca, Gavelinella monterelensis* and *Globorotalites micheliana* are used here in addition to conventional taxa for the Campanian–Maastrichtian chalk of Denmark, perhaps allowing correlation with the North Sea area, and further afield.

References

Burnett, J.A. 1998: Upper Cretaceous. In: Bown, P.R. (ed.): Calcareous nannofossil biostratigraphy. British Micropalaeontological Society Series **5**, 132–199.

Deegan, C.E. & Scull, B.J. 1977: A standard lithostratigraphical nomenclature for the central and northern North Sea. The Institute of Geological Sciences Report **77/25**, 36 pp.

Fritsen, A. (ed.) 1999: A joint chalk stratigraphic framework. In: Joint chalk research program topic V **1**. Norwegian Petroleum Directorate. 206 pp.

Gradstein, F.M., Ogg, J.G., Schmitz, M.D. & Ogg, G.M. 2012: The geologic time scale 2012, 1176 pp. Amsterdam: Elsevier.

Hart, M.B., Feist, S.E., Price, G.D. & Leng, M.J. 2004: Reappraisal of the K–T boundary succession at Stevns Klint, Denmark. Journal of the Geological Society (London) **161**, 885–892.

Håkansson, E., & Pedersen, S.A.S. 1992: Geologisk kort over den danske undergrund. Map sheet. København: Varv.

King, C., Bailey, H.W., Burton, C.A. & King, A.D. 1989: Cretaceous of the North Sea. In: Jenkins, D.G. & Murray, J.W. (eds): Stratigraphic atlas of fossil foraminifera, 372–417. Chichester: Ellis Horwood.

Lieberkind, K., Bang, I., Mikkelsen, N. & Nygaard, E. 1982: Late Cretaceous and Danian limestone. Danmarks Geologiske Undersøgelse Serie B **8**, 49–62.

Rambøll Arup JV 2011: Summary of geological conditions. Geotechnical Data Report **01.3-002**, 53 pp. Virum: Femern A/S.

Sheldon, E. 2008: Upper Campanian–Maastrichtian calcareous nannofossil biostratigraphy of the Stevns-1 borehole, Denmark. Journal of Nannoplankton Research **30**, 39–49.

Sheldon, E., Gravesen, P. & Nøhr-Hansen, H. 2012: Geology of the Femern Bælt area between Denmark and Germany. Geological Survey of Denmark and Greenland Bulletin **26**, 13–16.

Smith A.G., Smith, D.G. & Funnel, B.M. 1994: Atlas of Mesozoic and Cenozoic coastlines, 99 pp. Cambridge: Cambridge University Press.

Surlyk, F. 1997: A cool-water carbonate ramp with bryozoan mounds: Late Cretaceous – Danian of the Danish Basin. SEPM Special Publication **56**, 293–307.

Surlyk, F., Rasmussen, S.L., Boussaha, M., Schiøler, P., Schovsbo, N.H., Sheldon, E., Stemmerik, L. & Thibault, N. 2013: Upper Campanian – Maastrichtian holostratigraphy of the eastern Danish Basin. Cretaceous Research **46**, 232–256.

Thibault, N. 2010: Biometric analysis of the Arkhangelskiella group in the upper Campanian–Maastrichtian of the Stevns-1 borehole, Denmark: taxonomic implications and evolutionary trends. Geobios **43**, 639–652.

Thibault, N., Harlou, R., Schovsbo, N., Schiøler, P., Minoletti, F., Galbrun, B., Lauridsen, B.W., Sheldon, E., Stemmerik, L. & Surlyk, F. 2012: Upper Campanian – Maastrichtian nannofossil biostratigraphy and high resolution carbon isotope stratigraphy of the Danish Basin: towards a standard $\delta^{13}C$ curve for the Boreal Realm. Cretaceous Research **33**, 72–90.

Varol, O. 1998: Palaeogene. In: Bown, P.R. (ed.): Calcareous nannofossil biostratigraphy. British Micropalaeontological Society Publication Series, 200–224.

Authors' address

Geological Survey of Denmark and Greenland, Øster Voldgade 10, DK-1350 Copenhagen K, Denmark. E-mail: *es@geus.dk*

Palynological and microfossil biostratigraphy and palaeoecology over the Paleocene–Eocene transition, Femern Bælt, northern Germany

Patrick Alexander Richardt and Emma Sheldon

A palynological and micropalaeontological biostratigraphic and palaeoecological investigation has been carried out on the Paleocene–Eocene transition of core 10.A.057 from the Femern Bælt (Fig. 1). Initial investigations of boreholes from the Femern Bælt indicated that core 10.A.057 included a thick succession of Upper Paleocene – Lower Eocene clay (Sheldon & Nøhr Hansen 2010; Rambøll Arup JV 2011; Fig 2). Complete Paleocene–Eocene sections have been described from Jylland and the Storebælt (Heilmann-Clausen 1985, Laursen & Andersen 1997; Laursen & King 2000, Nielsen *et al.* 1986), but no detailed studies have been published on these successions from the Femern Bælt. Boreholes were drilled on Lolland in Denmark, under the Femern Bælt and on Fehmarn island, Germany from 2009 to 2011 as part of geological and geophysical investigations performed in preparation for the construction of a fixed road and rail link connecting Denmark and Germany. The boreholes penetrated Campanian – Upper Eocene strata, overlain by Quaternary deposits. Borehole 10.A.057 is located in the southern part of the Femern Bælt (Figs 1, 2).

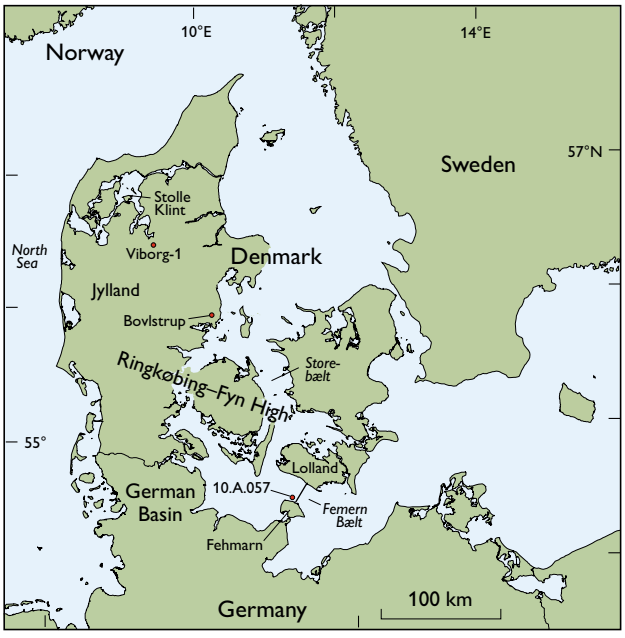

Fig. 1. Map of Denmark and northern Germany showing the location of the planned fixed road and rail link across the Femern Bælt and the location of borehole 10.A.057 at 54°31.8′N, 11°15.9′E.

Geology and palaeoecology

The Femern Bælt is located in the German Basin south of the Ringkøbing–Fyn High. During the Late Cretaceous, the Danish area was characterised by an epicontinental sea resulting in chalk deposition. The sea became more restricted in the early–middle Paleocene and several highs bordered the marine area (Clausen & Huuse 2002). Transgression during the Selandian resulted in clastic marine sedimentation and the North Sea, Denmark and the German Basin formed a partially enclosed shelf area. During the late Paleocene and Early Eocene, sediment deposition occurred in a relatively deep marine basin, at some distance from the shore. Intense volcanic activity caused by the opening of the North Atlantic resulted in deposition of ash and tuff layers during this period. The present distribution of the upper part of the Palaeogene sediments is a result of erosion and glaciotectonic deformation during the Quaternary (Fig. 2).

In the 10.A.057 core, the very fine-grained clays of the Upper Paleocene Holmehus Formation and Østerrende Clay (informal lithostratigraphic unit of Nielsen *et al.* 1986) are overlain by the Lower Eocene Ølst Formation, which is characterised by dark grey clay with abundant layers of black volcanic ash (Heilmann-Clausen *et al.* 1985).

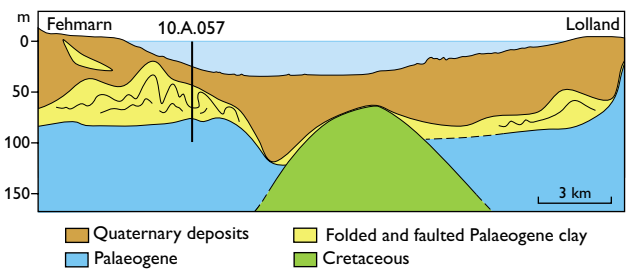

Fig. 2. Sketch south–north cross-section of the Femern Bælt area showing the location of borehole 10.A.057.

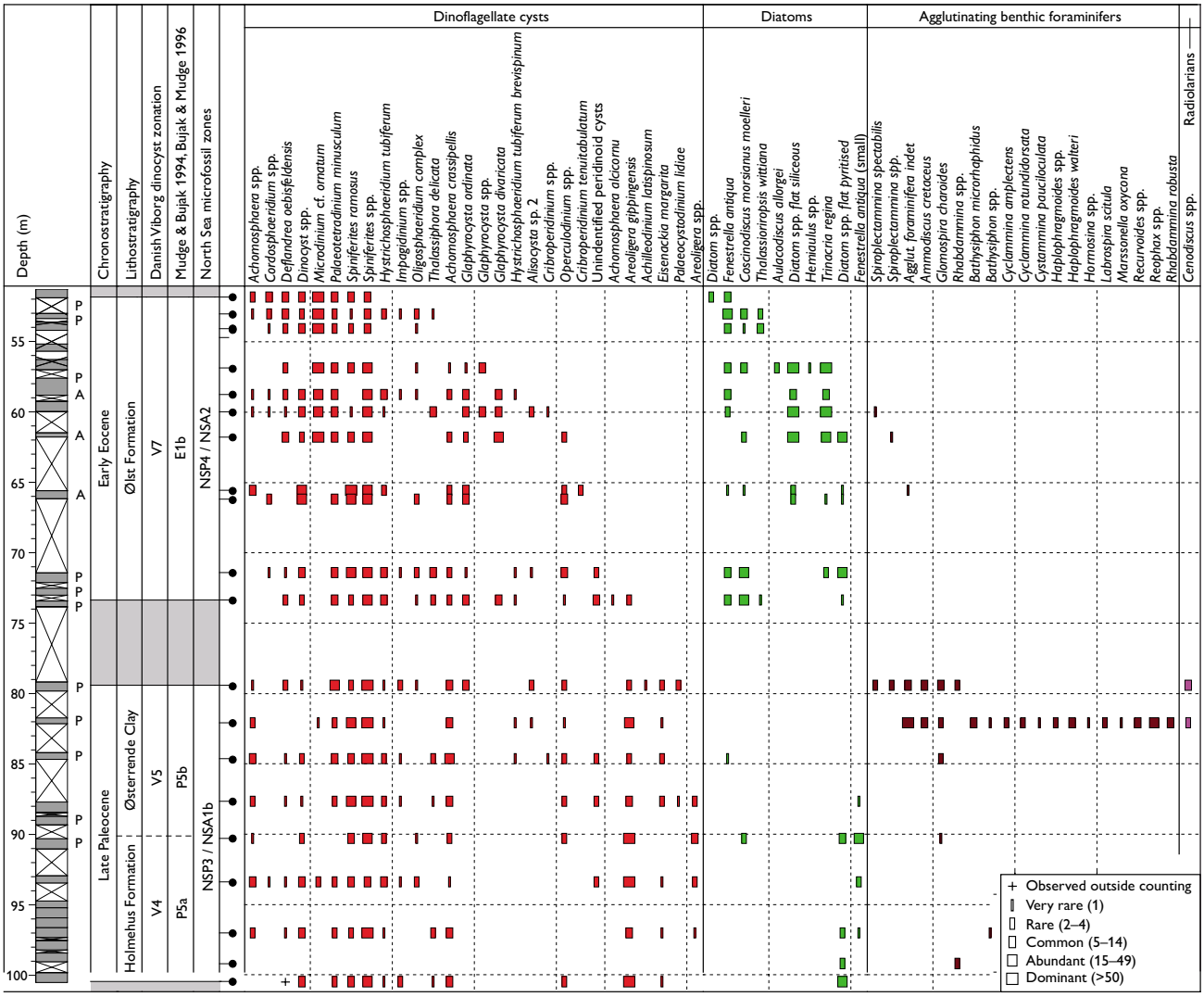

Fig. 3. Range chart showing the distribution (number of specimens) of dinocysts, diatoms, foraminifers and radiolarians from borehole 10.A.057. **P**: pyrite, **A**: ash layer.

Biostratigraphy

A total of 19 samples were analysed for dinocysts, diatoms, foraminifers and radiolarians (Figs 3, 4). The Danish Paleocene–Eocene zonation of the Viborg-1 cored borehole (Heilmann-Clausen 1985) and the North Sea zonation of Mudge & Bujak (1996) were used for the dinoflagellate cyst stratigraphy. The North Sea Cenozoic zonation of King (1989) was used for microfossils.

Dinocysts

The samples from 100.49 to 90.31 m are assigned to the *Areoligera gippingensis* Acme Subzone P5a (Mudge & Bujak 1996; Fig. 3). This subzone represents the uppermost part of zone V4 (Heilmann-Clausen 1985) and is equivalent to the uppermost part of the Holmehus Formation (Mudge & Bujak 1996). P5a is characterised by an acme of *A. gippingensis* and the presence of *Eisenackia margarita*. The top of P5a is defined by the top of the *A. gippingensis* acme. Nielsen *et al.* (1986) found low abundances of *Deflandrea oebisfeldensis* in V4 in a borehole from the Storebælt but Heilmann-Clausen (1985) did not find this species in V4. The boundary between V4 and the overlying V5 is tentatively placed, since relatively high abundances of *A. gippingensis* continue into V5.

The samples from 90.31 to 79.42 m are assigned to the *E. margarita* Subzone P5b (V5) based on the last occurrence (LO) of *E. margarita* (Mudge & Bujak 1996). *E. margarita* has its LO in the Østerrende Clay (Nielsen *et al.* 1986).

Zone V6, which is characterised by a dominance of the warm-water genus *Apectodinium* and an acme of *Apecto-*

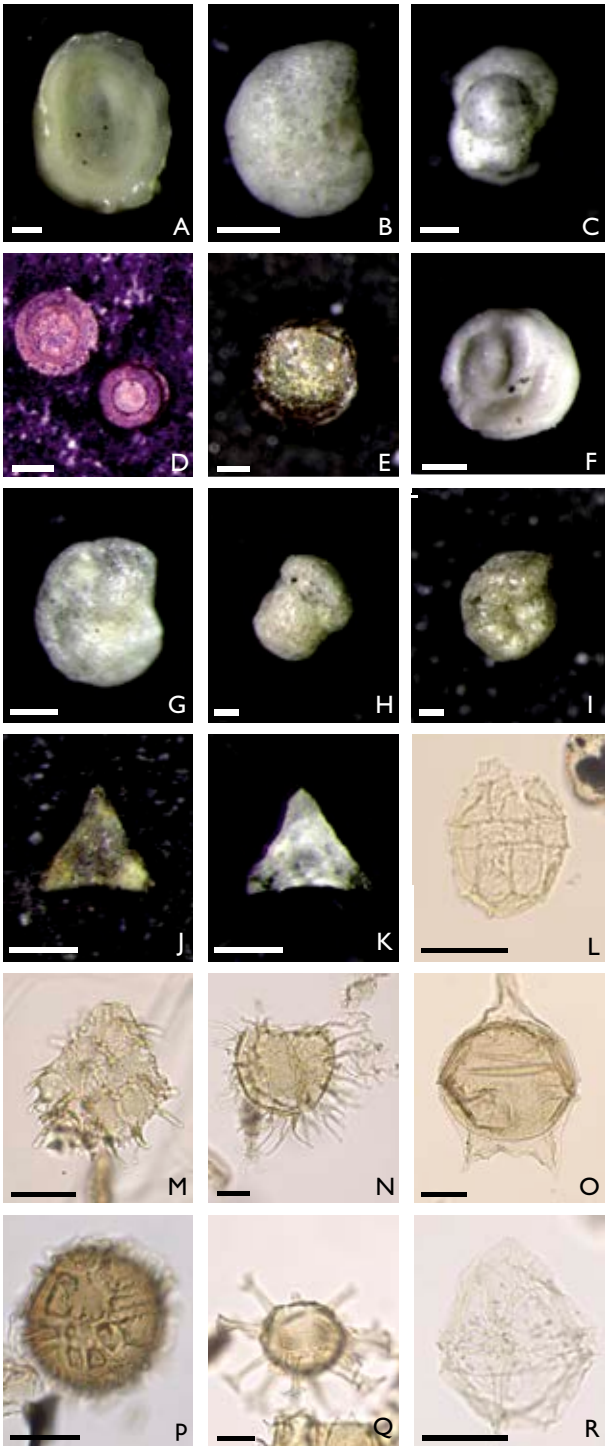

Fig. 4. Selected fossils: **A**–**C** and **F**–**I**: foraminifers, **D**, **E**, **J**, **K**: diatoms, **L**–**R**: dinocysts. **A**: *Ammodiscus cretaceous*. **B**: *Cyclammina amplectens*. **C**: *Cystammina pauciloculata*. **D**: *Coscinodiscus morsianus moelleri*. **E**: *Fenestrella antiqua*. **F**: *Glomospira charoides*. **G**: *Haplophragmoides walteri*. **H**: *Labrospira scitula* (front). **I**: *Labrospira scitula* (side). **J**: *Trinacria regina*. **K**: *Trinacria regina* (siliceous). **L**: *Microdinium* cf. *ornatum*. **M**: Piece of dinocyst. **N**: *Areoligera gippingensis*. **O**: *Deflandrea oebisfeldensis*. **P**: *Eisenackia margarita*. **Q**: *Hystrichospharidium tubiferum*. **R**: Unidentifiable peridinoid cyst. Scale bars: 100 μm (**A**–**K**), 20 μm (**L**–**R**).

dinium augustum, was not found in this study. A missing core section from 79.42 to 73.36 m could represent Zone V6, but V6 has not been observed previously in the Femern Bælt area (C. Heilmann-Clausen & H. Nøhr-Hansen, personal communication 2013). However, V6 is present in the Stolle Klint Clay, north-western Jylland. The base of the *Apectodinium* acme in the earliest Eocene is a global event and is coupled with a carbon isotope excursion denoting the start of the Paleocene–Eocene Thermal Maximum (PETM).

The samples from 73.36 to 51.81 m are referred to Early Eocene *D. oebisfeldensis* Acme Subzone E1b (upper V7; Bujak & Mudge 1994). The interval from 66.18 to 51.81 m is characterised by a minor acme of *Glaphyrocysta divaricata* and a high abundance of *Microdinium* cf. *ornatum* (Fig. 3). Zone V7 is found in the upper part of the Ølst Formation (Heilmann-Clausen 1985).

Foraminifers and diatoms

The assemblages mainly consist of poorly preserved agglutinating benthic foraminifers and diatoms. Samples from 100.49 to 79.42 m are assigned to zone NSA1b. Most samples only contain few foraminifers, but two samples from the upper *c.* 2 m contain rich faunas with *Spiroplectammina spectabilis*, *Labrospira scitula*, *Ammodiscus cretaceus*, *Glomospira charoides*, *Marsonella oxycona*, *Cystammina pauciloculata*, *Recurvoides* spp., *Hormosina* spp., *Rhabdammina robusta*, *Cyclammina rotundidorsata*, *Haplophragmoides walteri*, *Bathysiphon* spp. and *Cyclammina amplectens*. This assemblage is known as the '*Rhabdammina* biofacies'. The shift from low to higher diversity benthic assemblages in NSA1b was also noted in the Bovlstrup borehole, eastern Jylland (Laursen & Andersen 1997) and was interpreted as a shift from very poor to slightly improved life conditions on the sea floor. A low-diversity diatom flora with pyritised *Fenestrella antiqua* (var. small) and *Diatom* spp. (flat) is also present, in addition to sponge debris and radiolarians (*Cenodiscus* spp.). NSA1 is assigned to the Holmehus Formation in Denmark (King 1989).

Samples from 73.36 to 51.81 m are assigned to zone NSP4. The assemblages are dominated by resting spores of centric diatoms, comprising *Coscinodiscus morsianus moelleri*, *Fenestrella antiqua*, *Diatom* spp. (flat), *Thalassiophora wittiana*, *Trinacria regina*, *Aulacodiscus allorgei* and *Hemiaulus* spp. From 66.18 to 56.87 m pyritised and translucent diatoms occur in equal numbers; above and below this level only pyritised specimens occur. This difference in preservation is probably due to variations in the oxygen level in the water column and the amount of sulphide present in the sediment (De Jonghe *et al.* 2011). Zone NSP4 also includes bryozoan

fragments, fish teeth, *Inoceramus* fragments, sponge spicules and rare agglutinating foraminifers. NSP4 is assigned to the Early Eocene Ølst Formation (King 1989).

Discussion and conclusions

A dominance of agglutinating foraminifers of the '*Rhabdammina* biofacies' in subzone NSA1b suggests a middle to lower bathyal palaeoenvironment characterised by restricted water circulation, with low oxygen levels and a reducing environment at the sea floor (Jones & Charnock 1985; King 1989). The low oxygen level may have led to decreasing degradation of organic matter by bacteria and benthic organisms, giving rise to the dark grey colour of the Holmehus Formation compared with those described by Heilmann-Clausen *et al*. (1985).

A relatively high abundance of the supposed heterotrophic dinoflagellate *Deflandrea oebisfeldensis* and the rich diatom flora in the Ølst Formation may be due to increased productivity in the surface layers perhaps due to enhanced upwelling in coastal areas. The rich diatom flora, preserved as resting spores, also suggests stressed sea-surface and seabed conditions, perhaps due to volcanic ash falls and periods of anoxia (Bidgood *et al.* 1999). The scarcity of agglutinating foraminifers is probably due to reducing conditions at the sea floor. Schiøler *et al.* (2007) suggested that the Balder Formation (the North Sea equivalent of the Ølst Formation) was deposited in a restricted marine environment at upper bathyal depths with dysoxic to anoxic bottom conditions.

In core 10.A.057, palynological biostratigraphy indicates that Zone V6 is absent, either due to erosion or non-deposition, therefore the Paleocene–Eocene Thermal Maximum is not preserved at this location. A hiatus with V6 missing was noted in the Lillebælt area (Heilmann-Clausen *et al.* 1985), supporting the Femern Bælt data. However it is possible that Zone V6 is found in the missing core interval between 79.42 and 73.36 m.

References

Bidgood, M.D., Mitlehner, A.G., Jones, G.D. & Jutson, D.J. 1999: Towards a stable and agreed nomenclature for North Sea Tertiary diatom floras – the *'Coscinodiscus'* problem. In: Jones, R.W. & Simmons, M.D. (eds): Biostratigraphy in production and development geology. Geological Society (London) Special Publications **152**, 139–153.

Bujak, J. & Mudge, D. 1994: A high-resolution North Sea Eocene dinocyst zonation. Journal of the Geological Society **151**, 449-462.

Clausen, O.R. & Huuse, M. 2002: Mid-Paleocene palaeogeograhpy of the Danish area. Bulletin of the Geological Society of Denmark **49**, 171–186.

De Jonghe, A., Hart, M.B., Grimes, S.T., Mitlehner, A.G., Price, G.D. & Smart C.W. 2011: Middle Eocene diatoms from Whitecliff Bay, Isle of Wight, England: stratigraphy and preservation. Proceedings of the Geologists' Association **122**, 472–483.

Heilmann-Clausen, C. 1985: Dinoflagellate stratigraphy of the uppermost Danian to Ypresian in the Viborg 1 borehole, central Jylland, Denmark. Danmarks Geologiske Undersøgelse Serie A **7**, 69 pp.

Heilmann-Clausen, C., Nielsen, O.B. & Gersner, F. 1985: Lithostratigraphy and depositional environments in the Upper Paleocene and Eocene of Denmark. Bulletin of the Geological Society of Denmark **33**, 287–323.

Jones R.W. & Charnock, M.A. 1985: 'Morphogroups' of agglutinating foraminifera: their life positions, feeding habits and potential applicability in (paleo)ecological studies. Revue de Paléobiologie **4**, 311–320.

King, C. 1989. Cenozoic of the North Sea. In: Jenkins, D.G. & Murray, J.W. (eds): Stratigraphical atlas of fossil foraminifera, 418–489. Chichester: Ellis Horwood.

Laursen, G.V. & Andersen, S.B. 1997: A Late Palaeocene–Early Eocene benthic foraminiferal record from Bovlstrup, Denmark, showing a remarkable agglutinated fauna. Journal of Micropalaeontology **16**, 19–29.

Laursen, G.V. & King, C. 2000: Preliminary results of a foraminiferal analysis of a core from Østerrende, Denmark. Geologiska Föreningen i Stockholm Förhandlingar (GFF) **122**, 92 only.

Mudge, D.C. & Bujak, J.P. 1996: Palaeocene biostratigraphy and sequence stratigraphy of the UK central North Sea. Marine and Petroleum Geology **13**, 295–312.

Nielsen, O.B., Baumann, J., Zhang, D., Heilmann-Clausen, C. & Larsen, G. 1986: Tertiary deposits in Store Bælt. The Tertiary section of borehole D.G.I. 83101, Østerenden, Storebælt, Denmark. In: Møller, J.T. (ed.): Twentyfive years of geology in Aarhus. Geoskrifter **24**, 237-249. Department of Geoscience, Aarhus University, Denmark.

Rambøll Arup JV 2011: Summary of geological conditions. Geotechnical Data Report **01.3-002**, 53 pp. Virum: Femern A/S.

Schiøler, P. *et al*. 2007: Lithostratigraphy of the Palaeogene – Lower Neogene succession of the Danish North Sea. Geological Survey of Denmark and Greenland Bulletin **12**, 77 pp.

Sheldon, E. & Nøhr-Hansen, H. 2010: Fehmarn Belt fixed link pre-Quaternary biostratigraphy – a final status report for Ramboll Arup Joint Venture. Danmarks og Grønlands Geologiske Undersøgelse Rapport **2010/134**, 53 pp.

Authors' address

Geological Survey of Denmark and Greenland, Øster Voldgade 10, DK-1350 Copenhagen K, Denmark. E-mail: *par@geus.dk*

Ribbed moraines formed during the retreat of the Scandinavian ice sheet from eastern Himmerland, NE Jylland, Denmark

Hans Lerche, Peter Roll Jakobsen and Stig A. Schack Pedersen

The glacial geology of Himmerland in the north-eastern part of Jylland, south of Limfjorden (Fig. 1) has never received any special attention. However, the occurrence of parallel ridges south of Torup was mentioned by Milthers (1948) who interpreted them as marginal moraines. The ridges were recently studied during mapping of eastern Himmerland. Systematic geological mapping of the area north and south of Mariager Fjord started in 2009 and was completed in 2013 (map sheet 1316 III; Pedersen *et al.* 2013). This was followed by the map sheet to the north (1316 IV). During the recent mapping the extent of the terrain with parallel ridges was determined (Fig. 2); the western boundary is found in Rold Skov (Pedersen & Jakobsen 2005) and the eastern boundary follows an ancient coastline in eastern Himmerland. The most impressive parallel ridges occur in a forested area east of Madum Sø where the top level of the ridge crests reaches an elevation of 95 m a.s.l. However, the majority of the crests are at 60–70 m a.s.l. and most of the ridges are *c.* 10–15 m high. The sediments in the ridges are dominated by coarse-grained sand and gravel, and accumulations of erratic boulders are found on the surface of the ridges.

After completion of the mapping of the area, we decided to make a detailed investigation of the ridges using ground-penetrating radar (GPR) to map the internal structures of the ridges. We also studied sections in a small gravel pit at the northern boundary of Siem Skov (Figs 3, 4).

The aim of this paper is to describe the terrain with parallel ridges, which we interpret as ribbed moraines. We discuss the geological setting of the ridges in relation to the data acquired during the systematic geological mapping and the accompanying GPR survey. A glaciodynamic model for the formation of the ridges is proposed related to the recession of the ice that had its source area in south central Sweden.

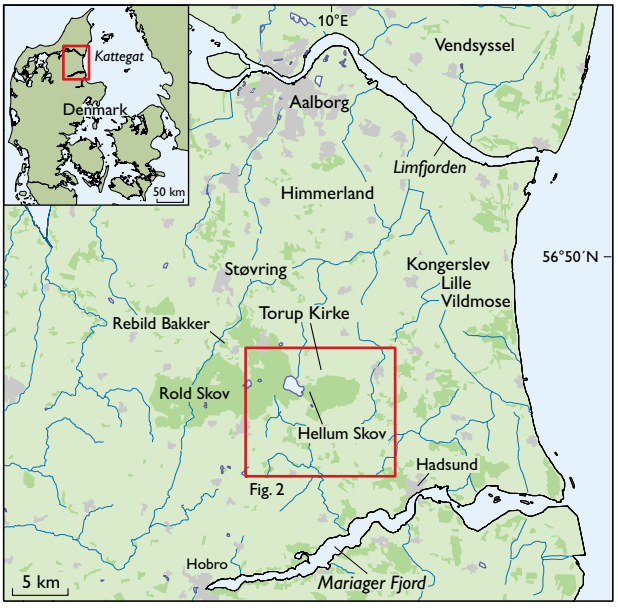

Fig. 1. Map of the north-eastern part of Himmerland where systematic geological mapping has been conducted over the past five years. The area with moraine ridges is indicated by a rectangle. The locations of place names mentioned in the text are shown.

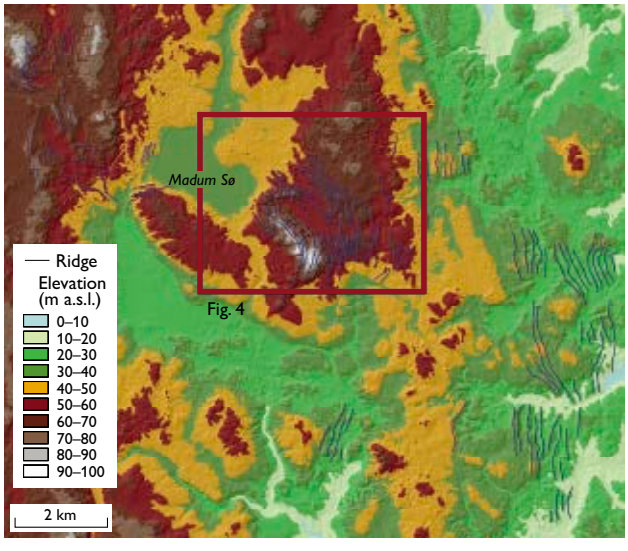

Fig. 2. LiDAR-based digital elevation model of the study area showing moraine ridges. Most of the ridges are found in three separate areas. The most densely spaced and largest ridges occur in the central area.

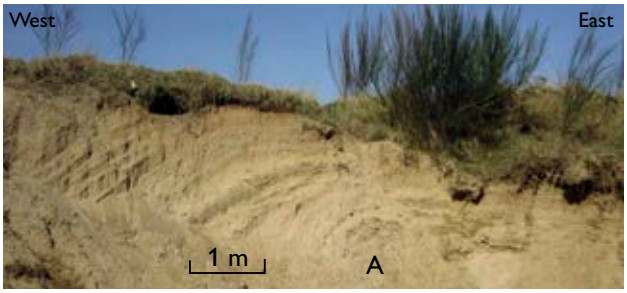

Fig. 3. Exposure in a small gravel pit located *c.* 1.2 km SSW of Torup Kirke showing a section through one of the ridges. West of the anticline (**A**) dipping layers of glaciaofluvial sand and gravel are seen, and east of the anticline layers of flow till occur. The architecture can be compared to the structures seen in the GPR profiles (Fig. 5). Photograph: Elina Kamla.

Geological setting

The bedrock in Himmerland is dominated by Maastrichtian chalk which is exposed in pits throughout the region. An erosional unconformity separates chalk from Quaternary deposits. Major parts of the region between Mariager Fjord and Limfjorden are covered by glaciofluvial sand that reaches a thickness of *c.* 40 m at Hadsund. In the small gravel pit at the northern boundary of Siem Skov, the succession begins with a glaciolacustrine unit, which increases in thickness towards the east. This unit is interpreted as a palaeo-Kattegat deposit and may correlate with the Lønstrup Klint Formation in Vendsyssel (Pedersen 2005). It is overlain by glaciofluvial sand and gravel that may correlate with the Rubjerg Knude Formation (Pedersen 2005). These proglacial deposits of the glaciodynamic sequence (according to the concept of Pedersen 2012) are overlain by *c.* 3 m of till. The till is classified as a sandy till; it contains indicator boulders from the Oslo Fjord region and its fabric indicates an ice-flow direction from north to south. Based on this ice movement direction the till is correlated with the Kattegat Till Formation (Houmark-Nielsen & Kjær 2003; Pedersen 2005). The top of the till is at 56 m a.s.l. in Siem Skov where it forms the base of the 10–25 m high ridges.

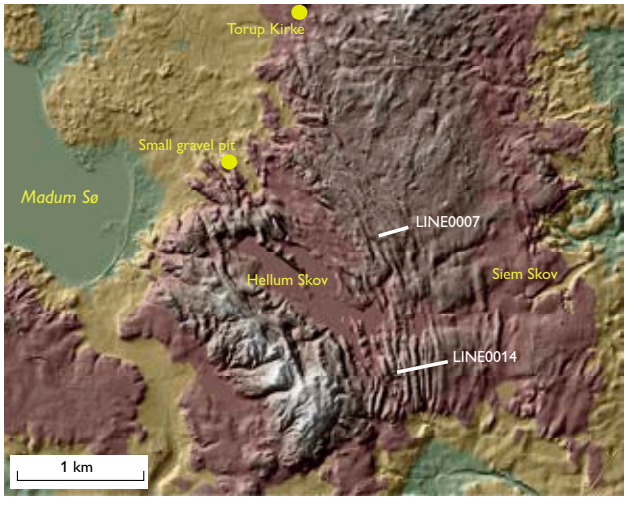

Fig. 4. Hill shade image of the central part of the ridge terrain. The ridges are almost parallel, mainly N–S-oriented but NW–SE-oriented in the north. The locations of the two GPR profiles (Fig. 5) are also shown. LINE0007 was acquired in a spruce plantation across relatively smooth ridges, whereas LIN0014 was acquired along a gravel road crossing 11 steep-sided ridges.

Meltwater related to the Swedish Ice Advance only played a small role in the region with the parallel ridges. To the west, glaciofluvial deposits from the Swedish Ice Advance are found in the upper part of the Rebild Bakker (Pedersen & Jakobsen 2005). After the parallel ridges had formed, depressions were created in the landscape due to melting of bodies of stagnant ice that were left from the retreating ice front. During the early Holocene valleys were eroded when the relative sea level was low.

Geomorphology of the parallel ridges

The elongate ridges cover an area of 15 × 8 km. Most of them are N–S-oriented, but there are NW–SE-oriented ridges in the north-western part of the area. The ridge density is highest in the central part of the area, in Hellum Skov and Siem Skov (Fig. 4) where the ridges reach elevations of 70 m a.s.l. and are *c.* 10 m high. The mean spacing between the ridges is 48 m in Hellum Skov and Siem Skov and the longest ridges are *c.* 2500 m long. Towards the east and south, ridges may still be recognised but are somewhat obscured. In these areas, ridge crests are at *c.* 30 m a.s.l. and the ridges are 5–10 m high.

Georadar survey of the parallel ridges

In September 2013, ground penetrating radar (GPR) surveys were carried out in Hellum Skov where the most pronounced ridge terrain is found. An EKKO 100TM device mounted on a cart was used, and six lines perpendicular to the ridges were recorded; five lines in the northern part of the forest and one line *c.* 1 km to the south. Transmitter voltage was 400 V and antenna frequency was centered at 100 MHz. The antennas were oriented broadside to the survey direction and separated by 1 m. Traces were recorded every 20 cm and consist of stacks of eight.

Two representative profiles, LINE0007 and LINE0014, illustrate the internal architecture of the ridges (Fig. 5). Assuming a mean velocity of 0.1 m/ns, 1 m equals 20 ns. In LINE0014 the layers below the ridges are predominantly

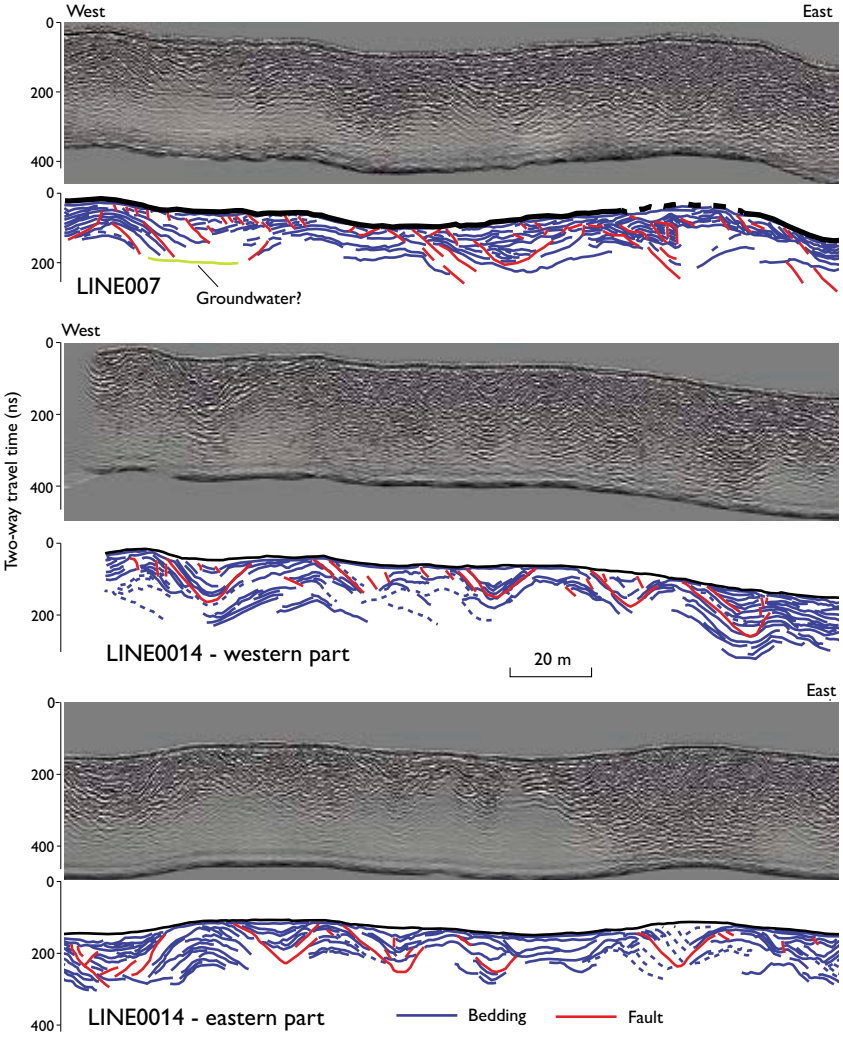

Fig. 5. Two examples of processed ground-penetrating radar records and their interpretations (LINE0014 is divided into two parts). The GPR data were processed using Reflex2DQuick analysis. The following steps were followed prior to the interpretation of the data: (1) X-axis flip, (2) move start time to –45.2 ns, (3) normal move-out, 1 m separation, (4) dewow noise filtered, time window 10 ns, (5) bandpass frequency, 20/187 MHz, (6) topographic migration, summation width 50 traces, (7) divergence compensation gain, scaling value 1 and (8) topographic correction, square interpolation. Our knowledge of radar-wave velocity variations in the survey area is limited, and hence we refrained from converting the recorded two-way travel time to depth. However, hyperbola velocity adaptions provided approximate mean velocities for each survey line.

subparallel anticlines, whereas layers below depressions are dominantly subparallel synclines. In both profiles two types of faults are found: (1) small, dominantly eastward-dipping faults and (2) larger, possibly superimposed folded thrust faults, which can be traced from near the surface down to 7–10 m below the surface (Fig. 5).

Formation of the ridges

The small E-dipping faults recognised in the GPR profiles are interpreted as thrust faults caused by pushing from the east. Small W-dipping faults may indicate landslides on steep ridge flanks. Large thrust faults are interpreted as listric faults with décollement surfaces *c.* 7–10 m below the ground. The folded lower layers of LINE0014 suggest ductile deformation within the ridges and the depressions.

GPR data indicate that the ridges were formed by ice pushing from the east under non-permafrost conditions. We suggest that the ridges reflect a net ice recession with a mean rate of *c.* 50 m/year, but with a number of small advances (Fig. 6). The east–west extent with ridges is almost 10 km wide, corresponding to a period of *c.* 200 years. A similar magnitude of recession rate of the Scandinavian Ice Sheet has been suggested for Vendsyssel, where recession from the coastal area along Kattegat north of Limfjorden is estimated to have occurred in the interval from 19 to 18.5 ka (Sandersen *et al.* 2009). We suggest that shortly after termination of the Last Glacial Maximum temperature increased rapidly, which lead to a significant recession of the ice margin.

The moraines show some similarities to de Geer moraines (De Geer 1940; Lundquist 1986; Lundquist & Viborg 1998; Lindén & Möller 2005). However, de Geer moraines formed in water depths of 150–250 m, during retreat of a grounding line with a calving glacier front. In contrast, the Himmerland moraines formed on dry land.

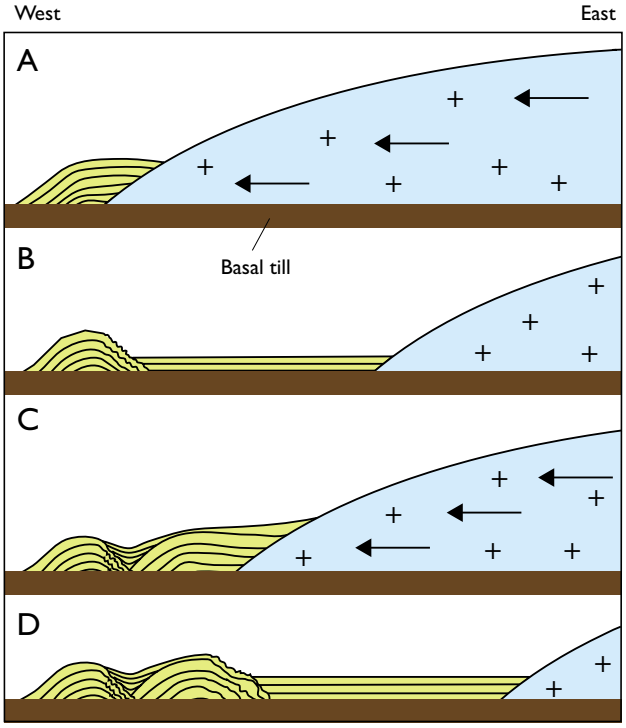

Fig. 6. Conceptual model showing the formation of moraine ridges in north-eastern Himmerland. **A**: In winter the glacier front advances, pushing up and deforming deposits in front of the glacier. **B**: In summer the mass balance of the glacier is negative and the glacier front recedes. The proximal part of the deformed deposits collapses and a ridge is formed. A new outwash fan forms between the glacier margin and the ridge. **C**: The next winter the new outwash fan is pushed up and deformed. Syntectonic deposition in the form of flow till and alluvial sediments also occurs. **D**: The next summer another outwash fan is formed.

Conclusions

As part of the systematic mapping of eastern Himmerland, a detailed investigation was made of a terrain with parallel ridges located in a 120 km^2 large area centred on Siem Skov. The individual ridges are up to *c.* 2.5 km long. The ridges are 10–25 m high, and the spacing between the ridge crests varies from 50 to 100 m. The parallel ridges are interpreted as ribbed moraines that formed during recession of the ice margin at *c.* 19 ka. The detailed architecture of the ridges was investigated by GPR surveys which show an integrated depositional and deformational dynamic picture with narrow and steep-sided depressions filled with flow-till materials contemporaneous with fold-push and up-thrusting.

References

De Geer, G. 1940: Geochronologia Suecica, Principles. Kungliga Svenska Vetenskapsakademiens Handlingar Ser. III **18**(6), 367 pp.

Houmark-Nielsen, M. & Kjær, K.H. 2003: Southwest Scandinavia, 40–15 kyr BP: palaeogeography and environmental change. Journal of Quaternary Science **18**, 769–786.

Lindén, M. & Möller, P. 2005: Marginal formation of De Geer moraines and their implications to the dynamics of grounding-line recession. Journal of Quaternary Science **20**, 113–133.

Lundqvist, J. 1986: Late Weichselian glaciation and deglaciation in Scandinavia. Quaternary Science Reviews **5**, 269–292.

Lundqvist, J. & Viborg, L. 1998: Isavsmältning och israndlinjer i Sverige and Lokaler i Sverige. In: Andersen, S. & Pedersen, S.A.S. (eds): Israndslinier i Norden, 61–81 and 161–215. Copenhagen: Nordisk Ministerråd.

Milthers, V. 1948: Det danske Istidslandskabs Terrænformer og Deres Opstaaen. Danmarks Geologiske Undersøgelse III. Række **28**, 234 pp. (with summary in English).

Pedersen, S.A.S. 2005: Structural analysis of the Rubjerg Knude glaciotectonic complex, Vendsyssel, northern Denmark. Geological Survey of Denmark and Greenland Bulletin **8**, 192 pp.

Pedersen, S.A.S. 2012: Glaciodynamic sequence stratigraphy. In: Huuse, M. *et al.* (eds) 2012: Glaciogenic Reservoirs and Hydrocarbon Systems. Geological Society (London) Special Publication **368**, 29–51.

Pedersen, S.A.S. & Jakobsen, P.R. 2005: Geologisk kortlægning af statsskovarealerne i Rold Skov. Systematisk geologisk kartering af statsskovarealerne i Rold Skov, som udgør dele af 1:25 000 kortbladene 1216 I SØ og 1216 II NØ, nordlige Jylland. Danmarks og Grønlands Geologiske Undersøgelse Rapport **2005/81**, 28 pp.

Pedersen, S.A.S., Jakobsen, P.J., Tougaard, L. & Gravesen, P. 2013: Geological map of Denmark 1:50 000, map sheet Mors, NW Denmark. Geological Survey of Denmark and Greenland Bulletin **28**, 29–32.

Sandersen, P.B.E., Jørgensen, F., Larsen, N.K., Westergaard, J.H., & Auken, E. 2009: Rapid tunnel-valley formation beneath the receding Late Weichselian ice sheet in Vendsyssel, Denmark. Boreas **38**, 834–851.

Authors' addresses

H.L., *Department of Geosciences and Natural Resource Management, University of Copenhagen, Øster Voldgade 10, DK-1350 Copenhagen K, Denmark.*
E-mail: *hans_lerche@hotmail.com*

P.R.J. & S.A.S.P., *Geological Survey of Denmark and Greenland, Øster Voldgade 10, DK-1350 Copenhagen K, Denmark.*

Arctic plant remains of Weichselian age from the Danish North Sea

Ole Bennike, Jørgen O. Leth, Jørn Bo Jensen, Niels Nørgaard-Pedersen and Steen Lomholt

The North Sea is a large, shallow epicontinental sea dominated by a sandy bottom that reflects a high-energy environment. Little is known about the environmental history of the Danish part of this large area during the Weichselian, the last ice age. Parts of it were glaciated during the last glacial maximum and probably also during older glaciations. Shallow parts were dry land, and deeper parts were covered by the sea during ice-free intervals. Large, partly ice-dammed lakes also existed.

Three remains of walrus (*Odobenus rosmarus*) have been radiocarbon dated (Möhl 1985; Kim Aaris-Sørensen, unpublished). One of the finds was dated to *c.* 35 cal. ka BP, whereas the two others finds gave somewhat younger ages of *c.* 30 cal. ka BP (Table 1).

Knudsen (1985) described the stratigraphy of sediment cores from the western part of the Danish North Sea. From the Roar 41 core, she reported on Eemian deposits overlain by Weichselian marine deposits with an Arctic or Boreo-Arctic foraminiferal fauna. An age of 30–50 cal. ka BP was suggested for this deposit by Larsen *et al.* (2009, fig. 8H). Leth (1998) obtained three radiocarbon ages of 43–45 cal. ka BP on marine bivalve shells from two vibrocores from Jyske Rev.

In connection with mapping of sand and gravel deposits in 2012, a number of 6 m long vibrocores were collected by the Geological Survey of Denmark and Greenland (GEUS). During description of the sediment cores, remains of plants were noted; most of them were early Holocene. However, a few samples from two sediment cores contained macrofossils of Arctic plants and two samples were dated. The aim of this paper is to report on these ages and their implications. The locations of the coring sites are shown in Fig. 1.

Material and methods

Sediment coring was carried out with a vibrocorer with a 6 m long, 10 cm wide steel core barrel with a PVC tube mounted. Coring positions were selected from high-resolution, shallow seismic profiles. The cores were collected in PVC tubes and cut into 1 m long sections and shipped to GEUS, where they were split and described. A few 1–2 kg samples with plant remains were wet sieved and the residue left on the sieves was analysed using a dissecting microscope. Two samples of terrestrial plant remains were dried and dated by radiocarbon accelerator mass spectrometry.

A Late Weichselian deposit

Lithological logs of the cores are shown in Fig. 2. NS 12-2-13 consists of 100 cm of Holocene marine silt and very fine-grained sand, underlain by 178 cm indistinctly laminated clay and silt, 180 cm of alternating layers of fine-grained sand, medium-grained sand and silt, 15 cm silt and 71 cm of alternating layers of fine-grained sand, medium-grained sand and silt. The deposits below the marine unit were interpreted as Late Glacial. Plant remains were noted near the bottom of the core.

Remains of terrestrial plants include leaves of *Salix herbacea*, a leaf of *Salix phylicifolia*, a leaf of *Betula nana*, seeds of *Empetrum nigrum*, a seed of *Lychnis flos-cuculi*, a megaspore of *Selaginella selaginoides* and a stem of *Distichium* sp.

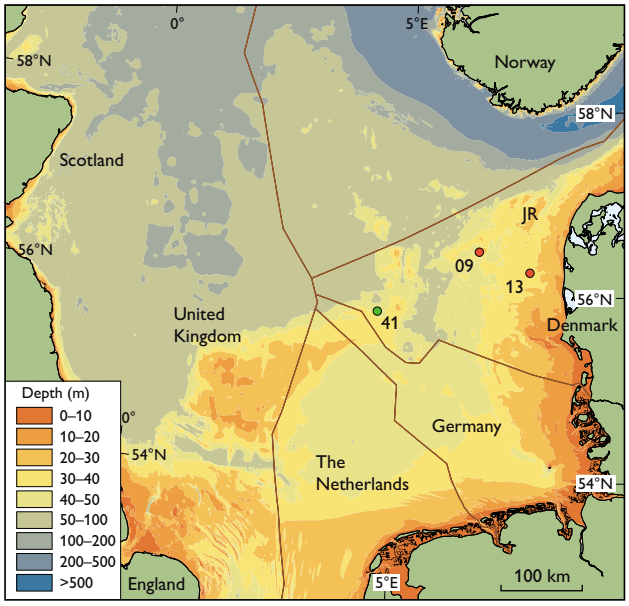

Fig. 1. Bathymetrical map of the North Sea. The dots show the locations of the studied sediment cores (13 = NS 12-2-13, 09 = NS 12-3-09). The green dot shows the location of core Roar 41 discussed by Knudsen (1985). **JR**: Jyske Rev.

Table 1. Pre-Holocene radiocarbon ages from the Danish North Sea

Core no.	N. Lat.	E. long.	Laboratory no.	Species	Depth b.c.t. (cm)*	Age (^{14}C years BP)	Calibrated age (years BP)†
NS 12-2-13	56°15.862′	7°27.819′	LuS-10493	*Salix herbacea*	542	10 730 ± 75	12 554–12 746
NS 12-2-09	56°28.478′	6°27.794′	LuS-10494	*S. herbacea, D. octopetala*	495	30 530 ± 300	33 957–35 010
562026‡	56°39.3′	7°39.9′	AAR-3291	*Spisula subtruncata*	230	39 200 ± 1100	41 136–44 666§
562026	56°39.3′	7°39.9′	AAR-3292	*Macoma balthica*	550	41 500 ± 1450	42 298–47 250§
562028	56°46.3′	7°33.2′	AAR-3293	*Donax vittatus*	310	39 300 ± 1300	40 807–45 085§
	Off Esbjerg		K-3727	*Odobenus rosmarus*		24 380 ± 620	27 033–29 417¶
	c. 56°30′	*c.* 7°	K-3726	*Odobenus rosmarus*		30 880 $^{+1270}_{-1110}$	31 578–36 940¶
	c. 57°12′	*c.* 8°28′	K-5746	*Odobenus rosmarus*		26 700 ± 1500	27 616–33 475[a]

* Below core top.
† Calibrated according to the CALIB 7.0 program.
‡ Core numbers refer to the numbering system used by the marine geologists at GEUS.
§ Leth (1998).
¶ Möhl (1985).
[a] K. Aaris-Sørensen, unpublished data.

(Table 2). Freshwater plants are represented by *Potamogeton filiformis*, and freshwater invertebrates are represented by *Cristatella mucedo* and *Fredericella indica*. Stems of *Scorpidium scorpioides* and *Drepanocladus* s.l. sp. are common; these mosses as well as *Carex* spp. probably grew in wet areas. A sample of *Salix herbacea* leaves gave an age of *c.* 12.6 cal. ka BP, corresponding to a Younger Dryas age (Table 1).

Younger Dryas deposits are common in Denmark, and several submarine deposits from inner Danish waters have also been found (e.g. Bennike *et al.* 2004; Bennike & Jensen

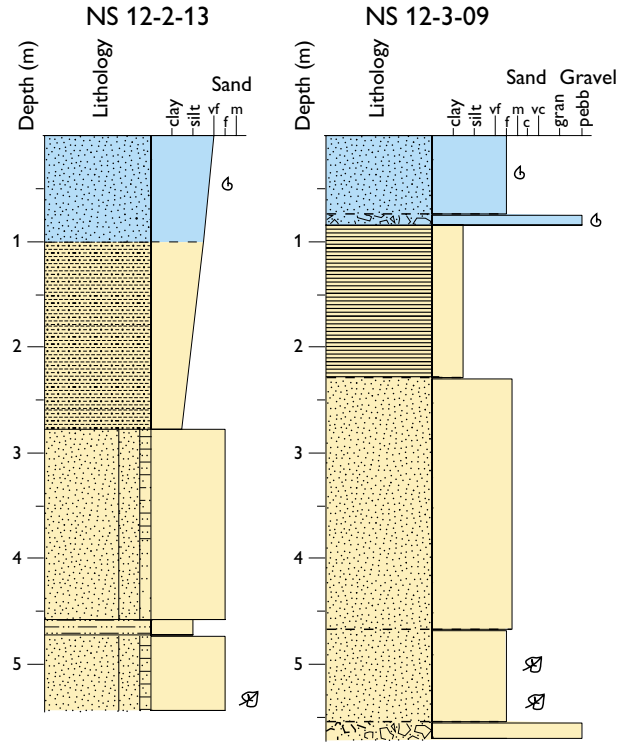

Fig. 2. Lithological logs of core NS 12-2-13 and NS 12-3-09. NS 12-2-13 was sampled at a water depth of 32.0 m and core NS 12-3-09 was sampled at a water depth of 43.5 m. Blue: Marine Holocene. Yellow: non-marine pre-Holocene.

Table 2. Macrofossils of Weichselian age from the North Sea

	NS 12-2-13 *c.* 12.6 ka	NS 12-3-09 *c.* 35 ka
PLANTS		
Cenococcum geophilum sclerotia	3	15
Distichium sp. stems	–	1
Ditrichum sp. stem	–	4
Bryum sp. stems	–	r
Paludella squarrosa stem	–	1
Drepanocladus revolvens stems	–	2
Drepanocladus s.l. sp. stems	c	r
Scorpidium scorpioides stems	c	r
Polytrichum sp. leaves	1	3
Selaginella selaginoides megaspores	1	1
Ranunculus sp. achene	1	–
Betula nana leaf fragment	1	–
Salix herbacea leaves	7	16
Salix phylicifolia leaves	2	–
Dryas octopetala leaves	–	11
Empetrum nigrum endocarps	4	–
Juncus sp. seed	–	1
Carex spp. achenes	6	14
Potamogeton filiformis achenes	–	3
ANIMALS		
Cladocera indet. shells	–	r
Staphylinidae indet. wing	1	–
Chironimidae indet. head capsules	–	r
Trichoptera indet. sclerite	–	1
Oribatida indet. skeletons	–	r
Fredericella indica statoblast	1	–
Cristatella mucedo statoblast	1	–

r: rare, c: common.

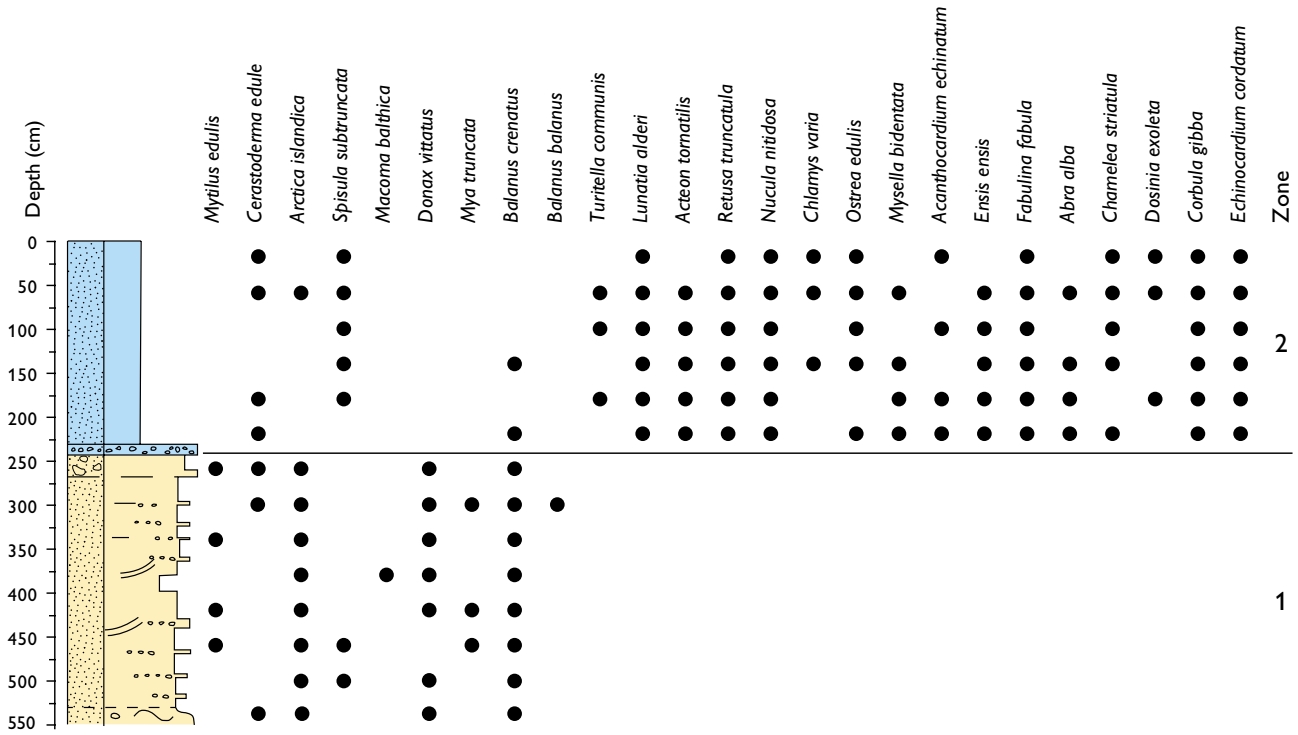

Fig. 3. Simplified macrofossil diagram of core 562028 from Jyske Rev (see Fig. 1 for location). Blue: Holocene marine fine-grained sand. Yellow: Pre-Holocene medium- and coarse-grained sand with pebbles.

2011; Mortensen *et al.* 2014). However, the present article is the first that reports on a Younger Dryas deposit from the Danish part of the North Sea. The deposit shows that the coring site had not yet been transgressed by the sea.

A Middle Weichselian deposit

Core NS 12-3-09 consists of 75 cm of Holocene marine fine-grained sand, underlain by 10 cm of Holocene marine gravel, 145 cm clay and silt, 238 cm fine- and medium-grained sand, 87 cm fine-grained sand with plant remains and 15 cm gravel.

Remains of terrestrial plants include leaves of *Salix herbacea*, leaves of *Dryas octopetala*, a megaspore of *Selaginella selaginoides*, 2 stems with leaves of *Ditrichum* sp., 1 stem with leaves of *Distichium* sp. and sclerotia of *Cenococcum geophilum* (Table 2). Wetland species are represented by *Carex* sp., *Juncus* sp., *Scorpidium scorpioides*, *Drepanocladus revolvens* and *Paludella squarrosa*. Lake or pond species are represented by *Potamogeton filiformis*, and freshwater invertebrates are represented by cladocerans, chironomid larvae and Trichoptera. A sample of *S. herbacea* and *D. octopetala* leaves gave an age of *c.* 35 cal. ka BP, corresponding to a Middle Weichselian age – prior to the last glacial maximum (Table 1).

Most of the species are known from Middle Weichselian deposits in Denmark, and indicate an open, treeless, tundra-like environment with wetlands and lakes. *S. herbacea* grows in areas with a long-lasting snow cover, whereas *D. octopetala* prefers areas with little snow cover. The presence of both of these dwarf shrubs indicates that wind-swept hills and places where snow could accumulate were present in the area.

Non-marine Middle Weichselian deposits with organic remains are rare in Denmark. Deposits of broadly the same age as the deposit from the North Sea have been discussed by Bennike *et al.* (1994, 2007) and Houmark-Nielsen *et al.* (1996); in addition, a number of re-deposited mammal bones and teeth, especially of mammoth (*Mammuthus primigenius*) have been found. The flora and fauna from the other Danish sites are similar to those from the North Sea. The Ålesund interstadial in south-west Norway, dated to 28–35 cal. ka BP, is characterised by an Arctic vertebrate fauna.

Pre-Holocene bivalve shells and bones

As mentioned in the introduction, dating of pre-Holocene marine shells from two cores from Jyske Rev gave ages of 43–45 cal. ka BP (Table 1; Leth 1998). Two of the dated species are boreal and warmth-demanding, which contrasts with indications of Arctic conditions during the same time period, as seen in other records from the region. A number

of samples from the two cores were analysed in connection with this study.

The studied fauna includes a number of boreal species (Fig. 3, zone 1). In addition to *Donax vittatus* and *Spisula subtruncata* reported by Leth (1998), boreal species are also represented by *Arctica islandica* and *Cerastoderma edule*. These four species are known from Holocene and Eemian deposits in the region, but not from Weichselian deposits. The fauna from the cores also comprises *Macoma balthica*, *Macoma calcarea*, *Mytilus edulis*, *Hiatella arctica*, *Mya truncata*, *Balanus crenatus* and *Balanus balanus* that are boreal and Arctic. No species that are confined to the Arctic were found, and the fauna can be characterised as of interglacial type. The fauna in zone 2 is typical for Holocene fine-grained deposits in the region.

There are no reports of interglacial-type deposits from the region from the Middle Weichselian. For example, in France where the nearest continuous Weichselian deposits are found, the Middle Weichelian was characterised by open vegetation with cold-adapted beetles. Hence we suggest that the pre-Holocene fauna from Jyske Rev is of Eemian age. That means that the radiocarbon dates should be considered minimum ages. There are numerous examples in the literature of interglacial shells that have yielded non-finite radiocarbon ages which are usually assigned to post-mortem recrystallisation. The deposits with the pre-Holocene shells consist of medium- and coarse-grained sand and fine-grained gravel. During periods of low relative sea level, these sandy deposits may have been subject to groundwater flow, which could lead to recrystallisation and introduction of younger carbon.

In some areas of the Dutch sector of the North Sea, bones of cold-adapted mammals are common. The fauna includes terrestrial species such as mammoth (*Mammuthus primigenius*), musk-ox (*Ovibos moschatus*) and reindeer (*Rangifer tarandus*), but also marine species such as walrus, white whale (*Delphinapterus leucas*) and bearded seal (*Erignatus barbatus*). Radiocarbon dating of bones from marine mammals yielded Middle Weichselian ages and non-finite ages (Post 2005). We suggest that the finite ages should also be regarded as minimum ages, because we find it doubtful that the sea extended this far south during the Middle Weichselian, when the global sea level was much lower than at present. We consider it likely that Arctic marine mammals lived in the southern North Sea during the Early Weichselian.

Summary

During parts of the Weichselian, parts of the Danish North Sea were land with an open, treeless, tundra-like environment with wetlands and lakes. Two radiocarbon-dated Arctic floras are dated to the Younger Dryas and the Middle Weichselian. A marine fauna from Jyske Rev gave non-finite Middle Weichselian ages and we conclude that it is an interglacial-type fauna probably of Eemian age.

Acknowledgement

The mapping of sand and graval deposits was funded by the Danish Nature Agency.

References

Bennike, O. & Jensen, J.B. 2011: Postglacial, relative shore-level changes in Lillebælt, Denmark. Geological Survey of Denmark and Greenland Bulletin **23**, 37–40.

Bennike, O., Houmark-Nielsen, M., Böcher, J. & Heiberg, E.O. 1994: A multi-disciplinary macrofossil study of Middle Weichselian sediments at Kobbelgård, Møn, Denmark. Palaeogeography, Palaeoclimatology, Palaeoecology **111**, 1–15.

Bennike, O., Jensen, J.B., Lemke, W., Kuijpers, A. & Lomholt, S. 2004: Late- and postglacial history of the Great Belt, Denmark. Boreas **33**, 18–33.

Bennike, O., Houmark-Nielsen, M. & Wiberg-Larsen, P. 2007: A Middle Weichselian interstadial lake deposit on Sejerø, Denmark: macrofossil studies and dating. Journal of Quaternary Science **22**, 647–651.

Houmark-Nielsen, M., Bennike, O. & Björck, S. 1996: Terrestrial biotas and environmental changes during the late Middle Weichselian in north Jylland, Denmark. Bulletin of the Geological Society of Denmark **43**, 169–176.

Knudsen, K.L. 1985: Foraminiferal stratigraphy of Quaternary deposits in the Roar, Skjord and Dan fields, central North Sea. Boreas **14**, 311–324.

Larsen, N.K., Knudsen, K.L., Krohn, C.F., Kronborg, C., Murray, A.S. & Nielsen, O.B. 2009: Late Quaternary ice sheet, lake and sea history of southwest Scandinavia – a synthesis. Boreas **38**, 732–761.

Leth, J.O. 1998: Late Quaternary geology and recent sedimentary processes of the Jutland Bank region, NE North Sea, 173 pp. Unpublished PhD thesis, University of Aarhus, Denmark.

Möhl, U. 1985: The walrus, *Odobenus rosmarus* (L.), as a "Danish" faunal element during the Weichsel Ice Age. Bulletin of the Geological Society of Denmark **34**, 83–85.

Mortensen, M.F., Henriksen, P.S. & Bennike, O. 2014: Living on the good soil: relationships between soils, vegetation and human settlement during the late glacial. Vegetation History and Archaeobotany **23**, 195–205.

Post, K. 2005: A Weichselian marine mammal assemblage from the southern North Sea. Deinsea **11**, 21–27.

Authors' address

Geological Survey of Denmark and Greenland, Øster Voldgade 10, DK-1350 Copenhagen K, Denmark. E-mail: *obe@geus.dk*

Stormwater management: methods for measuring near-surface infiltration capacity in clayey till

Britta Bockhorn, Marina Bergen Jensen and Knud Erik S. Klint

Glacial till forms a major proportion of the surface deposits in Northern Europe, and in Denmark more than 40% of the land surface is covered by clayey till. At the same time the majority of densely populated areas are situated on this fertile sediment type. In urban areas, one of the major tools in adaptation to climate change are sustainable drainage systems (SuDS). Their function is to manage the increasing amounts of stormwater on site, often by direct infiltration into the sediment. Accordingly, a realistic estimate of near-surface hydraulic properties is required when dimensioning SuDS for infiltration.

Clayey tills are generally believed to have a low-bulk hydraulic conductivity and thus a low infiltration capacity. However, clayey tills can be very heterogeneous and especially their bulk hydraulic properties can vary significantly depending on the distribution of permeable structures such as macropores (e.g. earthworm holes and fractures) and sand lenses within the till matrix (Klint & Gravesen 1999; Nilsson *et al.* 2001; Kessler *et al.* 2012). The saturated hydraulic conductivity (K_{sat}) of clayey tills varies from *c.* 1.0×10^{-10} to *c.* 1.0×10^{-4} m/s and thus covers a significant span (Fredericia 1990; McKay *et al.* 1993). Assessment of this value is a major challenge when considering the variability of this sediment type. It is therefore important to determine how representative standard infiltration tests are, specifically in tills, when used to formulate infiltration strategies.

Goals and scope

In this study we compare three different methods for measuring K_{sat} close to the surface: the double ring infiltrometer, the Guelph permeameter and infiltration tests in a small excavation. Each of these methods represents different scales and depths using different flow mechanisms. The goal of the study is to:

1. evaluate the suitability of these methods to return realistic K_{sat} values in tills, taking into account the geological heterogeneity of a clayey till from infiltration scale (0.5 m × 0.5 m) to field scale (100 m × 100 m), and
2. suggest relevant scales and strategies for infiltration tests in future experiments.

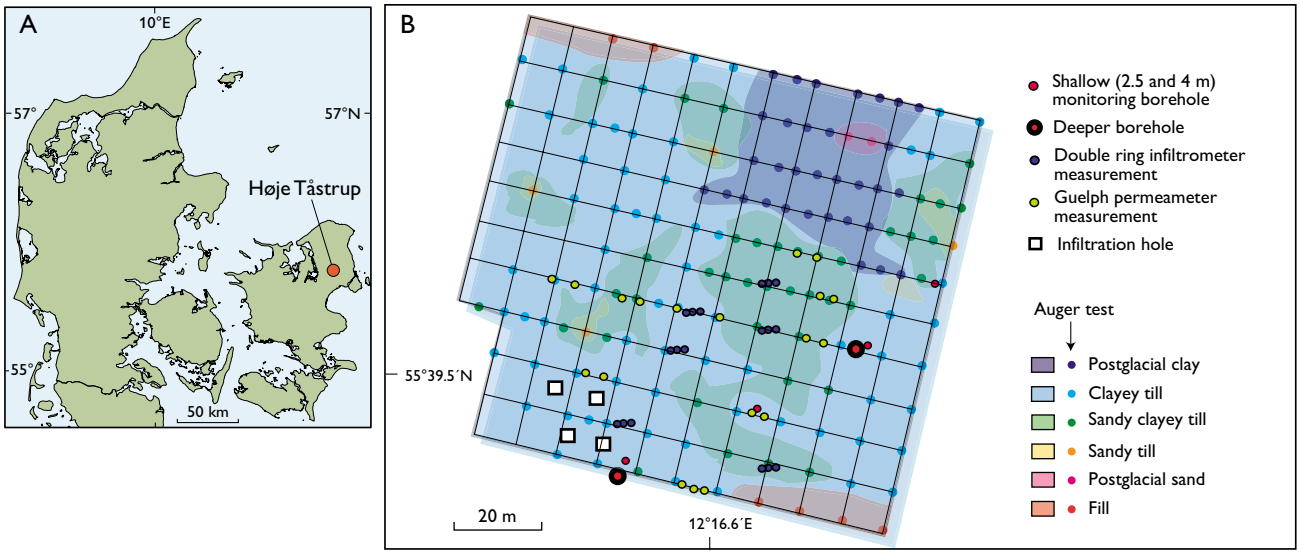

Fig. 1. **A**: Map of Denmark showing the location of the test site. **B**: Map of the test site showing the distribution of various sediment types and the locations of the infiltration tests.

Field experiments

The infiltration tests were conducted on former agricultural land next to the Technological Institute in Høje Taastrup, Denmark (Fig. 1). The area represents a site with a typical Danish clayey till. The geological setting is dominated by two basal till beds overlying glaciofluvial deposits and flow tills deposited in a supraglacial environment. The glacial deposits overlie highly fractured limestone bedrock *c.* 14–16 m below the ground surface. The primary groundwater table is located in the limestone bedrock at depths greater than 16 m and a secondary groundwater table is found in the upper till unit. The latter is located around 3 m below the surface during summer and around 1.0 to 0.5 m below the surface during winter.

An area of *c.* 100 m × 100 m was mapped in great detail using a hand auger (Jakobsen *et al.* 2011) with sampling in a 10 × 10 m grid. Shallow boreholes were cored to depths of 2.5 –4 m and used for monitoring the annual fluctuation of the secondary groundwater table. Two deeper boreholes were cored to a depth of *c.* 16 m. Two large holes were excavated to 5 and 8 m below the ground surface and used for detailed mapping of fractures and collection of large, intact samples for hydraulic tests in the laboratory.

The Guelph permeameter method measures the steady-state rate of water flow required to maintain a constant depth of water in a 40 cm deep and 8 cm wide cylindrical borehole. Water flows out of the outlet tube through a perforated section located above the permeameter tip. The Guelph

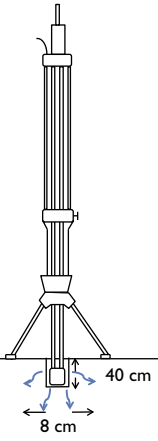

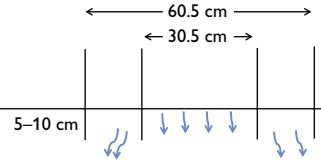

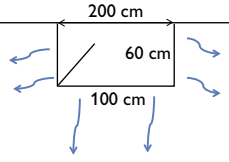

	GUELPH PERMEAMETER	DOUBLE RING INFILTROMETER	INFILTRATION HOLE
Direction of measured water flow	3-dimensional	1-dimensional	3-dimensional
Effect on soil structure	Smearing during excavation causing potential underestimation of K. Counteraction: careful removal of smearing with knife	Formation of cracks during insertion of cylinders into the soil → creation of preferential flow routes causing potential overestimation of K. Counteraction: sealing of contact with clay on the outside of the inner cylinder	Smearing during excavation of hole causing potential underestimation of K. Counteraction: careful removal of smearing with knife or use of excavation technologies that prevent or minimise smearing, e.g. chain excavator
Expenditure of time (time required to achieve full saturation)	1–2 hours depending on soil moisture	1–2 hours depending on soil moisture	1.5 hours to several hours depending on soil moisture
Degree of disturbance	Minimally invasive	Non-invasive	Highly invasive
Suitability to represent geological heterogeneity	Poor → Rather poor → Good Counteraction: conduct as many measurements as possible	Counteraction: conduct at least a triplet of measurements	
Literature on estimation of K_{sat}	Reynolds & Elrick (1985)	Reynolds *et al.* (2002)	

Fig. 2. Overview and principle of the different techniques used in this study. The blue arrows represent water flow. **K**: hydraulic conductivity.

permeameter method is based on the assumption of three-dimensional steady-state infiltration from a cylindrical test hole into the sediment.

Two concentric metal cylinders with diameters of 30.5 and 60.5 cm were used for the double ring infiltrometer method. After removal of the sward, the cylinders were carefully pressed 5–10 cm into the sediment. Water was poured into the inner cylinder, and also into the outer cylinder to prevent lateral movement of water beneath the inner cylinder, thus maintaining one-dimensional flow conditions. The amount of cumulative infiltration with time under falling-head conditions was recorded and K_{sat} values determined.

The infiltration holes were excavated to a depth of 60 cm with an inner area of 100 × 200 cm. Smearing caused by the excavation process was carefully removed with a knife. The holes were filled with water and when a steady state was attained, the infiltration rate from the hole into the sediment was measured directly.

A total of 41 infiltration tests were conducted across the site: 19 Guelph permeameter measurements, 18 double ring infiltrometer measurements and four infiltration tests in the excavated holes. More information on the methods is provided in Fig. 2.

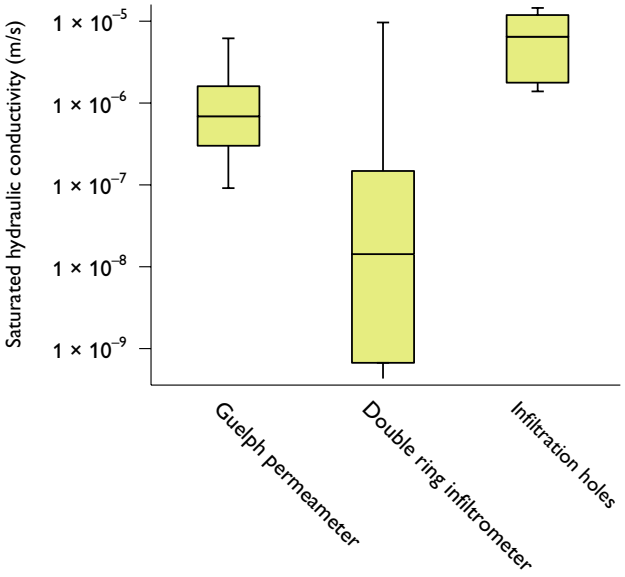

Fig. 3. Box and whisker diagram illustration of the range of saturated hydraulic conductivity values obtained using the Guelph permeameter, double ring infiltrometer and infiltration hole techniques. The scale is logarithmic. Whiskers are plotted at the maximum and minimum values, however, the minimum value for the double ring infiltrometer test is below the scale and not shown.

Results and discussion

The application of conventional infiltration technologies indicates that the saturated hydraulic conductivity (K_{sat}) of tills is a spatially highly variable property. In two Guelph permeameter measurements no infiltration at all was observed, which might be due to smearing during preparation of the borehole or compaction by heavy machines as the field site is former agricultural land. Compaction might also be the reason for one no-flow measurement in the double ring infiltrometer.

The results are presented in Table 1 and Fig. 3. The Guelph permeameter and the double ring infiltrometer average values are lower than those from the infiltration holes. This is probably due to not fully saturated conditions around the holes as the area is rather large compared to the area used for the Guelph permeameter and double ring infiltrometer measurements, where saturated conditions are attained reasonably quickly. The fact that the holes involve a much larger area than the Guelph permeameter and the double ring infiltrometer means that they involve more than one sediment type and accounts best for macro-pores, confirming that geological heterogeneity on clayey till plains influences the hydraulic conductivity even at infiltration plot scales.

A realistic estimate of hydraulic conductivity is crucial when planning how to manage stormwater infiltration. The present field-based study shows that hydraulic conductivity values are strongly influenced by the physical scale of the field measurements. This is mainly due to the local distribution of macro-pores and how well the geological heterogeneity is represented. The importance of scale-dependent variability of K_{sat} has also been demonstrated in previous studies (e.g. Jenssen 1990; Ronayne *et al.* 2012), but is still widely neglected when hydraulic conductivity values are used for stormwater management practices.

Due to the large variation of grain-size distribution in tills, it is not recommended to apply methods that define K_{sat} based on grain-size distribution. Neither is it recommended

Table 1. Summary statistics of saturated hydraulic conductivity values

Method	Number	Mininum	Maximum	Arithmetic mean
Guelph permeameter	19	9.12×10^{-8}	6.18×10^{-6}	1.44×10^{-6}
Double ring infiltrometer	18	7.43×10^{-13}	9.7×10^{-6}	8.26×10^{-7}
Infiltration holes	4	1.4×10^{-6}	1.46×10^{-5}	7.25×10^{-6}

to use K_{sat} values obtained with a double ring infiltrometer or a Guelph permeameter alone as they can vary by several orders of magnitude already on a infiltration plot scale. In our study we found a variable of more than two orders of magnitude. Data from infiltration holes give more realistic values. However, they are highly invasive and it may be difficult to excavate adequate holes in densely populated areas.

Instead of using highly invasive infiltration holes, we recommend to carry out combined hydrogeological investigations where double ring infiltrometer and Guelph permeameter measurements are supported by geological information from maps of near-surface deposits and borehole descriptions. In that less-destructive way, small-scale geological heterogeneity can be revealed and the most suitable areas for stormwater infiltration can be selected to enhance work efficiency of infiltration devices.

Acknowledgement

The work was conducted as part of the innovation consortium Cities in Waterbalance (Byer i Vandbalance) financed by the Danish Council for Technology and Innovation.

References

Fredericia, J. 1990: Saturated hydraulic conductivity of clayey tills and the role of fractures. Nordic Hydrology **21**, 119–132.

Jakobsen, P.R., Hermansen, B. & Tougaard, L. 2011: Danmarks digitale jordartskort. Danmarks og Grønlands Geologiske Undersøgelse Rapport **2011/40**, 28 pp.

Jenssen, P.D. 1990: Methods for measuring the saturated hydraulic conductivity of tills. Nordic Hydrology **21**, 95–106.

Kessler, T.C., Klint, K.E.S., Nilsson, B. & Bjerg, P.L. 2012: Characterization of sand lenses embedded in tills. Quaternary Science Reviews **53**, 55–71.

Klint, K.E.S. & Gravesen, P. 1999: Fractures and biopores in Weichselian clayey till aquitards at Flakkebjerg, Denmark. Nordic Hydrology **30**, 267–284.

McKay, L.D., Cherry, J.A. & Gillham, R.W. 1993: Field experiments in a fractured clay till. 1. Hydraulic conductivity and fracture aperture. Water Resources Research **29**, 1149–1162.

Nilsson, B., Sidle, R.C., Klint, K.E., Bøggild, C.E. & Broholm, K. 2001: Mass transport and scale-dependent hydraulic tests in a heterogeneous glacial till–sandy aquifer system. Journal of Hydrology **243**, 162–179.

Reynolds, W.D. & Elrick, D.E. 1985: In situ measurement of field-hydraulic conductivity, sorptivity, and the alpha-parameter using the Guelph permeameter. Soil Science **140**, 292–302.

Reynolds, W.D., Elrick, D.E., Youngs, E.G., Amoozegar, A., Booltink, H.W.G. & Bouma, J. 2002: Saturated and field-saturated water flow parameters. In: Dane, J.H. & Topp, G.C. (eds): Methods of soil analysis, Part 4, Physical methods, 797–878. Madison, Wi: Soil Science Society of America.

Ronayne, M.J., Houghton, T.B. & Stednick, J.D. 2012: Field characterization of hydraulic conductivity in a heterogeneous alpine glacial till. Journal of Hydrology **458–459**, 103–109.

Authors' addresses

B.B. & M.B.J., *Department of Geosciences and Natural Resource Management, University of Copenhagen, Rolighedsvej 23, DK-1958 Frederiksberg, Denmark*. E-mail: *bboc@ign.dk.ku*

K.E.S.K., *Geological Survey of Denmark and Greenland,* Øster *Voldgade 10, DK-1350 Copenhagen K, Denmark*.

A multidisciplinary study of a geothermal reservoir below Thisted, Denmark

Morten Leth Hjuler, Henrik Vosgerau, Carsten Møller Nielsen, Peter Frykman, Lars Kristensen, Anders Mathiesen, Torben Bidstrup and Lars Henrik Nielsen

The first geothermal plant in Denmark was established in 1984 near the town of Thisted (Fig. 1). For nearly 30 years the plant has successfully produced *c.* 43°C hot water (surface temperature) from a highly permeable sandstone reservoir in the Late Triassic to Early Jurassic Gassum Formation and used the heat from the geothermal water for district heating. The 45°C hot water (formation temperature) is pumped up from a vertical production well, Thisted-2, from a depth of *c.* 1250 m and the cooled water (*c.* 12°C) is re-injected into the formation through a vertical injection well, Thisted-3, located 1.5 km east of the production well.

In order to increase the capacity of the plant the supplier of district heating, Thisted Varmeforsyning, plans to add a new well to the current configuration. In 2013 the Geological Survey of Denmark and Greenland was assigned the task to propose suitable sites for a new well. The sites will be proposed based on the quality, continuity and temperature of the reservoir(s) within the Gassum Formation. Three possible well sites (Thisted-5A–C) were considered (Fig. 1).

Well-log information and core-analysis data from four existing wells, Thisted-1–4, indicate significant variations in reservoir properties and spatial extent of the reservoir bodies within the Gassum Formation. In order to establish a robust geological reservoir model that covers all reservoir-qualifying aspects it was decided to conduct the evaluation as a multidisciplinary study that included: (1) seismic interpretation and mapping, (2) determination of reservoir temperature, (3) petrophysical interpretation of well logs and (4) sedimentological description of well cores.

Two possible well configurations were considered: (1) The new Thisted-5 is used as an injection well and Thisted-2 continues as a production well. Production can be increased with additional injection capacity, and by using Thisted-5 as the principal injection well the breakthrough of cold injection water is postponed. (2) The new Thisted-5 is used as a production well with Thisted-2 and -3 as injection wells. Thisted-5 will be located downflank of the Thisted salt structure and will produce geothermal water from greater depths and expectedly with higher temperature than the existing production well.

Geological setting and seismic mapping

Thisted is located in the central to northern part of the Norwegian–Danish Basin in an area characterised by numerous salt pillows and diapirs. The Upper Permian – Mesozoic suc-

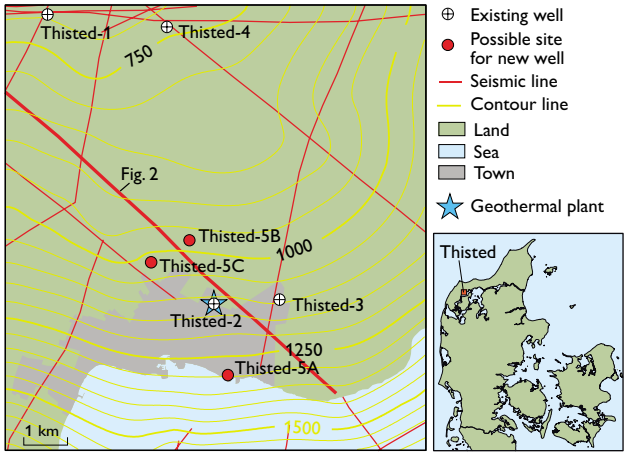

Fig. 1. Depth structure map of near top Gassum Formation (contour interval: 50 m) of the Thisted area showing seismic lines, well locations and possible locations of the planned Thisted-5 wells.

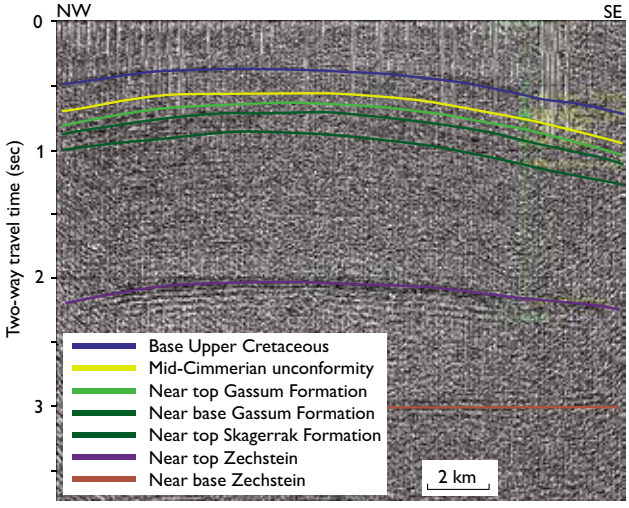

Fig. 2. Seismic section (PRKL7374A no 74249) across the Thisted salt pillow.

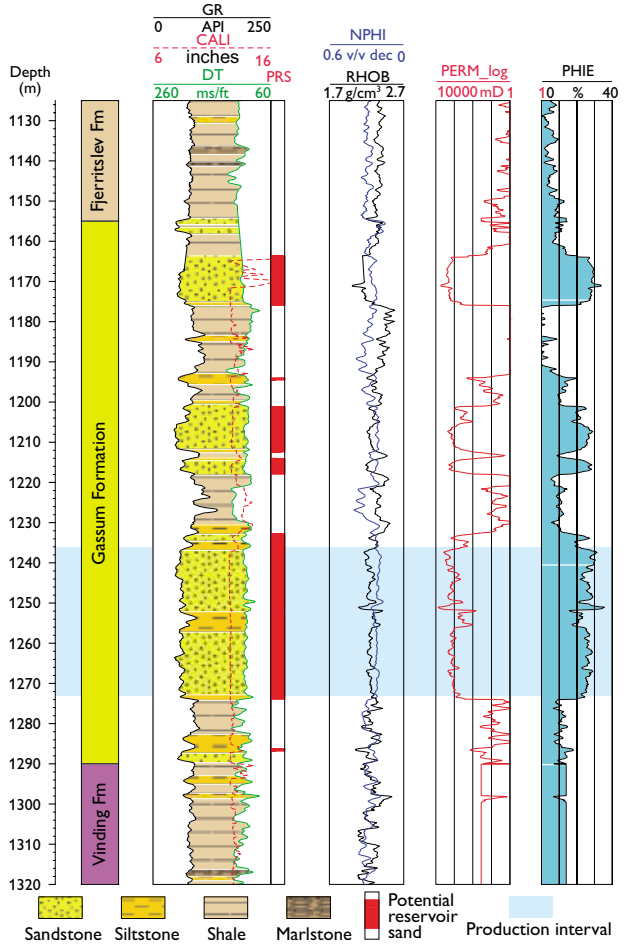

Fig. 3. Petrophysical evaluation of the Gassum Formation in the Thisted-2 well, including a lithological interpretation.

cession consists of 5–5.5 km of sediments (Vejbæk & Britze 1994). Thick Zechstein salt layers are overlain by Triassic sandstone, mudstone, carbonate and salt, followed by Lower Jurassic mudstone, Middle Jurassic sandstone, Upper Jurassic – Lower Cretaceous mudstone and siltstone with few sandstone beds. This succession is overlain by thick layers of chalk and limestone.

Thisted is situated over the southern part of a gently sloping salt pillow and the strata above the salt pillow in the area of the Thisted-2 and 3 wells dip towards the south. Thisted-1 and 4 are located on top of the structure.

All relevant 2D seismic profiles in the Thisted area were interpreted in order to map the presence and variations of the reservoirs including depth, changes in thickness and the occurrence of faults which may affect the lateral continuity of the reservoirs. Due to low resolution of the seismic data

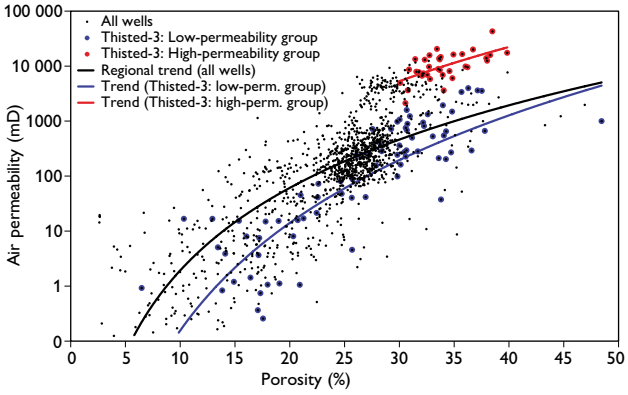

Fig. 4. Porosity–permeability plot based on conventional core analysis data from the Gassum Formation.

near the potential sites of Thisted-5, it was difficult to map faults and lateral changes in lithology and to trace seismic horizons. However, seven horizons could be identified, including the near top and near base of the Gassum Formation (Fig. 2). Mapping of single reservoir intervals within the Gassum Formation was impossible and no faults were identified.

Based on the seismic interpretation, four depth structure maps were compiled, including one of the near Top Gassum Formation (Fig. 1). From this map the depth of the Gassum Formation at the three suggested well sites can be estimated. Relative to the Thisted-2 well, the Thisted-5A site is located downflank of the Thisted structure whereas the Thisted-5B and 5C are situated upflank. Due to deeper burial and expected higher temperature of the geothermal target, the Thisted-5A site is suitable as a production well, whereas Thisted-5B and 5C are injection well candidates.

Reservoir temperature

Temperature data from Danish onshore wells are limited and include values from different depths and different formations, thus the geothermal gradient covers a wide range of 28–20°C/km. In the Thisted-2 production well, *c.* 43°C warm water (surface temperature) is produced from a depth of 1250 m (formation temperature 45°C). The geothermal target in Thisted-5A is estimated to be located at a depth of *c.* 1450 m, which corresponds to a temperature up to 52°C, if extrapolated from a continuation of the regional gradient and the temperature data from the Thisted-3 well. The geothermal target in the Thisted-5B and 5C injection sites is located at a depth of *c.* 1150 m corresponding to a reservoir temperature of 41°C using Thisted-3 data.

Table 1. Reservoir parameters for net sand from the Gassum Formation*

Well no.	Formation thickness (m)	Gross sand thickness (m)	Net sand thickness (m)	N/G†	Average porosity (%)	Estimated gas perm. (mD)	Estimated reservoir perm. (mD)‡
Thisted-1	137	94.4	84.4	0.62	28.3	2500	3125
Thisted-2	135	94.9	70.3	0.52	25.3	1300	1625
Thisted-3	115	67.4	54.5	0.47	28.6	3500	4375
Thisted-4	114	36.6	–	–	–	–	–

* Shale and porosity cut-off applied, net sand is defined as sandstone with <30% shale and porosity >15%.
† N/G: net sand thickness divided by formation thickness.
‡ Estimated reservoir permeability: estimated gas permeability multiplied by 1.25 (upscaling factor).

Well-log interpretation and core description

The evaluation of the reservoir quality of the Gassum Formation is primarily based on wireline logs and core-analysis data from Thisted-1–4 (Fig. 3). The quality of the logs is fairly good, but at certain intervals indications of caving lead to uncertain porosity estimates. Lithology, clay content, porosity and permeability are evaluated from combined analyses of log data, lithological descriptions of cores and core analysis data.

High, well test-based, porosities and permeabilities for the Thisted wells were validated by gas permeability measurements from core analysis and are possibly caused by the relatively shallow depth of the Gassum Formation (Hjuler *et al.* 2013). The regional porosity–permeability trend (Fig. 4) significantly underestimates the actual (well test) permeability and was therefore calibrated to more closely approximate the well test results. Evaluation of the sandstones indicates high average porosities exceeding 28% for the Thisted-1 and 3 wells (Table 1). The interpreted porosity of 25.3% for the Thisted-2 well seems too low considering the fairly high test permeability of 3670 mD; this is possibly due to erroneous log data. Despite considerable variation of the assessed net sand thickness within the study area all thicknesses are considered sufficient for geothermal exploitation (Table 1).

Detailed sedimentological descriptions and interpretations of the cores from the Thisted-3 well indicate that the reservoir sandstones were mainly deposited in fluvial and estuarine environments (Nielsen 2003; Hjuler *et al.* 2013). Considerable lateral and stratigraphical variations of the logs from the Thisted wells indicate spatial and temporal variations of the sedimentary environment, which must have a significant influence on reservoir distribution and quality. It is thus important for the mapping of reservoir intervals to

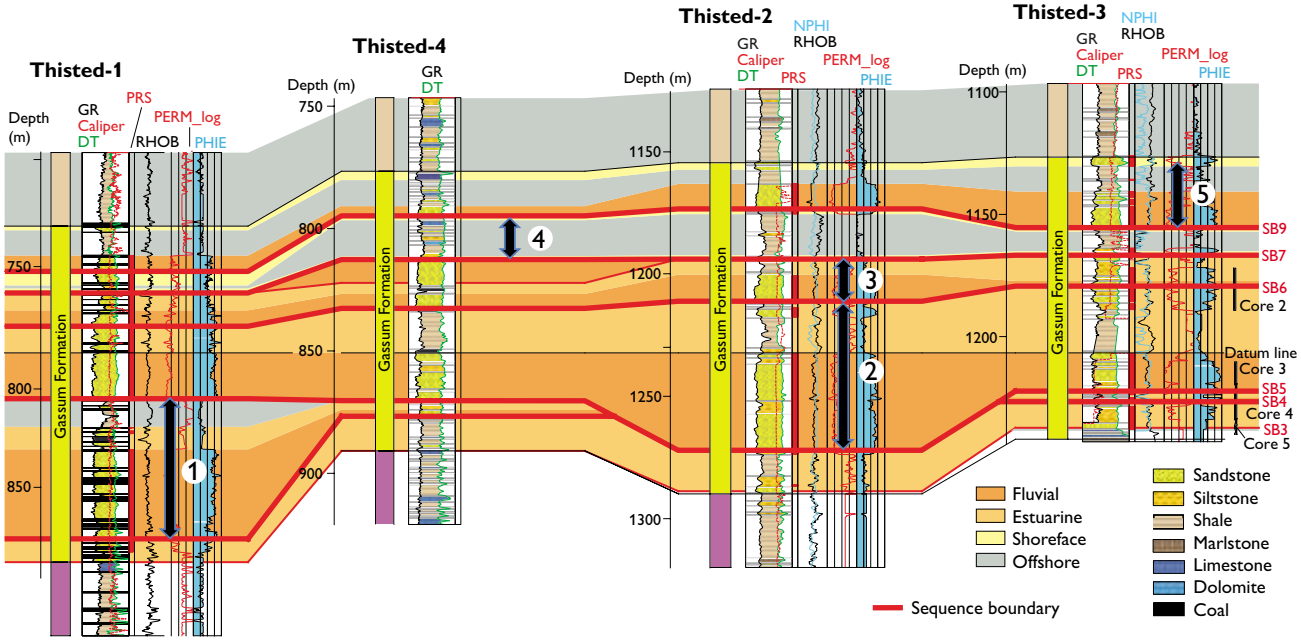

Fig. 5. Log correlation of sedimentary units within the Gassum Formation in the four Thisted wells. 1–5: sequences, red lines: sequence boundaries (corresponding to incised valley floors), **PRS**: potential reservoir sand. The sediments of the incised valleys are fluvial and estuarine.

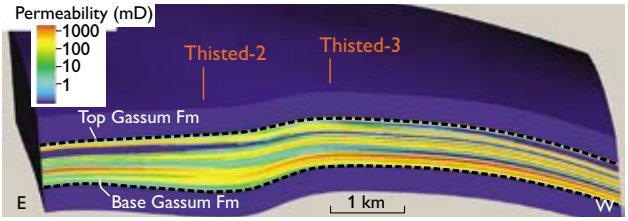

Fig. 6. Permeability model that crosses the Thisted-2 and 3 wells.

understand the variations in the sedimentary environment. Hence the logs of the four wells have been correlated (Fig. 5).

Five periods of sea-level rises and falls were identified within the Gassum Formation. During sea-level falls, incised valleys formed which were filled with fluvial and estuarine sediments during subsequent rises in sea level. The extent of reservoir sandstone deposits is limited by the extent of the valleys. To estimate the dimensions of sandstone bodies in the Thisted area the extent of present-day estuaries has been studied. It was found that the width of estuarine sediment bodies exceeds 8 km and the lengths are probably several tens of kilometres. In the Late Triassic – Early Jurassic the overall shoreline was NW–SE oriented. The seismic data do not allow the determination of the relief and extent of the incised valleys, but an overall NE–SW-orientation of the estuarine sediment bodies is assumed.

The reservoir lithology is limited to fluvial and estuarine sandstones with the fluvial sandstones being *c.* 20 times more permeable than the estuarine sandstones because detrital clay clogs the pores of the latter. As expected, the reservoir properties of clay- and siltstones outside the estuaries are poor and thus fluvial sandstones in the valleys may be hydraulically separated from each other. Log correlation implies that the estuarine deposits may coalesce into larger reservoir units, or may be partly separated by layers of low permeability. In a more landward position towards the NE fluvial reservoir sandstones may amalgamate into more coherent reservoir units, leading to improved reservoir continuity.

A reservoir model

Petrel® software was used to establish a reservoir model that covers an area of 11 × 13.5 km; flow simulations and dynamic modelling were performed using the Eclipse® 100 software (Fig. 6). Input data for the reservoir model were prepared by integration of interpreted seismic data, depth structure maps, temperature assessment, petrophysical evaluation, core description and log correlations as described above.

Comparison with historic data was not possible as no pressure data of the Thisted-2 and 3 wells are available; the simulated response from the dynamic modelling could only be adjusted because no significant temperature drop has been recorded in the production water since 1984. Hence the model results are uncertain and should be evaluated with caution due to lack of calibration data. With this limitation in mind, and using the current well configuration, the model simulations indicate another 15 years of production with no alarming decrease in water temperature (less than 1°C).

With Thisted-5A as a new production well situated downflank of the existing well pair, the production could benefit from a higher temperature with no sign of cooler water arriving during an operational time of 30 years (uncertainty in modelling results as above). With Thisted-5B or -5C as a new injection well situated at shallower depth than the existing well pair, and with Thisted-2 still used as production well, the new injection well can benefit from higher permeability.

Concluding remarks

By integrating data from geological, geophysical and petrophysical disciplines, a detailed geological model was established that provides a structural framework and demonstrates how depositional environment controls the lateral extent, continuity and quality of reservoirs. A detailed reservoir model was also established, which can simulate the remaining lifetime of the geothermal plant with the current well configuration, or the lifespan of the plant with the addition of a new production or injection well. The combination of geological and reservoir models provides indications of the best sites for additional production or injection wells.

References

Hjuler, M.L., Vosgerau, H., Nielsen, C.M., Frykman, P., Kristensen, L., Mathiesen, A., Bidstrup, T. & Nielsen, L.H. 2013: Assessment of potential capacity increase of the geothermal plant at Thisted by adding a new geothermal well. Danmarks og Grønlands Geologiske Undersøgelse Rapport **2013/80**, 90 pp.

Nielsen, L.H. 2003: Late Triassic – Jurassic development of the Danish Basin and Fennoscandian Border Zone, southern Scandinavia. In: Ineson, J.R. & Surlyk, F. (eds): The Jurassic of Denmark and Greenland. Geological Survey of Denmark and Greenland Bulletin **1**, 459–526.

Vejbæk, O.V. & Britze, P. 1994: Geological map of Denmark 1:750 000. Top pre-Zechstein (two-way traveltime and depth). Danmarks Geologiske Undersøgelse Kortserie **45**, 8 pp.

Authors' address

Geological Survey of Denmark and Greenland, Øster Voldgade 10, DK-1350 Copenhagen K, Denmark; E-mail: *mlh@geus.dk*

Estimating thermal conductivity from lithological descriptions – a new web-based tool for planning of ground-source heating and cooling

Claus Ditlefsen, Inga Sørensen, Morten Slott and Martin Hansen

It is the overall policy of the Danish Government that by 2050 electricity, heating and transport will be 100% based on renewable energy. In order to reach this goal a number of different green technologies will have to interact. In areas with no district heating, ground-source heating by heat pump technology (Sanner 2011) could well be one of the solutions.

The potential energy extraction from closed-loop boreholes for ground-source heating depends to a large degree on the thermal conductivity of the surrounding geological formations, although other parameters such as the thermal gradient and the extent of groundwater flow also affect the transport of heat to the borehole. Initial estimates indicate that in Denmark there may be as much as 40% difference between the most and the least favourable geological conditions, determined by the thermal conductivity of the different sediment or rock types alone (Vangkilde-Pedersen *et al.* 2012). Therefore specific knowledge of the thermal conductivity of the geological formations is essential when estimating the optimal drilling depth and the number of boreholes required for a specific plant. In co-operation with research and industrial partners, the Geological Survey of Denmark and Greenland is conducting a three-year project with the title 'GeoEnergy, tools for ground-source heating and cooling based on closed-loop boreholes' (***www.geoenergi.org***). The objective of the project is to acquire knowledge and develop tools and best practices for the planning, design and installation of shallow geothermal energy systems. This paper describes a web-based tool developed to estimate the thermal conductivity in the area surrounding a potential new plant. The tool was developed within the GeoEnergy project and can be used by administrators, energy planners and drillers of closed-loop boreholes.

Thermal conductivity of shallow Danish sediments

The thermal conductivity of sediments or rocks depends on their mineral composition, the texture, and the water content. Above the water table, where air is present in the pore spaces, sediments generally have a low thermal conductivity. Hence information about the position of the water table in the borehole is important when planning a new site.

Relatively few investigations of thermal properties of Danish sediments have been carried out (Balling *et al.* 1981; Porsvig 1986) and thermal conductivity values published in international literature show broad ranges for the individual sediment types (e.g. Banks 2008; VDI 2010). This is generally the case for clayey sediments and particularly for glacial till, see Vangkilde-Pedersen *et al.* (2012) for details. Therefore a programme was initiated to investigate the thermal properties of common shallow sediments. The work focused on determining the thermal conductivity of prevalent water-saturated sediments. The range of the thermal conductivities within common sediment types was determined from measurements of 51 samples from well-characterised exposures at different localities (Figs 1, 2). The samples were water saturated in the laboratory and placed in a thermal cupboard at 20°C for at least 16 hours before measurements were made. The thermal conductivity was determined using the needle probe method (Wechsler 1992; Hukseflux 2003). Detailed

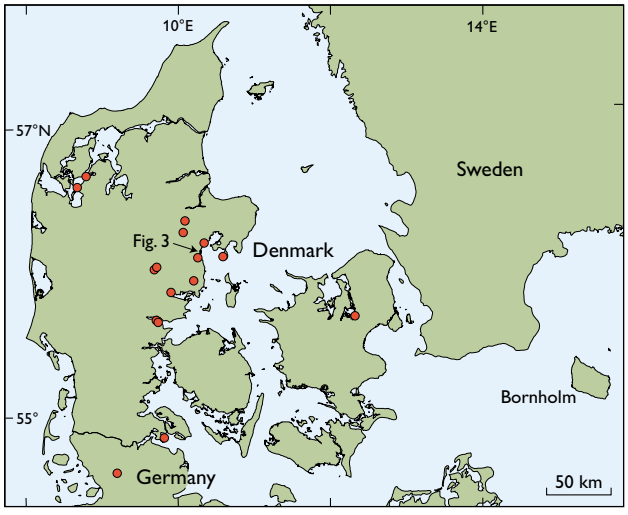

Fig. 1. Map showing sample locations. One sample from northern Germany was kindly provided by Reinhard Kirsch, Landesamt Schleswig-Holstein. For sample details see Ditlefsen & Sørensen (2014). The arrow shows the location of the map included in Fig. 3.

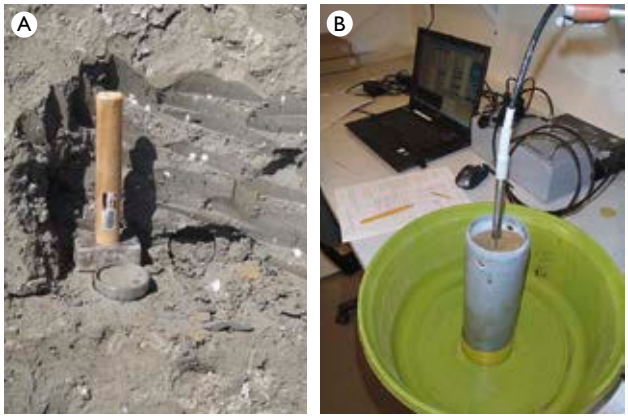

Fig. 2. **A**: Sampling of clayey till. **B**: A sediment sample with a needle probe installed.

descriptions of sampling and laboratory procedures, as well as data analysis and statistical analysis were published by Ditlefsen & Sørensen (2014) and Sørensen *et al.* (in press). A summary of the results is provided in Table 1. Each sample has been measured 2 to 5 times and an average value representing the sample was calculated. The variation amongst samples of the same sediment type is given as one standard deviation using the average values of each sample. The results indicate that the different sediment types have thermal conductivities within characteristic ranges with one standard deviation corresponding to approximately 20% of the mean. This further implies that it will be possible to estimate the thermal conductivity around a specific borehole from thorough descriptions of borehole samples alone.

The national borehole database Jupiter

The Geological Survey of Denmark and Greenland has acquired data on boreholes since 1926 in accordance with the Danish water supply legislation. The data include information about location, construction, geology, water table and groundwater chemistry (Hansen & Pjetursson 2011). Samples from approximately one third of the boreholes have been described and interpreted by geologists; the rest have been described by drillers in the field. Since 1969, drillers have also been obliged to submit representative borehole samples to the Survey where they are described according to strict standards as outlined by Larsen *et al.* (1995). In addition, geological interpretations of age and depositional environment are made (Gravesen & Fredericia 1984). The data are stored in the national borehole database, Jupiter, which can be accessed on the internet free of charge (www.geus.dk). The database includes data on more than 270 000 boreholes, corresponding to about six boreholes per square kilometre. In 2001, training and certification of drillers operating in Denmark became mandatory, including instruction in making a simple but rigorous description of borehole samples. This allows for an overall assessment of the character and possible origin of samples that have been described in the field by drillers. All in all, the national borehole database provides planners, drillers and administrators with a unique possibility to evaluate local geological conditions at a given site.

Estimating thermal conductivity values from sediment descriptions

As described above, it has been possible to establish a relationship between lithology and thermal conductivity for a number of common Danish sediment types. The national database holds a large number of lithological descriptions from throughout the country, and by combining the lithological and thermal conductivity data the borehole database can be used in a new way. To do this it has been necessary to develop a routine that could relate a lithological description to one of the sediment groups in Table 1. This task was facilitated by the structure of the lithological table in Jupiter, where different components of the lithological description e.g. *rock type, minor components, mineralogy, grain size, overall interpretation* etc. are stored with unique codes

Table 1. Thermal conductivity of some common, shallow, Danish sediments

Sediment type	Number of samples	Average thermal conductivity W mK^{-1}	Range W mK^{-1}	One standard deviation W mK^{-1}
Gyttja	3	0.68	0.58–0.86	0.15
Smectite-rich clay	3	0.98	0.80–1.14	0.17
Silty clay	10	1.15	0.90–1.42	0.17
Chalk*	4	1.62	1.49–1.80	0.13
Mica-rich, fine-grained sand	8	1.81	1.48–2.19	0.27
Till	19	1.89	1.40–2.66	0.30
Glacial sand, gravelly	4	2.24	1.98–2.43	0.19
Pure quartz sand	3	2.75	2.41–3.34	0.51

* Selected data from Balling *et al.* (1981).
Measurements were conducted with a needle probe (Hukseflux 2008) using water-saturated samples.

Table 2. Interpretation of thermal conductivity

Sediment type*	Supplementary information from driller	Suggested thermal conductivity (W mK^{-1})§
Sand		2.24
Limestone		1.62
Clay		1.15
Clay$^{\$}$	Containing, sand, gravel or stones	1.89
Clay, sand, and stones$^{\$}$		1.89

* Sediment type according to driller.
§ The values are based on measurements of thermal conductivity (Table 1) and our interpretations of sediment types.
$^{\$}$ Clay deposits with sand, gravel or stones are interpreted as till. Other clay deposits are interpreted as clay deposited in water.

in individual data fields, which makes rigorous queries into the lithological data possible. In this way most samples described and interpreted by geologists could fairly easily be assigned to one of the sediment groups in Table 1. In addition granite, gneiss and sedimentary rocks found near the surface on the island of Bornholm (Fig. 1) are tentatively ascribed thermal conductivities in accordance with VDI (2010). Water-lain sediments consisting of alternating layers of sand and clay are tentatively ascribed an average thermal conductivity of 1.5 W mK^{-1} in accordance with the values for sand and clay (Table 1). For samples where only the overall sediment type was noted by the driller, interpretations had to be made (Table 2). Finally, to compensate for the fact that sediments which are not water saturated have reduced thermal conductivities (VDI 2010), all deposits above the water table in the borehole are tentatively ascribed a conductivity of 1.0 W mK^{-1}.

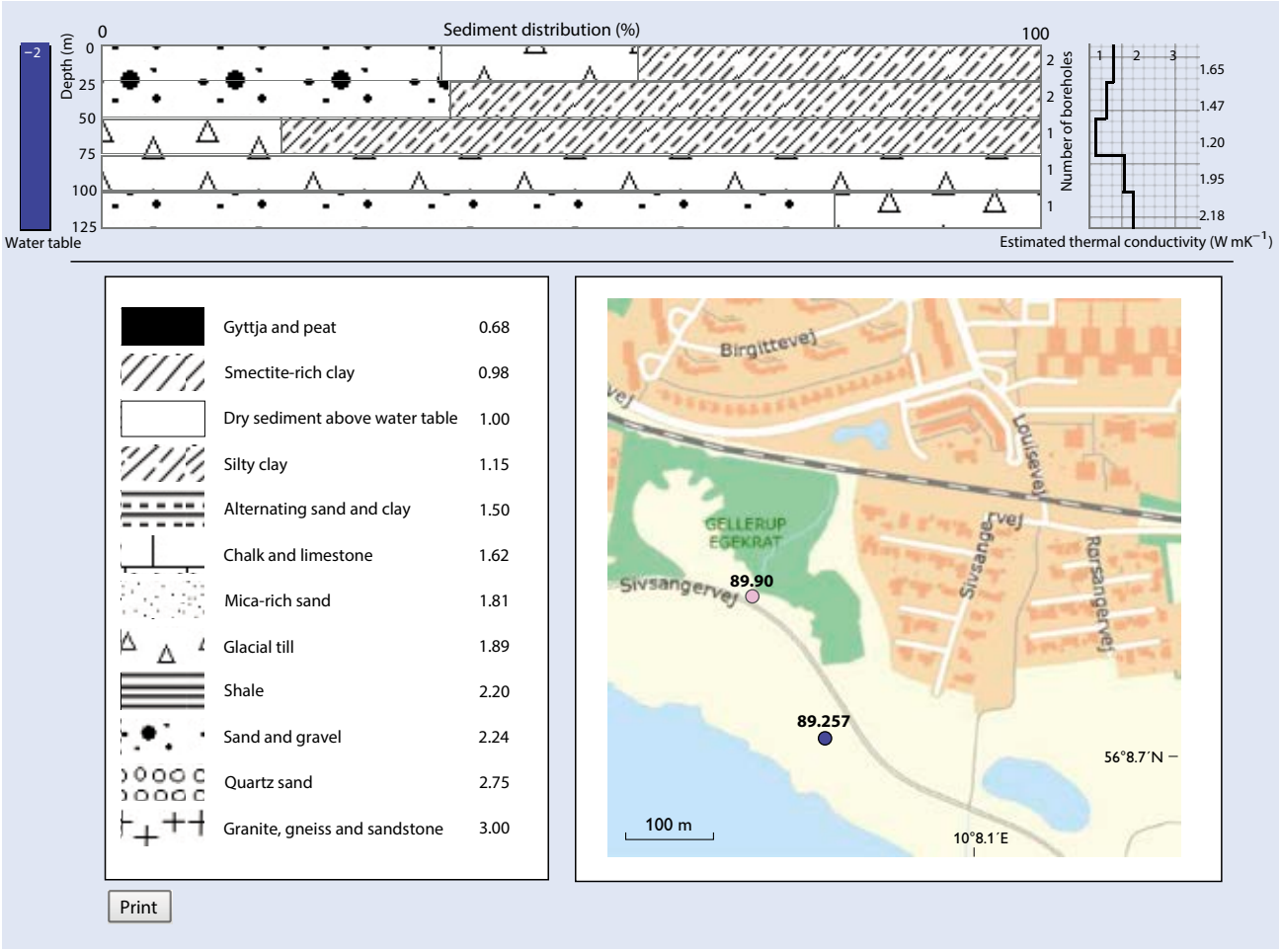

Fig. 3. Results from the web application shown in a standardised report window. *http://geuskort.geus.dk/termiskejordarter/*

It is the intention of the web application to show the expected thermal conductivity in a new project area from existing lithological descriptions and further to show the variation in thermal conductivity with depth as a function of the lithological variations. The calculations include all available boreholes within a user-defined rectangle, and the estimated thermal conductivity is calculated in depth intervals of 25 m from the available lithological descriptions. Furthermore, it is required that at least 80% of the interval is covered by descriptions that can be related to a thermal conductivity value. If this requirement is not met, the borehole is excluded from the calculations for the specific depth interval. Within each interval the percentage of each sediment type is then calculated and from this distribution the resulting thermal conductivity of the interval is estimated from the reference values for water-saturated sediments or rocks (Fig. 3). Furthermore, the average depth to the water table is calculated from the most recent soundings in each borehole. Above this depth a reduced thermal conductivity of 1 W mK^{-1} is estimated overruling the thermal conductivity related to the water saturated sediment.

The web application is available at ***http://geuskort.geus.dk/termiskejordarter/***. From the initial map, the user can zoom in on the relevant project area and see all boreholes. By using the box search button and clicking on the individual boreholes, a standard lithological report appears and the quality of the individual borehole data can be accessed. By dragging a rectangle over one or more boreholes, calculations based on the selected boreholes are made as described above. In order to obtain a reliable estimate of the thermal conductivity, it is important that the selected boreholes represent the geology at the new site, and a rectangle size of not more than 1 km^2 is recommend unless an initial data inspection indicates otherwise.

The results are shown in a standardised report window (Fig. 3). The report shows the average lithological composition of each 25 m interval as bars and a plot of expected thermal conductivity values versus depth. A plot of the depth to the water table calculated from soundings in the area is shown to the left. The report also contains a locality map that shows the boreholes in the area and a legend that includes average thermal conductivities of different sediment and rock groups. The properties of the different groups can easily be adjusted or more groups can be added by the web administrator when more information about the thermal conductivity of different sediments and rocks becomes available.

So far, the web application has been tested and released. The next step will be to introduce it to different end users such as administrators, drillers and energy planners. We also plan to conduct a number of interviews to get feedback, which may lead to adjustment of the system.

Acknowledgement

The EUDP programme of the Danish Energy Agency is thanked for financial support of the GeoEnergy project.

References

Balling, N., Kristiansen, J.I., Breiner, N., Poulsen, K.D., Rasmussen, R. & Saxov, S. 1981: Geothermal measurements and subsurface temperature modelling in Denmark. GeoSkrifter **16**, 176 pp.

Banks, D. 2008: An introduction to thermogeology: ground source heating and cooling, 351 pp. Oxford: Blackwell Publishing.

Ditlefsen, C. & Sørensen, I. 2014: D6 Overfladenære jordarters termiske egenskaber (in Danish with English summary), 30 pp. *http://geoenergi.org/xpdf/d6_jordarters_termiske_egenskaber.pdf*

Gravesen, P. & Fredericia, J. (eds) 1984: ZEUS-geodatabase system. Borearkivet. Databeskrivelse, kodesystem og sideregistre. Danmarks Geologiske Undersøgelse Serie D **3**, 259 pp.

Hansen, M. & Pjetursson, B. 2011: Free, online Danish shallow geological data. Geological Survey of Denmark and Greenland Bulletin **23**, 53–56.

Hukseflux 2003: TP02 Non-steady-state probe for thermal conductivity measurement. TP02 manual v1209. Delft: Hukseflux.

Hukseflux 2008: TPSYS02 Thermal conductivity measurement system user manual TPSYS02 manual v0806.doc. Delft: Hukseflux.

Larsen, G., Frederiksen, J., Willumsen, A., Fredericia, J., Gravesen, P., Foged, N., Knudsen, B. & Baumann, J. 1995: A guide to engineering geological soil description. Danish Geotechnical Society Bulletin **1E**, 130 pp.

Porsvig, M. 1986: Varmeovergangsforhold omkring jordslanger. Energiministeriets varmepumpeforskningsprogram **33**, 56 pp.

Sanner, B. 2011: Concept and feasibility studies. In: Mc Corry, M. & Jones, G.L. (eds): Geotrainet training manual for designers of shallow geothermal systems, 21–24. Brussels: Geotrainet.

Sørensen, I., Palola, M.A. & Ditlefsen, C. 2014: D8 Guidelines for equipment, methods and calibration, part 1: Measurement of thermal conductivity. GeoEnergy report, 37 pp. *www.geoenergy.dk*

Vangkilde-Pedersen, T., Ditlefsen, C. & Højberg, A.L. 2012: Shallow geothermal energy in Denmark. Geological Survey of Denmark and Greenland Bulletin **26**, 37–40.

VDI (Verein Deutscher Ingenieure) 2010: Thermische Nutzung des Untergrundes: Grundlagen, Genehmigungen, Umweltaspekte. Richtlinie 4640, Blatt 1, 33 pp. Düsseldorf: Verein Deutscher Ingenieure.

Wechsler, A.E. 1992: The probe method for measurement of thermal conductivity. In: Maglic, K. D., Cezairliyan, A. & Peletsky, V.E. (eds): Compendium of thermophysical property measurement methods **2**, Recommended measurement techniques and practices, 161–185. New York: Plenum Press.

Authors' addresses

C.D., *Geological Survey of Denmark and Greenland, Lyseng Allé 1, DK-8270, Højbjerg, Denmark*. E-mail: *cd@geus.dk*

M.S. & M.H., *Geological Survey of Denmark and Greenland,* Øster *Voldgade 10, DK-1350 Copenhagen K, Denmark*.

I.S., *VIA University College, Campus Horsens, Chr. M.* Østergaards *Vej 4, DK-8700 Horsens, Denmark*.

Six years of petroleum geological activities in North-East Greenland (2008–2013): projects and a view of the future

Jørgen A. Bojesen-Koefoed, Peter Alsen and Flemming G. Christiansen

The deadline for applications to the first licence round for petroleum exploration offshore North-East Greenland was 15 December 2012. The round was restricted, allowing only members of the KANUMAS consortium to be operators (BP, Chevron, Exxon, JOGMEG, Shell and Statoil). Nunaoil is also part of KANUMAS, but it is a carried, non-operator partner. An ordinary licensing round followed shortly after with a deadline on 15 October 2013.

At the end of 2013, pre-round licences were awarded and the results of the ordinary round are expected in 2014. Irrespective of the outcome of future exploration activities, this milestone marks an important step in Greenland's long way towards becoming an oil nation. It also offers an opportunity to summarise petroleum-directed activities in North-East Greenland since 2008, through which the Geological Survey of Denmark and Greenland (GEUS) has provided crucial knowledge to both the industry and the Greenland Bureau of Minerals and Petroleum (BMP) in their preparations for the licence rounds.

Background

Almost a decade ago, a licence round offshore North-East Greenland, including the Danmarkshavn Basin (Figs 1, 2), was discussed between the KANUMAS partners and the BMP, and the details of timing and block locations were negotiated over several years. In keeping with this, GEUS initiated discussions with the petroleum industry to clarify its needs in order to be able to provide optimal service to both companies and authorities when required. Concurrently, the United States Geological Survey's (USGS) 'Circum Arctic Resource Appraisal' directed focus to subjects that required further study. The North-East Greenland part was carried

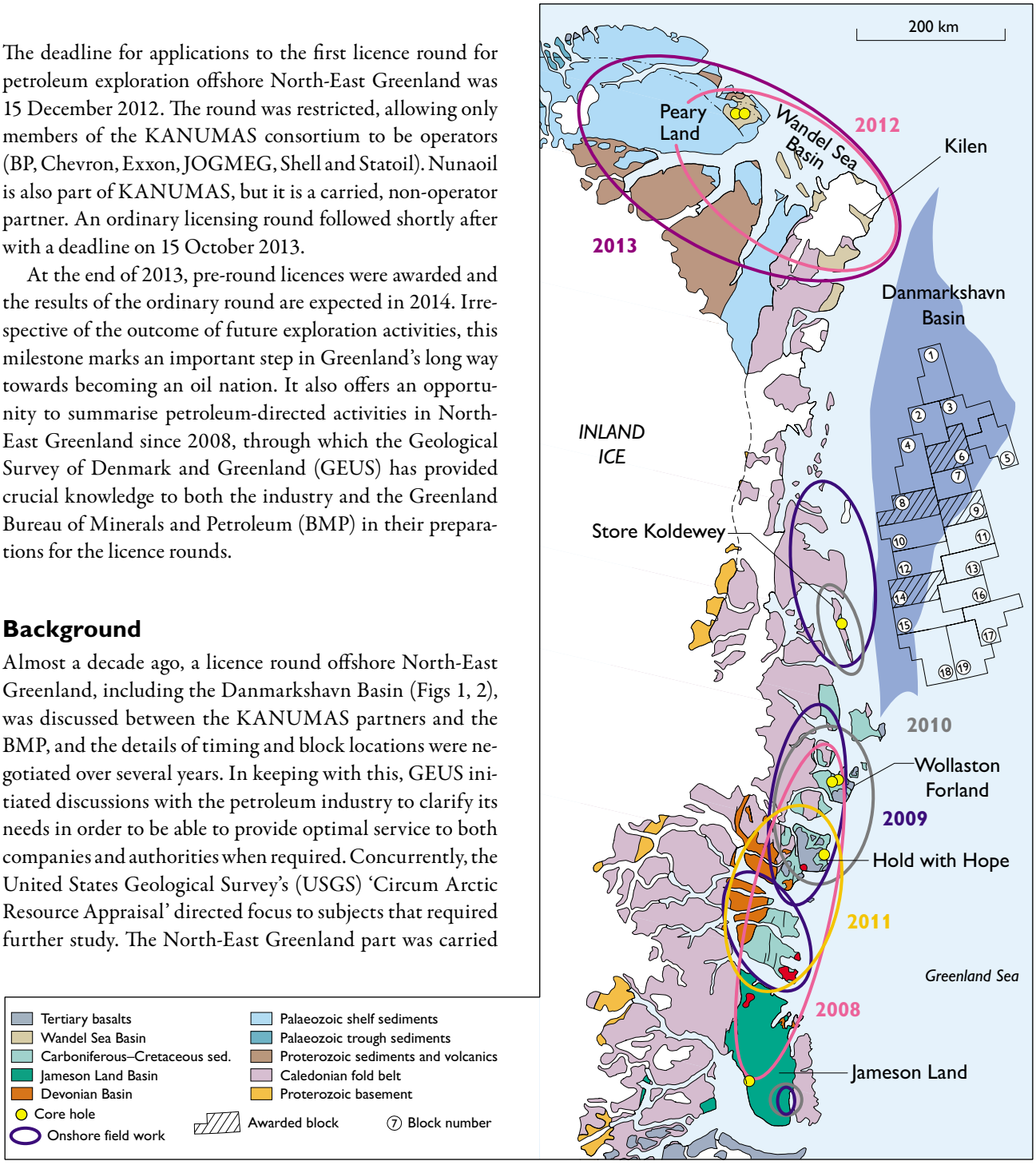

Fig. 1. Map of North-East Greenland, showing the offshore licence area, onshore field work areas (colour-coded according to year) and the locations of core holes.

 Geological Survey of Denmark and Greenland Bulletin 31, 59–62. Open access: www.geus.dk/publications/bull

Fig. 2. Aerial view of Kilen, a key area for understanding the geology of the Wandel Sea Basin with exposures of Triassic to Cretaceous sediments. Kilen is approximately 10 × 30 km large and is surrounded by glaciers except to the south-east that faces the Northeast Water polynya. View towards the south. For location see Fig. 1.

out in collaboration with GEUS (Christiansen *et al*. 2006; Gautier 2007; Gautier *et al*. 2011; Christiansen 2011). The seismic coverage of the North-East Greenland shelf is scattered and there are no wells. Therefore an understanding of the onshore geology is indispensable to construct analogues for the offshore basins. Geologists from Danish research institutions have worked in NE Greenland for over a century, and the accumulated sample and knowledge base at GEUS is the largest existing geological database for Greenland. In 2008, a project was set up at GEUS to systematise relevant available data and samples from this database, which contains results from onshore field work, core drilling and subsequent analyses. The aim was to use this material as a starting point for addressing key risks and uncertainties for future offshore exploration. Risks for offshore NE Greenland petroleum exploration include in broad terms: (1) the distribution, quality and correlation of the main Upper Jurassic – Lower Cretaceous source rock units, which have an important bearing on the nature of the petroleum products generated, (2) the nature and stratigraphic distribution of potential reservoir and seal rocks (and possible source rocks), primarily in the rather poorly known Cretaceous succession, which is very thick according to the only published seismic interpretation of the Danmarkshavn Basin (Hamann *et al*. 2005) and (3) the subsidence and exhumation history of North-East Greenland.

Project portfolio

In late 2007, a collaboration project, 'Petroleum Geological Studies, Services and Data in East and North-East Greenland', was initiated between GEUS and a number of oil companies. From the start, only little more than a handful of companies chose to participate, but soon the number grew to approximately twenty. The activity was designed with an open end, i.e. to continue for as long as industry interest would last, and it is now entering its seventh year. Participation is open to all companies that actively explore for and exploit petroleum. Upon entry into the group of partners, each company gets: (1) a GIS compilation summarising all available relevant information from North-East Greenland, including geological and palaeogeographical maps, data on >17 000 samples, photographs, logs, potential field data, etc. from onshore North-East Greenland from 70° to 82°N, (2) three reports on 'Petroleum systems', 'Uplift' and 'Seabed Features' mainly based on existing knowledge but including some new and reprocessed data, (3) invitation to semi-annual workshops at GEUS of which the 12th took place in November 2013, (4) access to data, results, power point presentations, etc.

In addition, project partners are invited to participate in a number of projects dedicated to specific topics defined by GEUS. At the end of 2013, nine such projects, including a field excursion to North-East Greenland have been carried out, and an additional four new projects have recently been proposed (Table 1).

Field work and shallow core drilling

Onshore field work, often including shallow core drilling down to approximately 235 m, has been carried out every summer since 2008 (Fig. 1). Each year's field campaign in North-East Greenland lasted 3–6 weeks and comprised 20–30 participants. An overview of the 2008 field season, including preliminary results of the drilling of the Blokelv-1 core hole was presented by Bojesen-Koefoed *et al*. (2009).

A principal target for shallow core drilling was the Upper Jurassic – Lower Cretaceous source rock succession, which is the local equivalent of the deposits that have generated the main part of the petroleum found in the North Sea and its northward extension. The imperfect knowledge of this succession was one of the key problems for assessment of the petroleum potential offshore North-East Greenland (Greenland Sea), and based on available outcrop samples the potential seemed surprisingly poor. Three cores with nearly 100% recovery and a total length of more than 600 m were

Table 1. Overview of completed and proposed projects

Project title	Initiated	Completed	Comments
Data package, Blokelv-1 core, Jameson Land	Oct. 2008	Dec. 2009	Oxfordian–Volgian portion of U. Jurassic – L. Cretaceous source rock succession. Comprehensive sedimentological, stratigraphic and source rock study
Provenance study of possible reservoir sandstone units in East and North-East Greenland	Oct. 2008	Dec. 2010	Based on zircon ages and provenance sensitive minerals. Comprehensive study of potential reservoir sandstone units, >200 samples
Data package, Rødryggen-1 core, Wollaston Forland	Mar. 2010	Dec. 2010	Kimmeridgian–Ryazanian portion of U. Jurassic – L. Cretaceous source rock succession. Comprehensive sedimentological, stratigraphical and source rock study
North-East Greenland uplift history phase II	Mar. 2010	Nov. 2011	Extension of initial uplift study to 78°N
The Cretaceous of North-East Greenland	Jun. 2010	Jun. 2012	Comprehensive study of the entire exposed and mostly poorly known Cretaceous succession
Geology of Store Koldewey	Dec. 2010	Mar. 2012	Important area for understanding the Danmarkshavn Basin. GIS compilation, including core-hole data
Data package, Brorson Halvø-1 core, Wollaston Forland	Apr. 2011	Dec. 2011	Kimmeridgian–Ryazanian portion of U. Jurassic – L. Cretaceous source rock succession in different tectonic settings. Comprehensive sedimentological, stratigraphic and source rock study
Data package, Nanok-1 core, Hold with Hope	Nov. 2011	Nov. 2012	Poorly exposed Cenomanian–Turonian succession Comprehensive sedimentological, stratigraphic and source rock study
The Triassic of the Wandel Sea Basin	Pending		Also highly relevant for Barents Sea geology
The Jurassic–Cretaceous of the Wandel Sea Basin	Pending		Also highly relevant for Barents Sea geology
The tectonic evolution of the Wandel Sea Basin	Pending		Also highly relevant for Barents Sea geology
Northern East Greenland uplift history – focus on the Wandel Sea Basin	Pending		Extension of previous uplift studies to 83°N and northwards

collected, covering the full stratigraphy from the Oxfordian to the Ryazanian (Blokelv-1, Rødryggen-1 and Brorson Halvø-1). More than 600 samples were analysed for petroleum potential and numerous biological marker and isotopic analyses carried out. Integrated with detailed stratigraphic and sedimentological studies they provide a unique insight into the character and development of the succession. Based on these studies, it has been demonstrated that the petroleum potential is 2–3 times higher than expected from initial data and that the succession, contrary to previous beliefs, is complete with only local hiatuses in specific tectonic settings. Core drilling has also been carried out in unexposed intervals of the Cretaceous (Store Koldewey-1, Nanok-1), and in the Triassic (Dunken-1, 2) and Permian successions (Kim Fjelde-1) of Peary Land.

Traditional onshore field work focused on solving predefined problems related to the overall key risks and uncertainties listed in the foregoing. Each season, individual field teams dedicated most of their efforts to one of the various projects (Table 1), while also contributing to other projects where needed. For instance, although both sand provenance and uplift studies were carried out with dedicated field teams, all teams collected samples for mineralogical analysis, apatite fission track analysis (AFTA) and vitrinite reflectance analysis (R_o), ensuring proper geographical and stratigraphic coverage. A small degree of overlap between some projects exists. For instance, the Store Koldewey study was concentrated in a restricted geographical area, but included deposits ranging from Caledonian basement to Pleistocene mud and elements of uplift studies, sand provenance, etc. as integral parts of the study. In contrast, the Cretaceous study concerned a specific, poorly known, portion of the stratigraphic column with scattered outcrops over a huge area (including Store Koldewey). The study was divided into sub-projects such as the erection of a formal and consistent lithostratigraphy, an integrated biostratigraphy that included macrofossils, microfossils (palynomorphs), reservoir model studies, petroleum source rock studies and more.

Published Research

Generally, all results produced during the course of the project are subject to a five-year confidentiality clause that must expire before GEUS can publish detailed results. However, general observations of little or no relevance for the proprietary studies have been published and more are under way. These include studies of igneous rocks (Larsen *et al.* 2013, in press), coal deposits (Bojesen-Koefoed *et al.* 2012; Petersen *et al.* 2013), Palaeogene sediments (Nøhr-Hansen *et al.* 2011), stratigraphy and palaeoenvironments (Alsen & Mutterlose 2009; Nøhr-Hansen 2012; Pauly *et al.* 2012a, b, 2013) and integrated studies (Fyhn *et al.* 2012). A large number of pa-

pers by GEUS scientists are expected in the coming years as confidentiality expires.

Impact on offshore petroleum exploration and perspectives for the future

A better understanding of numerous critical parameters has been achieved, and many of the results have had a strong influence on the development of offshore exploration models. In particular, based on the onshore work a better understanding of source rock distribution, thickness and quality as well as the timing and magnitude of subsidence and uplift have been obtained. In addition, a detailed understanding of the Cretaceous succession will be very important for evaluating future prospects and for correlation when offshore core holes and wildcat wells are eventually drilled.

In recent years, the focus of onshore field activities has shifted northwards, where the deposits of the Wandel Sea Basin (Fig. 1) are important for the understanding of the geology of the northernmost portion of the licence area off North-East Greenland. The northern region is also important for understanding the geology of the Barents Sea shelf, which is an area under intense exploration. Hence, a gradual shift of focus towards the conjugate margin is expected to take place in the coming years.

The nature of the collaboration with the industry in North-East Greenland must be expected to change after allocation of licences. Companies holding licences may change their focus whereas others not holding licences are expected to downgrade their interests in the region. However, GEUS sees an obvious interest in a continued collaboration, since it provides a platform for studies that would otherwise be beyond the economic capacity of the institution, but which are nonetheless important elements of the raison d'être of a geological research institution.

References

Alsen, P. & Mutterlose, J. 2009: The Early Cretaceous of North-East Greenland: A crossroads of belemnite migration. Palaeogeography, Palaeoclimatology, Palaeoecology **280**, 168–182.

Bojesen-Koefoed, J.A., Bjerager, M. & Piasecki, S. 2009: Shallow core drilling and petroleum geology related field work in North-East Greenland 2008. Geological Survey of Denmark and Greenland Bulletin **17**, 53–56.

Bojesen-Koefoed, J.A., Kalkreuth, W., Petersen, H.I. & Piasecki, S. 2012: A remote coal deposit revisited: Middle Jurassic coals at Kulhøj, western Germania Land, northeast Greenland. International Journal of Coal Geology **98**, 50–61.

Christiansen, F.G. 2011: Greenland petroleum exploration: history, breakthroughs in understanding and future challenges. Memoir of the Geological Society (London) **35**, 647–661.

Christiansen, F.G., Gautier, D.L., Stemmerik, L., Bidstrup, T., Bojesen-Koefoed, J.A. & Sørensen, K. 2006: Petroleum resource potential of the East Greenland shelf. AAPG Hedberg Research Conference on Understanding World Oil Resources, Colorado Springs, Colorado, USA, 12–17 November 2006. Extended abstract, poster.

Fyhn, M.B.W., Rasmussen, T.M., Dahl-Jensen, T., Weng, W.L., Bojesen-Koefoed, J.A. & Nielsen, T. 2012: Geological assessment of the East Greenland margin. Geological Survey of Denmark and Greenland Bulletin **26**, 61–64.

Gautier, D.L. 2007: Assessment of undiscovered oil and gas resources of the East Greenland Rift Basins Province. U.S. Geological Survey Fact Sheet **2007-3077**, 4 pp.

Gautier, D.L., Stemmerik, L., Christiansen, F.G., Sørensen, K., Bidstrup, T., Bojesen-Koefoed, J.A., Bird, K.J., Charpentier, R.R., Houseknecht, D.W., Klett, T.R., Schenck, C.J. & Tennyson, M.E. 2011: Assessment of NE Greenland: prototype for development of Circum-Arctic resource appraisal methodology. Memoir of the Geological Society (London) **35**, 663–672.

Hamann, N.E., Whittaker, R.C. & Stemmerik, L. 2005: Geological development of the Northeast Greenland Shelf. In: Doré, A.G. & Vining, A.A. (eds): Petroleum geology: North-West Europe and global perspectives. Proceedings of the 6th Petroleum Geology Conference, 887–902. London: Geological Society.

Larsen, L.M., Pedersen, A.K., Sørensen, E.V., Watt, W.S. & Duncan, R.A. 2013: Stratigraphy and age of the Eocene Igtertivâ Formation basalts, alkaline pebbles and sediments of the Kap Dalton Group in the graben at Kap Dalton, East Greenland. Bulletin of the Geological Society of Denmark **61**, 1–18.

Larsen, L.M., Pedersen, A.K., Tegner, C. & Duncan, R.A. in press: Eocene to Miocene igneous activity in NE Greenland: northward younging of magmatism along the East Greenland margin. Journal of the Geological Society (London), *http://dx.doi.org/10.1144/jgs2013-118*

Nøhr-Hansen, H. 2012: Palynostratigraphy of the Cretaceous – lower Palaeogene sedimentary succession in the Kangerlussuaq Basin, southern East Greenland. Review of Palaeobotany and Palynology **178**, 59–90.

Nøhr-Hansen, H., Nielsen, L.H., Sheldon, E., Hovikoski, J. and Alsen, P. 2011: Palaeogene deposits in North-East Greenland. Geological Survey of Denmark and Greenland Bulletin **23**, 61–64.

Pauly, S., Mutterlose, J. & Alsen, P. 2012a: Lower Cretaceous (upper Ryazanian–Hauterivian) chronostratigraphy of high latitudes (North-East Greenland). Cretaceous Research **34**, 308–326.

Pauly, S., Mutterlose, J. & Alsen, P. 2012b: Early Cretaceous palaeoceanography of the Greenland–Norwegian Seaway evidenced by calcareous nannofossils. Marine Micropaleontology **90–91**, 72–85.

Pauly, S., Mutterlose, J. & Alsen, P. 2013: Depositional environments of Lower Cretaceous (Ryazanian–Barremian) sediments from Wollaston Forland and Kuhn Ø, North-East Greenland. Bulletin of the Geological Society of Denmark **61**, 19–36.

Petersen, H.I, Øverland, J.A., Solbakk T., Bojesen-Koefoed, J.A. & Bjerager, M. 2013: Unusual resinite-rich coals found in northeastern Greenland and along the Norwegian coast: Petrographic and geochemical composition. International Journal of Coal Geology **109–110**, 58–76.

Authors' address

Geological Survey of Denmark and Greenland, Øster Voldgade 10, DK-1350 Copenhagen K, Denmark. E-mail: *jbk@geus.dk.*

Aeromagnetic survey in south-eastern Greenland: project Aeromag 2013

Peter Riisager and Thorkild M. Rasmussen

Aeromagnetic surveys are nowadays used at a wide range of scales and purposes. In frontier and under-explored areas, where data are otherwise sparse or non-existent, aeromagnetic acquisition remains the cheapest and easiest way to obtain or refine a picture of the structural setting. Aeromagnetic data are also useful for strategic planning of geological mapping campaigns and detailed geophysical data acquisition. Moreover, aeromagnetic data are of importance for prospecting, helping to define prospects. Large aeromagnetic surveys can be carried out efficiently and safely almost everywhere, in a short period of time and at reasonable cost.

In the following we present the newly released *Aeromag 2013* aeromagnetic survey that covers a remote and relatively under-explored coastal region in south-eastern Greenland, stretching from 64°45′N and northward to 67°30′N (Fig. 1). The survey represents a total of 65 492 line km, and covers an area of 30 100 km^2, adding a significant new dataset to the already existing database of government-financed geophysical surveys in Greenland. With the completion of the *Aeromag 2013* project, the database presently contains a total of *c.* 633 500 line km of high-resolution aeromagnetic data and *c.* 75 000 line km of multi-parameter data (electromagnetic, magnetic and partly radiometric data). Further details on previous surveys on Greenland and the database of available aeromagnetic data are summarised in Rasmussen *et al.* (2013; see also Fig. 1).

Details of the Aeromag 2013 survey

EON Geosciences Inc. flew the *Aeromag 2013* survey between 13 June and 2 September 2013, using two Piper Navajo PA-31 aircraft equipped with geophysical instruments (detailed below), and operating out of the airport at Kulusuk. The magnetic base stations used for correction of diurnal magnetic variations were installed at two different locations in Kulusuk.

The survey was carried out by flying along a gently draped surface 300 m above the ground or sea level. Due to the severe topography ranging from sea level to *c.* 2450 m, the gentle drape resulted in an average height above ground of 711 m. The survey lines were NE–SW-oriented, parallel to the coastline with a separation of 500 m while orthogonal tie-lines were flown with a separation of 5000 m. Total magnetic field data were recorded with a sampling interval of 0.1 sec. which corresponds to a sample distance of *c.* 7 m. The magnetic field at the base station was recorded with a 1 sec. sampling interval. Aircraft positional data from differential GPS measurements were recorded with a 1 sec. sampling interval, and aircraft altitude measurements obtained from barometric altimeter and radar were recorded with a sampling interval of 0.1 sec. A continuous digital video recording of the terrain passing below was also produced. Further details on the survey operation and equipment can be found in a report by EON Geosciences Inc. (2013), which is available at the online DODEX database at the Geological Survey of Denmark and Greenland (Riisager *et al.* 2011).

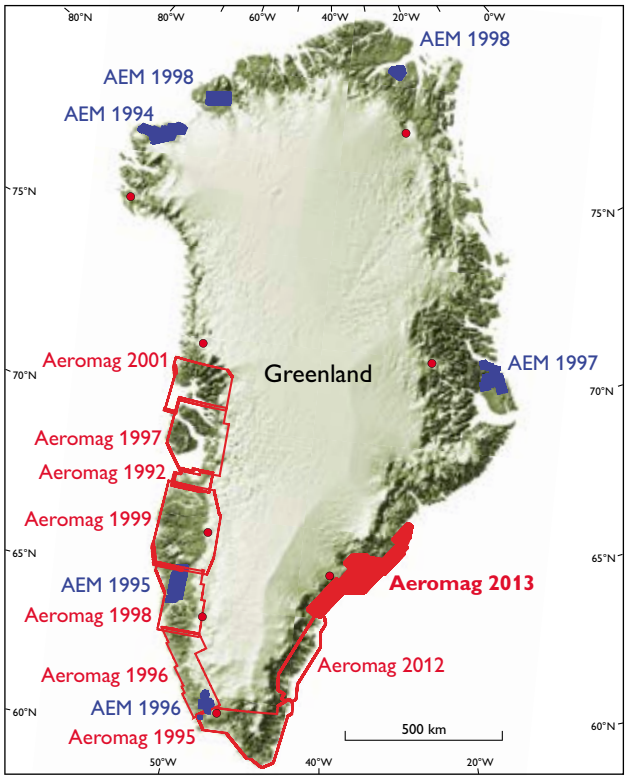

Fig. 1. Map of Greenland showing the location of government-financed high-resolution airborne geophysical surveys conducted from 1992 to 2014. Red: aeromagnetic surveys (Aeromag). Blue: combined electromagnetic and magnetic surveys (AEM).

Results and products

The *Aeromag 2013* survey dataset can be obtained as line data in the format of a Geosoft database. In addition two map sheets at scales of 1:250 000 and 35 map sheets at scales of 1:50 000 have been produced from interpolation and gridding of the data. The map sheets are available as both grid-files and pdf-files. Each of the map sheets shows the total magnetic field intensity and first and second vertical derivatives. Figure 2 shows the gridded total magnetic field intensity data for the entire survey area. The International Geomagnetic Reference Field corresponding to the date and location of the measurement has been subtracted from the data leaving the magnetic anomalies caused by the variation of magnetisation in the uppermost crust. Superimposed on the magnetic anomaly data in Fig. 2 is a shaded relief modelled by using a light-source illumination inclination of 45° and a declination of 45° (i.e. a light-source from the northwest).

Release of data

The completion of the *Aeromag 2013* project was marked by the release of the data on 3 March 2014. The data can be obtained for free from the Ministry of Industry and Mineral Resources in Greenland by submitting a form available at the Greenland Mineral Resources portal (***http://www.greenmin.gl/***).

Magnetic anomaly maps and geological implications

The surface geology of the surveyed region is shown on the map in Fig. 3. The survey covers the eastern part of the Nagssugtoqidian orogen that mainly consists of reworked Archaean gneisses with minor supracrustal rocks and several Palaeoproterozoic intrusives (Bridgwater *et al.* 1990; Kolb in press). Palaeogene intrusions and coast-parallel dykes are found in the northern part of the survey area (Tegner *et al.* 1998).

The magnetic anomalies mapped in the *Aeromag 2013* survey area range in amplitudes between –1318 nT and +3270 nT, with both the most negative and positive values relating to mapped intrusions (Figs 2, 3). In the southern part of the survey area, several NNE–SSW-trending subparallel linear and positive anomalies (marked I in Fig. 2) are clearly discernible, and most likely represent large dykes. The anomalies can be traced in the survey area over more than

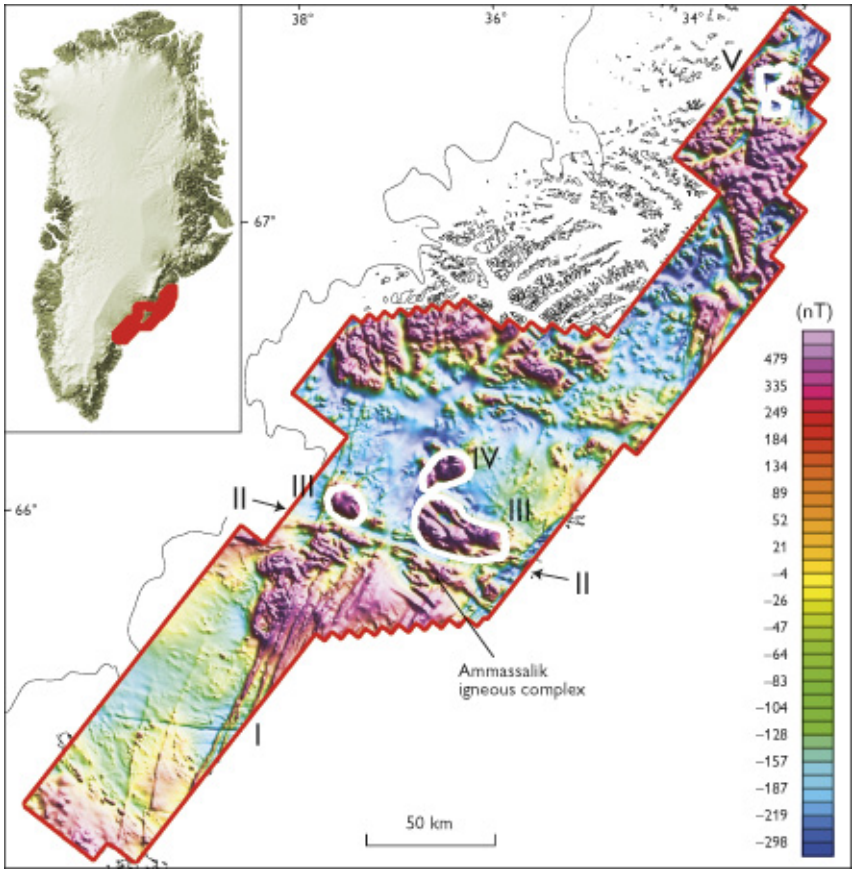

Fig. 2. Aeromagnetic anomaly map of the survey area in south-eastern Greenland covered during the *Aeromag 2013* project. **I–V**: magnetic anomalies discussed in the text. **I**: Possible large dykes NNE–SSW. **II**: Magnetic E–W low. **III**: Ammassalik igneous complex. **IV**: 1.9–2.2 Ga diorite intrusion. **V**: Kruse Fjord gabbro complex.

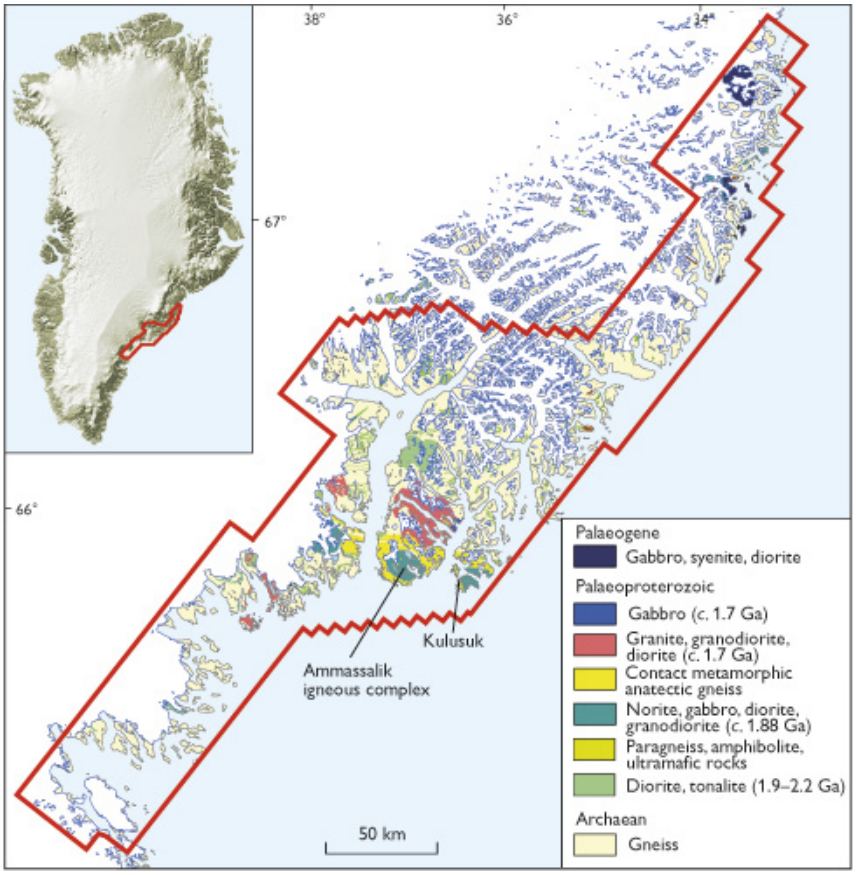

Fig. 3. Geological map of the survey area in south-eastern Greenland (modified from Escher 1990). Red: the Aeromag 2013 survey area. **I–V**: magnetic anomalies discussed in the text.

120 km and presumably extend offshore. To the north, several of these anomalies appear to be truncated by a magnetic low (II; Fig. 2) just north of the Ammassalik igneous complex. The magnetic anomalies measure 1–2 km across and have amplitudes in the order of 300 nT, with a magnetisation direction enhancing the present geomagnetic field suggesting a magnetisation dominated by induced magnetisation or a remanent magnetisation with a direction in the same general direction as the present geomagnetic field or both. The linear magnetic anomalies, which are mainly found offshore, are both much larger, and have a different orientation than the ENE–WSW-striking mafic dykes mapped in the area (Bridgwater *et al.* 1990). In order to estimate the depth of the source of the magnetic anomalies, Euler deconvolution (Reid *et al.* 1990) was carried out using the Standard Euler 3D method of the Geosoft package software v. 8.1. The method is based on Euler's homogeneity equation that relates the magnetic field and its gradient components to the location of the source. The system uses a least squares method to solve Euler's equation simultaneously for each grid position within a window and then determines the anomaly position, depth, and base level for a specific magnetic source. The most critical parameter in the Euler deconvolution is the structural index, which enters as an exponential factor corresponding to the rate at which the field falls off with distance, for a source of a given geometry. For our analysis we used a structural index value of 1, which is suitable for a dyke, and a window size of 2 km. The resulting depth estimates for the top of the dykes are generally below 400 m. Given the uncertainty of the depth estimates, and the up to 200 m water depth in the offshore area (Becker *et al.* 2009) where the magnetic anomalies are best defined, it is possible that the dykes are exposed near the coast. Finally, we note that the Kangâmiut dykes found in West Greenland, in a similar location on the North Atlantic craton (south of the central part of the Nagssugtoqidian orogen in West Greenland) are much less prominent magnetically (Rasmussen & van Gool 2000; Korstgård *et al.* 2006) than the linear magnetic anomalies seen in the *Aeromag 2013* survey area. We tentatively interpret the linear magnetic anomalies as massive dykes.

The E–W-trending magnetic low just north of the Ammassalik igneous complex marked II in Fig. 2 coincides with a suggested suture zone of the Nagssugtoqidian orogen, where the Rae craton to the north-east in an oblique WSW-directed subduction collided with the North Atlantic craton south of the suture zone at *c.* 1870–1885 Ma (Kolb in press). The suggested location of the suture zone is also supported by the apparent abrupt termination of several of the positive

NNE–SSW-trending anomalies marked I on Fig. 2 and discussed above.

North of the Ammassalik igneous complex the *c.* 1.7 Ga post-orogenic granodiorite intrusion marked III in Fig. 2 is clearly defined by positive magnetic anomalies with amplitudes up to almost 2000 nT. Similarly, the older 1.9–2.2 Ga diorite intrusion farther north marked IV in Fig. 2 is associated with a strong (*c.* 2500 nT) positive magnetic anomaly. The strongest magnetic anomalies in the Aeromag 2013 survey area are found in the northern part of the survey area and can be related to the Palaeogene intrusions in the area. The Kruuse Fjord gabbro complex marked V in Fig. 2 is related to a negative anomaly, hence having a magnetisation dominated by reversely magnetised remanent magnetisation, which is in excellent accordance with an Ar-Ar isochron age of 48.0 ± 1.2 Ma, and emplacement of the intrusive complex during the reverse C21R chron (Cande & Kent 1995).

Conclusions

In this paper we present the newly released *Aeromag 2013* survey that adds new and exciting data to the already extensive database of Greenland aeromagnetic data. The paper focuses on magnetic anomalies of regional extent, including sub-parallel linear and positive anomalies trending NNE–SSW (marked I on Fig. 2) that we suggest stem from hitherto undiscovered very large dykes. The suggested location of the suture zone of the Nagssugtoqidian just north of the Ammassalik igneous complex (II; Fig. 2) is supported by the aeromagnetic data. Finally, we note a general good correspondence between the mapped surface geology of the region and the aeromagnetic data; in particular, the intrusions which are clearly discernible. The magnetic data provide a basis for further analysis and modelling of the 3D geometry of the igneous intrusions. Many more local anomalies can be identified in the *Aeromag 2013* dataset but interpretations require further analyses.

Acknowledgements

Funding of the *Aeromag 2013* project was provided by the Ministry of Industry and Mineral Resources, Government of Greenland. Thanks are due to EON Geosciences Inc. for fulfilling all aspects of their contracts in a professional manner.

References

Becker, J.J. *et al*. 2009: Global bathymetry and elevation data at 30 arc seconds resolution: SRTM30_PLUS. Marine Geodesy **32**, 355–371.

Bridgwater, D., Austrheim, H., Hansen, B.T., Mengel, F., Pedersen, S. & Winter, J. 1990: The Proterozoic Nagssugtoqidian mobile belt of southeast Greenland: a link between the eastern Canadian and Baltic shields. Geoscience Canada **17**, 305–310.

Cande, S.C. & Kent, D.V. 1995: Revised calibration of the geomagnetic polarity timescale for the Late Cretaceous and Cenozoic. Journal of Geophysical Research, Solid Earth **100**, 6093–6095.

Eon Geosciences Inc. 2013: Final survey report. High resolution aeromagnetic survey, Southeast Greenland Aeromag 2013 Block, 31 pp. Unpublished report, Eon Geosciences Inc., Montreal, Quebec, Canada (in archives of the Geological Survey of Denmark and Greenland, report File **23712**).

Escher, J.C. 1990: Geological map of Greenland, 1:500 000, Sheet 14, Skjoldungen. Copenhagen: Geological Survey of Greenland.

Kolb, J. in press: Structure of the Palaeoproterozoic Nagssugtoqidian Orogen, South-East Greenland: model for the tectonic evolution. Precambrian Research, *http://dx.doi.org/10.1016/j.precamres.2013.12.015*

Korstgård, J.A., Stensgaard, B.M. & Rasmussen, T.M. 2006: Magnetic anomalies and metamorphic boundaries in the southern Nagssugtoqidian orogen, West Greenland. Geological Survey of Denmark and Greenland Bulletin **11**, 179–184.

Rasmussen, T.M., Thorning, L., Riisager, P. & Tukiainen T. 2013: Airborne geophysical data from Greenland. Geology and Ore, Exploration and Mining in Greenland. **22**, 12 pp.

Rasmussen, T.M & van Gool, J.A.M. 2000: Aeromagnetic survey in southern West Greenland: project Aeromag 1999. Geology of Greenland Survey Bulletin **186**, 73–77.

Reid, A.B., Allsop, J.M., Granser, H., Millett, A.J. & Somerton, I.W. 1990: Magnetic interpretation in three dimensions using Euler deconvolution. Geophysics **55**, 80–90.

Riisager, P., Pedersen, M., Jørgensen, M.S., Schjøth, F. & Thorning, L. 2011: DODEX – geoscience documents and data for exploration in Greenland. Geological Survey of Denmark and Greenland Bulletin **23**, 77–80.

Tegner, C., Duncan, R.A., Bernstein, S., Brooks, C.K., Bird, D.K. & Storey, M. 1998: ^{40}Ar–^{39}Ar geochronology of Tertiary mafic intrusions along the East Greenland rifted margin: relation to flood basalts and the Iceland hotspot track. Earth and Planetary Science Letters **156**, 75–88.

Authors' address

Geological Survey of Denmark and Greenland, Øster Voldgade 10, DK-1350 Copenhagen K, Denmark. E-mail: *pri@geus.dk*.

Combining exploration and multivariate techniques to detect the Bjørnesund West gold occurrence, southern West Greenland

Denis Martin Schlatter and Bo Møller Stensgaard

Gold exploration in the Bjørnesund region has been carried out since the early 1990s, and gold was found in the central part of the Bjørnesund East area by NunaOil and the Geological Survey of Denmark and Greenland (GEUS). Records of stream sediment samples with elevated gold concentrations up to several hundred parts per billion led to the recognition that amphibolites in the central part of the Bjørnesund East could be a promising target and work in 1996 led to the discovery of hydrothermally altered amphibolites with up to several hundred ppb gold. However, exploration work was limited to grassroots prospecting and none of the targets were drilled. The aim of new field work was to target areas in the Bjørnesund supracrustal belt which mainly consists of amphibolites but also comprises significant proportions of diorite, anorthosite, leucogabbro, granitoid rocks and ultramafic to mafic rocks that occur as relatively thin slivers in the amphibolite. We tested if the targeted areas were favourable for gold mineralisation and investigated the relationship between the mineral potential mapping and the actual geology. Here we demonstrate that based on older data we located new gold mineralising systems in the western part of the Bjørnesund supracrustal belt, identified platinum-enriched mafic to ultramafic rocks and located new occurrences of corundum at amphibolite-anorthosite contacts (Schlatter

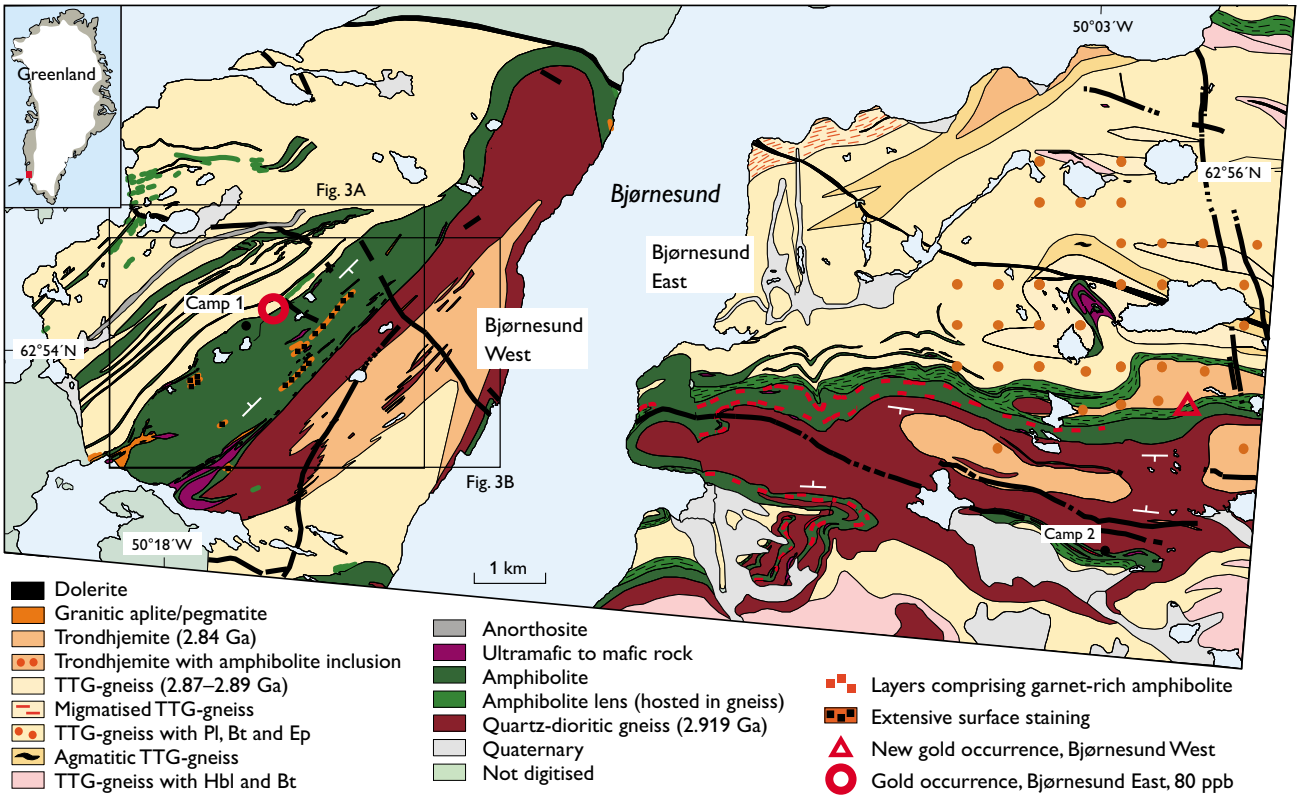

Fig. 1. Geological map of the Bjørnesund West and East areas showing the location of the newly discovered gold occurrence in Bjørnesund West. Prior to field work by GEUS in 2009, no gold occurrences were reported here. Black outlines indicate the sampled areas of Bjørnesund West, regarding sampling density see Fig. 3.

& Stensgaard 2012). We also show how lithogeochemical studies were useful to define the main rocks types, chemostratigraphic relations and hydrothermal alteration of the newly discovered gold mineralisation. Based on our study, we encourage the use of artificial neural network analysis and data interpretation prior to field work in Greenland in areas where only relatively little geological and mineral exploration work has been conducted and where the field season is relatively short.

Geology of the Bjørnesund area

The Bjørnesund supracrustal belt (Keulen *et al.* 2010) is of Mesoarchaean age, *c.* 50 km long and a few hundred metres to 3 km wide (Fig. 1). Amphibolites dated to 2947 ± 47 Ma are bounded towards the north and south by 2920–2810 Ma tonalite-trondhjemite-granodiorite (TTG) gneisses (Keulen *et al.* 2010; Kolb *et al.* 2013) that are interpreted to have been intruded into the amphibolites. Sheets of leucogabbro, gabbro and anorthosite are interpreted to have been intruded into the amphibolites at about 2950 Ma and were in turn intruded by quartz dioritic protoliths at 2920 Ma (Keulen *et al.* in press). Finally, late granites were intruded into the sequence of quartz-diorite amphibolite and anorthosite-gabbro between 2860 and 2830 Ma (Kolb *et al.* 2013). The rocks were affected by F1 folding into an isoclinal synform and F2 folding at 2850–2830 Ma with an E–W-trending fold axis, which is the most dominant structural feature in the Bjørnesund area (Keulen *et al.* in press). The F2 folding is associated with thrusting that caused shearing with only minor displacement. Finally, F3 NNW–SSE-trending folds have bent the regional foliation slightly.

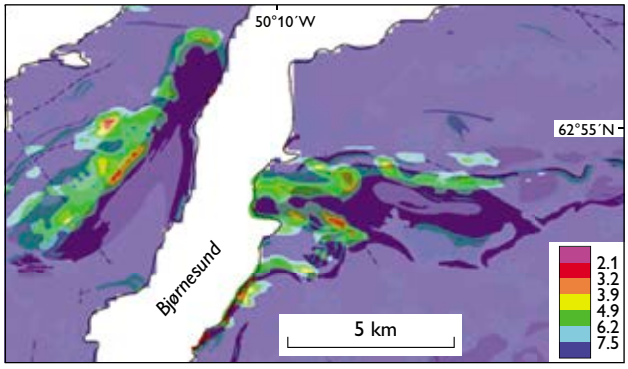

Fig. 2. Neural network analysis for gold favourable areas in the Bjørnesund West and East areas. Top 8.5% most favourable areas for gold in seven coloured intervals according to the neural network analysis of As, Cs, Rb, Sb and U stream sediment geochemistry and lineaments. A geological map is placed beneath the neural network analysis result, which is transparent.

Methods

A total of 116 rock samples (900 g) and 56 stream sediment samples (200 g) were collected during the field work and used for geochemical and petrographic investigations. Rock samples were crushed and milled by Actlabs laboratory in Ontario, Canada, and stream sediment samples were sieved at GEUS using a 0.18 mm sieve. The fine-grained fraction was sent to Actlabs for analysis. Gold was analysed by instrumental neutron activation whereas major and trace elements were analysed using Actlabs package '4Lithoresearch'. The U-Pb ages of zircon grains from four plutonic rock samples were also determined by Keulen *et al.* (in press). An artificial neural network is a mathematical and computational structure simulating the human neural network (the brain). Information, in the form of input data, which are presented to the network causes the network to learn and recognise patterns in the data. For instance, when a network is shown multiple datasets for known gold occurrences, it is able to identify and memorise possible patterns in the datasets associated with the occurrences which can be regarded as training points for the network. Afterwards, when the network is shown datasets from areas without any known gold occurrences, the network applies what it has learned and looks for patterns in the datasets that are similar to those recognised for the known gold occurrences. In that way, areas can be classified and mapped according to how similar their data patterns are to the patterns from the known gold occurrences. These areas can be regarded as potential to host gold occurrences.

Mineral potential mapping

Artificial neural network analysis (Stensgaard 2013) was used for mineral potential mapping (Fig. 2) together with Ni/Mg ratios from analysed stream sediment samples. This led to the identification of portions of the western and eastern parts of the Bjørnesund supracrustal belt as the most favourable for gold occurrences. Areas with anomalously high levels of Fe^{3+} were identified using ASTER satellite images, and correspond to ultramafic dunitic and pyroxenitic rocks (Schlatter & Stensgaard 2012). The most favourable areas, as identified from artificial neural network analysis, coincide with areas of stream sediments with elevated Ni/Mg ratios. Based on these detailed analyses, the Bjørnesund West and East areas were selected for field work with the aim to characterise the geological environment and evaluate the gold potential. A new detailed and geo-referenced digital geological map was compiled after the new field work (Fig. 1) and a new interesting gold occurrence was found in a hydrothermally altered shear zone in the amphibolites of the Bjørnesund

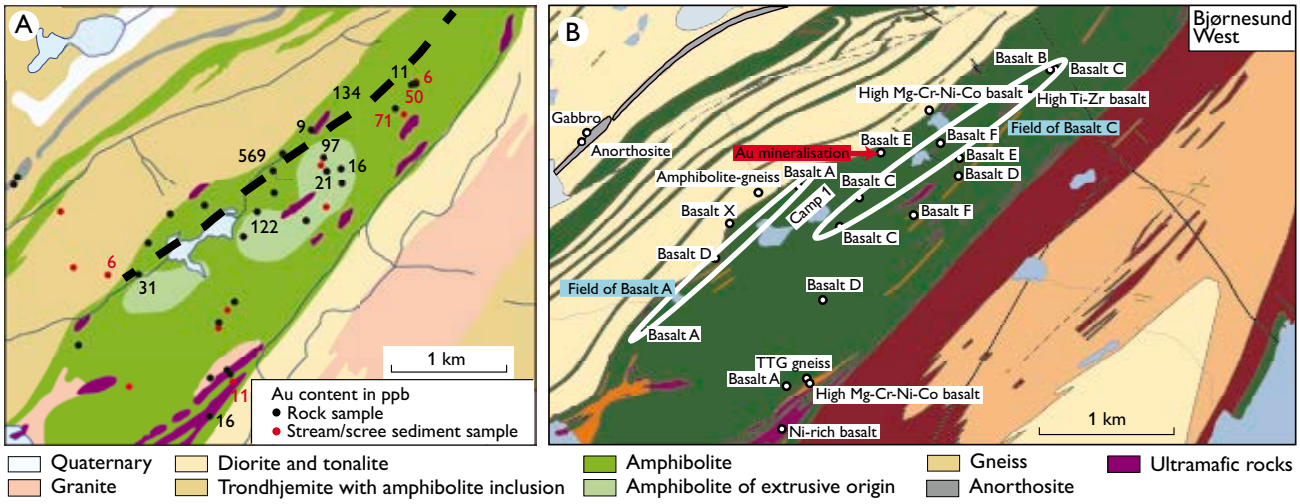

Fig. 3. **A**: Gold anomaly plot of sediment and rock samples from the Bjørnesund West area. A several tens-of-metres wide shear zone (dashed line) with gold-mineralised portions was discovered at 62°54.4′N, 50°16.2′W and at 555 m a.s.l. Legend below figure. **B**: Chemostratigraphic relation seen from the Bjørnesund West area. A rock unit which comprises mainly basalt A and a unit comprising mainly basalt C can be identified based on lithogeochemical immobile element techniques. The gold occurrence is found in rocks of basalt E type, and have basalt A and C in the structural footwall. For legend see Fig. 1.

West area. This several tens-of-metres wide NE–SW-trending shear zone (Figs 1, 3A) dips 80° SE. It can be followed over several hundred metres along strike and contains a 50 cm yellow-brownish, rusty-stained amphibolite, which hosts parallel quartz-carbonate-feldspar veinlets. Chip samples collected over this altered unit yielded 569 ppb Au (Fig. 3A), and alteration related to this gold occurrence was identified to be of the garnet-biotite-iron oxide-hydroxide type (Kolb *et al.* 2013). These new findings, together with elevated gold concentrations in stream sediment and rock samples along the same NE–SW-trending shear zone, indicate that the Bjørnesund supracrustal belt may host undiscovered gold occurrences and confirm that stream sediment sampling is a powerful exploration tool (Fig. 3A). Furthermore, nickel and platinum-group elements could also constitute a target as pentlandite was identified in an ultramafic rock sample with elevated concentrations of Ni, Cr, Co and PGE from Bjørnesund East (Fig. 1; Schlatter & Stensgaard 2012).

Chemostratigrapy and hydrothermal alteration

Based on lithogeochemical immobile-element-ratio classification (Barrett & MacLean 1994) seven types of amphibolite and three different types of other mafic to ultramafic rocks (high Mg-Cr-Ni-Co, Ni-rich and high-Ti-Zr basalt) were distinguished (Figs 1, 3B). The gold horizon was located at the contact of basalt A and basalt E (Fig. 3B). Amphibolites with elevated gold concentrations (less than 100 ppb) were also located in Bjørnesund East (Fig. 1, *c.* 2 km north-east of camp 2) where the ore horizon is also located at the contact of basalt A and basalt E (Schlatter & Stensgaard 2012). It appears that this basalt A – basalt E contact represents a good geochemical marker horizon in the Bjørnesund supracrustal belt. Changes were calculated for 35 basalt samples from the Bjørnesund area using the single precursor approach (MacLean & Barrett 1993). The results show that the richest gold-bearing basalt with 569 ppb Au from Bjørnesund West (Fig. 3B, encircled in white) is characterised by strong additions of FeO and silica (Fig. 4A) and by gain of CaO and loss of K_2O (Fig. 4B). In contrast, a basalt sample from Bjørnesund East with 80 ppb Au (Fig. 1) shows only a small loss of silica, no change of iron, gain of K_2O and loss of CaO (Fig. 4). We conclude that favourable alteration associated with gold mineralisation is characterised by silicification combined with addition of FeO and CaO.

Discussion and conclusions

Mineral potential mapping was successful because it indicated areas containing gold-mineralised rocks and pinpointed unusual mafic to ultramafic rocks where elevated concentrations of nickel and platinum-group metals were subsequently identified. Extensive rust zones were identified from ASTER satellite data, some of which correspond to the mafic to ultramafic rock units with elevated Ni, Cr, Co and PGE contents; several of the ultramafic to mafic rocks fall into the komatiite field and pentlandite was identified by microprobe analysis in one sample (Schlatter & Stensgaard 2012).

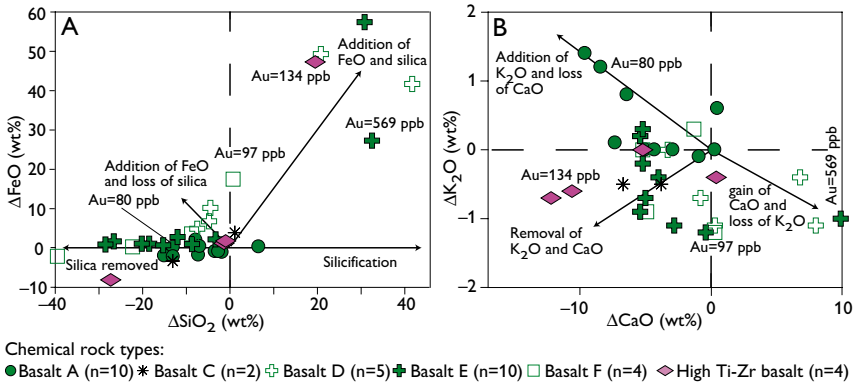

Fig. 4. Hydrothermal alteration based on mass-change calculations for 35 rocks from the Bjørnesund West and East areas. **A**: ΔSiO_2 versus Δ FeO. **B**: ΔCaO versus ΔK_2O. Mass changes were calculated using the method described by Barrett & MacLean (1994). Mass changes are reported in wt% change (Δ) relative to the precursor rock.

Chemostratigraphic interpretations show that the Au horizon is located at the contact between basalt A and basalt E and can be followed along the Bjørnesund supracrustal belt for at least 10 km (Figs 1, 3) so that this horizon represents an exploration target for gold and provides evidence of an E–W continuation. Alteration related to Au mineralisation is of garnet-biotite-iron oxide-hydroxide type and quartz-carbonate-feldspar veinlets occur in an amphibolite-hosted thrust-shear zone between quartz-dioritic gneiss and gneiss. Mass-change calculations show that favourable 'Au-alteration' is characterised by gains of FeO, SiO_2 and CaO and enrichment of As, Sb and Zn (Schlatter & Stensgaard 2012). The spatial association of gold occurrences and granite-trondhjemite rocks (Fig. 1) possibly indicates that the granitoids played a role in the emplacement of the gold. The association of gold and nickel is intriguing (Schlatter & Steensgaard 2013) and could be related to deep structures which might have been activated during events similar to those described by Fiorentini *et al.* (2012) from the highly nickel-enriched Agnew-Wiluna greenstone belt in western Australia where felsic and komatiitic magmas are related to deep crustal conduits.

With respect to the timing of events of the Bjørnesund supracrustal belt, we suggest that ultramafic rocks, leucogabbro and anorthosite were intruded into amphibolites (Fig. 1). This event may have been coeval with orthomagmatic nickel-platinum group-element mineralisation and isoclinal F1 folding. It is suggested that gold was then orogenically emplaced between 2860 and 2830 Ma (Kolb *et al.* 2013) at peak regional metamorphism. Finally, late F3 deformation events created faulting in a staircase-like outcrop pattern at 2710–2700 Ma (Keulen *et al.* in press). This study represents a coupled effort of artificial neural network analysis and targeted field exploration and shows that such an approach can be efficient and successful in identifying new exploration targets of gold, nickel-platinum group elements and corundum.

References

Barrett, T.J. & MacLean, W.H. 1994: Chemostratigraphy and hydrothermal alteration in exploration for VHMS deposits in greenstones and younger volcanic rocks. In: Lentz, D.R. (ed.): Alteration and alteration processes associated with ore-forming systems. St. John's: Geological Association of Canada. Short Course Notes **11**, 433–467.

Fiorentini, M., Beresford, S., Barley, M., Duuring, P., Bekker, A., Rosengren, N., Cas, R. & Hronsky J. 2012: District to camp controls on the genesis of komatiite-hosted nickel sulfide deposits, Agnew-Wiluna Greenstone Belt, Western Australia: insights from the multiple sulfur isotopes. Economic Geology **107**, 781–796.

Keulen, N., Kokfelt, T.F. & Scherstén, A. 2010: Notes on the common legend to the 1:100 000 digital geological map of southern West and South-West Greenland, 61°30′–64°N. Danmarks og Grønlands Geologiske Undersøgelse Rapport **2010/119**, 41 pp.

Keulen *et al.*, in press: Meso- and Neoarchaean geological history of the Bjørnesund Supracrustal Belt, southern West Greenland: settings for gold enrichment and corundum formation. Precambrian Research.

Kolb, J., Dziggel, A. &. Schlatter, D.M. 2013: Gold occurrences of the Archean North Atlantic craton, southwestern Greenland: a comprehensive genetic model. Ore Geology Reviews **54**, 29–58.

MacLean, W.H. & Barrett T.J. 1993: Lithogeochemical techniques using immobile elements. Journal of Geochemical Exploration **48**, 109–133.

Schlatter, D.M. & Stensgaard, B.M. 2012: Evaluation of the mineral potential in the Bjørnesund Greenstone Belt combining mineral potential mapping, field work and lithogeochemistry. Danmarks og Grønlands Geologiske Undersøgelse Rapport **2012/60**, 60 pp.

Schlatter, D.M. & Stensgaard, B.M. 2013: Evaluation of the mineral potential in the Bjørnesund greenstone belt, southern West Greenland, combining multivariate studies, field work and geochemistry. 11th Swiss Geoscience Meeting, Lausanne, 15–16 November 2013. Abstracts, 74–75.

Stensgaard, B.M. 2013: Analysis of regional data sets: predictive gold potential using neural network analysis. Danmarks og Grønlands Geologiske Undersøgelse Rapport **2013/15**, 27–81.

Authors' addresses

D.M.S.* & B.M.S., *Geological Survey of Denmark and Greenland,* Øster *Voldgade 10, DK-1350 Copenhagen K, Denmark.*

*Present address: *Helvetica Exploration Services GmbH, Carl-Spitteler-Strasse 100, CH-8053 Zürich, Switzerland.*

E-mail: *denis.schlatter@helvetica-exploration.ch*

Integrating 3D photogeology with aeromagnetic data as a tool for base-metal exploration in East Greenland

Anaïs Brethes, Pierpaolo Guarnieri and Thorkild M. Rasmussen

An 800 km long basin system developed along the East Greenland margin since the Late Palaeozoic in which the Jameson Land Basin forms the southern part of the system. Along the margins of the Jameson Land Basin there are occurrences of barite, copper, lead, zinc and silver, which are particularly abundant in the northern part of the basin's eastern margin in the Wegener Halvø area (Fig. 1). Structures and stratigraphic architecture play important roles in the mineralisation distribution, so detailed mapping is essential. We used 3D photogeology combined with geophysical data to map the different stratigraphic units, faults and dykes in three dimensions.

Geological setting of Jameson Land Basin

The East Greenland Basin began to develop during the Devonian following the Caledonian orogeny. In the Late Carboniferous and Early Permian rotational block faulting took place (Surlyk 1990). The faults were reactivated during the Late Permian and Early Triassic and synsedimentary faulting occurred at the same time (Seidler 2000). The resulting fault blocks were peneplained before transgression and onset of sedimentation in the Late Permian. On Wegener Halvø the up to 300 m thick Upper Permian sequence unconformably overlies deformed and peneplained Devonian sediments (Fig. 1). The sequence is dominated by karstified dolomitic limestone of the Karstryggen Formation, by carbonate buildups which developed on palaeotopographic highs (the Wegener Halvø Formation) and by bituminous dark shale of the Upper Permian Ravnefjeld Formation. These filled up the deepest and karstified parts of the previous formations and locally contain calcareous concretions and fossils derived from the carbonate buildups. The unconformable to conformable Permian–Triassic boundary is locally incised by submarine canyons (Seidler 2000). Laterally variable, the Triassic stratigraphic architecture was controlled by tectonics and rapid asymmetric subsidence. This entire sequence is mainly composed of continental deposits with some shallow marine incursions. In the Tertiary the Jameson Land Basin was covered by flood basalt and intruded by a complex of sills and E–W to NW–SE-trending dykes. The intrusions that are dated to the latest Paleocene to earliest Eocene (Soper *et al*. 1976) affect the entire sequence of basin fill. In Miocene time the northern part of the basin was uplifted more than 1 km (Mathiesen *et al*. 2000; Hansen *et al*. 2001).

Base-metal mineralisation on Wegener Halvø

The first rock samples were collected in East Greenland in 1822 and during the Three-year Expedition to East Greenland from 1931 to 1934 copper-, lead- and silver-bearing minerals were discovered on Wegener Halvø (Fig. 1), in the Upper Permian carbonates of the Wegener Halvø Formation. Subsequent investigations by Nordisk Mineselskab A/S (Nordmine) led to the discovery in 1968 of base-metal occurrences in the black shale of the Ravnefjeld Formation. Min-

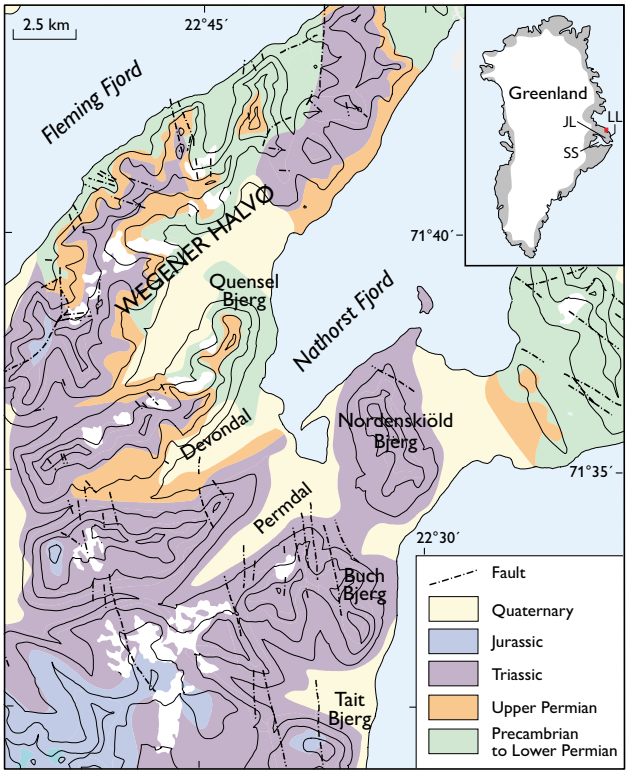

Fig. 1. Simplified geological map of the Wegener Halvø area (modified from Perch-Nielsen *et al*. 1983). **SS**: Scoresby Sund. **JL**: Jameson Land. **LL**: Liverpool Land. Contour interval 200 m.

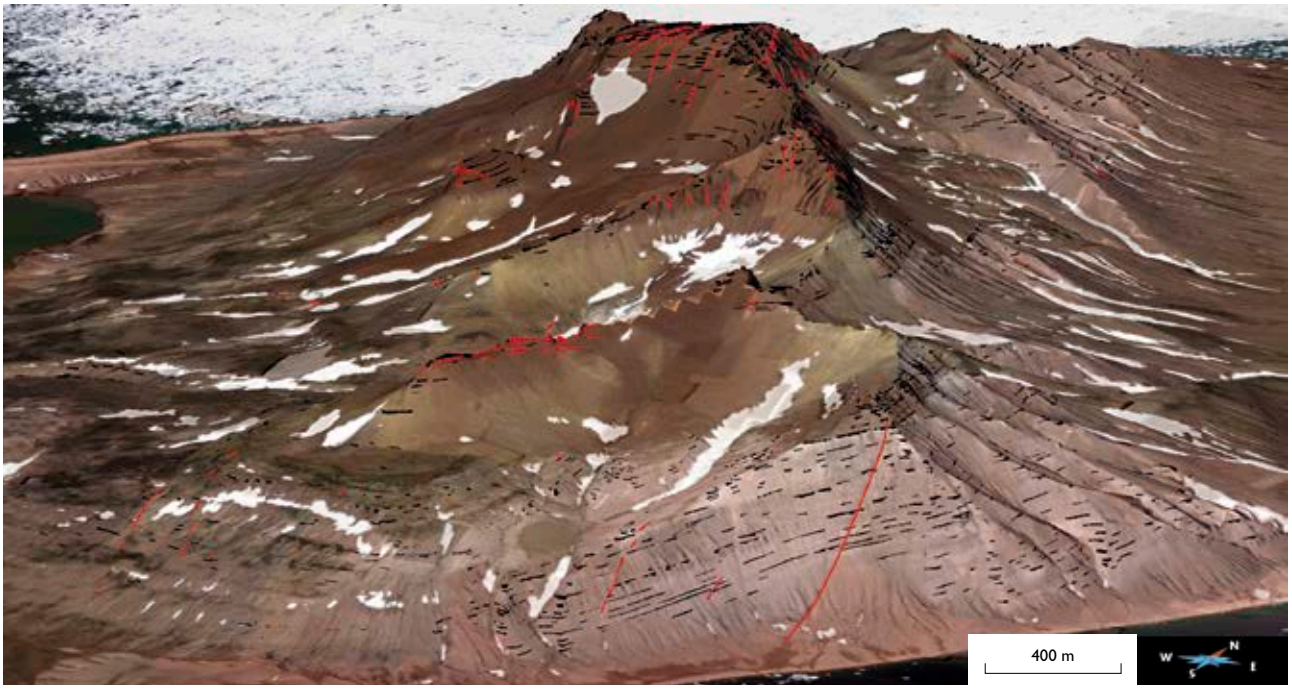

Fig. 2. 3D view from the south towards Nordenskiöld Bjerg created with orthophotographs draped on a digital elevation model developed from LIDAR data. The geological features collected from aerial photographs are: faults and fractures (red lines) and Triassic bedding (black lines).

eral exploration ceased because the ore was too low grade, but the oil industry became interested in the hydrocarbon source-rock potential of the Upper Permian shale. Harpøth *et al*. (1986) reviewed more than a century of these sporadic field campaigns and since 2011 Avannaa Resources Ltd has explored the area for base metals. Mineral occurrences are particularly abundant along the eastern margin of the Jameson Land Basin, especially in the Wegener Halvø area where they occur in three of the Upper Permian formations and three of the Triassic formations. One of the most interesting ore-bearing formations is the limestone buildups of the Wegener Halvø Formation. As described by Harpøth *et al*. (1986), Cu, Pb and Zn sulphides are scattered throughout the whole peninsula. They are also found as fine-grained material in inter-reef black-shale occurrences in the Ravnefjeld Formation. Base-metal minerals are mainly found in the upper part of the carbonates and in the lower part of the shales (Upper Permian formations), but stratiform occurrences occur in Triassic sediments. Early Triassic alluvial conglomerate and arkosic sandstone are mineralised with argentiferous chalcocite-covellite, and galena occurs as cement. According to soil sample geochemical analyses, the highest grades appear to be concentrated at the contact between two facies, in a trend perpendicular to the palaeocurrents (Harpøth *et al*. 1986). In the Late Triassic playa-lake mudstone and sandstone, fine-grained Cu sulphides are found over an area of 1000 km^2.

3D photogeology

The Geological Survey of Denmark and Greenland is equipped with a 3D stereoplotter to carry out multi-model photogrammetry that can be used to accurately map geological features from vertical and oblique aerial photographs. The instrument is equipped with two polarised monitors set one above the other with an angle of 110° separated by a half-mirror (Vosgerau *et al.* 2010). Each polarised screen displays one photograph of an overlapping stereopair. The half-mirror allows the viewer to see two photographs as one image with 3D polarised glasses getting a depth perception of the geological features that, in turn, can be digitised as 3D polylines. The geologic features and the database are automatically imported into a geographic information system where they can be edited. The photographs used for the present work were taken during a combined hyperspectral and LIDAR survey in 2012 (Thorning *et al.* in press). The spacing between the flight lines was *c.* 500 m and the pixel size in the centre of each image is 27 × 27 cm.

On Wegener Halvø, an area of 100 km^2 comprising Devondal and Nordenskiöld Bjerg was mapped on a scale of 1:1000 (Fig. 1). More than 5000 features were digitised, including bedding, stratigraphic boundaries as well as fractures and dykes (Fig. 2). Together with the digitised 3D polylines it is possible to calculate strata thicknesses and measure strike and dip of bedding of faults and dykes. The overall

stratigraphic succession is based on the published geological map (Perch-Nielsen *et al.* 1983). More than 900 faults, fractures and dykes were digitised in the Wegener Halvø area and the majority shows a N–S and NNW–SSE-orientation. The structures are steep and occur as flower structures affecting the entire succession. The vertical offset is small and decreases from south to north along the strike of the faults that in some cases have a strike-slip component.

Integrated 3D photogeology and aeromagnetic data

The dataset from the interpretation of the photographs has been combined with a new structural interpretation of airborne magnetic data from the AEM Greenland 1997 survey (Rasmussen *et al.* 2001). Different maps were obtained from the calculation of the magnetic gradient tensor elements to highlight structures in different directions (Pedersen & Rasmussen 1990). The total magnetic intensity anomalies of the structures of interest have small amplitudes (around 3 nT) that are close to the detection limit of *c.* 0.5 nT of an airborne survey. As differentiation works as a high-pass filter, the second vertical derivative of the total magnetic intensity was also calculated to emphasise the linear features. This processing provides a better dynamic range for visualising the structures than the measured field. To attenuate the short wavelength noise features generated by this differentiation, an upward continuation of the magnetic field to 100 m was applied. Lineaments defined by negative magnetic anomalies and interpreted as major structures were digitised on the resulting map (Fig. 3A). These features are N–S to NNW–SSE-trending and several kilometres long and they fit with the faults in the geological map (Fig. 1) and with the fault segments mapped with the 3D stereo-plotter (Fig. 3B). The accurate fault segments mapped by photogeology were integrated with the magnetic lineaments highlighted at a larger scale. Thus, an identified structure can be prolongated on the map using geophysical data and constrained in its precise location and dip using 3D photogeology. One of the N–S-trending faults mapped by 3D photogeology and visible on the magnetic data coincides with the so-called Vimmelskaft lineament defined by Pedersen (1997). This lineament corresponds to a zone where a N–S-trending fault and a N–S-running dyke cut through Upper Permian shales and karstified carbonates. Important mineral occurrences with high base-metal content are found along this lineament and the concentration decreases away from the lineament.

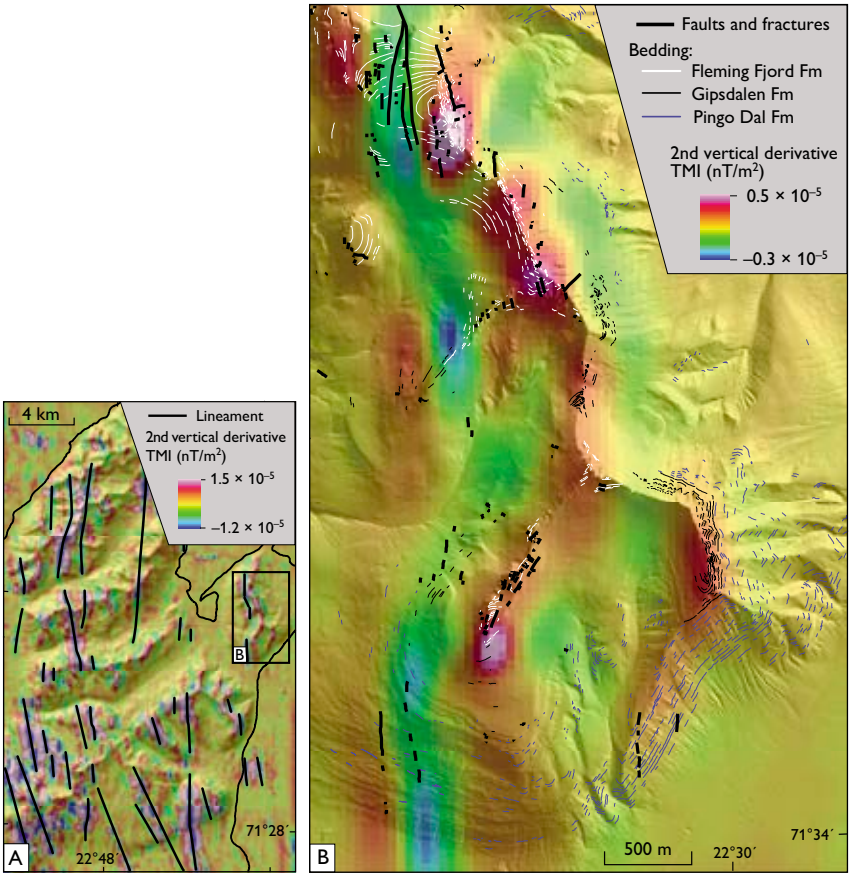

Fig. 3. **A**: Second vertical derivative of the total magnetic intensity (**TMI**) from the AEM Greenland 1997 survey (pixel size is 50 × 50 m) continued upward to 100 m and draped on the shaded elevation model. The negative magnetic lineaments are digitised and shown as black lines. **B**: Correlation between magnetic data and the faults, fractures and bedding collected from aerial photographs. Note the presence of eroded strata parallel to positive magnetic anomalies and faults and fractures related to negative anomalies.

The positive magnetic anomalies are not linear and appear to be associated with magnetic domains in the Triassic formations (Fig. 3B). The contours of these domains are parallel to the stratification collected from 3D photogeology (edges of eroded beds) and are mostly located on crests.

Concluding remarks

Using 3D photogeology we mapped a 100 km^2 area with good exposures on a scale of 1:1000. Formation boundaries and dip of strata are well constrained. New structures were mapped and the resulting dataset forms a good starting point for further studies of the stratigraphy or tectonic evolution using 3D modelling. The combination of 3D photogeology with new processing of the magnetic data has shown a good match between N–S-trending magnetic lineaments and N–S-trending normal steep faults. Structures of this type were highlighted by Pedersen (1997) for their possible role as pathways for mineralising fluids. The structures mapped during this study that affect the Upper Permian carbonates and shales, should be checked in the field. Furthermore, although mineral occurrences found in the Triassic formations are stratiform, remobilised sulphides are concentrated in cross-cutting fractures. The mapped faults and fractures that cut through Triassic formations could also be interesting targets for exploration. Detailed studies of structures and stratigraphic architecture are key points for mineral exploration. Accurate mapping using 3D photogeology combined with geophysical data can be efficient tools for this, especially in areas with difficult access and excellent outcrops.

References

Hansen, K., Bergman, S.C. & Henk, B. 2001: The Jameson Land basin (east Greenland): a fission track study of the tectonic and thermal evolution in the Cenozoic North Atlantic spreading regime. Tectonophysics **331**, 307–339.

Harpøth, O., Pedersen, J.L., Schønwandt, H.K. & Thomassen, B. 1986: The mineral occurrences of central East Greenland. Meddelelser om Grønland, Geoscience **17**, 139 pp.

Mathiesen, A., Bidstrup, T. & Christiansen, F.G. 2000: Denudation and uplift history of the Jameson Land basin, East Greenland – constrained from maturity and apatite fission track data. Global and Planetary Change **24**, 275–301.

Pedersen, M. 1997: Investigation of ore potential in black shales of the Upper Permian Ravnefjeld Formation in Scoresby Land and on Traill Ø, central East Greenland. Danmarks og Grønlands Geologiske Undersøgelse Rapport **1997/124**, 17 pp.

Pedersen, L.B. & Rasmussen, T.M. 1990: The gradient tensor of potential field anomalies. Some implications on data collection and data processing of maps. Geophysics **55**, 1558–1566.

Perch-Nielsen, K., Henriksen N. & Stemmerik, L. 1983: Geological map of Greenland, 1:100 000, Fleming Fjord, 71 Ø.1 Nord. Copenhagen: Geological Survey of Greenland.

Rasmussen, T.M., Thorning, L., Stemp, R.W., Jørgensen, M.S. & Schjøth, F. 2001: AEM Greenland 1994–1998 – summary report. Danmarks og Grønlands Geologiske Undersøgelse Rapport **2001/58**, 46 pp.

Seidler, L. 2000: Incised submarine canyons governing new evidence of Early Triassic rifting in East Greenland. Palaeogeography, Palaeoclimatology, Palaeoecology **161**, 267–293.

Soper, N.J., Downie, C., Higgins, A.C. & Costa, L.I. 1976: Biostratigraphic ages of Tertiary basalts on the East Greenland continental margin and their relationship to plate separation in the Northeast Atlantic. Earth and Planetary Science Letters **32**, 149–157.

Surlyk, F. 1990: Timing, style and sedimentary evolution of Late Palaeozoic – Mesozoic extensional basins of East Greenland. In: Hardman, R.F.P. & Brooks, J. (eds): Tectonic events responsible for Britain's oil and gas reserves. Geological Society, Special Publication (London) **55**, 107–125.

Thorning, L., Christensen, N.N., Olsen, S., Riisager, P., Sørensen, L.L., Sørensen, E.V. & Tukiainen, T. in press: High resolution airborne hyperspectral imaging spectroscopy in central East Greenland 2012 – data acquisition and pre-processing. Danmarks og Grønlands Geologiske Undersøgelse Rapport**.**

Vosgerau H., Guarnieri P., Weibel R., Larsen M., Dennehy, C., Sørensen, E.V. & Knudsen, C. 2010: Study of a Palaeogene intrabasaltic sedimentary unit in southern East Greenland: from 3-D photogeology to micropetrography. Geological Survey of Denmark and Greenland Bulletin **20**, 75–78.

Authors' addresses

A.B. & P.G., *Geological Survey of Denmark and Greenland, Øster Voldgade 10, DK-1350 Copenhagen K, Denmark*. E-mail: *aib@geus.dk*

T.M.R., *Division of Geosciences and Environmental Engineering, Luleå University of Technology, S-971 87 Luleå, Sweden***.**

Earthquake swarms in Greenland

Tine B. Larsen, Peter H. Voss, Trine Dahl-Jensen and Hans Peter Rasmussen

Two earthquake swarms have been detected in Greenland. One occurred on the island of Disko in August 2010, the other one was active from January 2008 to June 2009 near the South-East Greenland coast *c.* 200 km south of Tasiilaq. An earthquake swarm is defined as a series of earthquakes of similar magnitude located within a small area. The magnitude of the largest earthquakes in a swarm is typically less than 4 (Ma & Eaton 2009). Swarm activity is distinctly different from the more common mainshock–aftershock activity, which is characterised by one large earthquake (mainshock) followed by a series of smaller aftershocks. Earthquake swarms mainly occur in areas with tectonic and/or volcanic activity (Stykes 1970), but intraplate swarms are also found in otherwise stable environments (Gregersen 1979; Atakan *et al*. 1994; Uski *et al*. 2006; Ma & Eaton 2009). Geological boundaries and old fault zones appear to be a common setting for intraplate earthquake swarms. Earthquake swarms have previously been detected in North and North-East Greenland (Gregersen 1979) at a time when the seismograph coverage was very sparse. It was concluded that the earthquake swarms were caused by tectonic stresses in and around old sedimentary basins near the continental margin.

In this study we take advantage of the recently improved network of digital broadband seismographs in Greenland (Dahl-Jensen *et al*. 2010). The shorter distance between seismograph stations and the high quality digital data enable us to better detect small earthquakes. We have focused on the last decade during which the digital network has gradually been established (Fig. 1). We revisited the two regions where swarms have previously been detected, in North Greenland and in North-East Greenland (Gregersen 1979). Searching the GEUS earthquake database for recent earthquakes showed nothing in the area of the North Greenland swarm. The swarm described by Gregersen (1979) was primarily detected using data from a Canadian station (ALE) and a temporary station on the ice sheet, supplemented with data from Station Nord (NOR) for the largest earthquakes in the swarm. This particular region has not experienced an increase in station coverage in recent years. It is therefore impossible to distinguish whether the lack of recent detections is due to a lack of activity in that area. The location of the North-East Greenland earthquake swarm has also been searched without finding any new swarm activity in the last decade. Only two small earthquakes have been detected in the area, one in 2008 and another in 2011. In this area the station coverage has improved since 1974, so the lack of detections reflects that the area is currently seismically quiet.

Two new localities with earthquake swarms were uncovered in this study (Fig. 1). Both are areas with regular seismic activity. One swarm is located on the island of Disko near the Disko Gneiss Ridge (Fig. 2) where a fault zone runs N–S through the island (Chalmers *et al*. 1999). This is a very distinct swarm with its main activity concentrated on two days

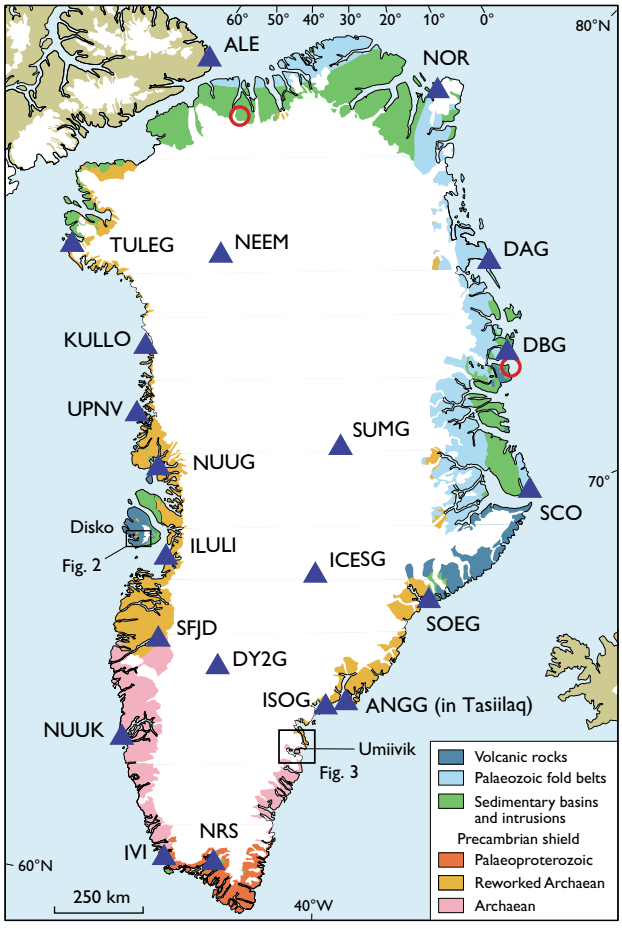

Fig. 1. Geological map of Greenland with seismograph stations marked by triangles. The locations of the swarms found by Gregersen (1979) are marked with red circles. The locations of the swarms presented in this study are marked with black boxes.

 Geological Survey of Denmark and Greenland Bulletin 31, 75–78. Open access: www.geus.dk/publications/bull

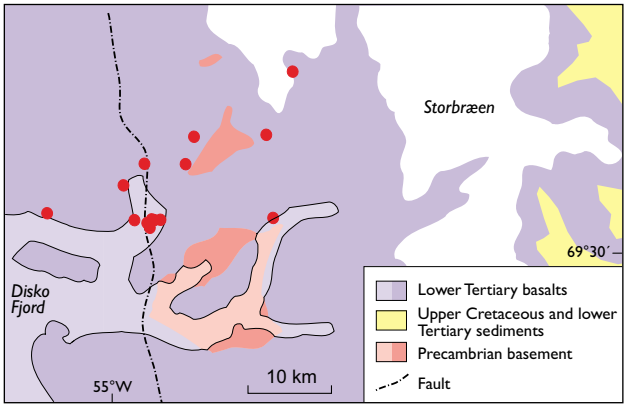

Fig. 2. The calculated epicentres for the swarm earthquakes on Disko, West Greenland. The Disko Gneiss Ridge runs along the fault line on the map.

in late August 2010, followed by slightly increased seismicity during the following two months. The other swarm is located in a remote area near the South-East Greenland coast, *c.* 200 km south of Tasiilaq (Fig. 3). This swarm is less distinct with two main pulses of activity in January 2008 and spring 2009. This area had increased seismicity for a year and a half, before it tapered off. The objective of this paper is to describe the two newly discovered earthquake swarms and how they relate to the local geology.

Data and analysis

Seismographs have been continuously operating in Greenland since 1927 (Hjelme 1996). Originally the instruments were large, difficult to install and labour intensive to maintain. It was only possible to operate a few stations in Greenland. This changed with the development of digital instruments, and during the last decade a network of 20 digital broadband seismographs with real-time data transmission has been installed in Greenland (Fig. 1). This massive undertaking is a result of the international collaboration in the Greenland Ice Sheet Monitoring Network (GLISN) project with funding from around the world (Dahl-Jensen *et al*. 2010). The latest seismological station was installed in Upernavik in 2013 by the Korean Polar Research Institute (see UPNV Fig. 1).

Data from the real-time network of seismographs are processed daily at GEUS using the SEISAN analysis software (Ottemöller *et al*. 2013). Earthquake phases are manually identified and combined to form earthquake locations when possible. Locations and phase readings are kept in the GEUS database for future reference. This includes phase readings not associated with an earthquake location. All the raw waveform data are also stored. The new earthquake swarms were discovered by performing a search in the database around locations, where clustering of seismicity was observed on a map of all earthquakes in Greenland. The search results were then examined for possible clustering of events in time. Two earthquake clusters fulfilled the criteria defining an earthquake swarm. Despite the improved station coverage, it is still challenging to determine the focal mechanism of most earthquakes in Greenland. Particularly the small swarm earthquakes that are only registered on one to four seismographs, which is insufficient for reliable focal mechanism calculations.

Earthquake swarm at the island of Disko

Disko and the surrounding areas are frequently shaken by small earthquakes, some large enough to be felt by the locals. Disko is also known for its warm springs formed where circulating surface water penetrates into the subsurface through deep cracks and is heated by the higher temperatures at depth. The flow of a warm spring is sometimes changed by a small earthquake, indicating that the earthquake sources are shallow. There are thousands of springs with constant temperature on Disko. The temperatures in individual springs vary between 1°C and 18.5°C (Kristensen 2006).

The number of earthquakes detected near the southern end of the Disko Gneiss Ridge per year for 2006–2013 varies between one and ten (Fig 4A). However, 2010 stands out with 27 detected earthquakes. The earthquake activity was particularly intense on 22 and 23 August (Fig 4B). The earthquakes ranged in magnitude from 1.9 to 3.2 with most

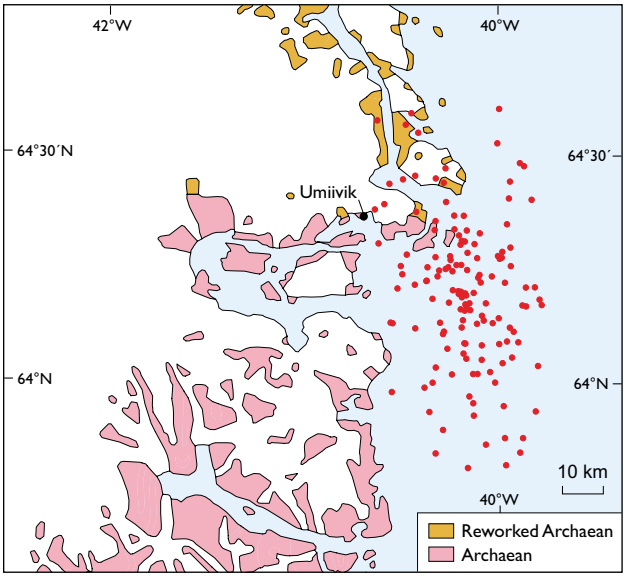

Fig. 3. The calculated epicentres for the swam earthquakes near Umiivik, on the South-East Greenland coast.

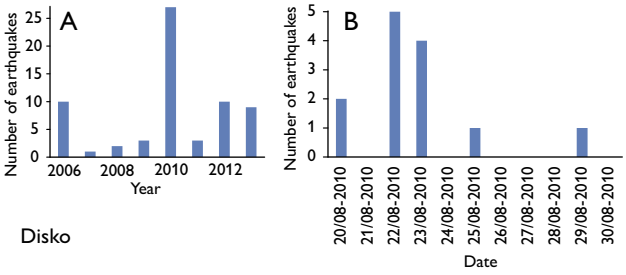

Fig. 4. **A**: Number of earthquakes per year for the period 2006–2013 around the location of the earthquake swarm on Disko. **B**: Number of earthquakes per day from 20 to 30 August 2010 in the same area.

clustering in the magnitude range between 2.2 and 2.8. The earthquake epicentres were spread out over a small area with the largest distance between two events being about 30 km. This distance is within the uncertainty on the locations. The uncertainty on the epicentres is in the order of 10 km in N–S direction and at least 50 km in E–W direction. This is caused by the geometry of the network relative to the events with seismographs primarily located north and south of the epicentres. As Fig. 2 shows, the scatter in the epicentres was indeed largest in E–W direction.

The closest seismograph where all earthquakes were registered is located in Ilulissat (ILULI) 110–120 km away. The earthquakes were also registered in Nuugaatsiaq (NUUG) *c*. 220 km to the north, in Kangerlussuaq (SFJD) 320 km to the south and at the Summit ice camp (SUMG) 650 km towards the north-east. A few earthquakes were registered on a total of eight seismographs in Greenland, but most of them were registered in just four locations. The depth of the earthquakes is poorly determined, but appears to be shallow. A major challenge in determining the depth is the limited knowledge of the crustal velocity structure. The depth to Moho is known from receiver function studies (Dahl-Jensen *et al*. 2003), and the crustal density structure in the Disko area has been modelled from seismic and potential field data (Chalmers *et al*. 1999). Relocating the earthquakes with a fixed depth of 5 km does not reduce the distance between the epicentres significantly. However, the variation in time difference between the *P*-wave arrival and the *S*-wave arrival was less than 1.5 sec. indicating a small source region.

The north–south-oriented fault along the Disko Gneiss Ridge is a known zone of weakness, and the area is characterised by a moderate earthquake activity with no seasonal variation. In SE Finland earthquake swarms are observed to be related to the intrusion of water and gas into fractures working in concert with the local stress field (Uski *et al*. 2006). A similar mechanism is likely on Disko. As warm water is circulating in deep cracks all year round a seasonal variation is not expected. Some of the warm springs on Disko are radioactive (Kristensen 2006) containing radon from the basement. Radon is also observed near earthquake swarms in Finland, and radon gas is believed to play a minor role in triggering earthquake swarms in SE Finland (Uski *et al*. 2006).

Earthquake swarm in South-East Greenland

The east coast of Greenland is frequently shaken by small earthquakes. In Tasiilaq earthquakes are felt almost every year. Many small earthquakes are registered farther down the coast, but it is not known if any of these events can be felt as the area is not populated. Earthquake swarm activity was detected in January 2008 and in the spring of 2009 just off the coast near Umiivik. The earthquakes in the swarm range in magnitude from 1.8 to 3.8. In the years before and after the swarm period, the level of earthquake activity in the area range between 12 and 21 earthquakes per year (Fig. 5A). However, in 2008 and 2009 respectively 71 and 114 earthquakes were registered. The earthquakes occurred primarily in January and April 2008 and again from January to July 2009 (Fig. 5B).

The uncertainty on most of the epicentres is several hundred kilometres in both the N–S and E–W directions. This is a consequence of the earthquakes being detected primarily by only two seismographs (four phases in total) in Kangerlussuaq (SFJD) and at Summit (SUMG) 550 km and 1000 km from the epicentres. The distance between the seismographs and the epicentres is well-determined, but the direction is poorly constrained. After improvements had been made to the seismograph network, a larger earthquake with a magnitude of 3.6 occurred in the area on 13 October 2009. This earthquake was well-recorded at four locations: Narsarsuaq (NRS), Kangerlussuaq (SFJD), Ilulissat (ILULI) and Summit (SUMG) with an uncertainty of less than 10 km in N–S direction and less than 20 km in E–W direction. This earth-

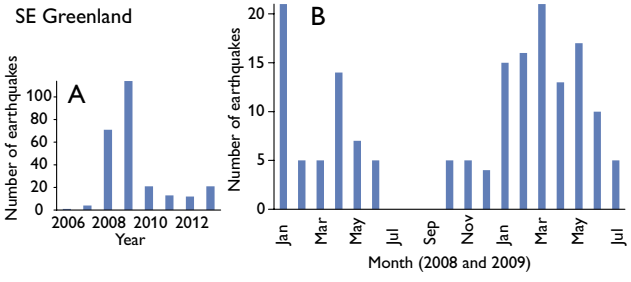

Fig. 5. **A**: Number of earthquakes per year for the period 2006–2013 around the location of the earthquake swarm at the SE Greenland coast. **B**: Number of earthquakes per month from January 2008 to July 2009 in the same area.

quake is located near the centre of the cloud of epicentres, and it can be used to evaluate the relative locations of the swarm earthquakes.

The waveforms for the small earthquakes are very noisy, making a direct comparison difficult. Instead we examine the variation in time difference between the *P*-wave and *S*-wave arrival for individual earthquakes. Despite the epicentres being scattered over almost 100 km in N–S direction and *c*. 50 km in E–W direction, the variation in *S*–*P* time (i.e. the distance to the earthquake) at each seismograph station fluctuated only in rare cases by more than 1.5 sec. relative to the 13 October 2009 earthquake. The large scatter in epicentres is probably an artefact of the focal depth being unconstrained.

The Umiivik area marks a major geological transition between the relatively unreworked Archaean rocks to the south and rocks highly deformed in the Proterozoic to the north (Henriksen *et al*. 2009). Offshore the existence of a failed rift arm was proposed by Hopper *et al*. (1998). The earthquake swarm was thus located close to two old geological boundaries. This is in good accordance with the general observations by Stykes (1978) that intraplate earthquakes indeed occur in old zones of weakness.

Conclusion

As shown by this initial search for earthquake swarms, the improvements to the seismograph network in Greenland enable us to better uncover and analyse swarms in the future. The swarms presented in this paper could not have been detected a decade ago. Intraplate earthquake swarms can contribute to the understanding of geological processes currently at work near old geological boundaries in remote areas. Both swarms presented here were active near old geological boundaries. The swarm on Disko is located at the southern end of the Disko Gneiss Ridge where a large fault runs through the island. Circulating water in deep cracks may possibly play a role. The SE Greenland swarm is located close to a major geological boundary between reworked and unreworked Archaean rocks. Furthermore, the swarm is close to the proposed location of a failed rift arm in the Atlantic. Finding earthquake swarms close to old, major, geological boundaries is well in accordance with the literature. The earthquake swarms presented in this paper are not associated with known sedimentary basins such as the swarms described in Gregersen (1979). This indicates a diversity of swarm sources in Greenland. Further work will be carried out on the earthquake swarms in Greenland and data from temporary and Canadian seismographs will be included in the analysis.

Acknowledgement

The data were collected and distributed by the GLISN project and its members, www.glisn.info.

References

Atakan, K., Lindblom, C.D. & Havskov, J. 1994: Earthquake swarm in Steigen, northern Norway: an unusual example of intraplate seismicity. Terra Nova **6**, 180–194.

Chalmers, J.A., Pulvertaft, T.C.R., Marcussen, C. & Pedersen, A.K. 1999: New insight into the structure of the Nuussuaq Basin, central West Greenland. Marine and Petroleum Geology **16**, 197–224.

Dahl-Jensen, T. *et al*. 2003: Depth to Moho in Greenland: receiver function analysis suggests two Proterozoic blocks in Greenland. Earth and Planetary Science Letters **205**, 379–393.

Dahl-Jensen, T., Larsen, T.B., Voss, P.H. & the GLISN group 2010: Greenland ice sheet monitoring network (GLISN): a seismological approach. Geological Survey of Denmark and Greenland Bulletin **20**, 55–58.

Gregersen, S. 1979: Intraplate earthquake swarms in Greenland and adjacent continental regions. Nature **281**, 661–662.

Henriksen, N., Higgins, A.K., Kalsbeek, F. & Pulvertaft, T.C.R. 2009: Greenland from Archaean to Quaternary. Descriptive text to the Geological map of Greenland 1:2 500 000. 2nd edition. Geology of Greenland Survey Bulletin **18**, 126 pp.

Hjelme, J. 1996: History of seismological stations in Denmark and Greenland. In: Wahlström, R. (ed.): Seismograph recording in Sweden, Norway – with arctic regions, Denmark – with Greenland, and Finland. Proceedings from the Uppsala Wiechert Jubilee Seminar, 49–57. Uppsala: Seismological Department, Uppsala University, Sweden.

Hopper, J.R., Lizarralde, D. & Larsen, H.C. 1998: Seismic investigations offshore South-East Greenland. Geology of Greenland Survey Bulletin **180**, 145–151.

Kristensen, R.M. 2006: De varme kilder. In: Bruun, L. *et al*. (eds): Arktisk Station 1906–2006, 310–315. Copenhagen: Rhodos.

Ma, S. & Eaton, D.W. 2009: Anatomy of a small earthquake swarm in southern Ontario, Canada. Seismological Research Letters **80**, 214–223, *http://dx.doi.org/10.1785/gssrl.80.2.214*

Ottemöller, L., Voss, P.H. & Havskov, J. 2011: SeisAn earthquake analysis software for Windows, Solaris, Linux and MacOSX. University of Bergen.

Stykes, L.R. 1970: Earthquake swarms and sea-floor spreading. Journal of Geophysical Research **75**, 6598–6611.

Stykes, L.R. 1978: Intraplate seismicity, reactivation of pre-existing zones of weakness, alkaline magmatism, and other tectonism postdating continental fragmentation. Reviews of Geophysics and Space Physics **16**, 621–688.

Uski, M., Tiira, T., Korja, A. & Elo, S. 2006: The 2003 earthquake swarm in Anjalankoski, south-eastern Finland. Tectonophysics **422**, 55–69.

Authors' address

Geological Survey of Denmark and Greenland, Øster Voldgade 10, DK-1350 Copenhagen K, Denmark; E-mail: *tbl@geus.dk*

Outlet glacier dynamics and bathymetry at Upernavik Isstrøm and Upernavik Isfjord, North-West Greenland

Camilla S. Andresen, Kristian K. Kjeldsen, Benjamin Harden, Niels Nørgaard-Pedersen and Kurt H. Kjær

During the past decades, the Greenland ice sheet has experienced a marked increase in mass loss resulting in an increased contribution to global sea-level rise. The three largest outlet glaciers in Greenland have increased their discharge, accelerated, thinned and retreated between 1996 and 2005. After 2005 most of them have slowed down again although not to previous levels. Geodetic observations suggest that rapid increase in mass loss from the north-western part of the ice sheet occurred during 2005–2010 (Kjeldsen *et al.* 2013).

Warming of the subsurface water masses off Greenland may have triggered the acceleration of outlet glaciers from the ice sheet (Straneo & Heimbach 2013). The North Atlantic subpolar gyre, which transports water to South-East and West Greenland via the warm Irminger Current, warmed in the mid-1990s. Increased inflow of warm subpolar waters likely led to increased submarine melting of tidewater glaciers.

Climate, glacier configuration and fjord bathymetry play fundamental roles for outlet glacier dynamics and thus knowledge of these parameters is warranted. In particular, the bathymetry of a fjord gives important information about the exchange between fjord waters close to marine-terminating glaciers and the shelf and ocean. However, only sparse bathymetric data are available for the majority of fjords in Greenland. The International bathymetry chart for the Arc-

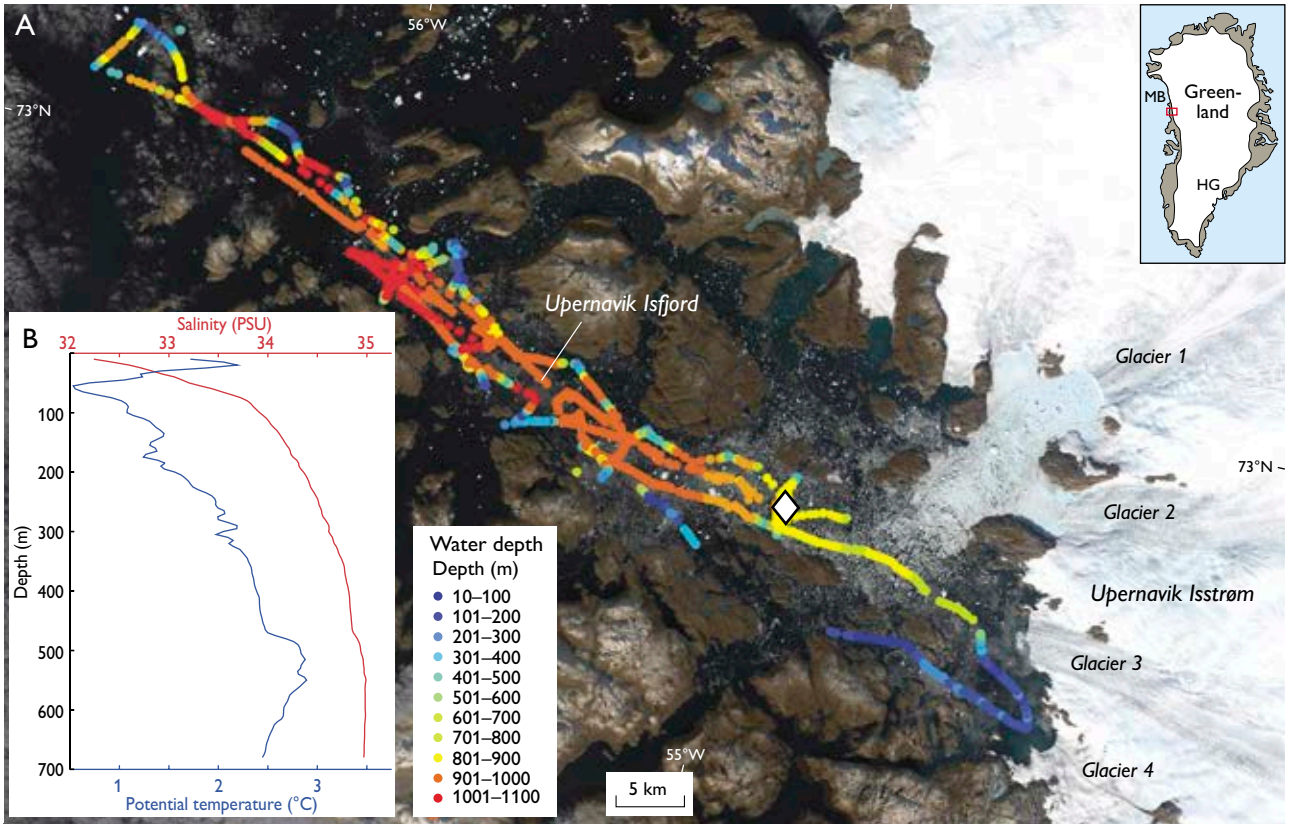

Fig. 1. **A**: Landsat 8 satellite image from August 2013 of the Upernavik Isfjord region with recorded water depths in the fjord. **B**: Temperature and salinity profiles at a mid-fjord site (white diamond). Data acquired in 2013 by oceanographers from Woods Hole Oceanographic Institution. **MB**: Melville Bugt. **HG**: Helheimgletscher.

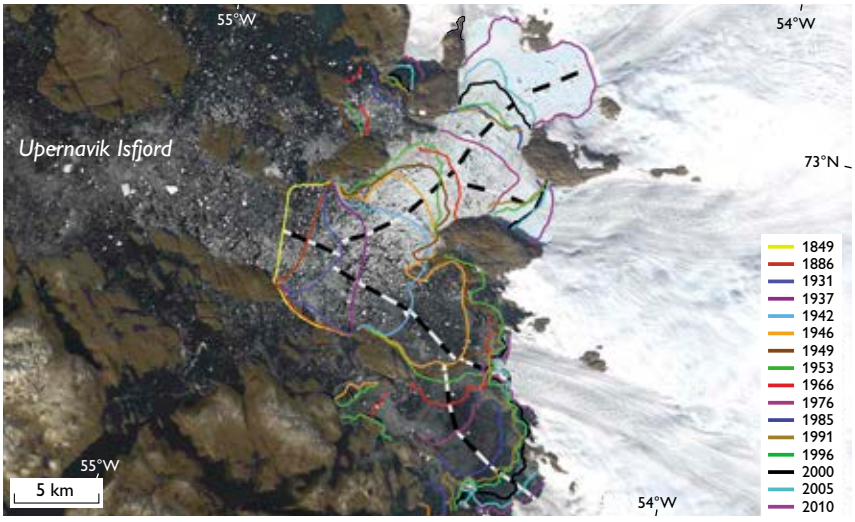

Fig. 2. Glacier frontal positions based on maps from historical expeditions, aerial photographs and satellite images (Weidick 1958; Khan *et al.* 2013), supplemented with a Corona satellite image from 1966 and a Landsat MSS image from 1976. The black and white lines show the tracks used for calculating single-point distances from the glacier margin.

tic Ocean (IBCAO) does not provide adequate data for the fjords and gives the impression that water depths in fjords are typically <200 m.

Here we present the first detailed bathymetric data from Upernavik Isfjord in North-West Greenland, which were obtained during a cruise led by the Geological Survey of Denmark and Greenland in August 2013. The purpose of the cruise was to retrieve sediment cores, collect hydrographic data and map the bathymetry of the fjord. In this paper, we also estimate retreat rates of the Upernavik Isstrøm since 1849 and evaluate them in the context of climate variability, glacier setting and fjord bathymetry.

Upernavik Isstrøm and Upernavik Isfjord

Upernavik Isstrøm consists of four main ice streams (glaciers 1–4, Fig. 1) that had a total mass loss of 53.5 ± 12.8 Gt during the period 2005–2010 (Khan *et al.* 2013). The four glaciers terminate in the *c.* 80 km long Upernavik Isfjord. Glaciers 1 and 2 are the most productive and the fjord in front of these glaciers is packed with icebergs throughout the year. The bathymetric data (Fig. 1) show that most of the fjord is over 900 m deep, but water depths of 600–800 m are found near its head. Due to ice conditions, water depths could only be measured near glacier 4 where there is an area with water depths around 200 m. Local fishermen report water depths of 600–700 m at a distance of *c.* 5–10 km from the fronts of glaciers 1–3. The survey ended slightly west of the fjord mouth and there was no indication of a sill.

The hydrographic measurements show a *c.* 2°C warm, low-salinity, 50 m thick surface layer. From 50 to 150 m cold polar water with a temperature of 0.5–1.5°C is found, and below this the water gradually warms from 1 to 3°C and becomes more saline, which shows that Atlantic water penetrates into the fjord (Fig. 1). This also indicates that there is no shallow sill at the entrance to the fjord. Radar-based surveys suggest grounding line depths of 400–700 m for glaciers 1–3 and 100 m for glacier 4 (Morlighem *et al.* 2014). This suggests that Atlantic water comes into contact with the fronts of glaciers 1–3, whereas the front of glacier 4 is in contact with polar water. This finding has implications for understanding the history of glacier retreat.

Glacier retreat and climate change

Frontal positions of Upernavik Isstrøm were compiled for the period from 1849 to 1953 by Weidick (1958; Fig. 2). Along with satellite images from 1966 and 1976 (this study) and more continuously since 1985 (Khan *et al.* 2013) these compilations provide a 150 years long record of glacier retreat since the Little Ice Age maximum position. Using the centre flow-line we estimate average annual retreat rates between glacier margin positions (Fig. 3C). From the Little Ice Age until *c.* 1931, the four glaciers were merged into one and retreated relatively slowly. The frontal retreat rate accelerated around 1931 and glaciers 1 and 2 and glaciers 3 and 4 started to split into two separate arms, and after 1946 glaciers 3 and 4 were decoupled from each other. The relatively high retreat rates lasted until the mid-1940s and were followed by lower retreat rates. Glaciers 1 and 2 decoupled from each other after 1966. Three subsequent episodes of increased retreat rates are seen: (1) between 1966 and 1985 (glaciers 1, 2 and 4), (2) late 1990s (glaciers 1, 2 and 4) and (3) 2005–2009 (all glaciers). During the latter period, the retreat rate of glacier 1 was exceptionally high. The temporal resolution of the data does not allow us to detect earlier similar rapid retreat events. In a recent study, data on frontal changes, thinning, and glacier velocity since 1985 were obtained from aerial photos and sat-

ellite data and used to estimate dynamic mass loss (Khan *et al.* 2013). Glacier 4 experienced a marked mass loss episode, including >100 m thinning, prior to 1991. At the same time no marked changes were recorded for glaciers 1–3. In contrast, between 2005 and 2009, glacier 1 sped up, retreated and thinned markedly, whereas glaciers 2–4 were relatively stable. Kjær *et al.* (2012) documented two events of dynamic mass loss along the Melville Bugt coast but also noted a spatially variable pattern in the magnitude of these events. The extended retreat data presented here may indicate that the marked dynamic mass loss prior to 1991 of glacier 4 was preceded by an even more marked event between 1966 and 1985 affecting not only glacier 4 but also glaciers 1 and 2.

Care should be taken in comparing magnitude and timing of retreat rates from merged and decoupled glaciers due to their different and temporally variable tributary sizes, glacier tongue widths and flow rates. Moreover, the estimated frontal positions are based on single points and may be subject to seasonal fluctuations and are thus only approximate. However, the timing of accelerated retreat rates in the different glaciers is fairly synchronous over inter-annual time scales. The onset of increased retreat rates in the 1930s of glaciers 1 + 2 and 3 + 4 as well as the increased retreat rates of glaciers 1 + 2 around 1966 may have been initiated by their decoupling from the merged glacier and glaciers 1 + 2 at this time. This would suggest that topographical constraints are important for retreat rates. Alternatively, a common climate change may have forced accelerated retreat and in this way caused the decoupling of glaciers.

The marked retreat episodes in 1931–1946 (of the merged glacier), in the late 1990s (glaciers 1, 2, 4) and in 2005–2009 (all glaciers, but most markedly glacier 1) occurred at times of marked warming near Upernavik and entire Greenland (Chylek *et al.* 2006). Marked retreat from 1930 to the 1940s has also been documented elsewhere in Greenland, specifically for Helheimgletscher in South-East Greenland (Andresen *et al.* 2012; Figs 1, 3D) and has been ascribed to variations in the Atlantic multi-decadal oscillation (AMO). The AMO is a mode of variability with its main expression in sea-surface temperatures in the North Atlantic Ocean and influencing circum-Atlantic climate, including coastal Greenland. The AMO has a periodicity of *c.* 60 years, and a positive AMO

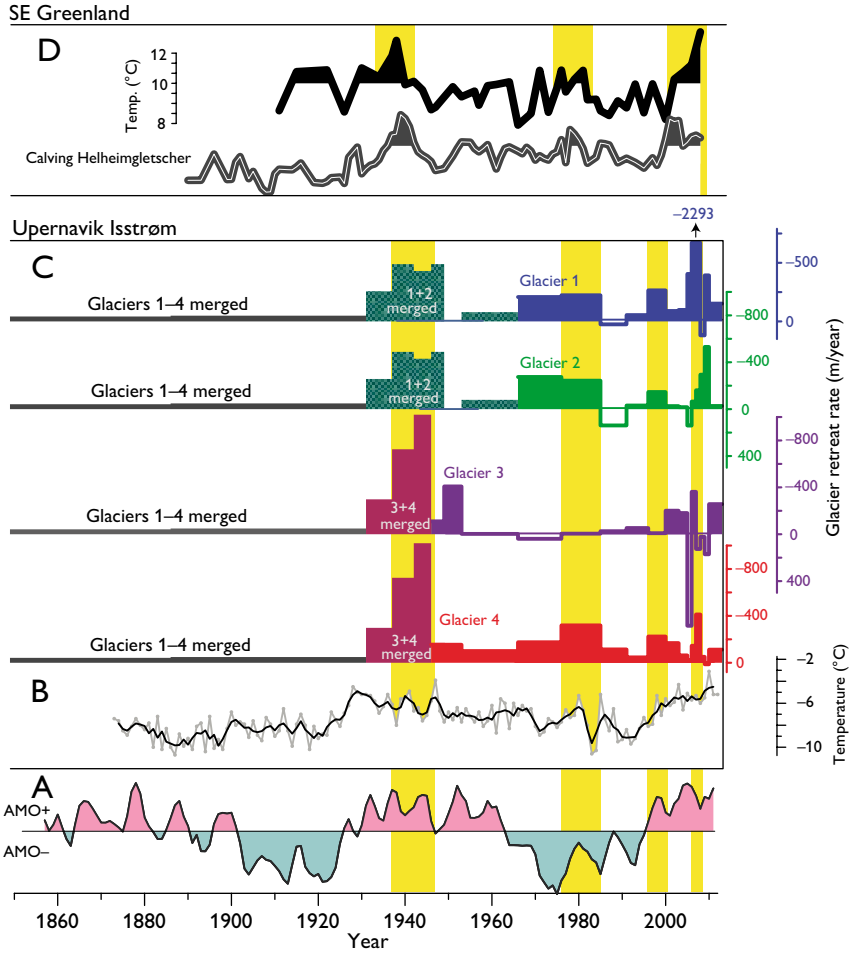

Fig. 3. **A**: Atlantic multi-decadal oscillation (AMO) index (Schlesinger & Ramankutty 1994). **B**: Annual average air temperature for Upernavik (data from the Danish Meteorological Institute). **C**: Calculated changes in rate (m yr^{-1}). Negative values and colour-filled boxes: glacier retreat. Positive values and white boxes: glacier advance. Episodes characterised by increased retreat rates by Upernavik are highlighted with yellow boxes. **D**: Marine sediment-based proxy data from South-East Greenland. Relative variability in calving from Helheimgletscher based on sand fluxes (Andresen *et al.* 2012) and shelf sea-surface temperatures based on analyses of core ER07 from Sermilik fjord (Andresen *et al.* 2013). Yellow boxes highlight warm episodes with increased dynamic mass loss in South-East Greenland.

index is linked with higher sea-surface temperatures. The accelerated retreat episodes of Upernavik Isstrøm from 1930 to the 1940s, late 1990s and 2005–2009 could be associated with warming of subsurface waters during periods with positive AMO indexes (Fig. 3). However, since air temperatures co-vary with the AMO index on multi-decadal timescales (Figs 3A, B) it is not possible to differentiate directly between influence from increased air versus water temperatures on mechanisms that could lead to retreat of the glacier margin.

As noted the increased retreat rates of glaciers 1 and 2 between 1966 and 1985 may have been triggered by changed topographical constraints such as loss of pinning points as the combined glacier front widened considerably (Figs 2, 3C). However, due to the synchronous, high retreat rates of glacier 4 within its own tributary, as well as continued high retreat rates long after decoupling of glaciers 1 and 2, we speculate that climate forcing is also involved. The increased retreat differs from the other retreat episodes because it occurred during a negative AMO index. However, even though average sea-surface temperatures in the source region of Atlantic waters were generally low between the early 1960s and the mid-1990s and annual air temperatures in Upernavik decreased slightly, air temperatures increased between the early 1970s and 1980. Interestingly, sediment-based proxy glacier and ocean data document a marked warming of Atlantic waters in South-East Greenland at this time along with a marked increase in calving from Helheimgletscher (Fig. 3D). The concurrency between this climate warming and glacier instability in South-East Greenland supports the theory that the increased retreat rates of glaciers 1, 2 and 4 between 1976 and 1985 were forced by climate warming.

The front of glacier 4 has been located in a 200 m shallow area since the 1950s (Fig. 1) and the front of this glacier is not in direct contact with the deeper warm subsurface layer in the fjord. Although warming or increased thickness of the Atlantic water layer may increase the temperature of the polar water layer, we suggest that the accelerated retreat rates of glacier 4, including the 1985–1991 episode of marked thinning (Khan *et al.* 2013), may be linked with increased air temperatures. It has been suggested that meltwater percolating down the glacier being released as subglacial discharge may have a considerable influence on the submarine melt rates and thus glacier stabilisation.

We emphasise that the retreat record is not fully representative of glacier changes. Not only are the determined frontal positions rather sporadic and do not represent a continuous record of change, but in addition we need to assess thinning and flow-rate changes to obtain a more comprehensive picture of glacier changes since the Little Ice Age. One way to overcome this will be to analyse sediment cores to obtain a continuous proxy record of calving variability. This will add information on dynamic changes and can subsequently be linked to digital elevation models and mass-balance modelling to estimate mass loss. Our results also show that bathymetric conditions may partly explain asynchronous glacier responses to climatic warming. It is therefore important to incorporate bathymetric data when trying to understand and predict outlet-glacier behaviour. Hopefully future campaigns to collect and pool bathymetric data will provide improved bathymetric maps of the Greenland fjords.

Acknowledgements

The 'Upernavik Glacier Project' is funded by Geocenter Danmark. We thank Arctic Station on Disko for the use of the vessel *Porsild* and Hans Karl Petersen from Upernavik who was pilot during the survey of glacier 4 and provided water-depth information by glaciers 1–3.

References

Andresen, C.S. *et al.* 2012: Rapid response of Helheim Glacier in Greenland to climate variability over the past century. Nature Geoscience **5**, 37–41.

Andresen, C.S., Sicre, M.-A., Straneo, F., Sutherland, D.A., Schmith, T., Ribergaard, M.H., Kuijpers, A. & Lloyd, J.M. 2013: A 100-year record of alkenone-derived SST changes by Southeast Greenland. Continental Shelf Research **71**, 45–51.

Chylek, P., Dubey, M.K. & Lesins, G. 2006: Greenland warming of 1920–1930 and 1995–2005. Geophysical Research Letters **33**, L11707.

Khan, S.A., *et al.* 2013: Recurring dynamically induced thinning during 1985 to 2010 on Upernavik Isstrøm, West Greenland. Journal of Geophysical Research: Earth Surface **118**, 111–121.

Kjær, K.H. *et al.* 2012: Aerial photographs reveal late-20th-century dynamic ice loss in northwestern Greenland. Science **337**, 569–573.

Kjeldsen, K.K., *et al.* 2013: Improved ice loss estimate of the northwestern Greenland ice sheet. Journal of Geophysical Research: Solid Earth **118**, 698–708.

Morlighem, M., Rignot, E., Mouginot, J., Seroussi, H.& Larour, E. 2014: Deeply incised submarine glacial valleys beneath the Greenland Ice Sheet. Nature Geoscience **7**, 418–422.

Schlesinger, M.E. & Ramankutty, N. 1994: An oscillation in the global climate system of period 65–70 years. Nature **367**, 723–726.

Straneo, F. & Heimbach, P. 2013: North Atlantic warming and the retreat of Greenland's outlet glaciers. *Nature* **504**, 36–43.

Weidick, A. 1958: Frontal variations of Upernaviks Isstrøm in the last 100 years. Meddelelser fra Dansk Geologisk Forening **14**, 52–60.

Authors' addresses

C.S.A. & N.N.P., *Geological Survey of Denmark and Greenland,* Øster *Voldgade 10, DK-1350 Copenhagen K, Denmark*. E-mail: *csa@geus.dk*

K.K.K. & K.H.K., *Natural History Museum of Denmark, University of Copenhagen, Øster Voldgade 5-7, DK-1350 Copenhagen K, Denmark.*

B.H., *Woods Hole Oceanographic Institution, Woods Hole, MA 02543, USA.*

Katabatic winds and piteraq storms: observations from the Greenland ice sheet

Dirk van As, Robert S. Fausto, Konrad Steffen and the PROMICE project team*

In 2007 the Programme for Monitoring the Greenland Ice Sheet (PROMICE) was initiated to observe and gain insight into the mass budget of Greenland ice masses. By means of *in situ* observations and remote sensing, PROMICE assesses how much mass is gained as snow accumulation on the surface versus how much is lost by iceberg calving and surface ablation (Ahlstrøm *et al.* 2008). A key element of PROMICE is a network of automatic weather stations (AWSs) designed to quantify components of the surface mass balance, including the energy exchanges contributing to surface ablation (Van As *et al.* 2013).

The use of these AWS observations is not limited to studies of ice-sheet mass balance. PROMICE contributes to CryoNet (www.globalcryospherewatch.org/cryonet), the core network of surface measurement sites of the World Meteorological Organization (WMO) Global Cryosphere Watch. By real-time delivery through WMO, PROMICE observations contribute to improve both operational forecasting and climate analysis in the data-sparse Arctic. The Greenlandic population, highly dependent on accurate forecasting of weather conditions, benefits directly from these real-time observations. For instance, extreme surface wind speeds are a high-risk element in Greenland. The third-highest wind speed observed at the surface of the Earth (93 m/s or 333 km/h), was recorded in a 8–9 March 1972 storm at Thule in North-West Greenland (Stansfield 1972).

In this paper, we discuss the extent to which the Greenland ice sheet generates its own near-surface wind field. We use PROMICE data to gain insight into the interaction between air temperature, radiation and gravity-driven katabatic winds. We focus on a particularly powerful spring storm in 2013 that contributed to a fatality on an ice-sheet ski traverse attempt (Linden 2013).

Weather stations on the Greenland ice sheet

The original PROMICE network consisted of fourteen AWSs in seven ablation regions of the Greenland ice sheet, with each region monitored by a lower (L) and an upper (U) elevation station (Fig. 1; Ahlstrøm *et al.* 2008). PROMICE has collaborated logistically and financially with other projects in the regions of the TAS, QAS, NUK and KAN stations, leading to the installation of eight additional AWSs. The PROMICE

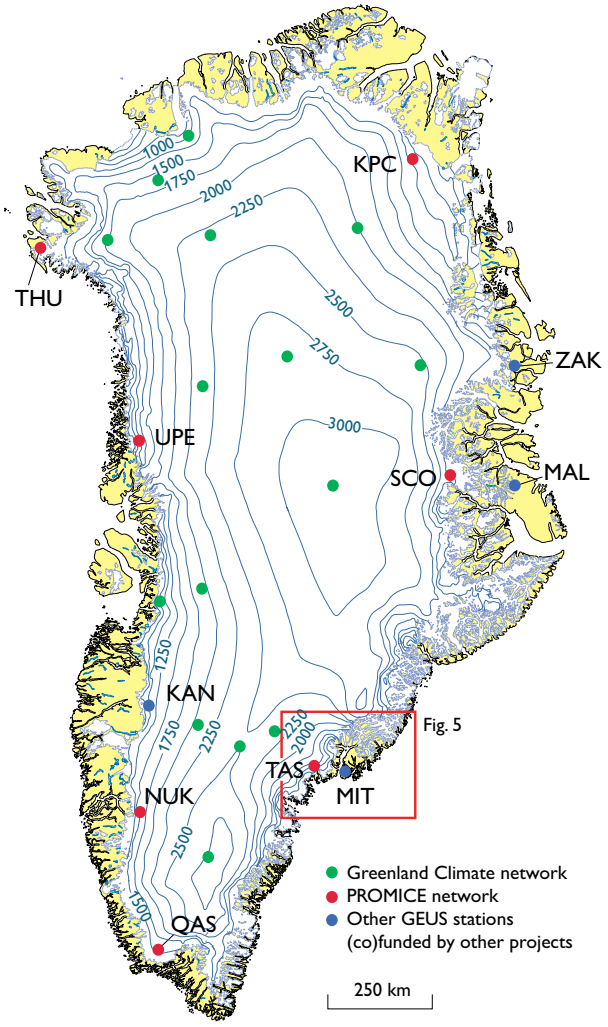

Fig 1. Map of Greenland showing the locations of automatic weather stations on the ice sheet and on local ice caps.

* Andreas P. Ahlstrøm, Signe B. Andersen, Morten L. Andersen, Jason E. Box, Charalampos Charalampidis, Michele Citterio, William T. Colgan, Karen Edelvang, Signe H. Larsen, Søren Nielsen, Martin Veicherts and Anker Weidick

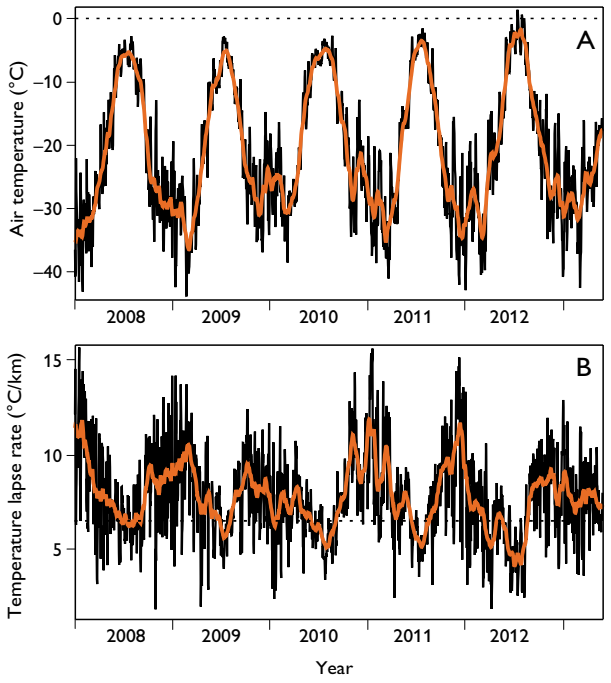

Fig. 2. **A**: Daily average (black) and 31-day average (red) air temperature over the Greenland ice sheet as determined from interpolated weather station observations from the GC-Net and PROMICE network. **B**: Same, but vertical near-surface temperature lapse rates. The dashed line shows a lapse rate of 6.5°C/km above which air masses are increasingly unstable.

AWS sites have been selected to complement the Greenland Climate Network (GC-Net), which chiefly monitors the ice-sheet accumulation area (Steffen *et al.* 1996).

Continuous PROMICE AWS observations include: air temperature (*c.* 2.7 m above surface), barometric pressure, air humidity, wind speed and direction (*c.* 3.1 m above surface) as well as down- and upward solar (shortwave) and terrestrial (longwave) radiation. The AWSs also record temperature profiles in the upper 10 m of the ice, GPS-derived location and diagnostic parameters such as station tilt angles. A pressure transducer and two sonic rangers measure snow and ice-surface height change associated with ablation and accumulation (Fausto *et al.* 2012). All data and metadata including sensor specifications are available at *www.promice.org*.

Here, we use averaged values of air temperature, wind speed and direction, and radiation components. Single wind measurements have an uncertainty of 0.3 m/s and 3° (Van As 2011) and are not adjusted for shifts in tilt, rotation or measurement height as this does not impact the outcome of this study. We also combine GC-Net and PROMICE temperature data to give the most complete observed meteorological depiction of the Greenland ice sheet currently possible. We calculated the daily average near-surface air temperature across the ice sheet between 2008 and 2013 by means of inverse-distance interpolation between as many as 32 AWSs that operated on a given day. We also determined the daily average vertical near-surface air-temperature lapse rate by means of a linear least-squares fit to all available data.

Atmospheric temperature and stability

The average near-surface air temperature over the Greenland ice sheet has a distinct annual cycle with minimum (winter) values between –20°C and –40°C (Fig. 2A). During the relatively short summer, temperatures are often around –5°C and are less variable due to (1) reduced cyclonic activity and (2) surface melting over large parts of the ice sheet. The latter is a moderating factor because near-surface temperatures are limited to near freezing. Since 2008, ice-sheet average air temperatures above 0°C have only been recorded on five days (11–13 and 28–29 July 2012) during which surface melting occurred over nearly the entire ice sheet (e.g. Nghiem *et al.* 2012).

The average near-surface air-temperature lapse rate over the ice sheet exhibits a reversed cyclicity as compared to air temperature with winter values often exceeding a 10°C decrease per vertical kilometre (Fig. 2B). Assuming a textbook value of a 6.5°C/km free-atmospheric lapse rate to be representative

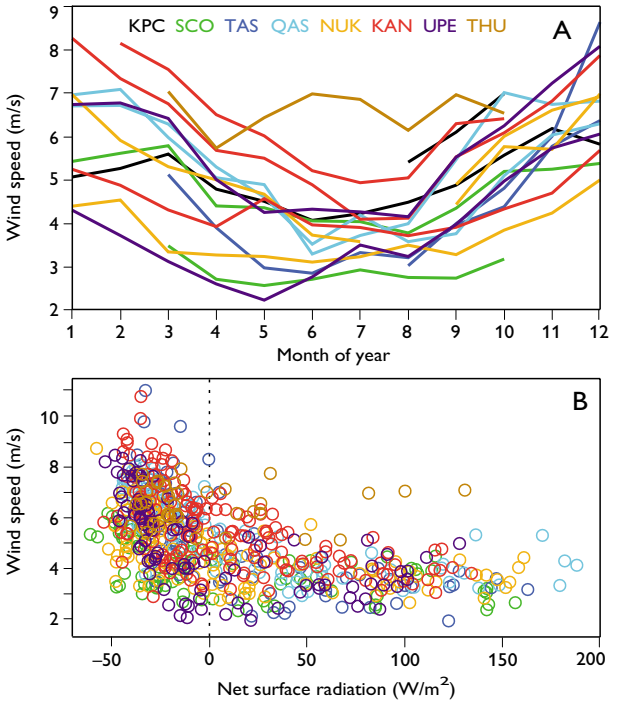

Fig. 3. **A**: The average annual cycle in wind speed at the PROMICE sites. Lines are drawn for each weather station, but only if three years of good data are available. **B**: The monthly average wind speed versus the net (shortwave + longwave) radiation budget. For locations of the stations see Fig. 1.

of the threshold between stable and unstable conditions over Greenland, this suggests that the near-surface atmosphere is commonly less buoyant (denser) at higher elevations than air at lower elevations. In a free atmosphere such a density difference over a few vertical kilometres would trigger an immediate adjustment through convection. Over the large horizontal scale of the Greenland ice sheet, the actual density gradients are roughly two orders of magnitude smaller, which adds insignificantly to the force balance. Figure 2B illustrates that during winter, the high elevation interior of the ice sheet cools more than lower elevation regions near the margin. As a result, the shallow (*c.* 100 m thick) stable atmospheric boundary layer that blankets the ice sheet attains an even larger temperature deficit compared to the free atmosphere at high elevation in winter. The larger this temperature deficit relative to the free atmosphere, the larger the density difference relative to the free atmosphere, and thus the larger the gravitational acceleration of the shallow boundary layer. This katabatic force increases linearly with increasing surface slope.

Katabatic winds

Winds over the Greenland ice sheet are strongest in winter (e.g. Steffen & Box 2001), as observed at every PROMICE AWS (Fig. 3A). While part of this increase is due to lower wintertime pressure and more frequent passage of cyclonic systems, the primary cause of stronger winter winds is surface radiative cooling. This well-known forcing mechanism of katabatic wind is apparent from stronger winds at more negative surface net radiation (Fig. 3B) and the strong correlation between the directions in slope and wind (see below). A negative radiation budget is common during winter due to little or no solar radiation at high latitudes when the upward emission of long-wave terrestrial radiation exceeds downward atmospheric radiation at the surface.

The wind regimes over the ice sheet do differ between regions. Winds are stronger at the higher-elevation AWSs due to the larger radiative cooling of the surface (provided a surface slope is present). The highest monthly-mean wind speed values in Fig. 3B were recorded at KAN_M and KAN_U (1270 and 1840 m a.s.l., red), and TAS_U and TAS_A (570 and 900 m a.s.l., blue).

Piteraq storms

The wind regimes at KAN and TAS are shown in a case study of the 2012/2013 winter (Fig. 4). Figure 4A illustrates that low-wind winter conditions are rare at KAN_U, PROMICE station at highest elevation. Figure 4B shows the dominant katabatic nature of winter winds. Nearly all measurements from KAN_U show the wind to blow from upslope direction (*c.* 90°, east), albeit deflected to the right (*c.* 135°, south-east) by the Coriolis effect due to the Earth's rotation. Typically, wind speeds at TAS_U are lower (but still non-zero) due to the weaker radiative cooling at lower elevation. Katabatic forcing also dominates here, given the persistent non-zero winds originating from the upslope direction of *c.* 0° (north) and more westerly directions due to Coriolis forcing. The major difference between the two data series in Fig. 4 is the frequency of strong wind events exceeding *c.* 20 m/s, which are more common in the TAS region. In the strongest storms, the wind direction pivots towards the regional free-atmospheric flow (Fig. 4B).

These storms are known in Greenland as piteraqs, and build up momentum due to the alignment of katabatic and large-scale (geostrophic) forcing (Oltmanns *et al.* 2014). These notorious storms have repeatedly caused severe damage to the towns such as Tasiilaq. The piteraq on 27 April 2013 (Fig. 4A), which jeopardised a sport expedition on the ice sheet (Linden 2013), was exceptionally strong at TAS_U in the context of the 2008 to 2013 PROMICE observational period, with 10-minute average wind speeds exceeding 42 m/s (150 km/h). During this event, four persons (C. Charalampidis, W.T. Colgan, H. Machguth and D. van As)

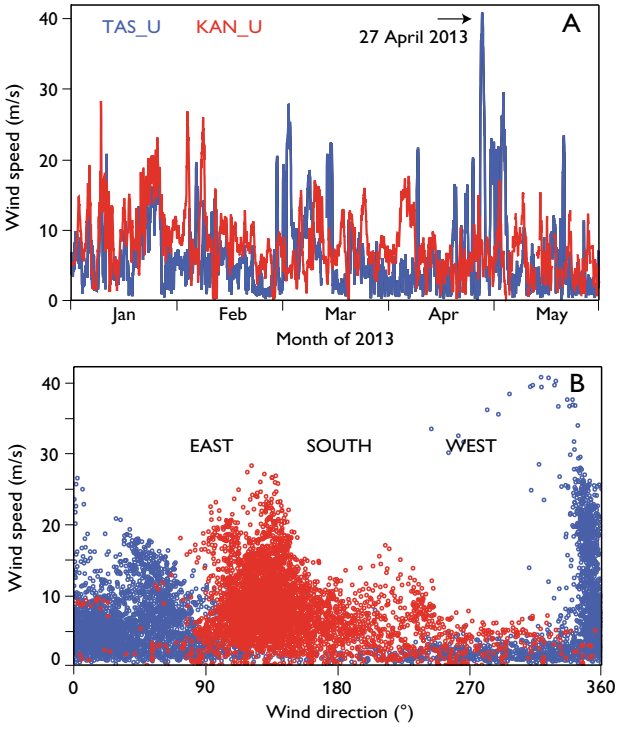

Fig. 4. **A**: Hourly average wind speed at TAS_U and KAN_U weather stations. The piteraq on 27 April 2013 is clearly visible in the TAS_U observations. **B**: Same, but wind speed plotted versus wind direction for the period from October 2012 to May 2013.

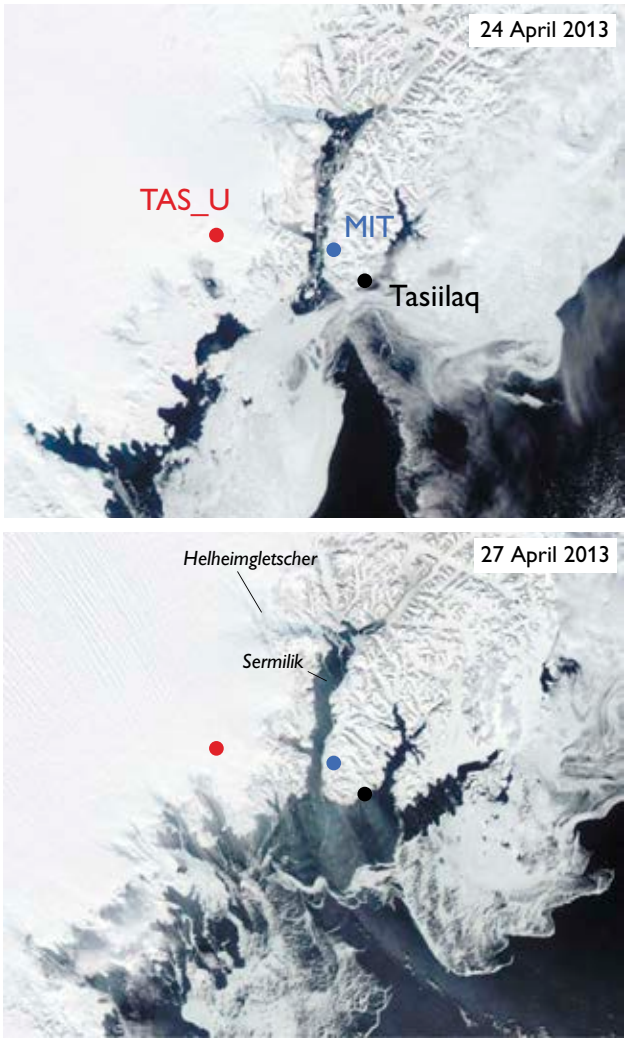

Fig. 5. MODIS satellite images of the Tasiilaq region of South-East Greenland on 24 and 27 April 2013, before and during a strong piteraq event. For location, see Fig. 1.

from the Geological Survey of Denmark and Greenland were in the field at KAN_U, and although they experienced wind speeds approximately one third of those at TAS_U (*c.* 300 km to the east) the white-out and heavy snowdrift yielded conditions too dangerous for them to leave shelter.

Satellite images from the 2013 piteraq event show that a large region was affected (Fig. 5). The striping on the ice sheet in the top left corner of the lower image shows the wind direction with snow transported toward and past the ice sheet margin. Large areas of sea and fjord ice disintegrated, and the 5–13 km wide Sermilik fjord, into which Helheimgletscher calves, was cleared of ice.

Clearly, katabatic winds and especially the piteraqs, have a large impact on the ice sheet and its immediate surroundings. Given increasing commercial activity around the periphery of the Greenland ice sheet, there is a growing impetus for understanding these winds and their response to climate change. Regional atmospheric model projections until the year 2100 suggests that while climate change will likely result in weaker winds in Greenland's flat interior, stronger winds may occur in steeper regions around the ice sheet periphery (Gorter *et al.* 2013).

Acknowledgements

PROMICE is funded by the Danish Ministry of Climate, Energy and Building and is operated by the Geological Survey of Denmark and Greenland. Several weather stations are (co)funded by the Greenland Analogue Project, the REFREEZE project and the Greenland Climate Research Centre.

References

Ahlstrøm, A.P. & the PROMICE project team 2008: A new programme for monitoring the mass loss of the Greenland ice sheet. Geological Survey of Denmark and Greenland Bulletin **15**, 61–64.

Fausto, R.S., Van As, D., Ahlstrøm, A.P. & Citterio, M. 2012: Assessing the accuracy of Greenland ice sheet surface ablation measurements by pressure transducer. Journal of Glaciology **58**(212), 1144–1150.

Gorter, W., van Angelen, J.H., Lenaerts, J.T.M. & van den Broeke, M.R. 2013: Present and future near-surface wind climate of Greenland from high resolution regional climate modelling. Climate Dynamics **42**, 1595–1611.

Linden, M. 2013: Greenland death: how 100 mph ice storms can blow in without warning. The Independent, 1 May 2013. London, UK.

Nghiem, S.V., Hall, D.K., Mote, T.L., Tedesco, M., Albert, M.R., Keegan, K., Shuman, C.A., DiGirolamo, N.E. & Neuman, G. 2012: The extreme melt across the Greenland ice sheet in 2012. Geophysical Research Letters **39**, L20502.

Oltmanns, M., Straneo, F., Moore, G.W.K. & Mernild, S.H. 2014: Strong downslope wind events in Ammassalik, Southeast Greenland. Journal of Climate **27**, 977–993.

Stansfield, J. 1972: The severe Arctic storm of 8–9 March 1972 at Thule Air Force Base, Greenland. Weatherwise **25**, 228–233.

Steffen, K. & Box, J.E. 2001: Surface climatology of the Greenland Ice Sheet: Greenland climate network 1995–1999. Journal of Geophysical Research: Atmospheres **106**(D24), 33951–33964.

Steffen, K., Box, J.E. & Abdalati, W. 1996: Greenland climate network: GC-Net. In: Colbeck, S.C. (ed.): Glaciers, ice sheets and volcanoes: a tribute to Mark F. Meier. CRREL special Report **96-27**, 98–103.

Van As, D. 2011: Warming, glacier melt and surface energy budget from weather station observations in the Melville Bay region of northwest Greenland. Journal of Glaciology **57**(202), 208–220.

Van As, D., Fausto, R.S., Colgan, W.T., Box, J.E. & PROMICE project team 2013: Darkening of the Greenland ice sheet due to the melt-albedo feedback observed at PROMICE weather stations. Geological Survey of Denmark and Greenland Bulletin **28**, 69–72.

Authors' addresses

D.v.A. and others, except K.S., *Geological Survey of Denmark and Greenland, Øster Voldgade 10, DK-1350 Copenhagen K, Denmark.* E-mail: *dva@geus.dk*

K.S., *Swiss Federal Institute for Forest, Snow and Landscape Research (WSL), Zürcherstrasse 111, CH-8903 Birmensdorf, Switzerland.*

Mass loss from an ice-sheet drainage basin in West Greenland

Morten L. Andersen, Signe B. Andersen, Lars Stenseng, Henriette Skourup, William Colgan, Steen S. Kristensen, John P. Merryman Boncori, Andreas P. Ahlstrøm, Xavier Fettweis, René Forsberg, Michele Citterio, Jason E. Box, Dirk van As and Robert S. Fausto

The Greenland ice sheet is losing mass to the ocean at an increasing rate (Thomas *et al*. 2006). During the 1980s the ice sheet was believed to be in near-equilibrium (van den Broeke *et al*. 2009). Within the first decade of the 21st century, however, a net negative balance was observed. Greenland's present rate of ice loss is *c*. 250 Gt yr^{-1}, equivalent to a sea-level rise contribution of *c*. 0.69 mm yr^{-1}. The rate of ice loss has increased over the post 1992 observation period (Shepherd *et al*. 2012).

The ice-sheet mass budget can be partitioned into two main components: (1) surface mass balance (SMB; the net difference between accumulation and surface ablation) and (2) marine ice loss (*D*; iceberg discharge via glacier dynamics plus subsurface melt at the glacier terminus). Over the past decade, the surface mass-balance proportion has accelerated relative to the *D* component, changing from *c*. 50% in 2000–2008 (van den Broeke *et al*. 2009) to more than two thirds (68%) in 2009–2012 (Enderlin *et al*. 2014).

Whereas modern climate models appear to capture the surface mass-balance response to climate change, the physical processes driving variability in glacier discharge are more complex. Recent increases in *D* may be due to: (1) changing force-balance at the ice-ocean interface as suggested by model simulations (e.g. Nick *et al*. 2009, 2013), (2) changing basal lubrication at the ice-bed interface due to increased meltwater availability (Zwally *et al*. 2002; Andersen *et al*. 2010), and/or (3) decreasing ice viscosity due to increasing ice temperature (van der Veen *et al*. 2011). The high spatial variability in these forcing mechanisms and a large sensitivity to local fjord geometry (Nick *et al*. 2013) require basin scale studies of glacier dynamics to elucidate local causes of glacier acceleration.

In 2007 the Programme for Monitoring the Greenland Ice Sheet (PROMICE) was initiated to gain insight into the changing mass balance of the Greenland ice sheet using quantitative meteorological observations, as well as airborne surveys of ice thickness and flow-velocity observations (Ahlstrøm *et al*. 2008). Here we present the first calculations of ice discharge using PROMICE observations, with focus on a West Greenland ice-sheet drainage basin previously defined as 'Basin 7' (Zwally *et al*. 2012; Fig. 1). The *c*. 400 km long ice-sheet margin within Basin 7 includes the 6 km wide Jakobshavn Isbræ, and several other marine-terminating outlet glaciers, such as Store Gletscher and Rink Isbræ (Figs 1, 2). We combine satellite-derived, ice-surface velocities, airborne ice-thickness measurements, and modelled surface mass balance to assess the dynamic discharge from Basin 7.

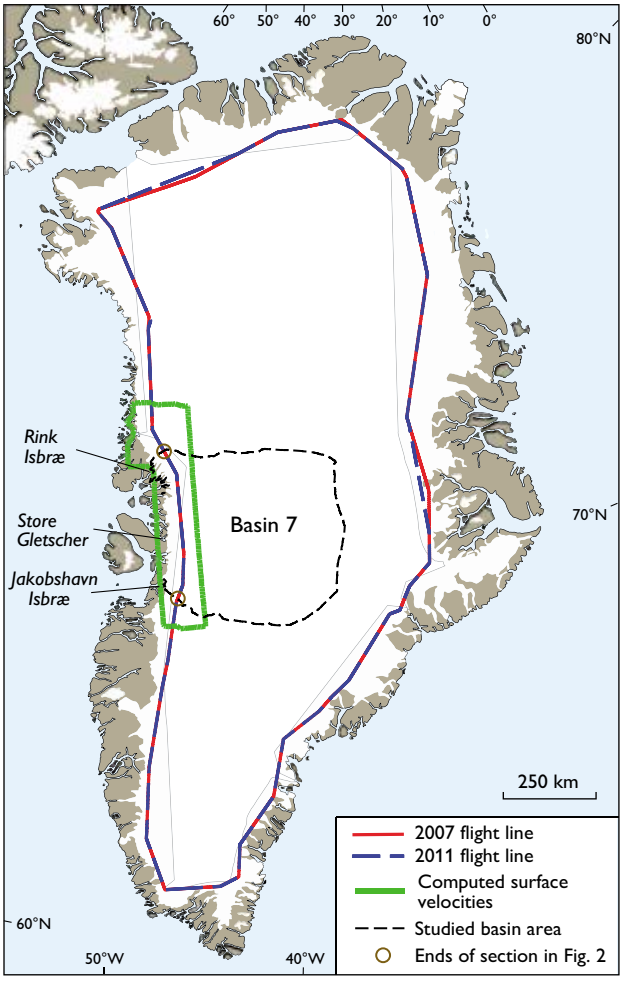

Fig. 1. Map of Greenland showing interpolated flight lines for 2007 and 2011, area of computed surface velocities for this study (Fig. 3) and the studied catchment area.

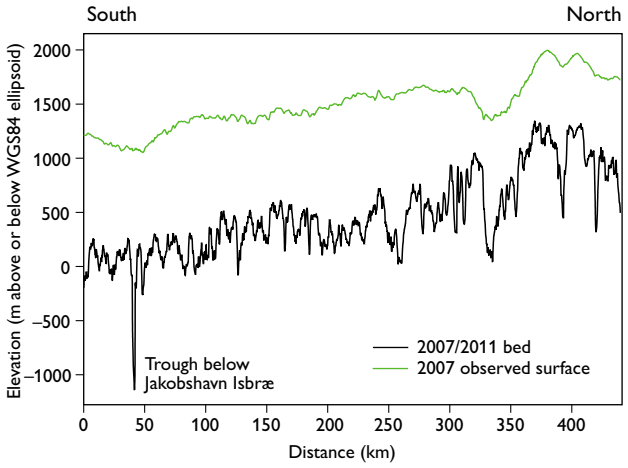

Fig. 2. South-to-north section of the studied basin along the 2007 and 2011 flight lines. For location see Fig. 1.

Data and methods

We estimate the solid ice discharge (D) into the ocean according to the input–output method of Rignot & Kanagaratnam (2006). First we quantify the mass flux (F) discharging across a flux gate, upstream of the boundary between the ice sheet and the ocean (the grounding line), defined by the path of the PROMICE airborne ice-thickness surveys conducted in the summers 2007 and 2011 (Fig. 1). The elevation of this flux gate is *c.* 1500 m a.s.l. in Basin 7 (Figs 2, 3). The ice-surface and bed elevations determined by the airborne surveys were interpolated to *c.* 30 m spacing along the flux gate to resolve spatial variability in ice flow.

The flux F at grid point i is computed as $F_i = H_i \cdot L_i \cdot v_i$, where H_i is the ice thickness, L_i is the spacing along the flight line (*c.* 30 m), and v_i is the depth-averaged ice velocity component that is perpendicular to the flux gate. Ice surface velocities were derived by applying offset tracking to ALOS/PALSAR synthetic aperture radar (SAR) data acquired between November 2009 and February 2010, using the SUSIE processing chain based on the commercial package GAMMA (Merryman Boncori *et al.* 2010; Ahlstrøm *et al.* 2011). Uncertainties associated with the ice velocities were estimated using the method of Mohr & Merryman Boncori (2008) and are under 10% (Fig. 3). We assume a uniform vertical velocity profile, where ice-surface velocity is equivalent to depth-averaged velocity (i.e. 'plug flow'; Rignot & Kanagaratnam 2006).

With the total basin flux $F (=\sum F_i)$ known, the grounding line discharge (D) can be estimated by adding the spatially integrated surface mass balance (SMB) of the area downstream ('ds') of the flux gate: $D = F + SMB_{ds,ref}$, where $SMB_{ds,ref}$ is a reference period (1961–1990) mean SMB field from the regional climate model MAR v3.2, forced at its boundaries by ECMWF reanalysis data and run at a spatial resolution of 25 km (Fettweis *et al.* 2013a). Similarly, the mass balance upstream of the flux gate (interior mass balance, IMB) can be computed by subtracting F from the upstream spatially integrated SMB for the reference period: $IMB = SMB_{us,ref} - F$.

Quantification of D allows us to estimate the total mass balance (TMB) of the drainage basin. The TMB value is calculated as $TMB = SMB_{tot,yr} - D$, where $SMB_{tot,yr}$ is the yearly SMB spatially integrated across the entire basin.

Estimated uncertainty (σb) on radar-derived bed elevation b values is 80 m and estimated uncertainty (σs) on laser-derived surface elevation observations (s) is 0.1 m. Assuming errors in b and s are random, we take uncertainty in ice thickness (σH) as the sum in quadrature of the fractional uncertainties of σb and σs (e.g. Colgan *et al.* 2008). Uncertainty in flux F at gridpoint i (σF_i) is similarly taken as the sum in quadrature of the fractional uncertainties of σH_i and σv_i, where the latter term is the uncertainty in the annual

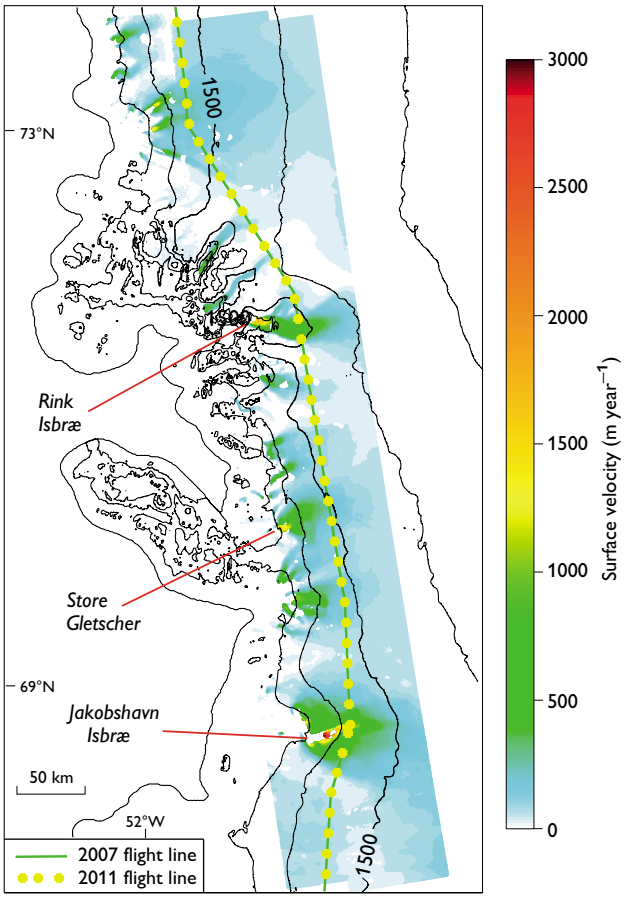

Fig. 3. Surface velocities derived from synthetic aperture radar (SAR) data for 2009–2010 used in this study. The contour lines are based on the digital elevation model of the *Greenland ice mapping project* (Howat *et al.* 2014).

depth-averaged velocity at i. We assume no uncertainty in L_i. Uncertainty in the total flux F in the basin is then $\sigma F = \sum \sigma F_i$. We take uncertainty in SMB to be 15% at basin scale (Fettweis *et al*. 2013a) and similarly propagate uncertainties in both F and SMB as the sum in quadrature of fractional uncertainties when assessing the cumulative uncertainty (σD) associated with the grounding-line ice discharge. Uncertainties on TMB and IMB are developed analogously.

The thickness observations were carried out in summer, and we do not account for the difference between summer and winter ice velocities. However, at *c.* 1500 m a.s.l., we expect the difference between summer and winter ice velocities to be small (<2%; Joughin *et al*. 2008).

Results

Both the upstream flux (F) and downstream discharge (D) in Basin 7 are within the uncertainty of their respective values in 2007 and 2011 (Table 1). Whereas we employ different airborne-derived, ice-geometry data for each year, the velocity field used is identical for the two years (winter 2009/2010 values), as is the surface mass-balance correction (1961–1990 values). The similar mass fluxes indicate that changes in ice geometry along the *c.* 1500 m contour were slight between 2007 and 2011.

Interior mass-balance values for both years are zero within the uncertainty, which is in good agreement with Zwally *et al*. (2011), who found a slight mass gain of 8 Gt yr^{-1} above 2000 m a.s.l.

The total mass-balance values are also, within uncertainty, similar for 2007 and 2011. Considering the *c.* 10 Gt yr^{-1} decrease in D, this suggests that yearly fluctuations in the dynamics of major tidewater outlet glaciers in Basin 7 are balanced by variations in surface mass balance. The mean total mass-balance value (–30.5 Gt yr^{-1}) corresponds to a sea-level rise contribution of *c.* 0.08 mm yr^{-1}, and agrees within uncertainty with a satellite gravimetry-derived total mass-balance estimate of –24 ± 1 Gt yr^{-1} for Basin 7 over the 2004 to 2010 period (Colgan *et al*. 2014), and a 2007 total mass-balance value reported in Rignot *et al*. (2008) of –36.7 Gt yr^{-1} for an analogous West Greenland basin. The 2007 value we present is more negative than a Basin 7 estimate of –14 ± 1 Gt yr^{-1} over the 2003 to 2007 period derived from satellite altimetry (Zwally *et al*. 2011). This latter study, however, preceded the 2007 to 2011 observation period, and may therefore reflect the less negative surface mass-balance regime prior to the observation period (Fettweis *et al*. 2013b).

Table 1. Mass fluxes in Gt per year

Year	Upstream flux (F)	Ice discharge (D)	Interior balance (IMB)	Total mass balance*
2007	79.5 ± 6.1	70.4 ± 6.2	–5.6 ± 12.6	–31.3 ± 8.6
2011	69.7 ± 5.3	60.6 ± 5.5	–4.1 ± 12.3	–29.7 ± 7.2

* Total mass balance = $SMB_{tot,yr}$ – D

Summary remarks

Rignot & Kanagaratnam (2006) invoked an assumption of negligible changes in ice geometry between their flux gates and the grounding line. As their flux gates are located at the *c.* 1000 m elevation contour, any dynamic thickening or thinning signals affect a relatively small proportion of the basin area. Given that the PROMICE flux gates are substantially farther inland from the grounding line, we are exploring approaches for explicitly correcting D values for recent changes in ice geometry between the upstream flux gate and the downstream grounding line. This may be particularly relevant in highly dynamic areas, such as the Jakobshavn Isbræ area. A preliminary assessment of such a correction for Basin 7 suggests that the rate of change in downstream ice volume is equivalent to *c.* 25% of D, which would further decrease the total mass balance by up to 15 Gt yr^{-1}. As more synthetic aperture radar data become available, we will improve the temporal coverage of the PROMICE ice-surface velocity product to annual resolution.

The plug-flow assumption adds a negative bias to the mass-loss estimates by assuming that all flow is caused by sliding at the bed, i.e., the surface speed is equal to the mean flow velocity of the ice column. This may be valid in the fast flowing coastal areas, but higher up on the ice sheet the assumption is less valid, where the surface velocity is a mix of sliding and deformation, and the vertically averaged flow speed can be as low as 80% of the observed surface speed.

In the PROMICE framework, this basin-scale mass-balance assessment will be extended to deliver basin-scale mass-balance and ice-discharge estimates of the entire Greenland ice sheet over multiple observation years. This survey aims to improve portioning of mass loss at basin scale, contributing to improved sea-level rise projections for the Greenland ice sheet.

Acknowledgments

PROMICE is funded by the Danish Ministry of Climate, Energy and Building, and is operated by the Geological Survey of Denmark and Greenland. This paper is contribution number 38 of the Nordic Centre of Excellence SVALI, Stability and Variations of Arctic Land Ice, funded by the Nordic Top-level Research Initiative.

References

Ahlstrøm, A. & the PROMICE project team 2008: A new programme for monitoring the Greenland ice sheet mass loss. Geological Survey of Denmark and Greenland Bulletin **15**, 61–64.

Ahlstrøm, A. *et al.* 2011: PROMICE 2007–2010. Final report for the establishment phase of the Programme for Monitoring of the Greenland Ice Sheet. Danmarks og Grønlands Geologiske Undersøgelse Rapport **2011/118**, 178 pp.

Andersen, M.L. *et al.* 2010: Spatial and temporal melt variability at Helheim Glacier, East Greenland, and its effect on ice dynamics. Journal of Geophysical Research, Earth Surface **115**, F04041.

Colgan, W., Davis, J. & Sharp, M. 2008: Is the high-elevation region of Devon Ice Cap thickening? Journal of Glaciology **54**, 428–436.

Colgan, W., Abdalati, W., Citterio, M., Csatho, B., Fettweis, X., Luthcke, S., Moholdt, G. & Stober, M. 2014: Hybrid inventory, gravimetry and altimetry (HIGA) mass balance product for Greenland and the Canadian Arctic. The Cryosphere Discussions **8**, 537–580.

Enderlin, E.M., Howat, I.M., Jeong, S., Noh, M.-J., van Angelen, J.H. & van den Broeke, M.R. 2014: An improved mass budget for the Greenland ice sheet. Geophyscial Research Letters **41**, 866–872.

Fettweis, X., Franco, B., Tedesco, M., van Angelen, J.H., Lenaerts, J.T.M., van den Broeke, M.R. & Gallee, H. 2013a: Estimating the Greenland ice sheet surface mass balance contribution to future sea level rise using the regional atmospheric climate model MAR. The Cryosphere **7**, 469–489.

Fettweis, X., Hanna, E., Lang, C., Belleflamme, A., Erpicum, M. & Gallée, H. 2013b: Brief communication: Important role of the mid-tropospheric atmospheric circulation in the recent surface melt increase over the Greenland ice sheet. The Cryosphere **7**, 241–248.

Howat, I.M., Negrete, A. & Smith, B. 2014: The Greenland ice mapping project (GIMP) land classification and surface elevation datasets. The Cryosphere Discussions **8**, 453–478.

Merryman Boncori, J.P., Dall, J., Ahlstrøm, A.P & Andersen, S.B. 2010: Validation and operational measurements with SUSIE – a SAR ice-motion processing chain developed within PROMICE (Programme for the monitoring of the Greenland ice sheet). In: Lacoste-Francis, H. (ed.): Proceedings of the ESA Living Planet Symposium, Bergen, Norway (ESA SP-686) Noordwijk: ESA Communications ESTEC.

Mohr, J.J. & Merryman Boncori, J.P. 2008: An error prediction framework for interferometric SAR data. IEEE Transactions on Geoscience and Remote Sensing 46, 1600–1613.

Nick, F.M., Vieli, A., Howat, I.M. & Joughin, I. 2009: Large-scale changes in Greenland outlet glacier dynamics triggered at the terminus. Nature Geoscience **2**, 110–114.

Nick, F.M., Vieli, A., Andersen, M.L., Joughin, I., Payne, A.J., Edwards, T.L., Pattyn, F. & van de Wal, R.S.W. 2013: Future sea-level rise from Greenland's main outlet glaciers in a warming climate. Nature **497**, 235–238.

Rignot, E. & Kanagaratnam, P. 2006: Changes in the velocity structure of the Greenland ice sheet. Science **311**, 986–990.

Rignot, E., Box, J.E., Burgess, E. & Hanna, E. 2008: Mass balance of the Greenland ice sheet from 1958 to 2007. Geophysical Research Letters **35**, L20502.

Shepherd, A. *et al.* 2012: A reconciled estimate of ice-sheet mass balance. Science **338**, 1183–1189.

Thomas, R., Frederick, E., Krabill, W., Manizade,S. & Martin, C. 2006: Progressive increase in ice loss from Greenland. Geophysical Research Letters **33**, L10503, doi:10.1029/2006GL026075.

Van den Broeke, M., Bamber, J., Ettema, J., Rignot, E., Schrama, E. & van den Berg, W.J., van Meijgaard, E., Velicogna, I. & Wouters, B. 2009: Partitioning recent Greenland mass loss. Science **326**, 984–986.

Van der Veen, C.J., Plummer, J.C. & Stearns, L.A. 2011: Controls on the recent speed-up of Jakobshavn Isbræ, West Greenland. Journal of Glaciology **57**, 770–782.

Zwally, H., Abdalati, W., Herring, T., Larson, K., Saba, J. & Steffen, K. 2002: Surface melt-induced acceleration of Greenland ice-sheet flow. Science **297**, 218–222.

Zwally, H., Giovinetto, M., Beckley, M. & Saba, J. 2012: Antarctic and Greenland drainage systems, NASA, Goddard Space Flight Center, Cryospheric Sciences Laboratory. http://icesat4.gsfc.nasa.gov/cryo_data/ant_grn_drainage_systems.php.

Zwally, H. J. *et al.* 2011: Greenland ice sheet mass balance: distribution of increased mass loss with climate warming; 2003–07 versus 1992–2002. Journal of Glaciology **57**, 88–102.

Authors' addresses

M.L.A., S.B.A., W.C., A.P.A., M.C., J.E.B., D.v.A. & R.S.F., *Geological Survey of Denmark and Greenland, Øster Voldgade 10, DK-1350 Copenhagen K, Denmark*. E-mail: *mola@geus.dk*

L.S., H.S., S.S.K. & R.F., *DTU Space, DK-2800 Lyngby, Denmark*.

X.F., *Department of Geography, University of Liège, 4000 Liège, Belgium*.

J.P.M.B., *Istituto Nazionale di Geofisica e Vulcanologia, 00142 Rome, Italy*.

Surface albedo as a proxy for the mass balance of Greenland's terrestrial ice

William Colgan, Jason E. Box, Robert S. Fausto, Dirk van As, Valentina R. Barletta and Rene Forsberg

Satellite observations are critical to understanding the mass balance of Greenland's terrestrial ice (Fig. 1). The Gravity Recovery and Climate Experiment (GRACE) satellite constellation provides monthly gravimetry observations that can directly assess mass balance. Temporal data gaps have begun to appear in the GRACE record due to declining satellite function. In anticipation of further deterioration in the coverage of GRACE, we have explored an empirical relation between ice-surface albedo (or reflectance) and ice-mass balance to fill the gaps in the gravimetry record of Greenland's ice-mass balance. As surface albedo observed by the moderate-resolution imaging spectroradiometer (MODIS) aboard the Terra satellite is available in near real-time, employing a MODIS-derived proxy permits near real-time estimates of Greenland ice-mass balance. The Geological Survey of Denmark and Greenland has begun employing the albedo – mass-balance relation described here to issue near real-time estimates of Greenland ice-mass balance during the summer melt season at www.polarportal.org.

Data and method

We employ ice-mass balance data for Greenland as assessed by the Technical University of Denmark monthly GRACE RL05 solutions from the 2003 to the 2012 summer melt seasons (May to September; Barletta *et al.* 2013). Monthly mass balance, calculated by node-centred finite differencing of this solution time series, is available for 44 out of 50 study-period months. Single, missing monthly solutions (Jun 2003, Jun 2011 and Jul/Aug 2012) prevent resolving mass balance for the months preceding and following the missing solutions (May/Jul 2003, May/Jul 2011 and Jun/Sep 2012; Tedesco *et al.* 2013). The 1σ uncertainty associated with monthly mass balance calculated in this way ranges from 45 to 149 Gt, with an average of 91 Gt over the study period. We take this average value as representative of the uncertainty in GRACE-derived monthly mass balance.

We employ the Greenland ice-surface albedo observed by Terra MODIS MOD10A1 during clear sky conditions. Clear sky conditions vary both temporally and spatially, especially in South Greenland, where *c.* 25% of the MODIS scenes show clear sky. Eleven-day running statistics are used to identify and reject <5% of the values within a given scene that exceed 2σ from the running multi-scene mean. To prevent rejecting potentially valid cases, data within 0.04 of the running multi-scene median are not rejected (Box *et al.* 2012). Mean monthly albedo is generated from these clear sky and filtered scenes for the melt-season months from 2003 to 2012. We compared the MODIS monthly albedo with *in situ* observations from the Programme for Monitoring of the Greenland Ice Sheet (PROMICE; van As *et al.* 2013) and the Greenland Climate Network (Steffen & Box 2001), and found that the root mean squared error reached a minimum of 0.039 in May and a maximum of 0.085 in September. The bias between MODIS and *in situ* albedo, which was less than the root mean squared error in all months, ranged from −0.027 in June to 0.022 in September. We therefore take the 1σ uncertainty associated with the ice-sheet-wide MODIS monthly albedo to be 0.059 during the summer melt season, the average May

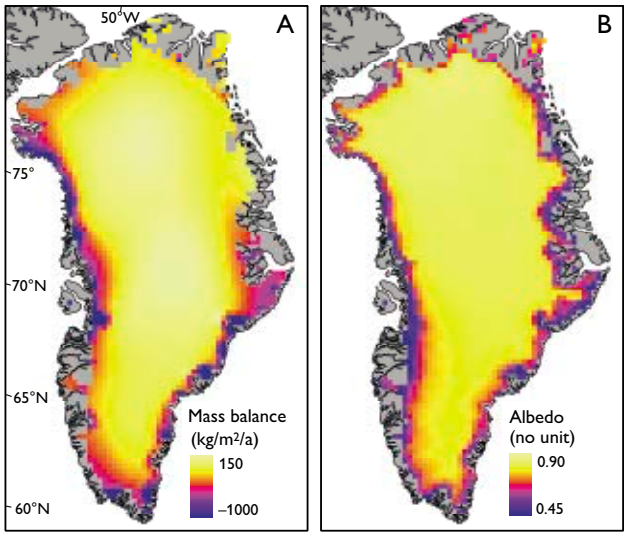

Fig. 1. **A**: Mean annual mass balance of Greenland's terrestrial ice, derived by an inversion of mass loss observed by satellite gravimetry that is constrained by satellite altimetry and fractional ice-coverage information (Colgan *et al.* 2014). **B**: June to August mean albedo, derived by averaging all available clear sky albedo scenes, each of which has been filtered using running statistics to reject invalid data (Box *et al.* 2012). Both datasets span the period from 2004 to 2010 and share a common ice mask where the local ice fraction exceeds 0.5 at 26 km resolution. Colour bars saturate at maximum and minimum values.

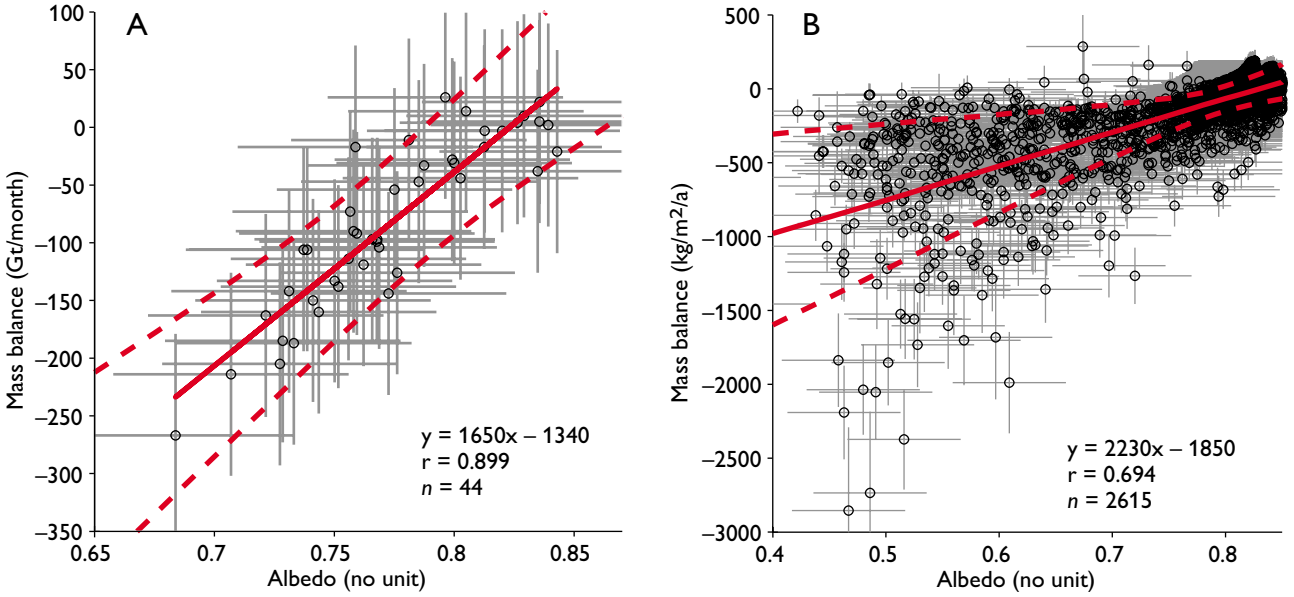

Fig. 2. Mass balance versus albedo in time and space. **A**: Greenland ice monthly mass balance derived from satellite gravimetry (Barletta *et al.* 2013) versus monthly average albedo derived from satellite imagery (Box *et al.* 2012), during May to September over the period from 2003 to 2012. **B**: Local mean annual mass balance derived from an inversion of satellite gravimetry (Colgan *et al.* 2014) versus local June to August mean albedo derived from satellite imagery (Box *et al.* 2012), averaged over the 2004 to 2010 period and across the domain shown in Fig. 1. Solid and dashed lines denote ordinary least squares regression (2σ uncertainty envelope).

through September root mean squared error between local *in situ* and MODIS observations. A portion of this apparent discrepancy likely results from footprint differences between *in situ* (*c.* 10 m^2) and MODIS (*c.* 500 m^2) albedo samples.

Using these GRACE-derived mass-balance and MODIS-derived albedo records, we evaluate a single variable regression model to estimate monthly mass balance as a function of monthly albedo. Monthly albedo (α) is strongly correlated with monthly mass balance ($\partial M/\partial t$) during the summer melt months within the study interval (r = 0.899, p <0.01; Fig. 2A). This implies that the Greenland ice-mass balance can be statistically approximated by

$$\frac{\partial M}{\partial t} = A\alpha + c$$

where A is a coefficient equal to 1650 Gt/month, and c is a constant of –1340 Gt/month. A is the apparent sensitivity of mass balance to albedo (e.g. a 0.01 decrease in monthly average albedo corresponds to a 16.5 Gt decrease in monthly mass balance), while c would be the theoretical minimum monthly mass balance when all solar radiation is absorbed (e.g. when $\alpha = 0$).

Application

Two sources of error arise when estimating the Greenland ice-mass balance via ice-surface albedo: the statistical uncertainty associated with albedo as a proxy for mass balance, and the underlying measurement uncertainty associated with resolving monthly mass balance. The monthly Greenland ice-mass balances predicted by single variable albedo regression agree with the monthly mass balances observed by GRACE within a root mean squared error of ±32 Gt/month. Combining, in quadrature, this statistical uncertainty with the characteristic measurement uncertainty in the GRACE-derived Greenland ice-mass balance (±91 Gt/month), yields a total uncertainty in albedo-regressed mass balance of ±96 Gt/month. We calculate uncertainty in, and assess stationarity of, A and c by calculating their values in overlapping four-year subsets of the ten-year study period. This subset analysis yields 1σ uncertainties associated with best-fit A and c parameters of 1650 ±400 and –1340 ±300 Gt/month, respectively. An apparent increase in A and decrease in c over time are suggestive of an increase in mass-balance sensitivity to albedo over time. This is consistent with indications that surface mass balance is now the dominant mechanism of Greenland ice loss (Enderlin *et al.* 2014). The drift in both A and c, however, is statistically insignificant over the satellite record length presently available for analysis. Within associated statistical uncertainty, we therefore suggest that average monthly ice-surface albedo is a stationary proxy for the monthly Greenland ice-mass balance during the 2003 to 2012 melt seasons.

The utility of ice albedo as a proxy for ice-mass balance may be evaluated by comparing GRACE- and MODIS-derived cumulative mass-balance anomalies and monthly mass-balance rates. The albedo-regressed cumulative anomaly captures both the rate and magnitude of mass loss in each melt season between 2003 and 2012 (Fig. 3A). Albedo-regressed mass-balance rates, however, generally overestimate mass loss early in the melt season (–26 Gt/month on average in May and June), and underestimate mass loss late in the melt season (+13 Gt/month on average in August and September). The single largest residual is a mass-loss overestimate of –92 Gt in June 2009 (Fig. 3C). Precipitation is recognised to decrease with air temperature, as a function of temperature-dependent absolute humidity. PROMICE weather data suggest the June 2009 outlier is most likely due to anomalously cold air temperatures and little snowfall after the initiation of spring melt, which resulted in an anomalously low June surface albedo and melt rate. While cumulative anomalies compound any systematic biases over the course of a season, the magnitude and associated uncertainty of the albedo-regressed, monthly mass-balance rates appear reasonable in the context of analogous GRACE values (Fig. 3B).

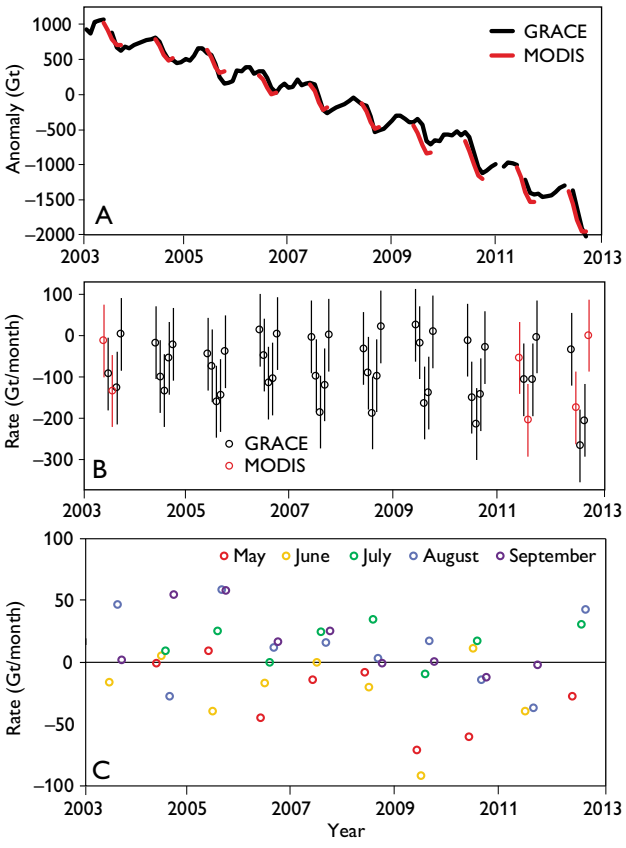

Fig. 3. **A**: Cumulative mass balance anomaly for Greenland's ice observed by GRACE satellite gravimetry over the period from January 2003 to October 2012 (Barletta *et al.* 2013), and the analogous albedo-regressed anomaly for May to September melt periods derived from MODIS satellite imagery. In each year, cumulative albedo-regressed mass loss is applied to the April anomaly assessed by Barletta *et al.* (2013). **B**: Melt season ice-mass balance rate (Barletta *et al.* 2013), and the analogous albedo-regressed rate when GRACE-derived values are not available. **C**: Residual (MODIS-derived minus GRACE-derived) in monthly ice-mass balance during the May to September melt season.

Discussion and summary

The mass balance of Greenland's ice reflects a combination of surface mass balance and underlying ice dynamic processes. The physical basis for surface albedo being a skilful proxy of surface mass balance is straightforward; albedo increases with fresh snowfall and decreases with melt or snowpack removal (Fig. 2B). Albedo therefore integrates the competing surface mass-balance processes of accumulation and ablation. Snow or ice albedo directly influences meltwater pro-

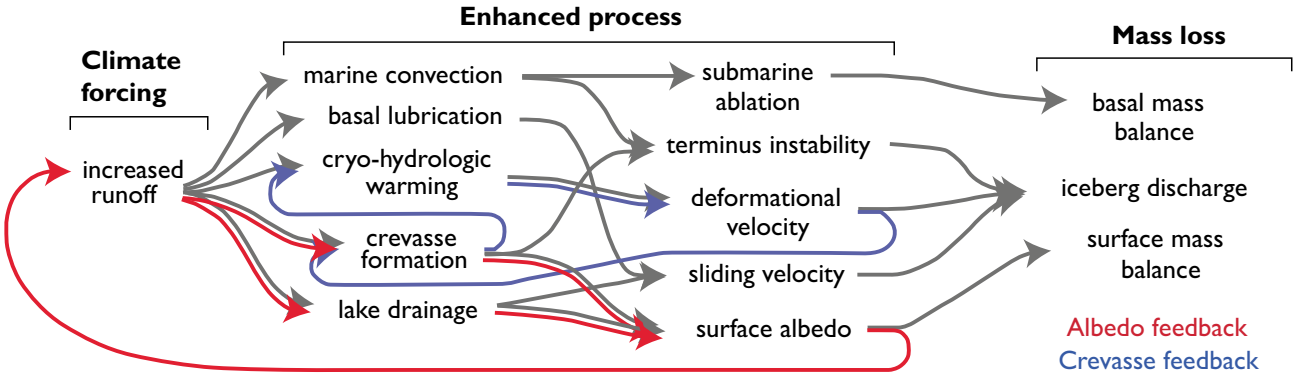

Fig. 4. Understanding the relation between surface albedo and mass balance: a schematic overview of previously recognised linkages between increased meltwater runoff and enhanced ice loss in Greenland (Box & Colgan 2013). Many intermediate processes convert increased meltwater runoff into increased ice loss via either iceberg discharge or surface or basal mass balance. Some processes involving ice-surface albedo and crevasses form positive feedback loops, potentially amplifying mass loss (Colgan *et al.* 2011).

duction and mass loss via runoff (Hock 2005). The indirect links between decreased surface albedo (and increased meltwater runoff) and enhanced mass loss via ice discharge from marine-terminating glaciers are numerous and diverse (Fig. 4; Box & Colgan 2013). Similar to surface-balance processes, however, processes enhancing ice dynamics, such as crevasses and supraglacial lakes, also generally decrease albedo with increasing mass loss.

For example, as crevassed ice absorbs approximately twice as much solar radiation as non-crevassed ice, small changes in crevasse extent can substantially modify albedo. A >10% increase in crevasse extent since *c.* 1998 within a West Greenland study area has been attributed to the acceleration of Jakobshavn Isbræ (Colgan *et al.* 2011). Crevasses can facilitate dynamic mass loss via enhanced terminus instability, as well as enhanced deformational velocity resulting from cryo-hydrologic warming. Similarly, a low-albedo 'dark zone' forms in the elevation band where meltwater accumulates, both within the snow and firn, as well as in supraglacial lakes. Within this 'dark zone', up to 40% of variability in annual mass balance is due to variability in summer ice-surface albedo (Greuell 2000). In high-melt years, lakes form at higher elevations and have a higher probability of rapidly draining large water volumes to the subglacial hydrological system (Liang *et al.* 2012). Albedo 'dark zone' width is therefore directly proportional to the delivery of water to the ice–bed interface.

Given previously recognised strong links between albedo and surface mass balance (Hock 2005), the high correlation between Greenland ice albedo and mass balance that we have explored supports the notion that the majority of recent Greenland ice-mass loss has occurred via meltwater runoff (Enderlin *et al.* 2014). Given the numerous and diverse previously postulated links between increased meltwater runoff and enhanced ice-dynamic mass loss, we suggest that a substantial portion of variability in dynamic mass loss is ultimately modulated by surface albedo and meltwater runoff (Box & Colgan 2013). The overarching inference from our preliminary data exploration is that a strong relation exists between Greenland's ice-surface albedo and mass balance, both through time and across space, and this merits further examination (Fig. 2). As near real-time albedo monitoring has proved successful in qualitatively forecasting extreme Greenland ice-mass loss events (Box *et al.* 2012), the Geological Survey of Denmark and Greenland has begun employing the albedo regression described here to issue near real-time estimates of Greenland ice-mass balance during the melt season at www.polarportal.org (Fausto *et al.* 2013).

Acknowledgement

This work is supported by the Danish Council for Independent Research, Natural Sciences (11-115166) and PROMICE.

References

Barletta, V.R., Sørensen, L.S. & Forsberg, R. 2013: Scatter of mass changes estimates at basin scale for Greenland and Antarctica. The Cryosphere **7**, 1411–1432.

Box, J., Fettweis, X., Stroeve, J.C., Tedesco, M., Hall, D.K. & Steffen, K. 2012: Greenland ice sheet albedo feedback: thermodynamics and atmospheric drivers. The Cryosphere **6**, 821–839.

Box, J. & Colgan, W. 2013: Greenland Ice Sheet mass balance reconstruction. Part III: Marine ice loss and total mass balance (1840–2010). Journal of Climate **26**, 6990–7002.

Colgan, W., Steffen, K., McLamb, W.S, Abdalati, W., Rajaram, H., Motyka, R.J., Phillips, T. & Anderson, R.S. 2011: An increase in crevasse extent, West Greenland: Hydrologic implications. Geophysical Research Letters **38**, L18502.

Colgan, W., Abdalati, W., Citterio, M., Csatho, B., Fettweis, X., Luthcke, S., Moholdt, G. & Stober, M. 2014: Hybrid inventory, gravimetry and altimetry (HIGA) mass balance product for Greenland and the Canadian Arctic. The Cryosphere Discussions **8**, 537–580.

Enderlin, E.M., Howat, I.M., Jeong, S., Noh, M.-J., van Angelen, J.H. & van den Broeke, M.R. 2014: An Improved Mass Budget for the Greenland ice sheet. Geophysical Research Letters **41**, 866–872.

Fausto, R.S., Colgan, W. & Langen, P.L. 2013: Real-time changes in Arctic ice presented in online portal. EOS, Transactions of the American Geophysical Union **94**, 397–398.

Greuell, W. 2000: Melt-water accumulation on the surface of the Greenland ice sheet: effect on albedo and mass balance. Geografiska Annaler **82A**, 489–498.

Hock, R. 2005: Glacier melt: a review of processes and their modelling. Progress in Physical Geography **29**, 362–391.

Liang, Y.-L., Colgan, W., Qin, L, Steffen, K., Abdalati, W., Stroeve, J., Gallaher, D. & Bayou, N. 2012: A decadal investigation of supraglacial lakes in West Greenland using a fully automatic detection and tracking algorithm. Remote Sensing of Environment 123, 127–138.

Steffen, K. & Box, J. 2001: Surface climatology of the Greenland ice sheet: Greenland climate network 1995–1999. Journal of Geophysical Research **106**, 33 951–33 964.

Tedesco, M., Fettweis, X., Mote, T., Wahr, J., Alexander, P., Box, J.E. & Wouters, B. 2013: Evidence and analysis of 2012 Greenland records from spaceborne observations, a regional climate model and reanalysis data. The Cryosphere **7**, 615–630.

Van As, D., Fausto, R.S., Colgan, W.T., Box, J.E. and the PROMICE project team 2013: Darkening of the Greenland ice sheet due to the melt-albedo feedback observed at PROMICE weather stations. Geological Survey of Denmark and Greenland Bulletin **28**, 69–72.

Authors' address es

W.C., J.E.B., R.S.F. & D.v.A., *Geological Survey of Denmark and Greenland, Øster Voldgade 10, DK-1350 Copenhagen K, Denmark.* E-mail: wic@geus.dk
V.R.B. & R.F., *Technical University of Denmark DK-2800 Kgs. Lyngby, Denmark.*

To what extent is Denmark vulnerable to mineral supply shortage?

Per Kalvig, Rune J. Clausen, Niels Fold and Karen Hanghøj

Mineral resources are building blocks of modern society and essential for progress and prosperity. Mankind has always depended on access to mineral raw materials, which have been a key factor for wealth, culture and development. Modern societies are characterised by a rapidly increasing demand for specialised mineral raw materials, determined by their stage of technological development, the number of consumers, and their standard of living. Generally, the availability of mineral raw materials has not, until recently, been considered an issue by the average consumer or by companies in the downstream end of the value chains, and mineral resources have not been part of the political agenda. In this context China's control over rare-earth elements (REE) has been an eye opener to both industry and politicians worldwide, and has subsequently led to discussions about the possible exhaustion of finite resources and potential threats to the availability of raw materials caused by geopolitical tension and market restrictions.

The increased concern has lead to several attempts to assess the risk of supply shortage which are however still at a rather qualitative stage. Inadequate knowledge about the current and future demand for mineral raw materials prevents political and industrial decision-makers from taking the necessary actions to predict and mitigate the national and industrial vulnerability to supply shortage. Thus, most modern societies, including Denmark, are vulnerable to mineral raw materials scarcity, but unaware of where and how it may appear, and how to prevent and address the problem.

Scarcity issues

Scarcity issues have been discussed since Thomas Malthus in 1798 initially predicted problems of food shortage due to increasing population and later also in relation to mineral resources. A number of organisations and individuals (e.g. Club of Rome, Gro Harlem Bruntland) have taken the lead in these discussions and emphasised that natural resources are finite and limited and that the global economy is growing disproportionately.

At the summit meeting in Rio de Janeiro in 1992, all nations were encouraraged to adopt the so-called Bruntland principles to ensure sufficient resources for future generations. The term sustainability was introduced to the mining industry. However, no clear effects can be identified neither in the policies nor in the overall mineral consumption, and global and national concern on how to secure raw material supply is increasing. Terms such as *critical minerals* were introduced, reflecting the risk of scarcity of some raw materials. The US National Research Council quantitatively addressed scarcity issues related to minerals in 2008 (National Research Council 2008), and since then a substantial number of reports have focused on the topic (e.g. Rosenou-Tornow *et al*. 2009; European Commission 2010; UNDP 2010; Graedel *et al*. 2012). The decoupling of wealth and mineral resource consumption remains to be seen.

Why are minerals important?

Mineral-based materials are present everywhere in our daily life – in houses, cars, computers, cooking utensils, paint, tiles, paper, plastic, batteries, wind turbines, roads, pipes etc. For each and all of these 'end products' the choice of raw materials – and thus the minerals that need to be mined – depends on the required physical and chemical properties of the products. In some cases more than one material may fulfil the product requirements and the choice will then be based on price and availability.

All societies need mineral resources for their development, but exactly which minerals and metals are in demand and how they are used depend on the stage of development of the particular society. During historic time the trend has been very clear; innovation and new technologies require an increasing number of specialised raw materials. Consequently, we need to explore for new types of minerals to meet new demands.

The demand for minerals is fueled by a number of drivers

Demographics – The United Nations has estimated that the world population will increase from currently 7 billion to 9 billion by 2050 and that about 6.5 billion people will

live in cities in 2050. This trend creates a need to develop new infrastructure to support the fast-growing urbanisation, which in turn creates an increased demand for minerals, in particular sand, gravel, iron and copper. Numerous other raw materials are also needed for basic infrastructure.

Wealth – The economic growth in some of the emerging markets – e.g. Brazil, Russia, India, Indonesia, China, the Republic of Korea, South Africa – creates millions of new customers for products like houses, household machines, bicycles, cars, computers, etc. These are all manufactured from raw materials which have to be mined and processed. An example of this is China that has the world's largest population and is globally the largest consumer of copper, aluminium and iron. However, the consumption of copper in China is still only 3 kg/person/year, much lower than in Europe where the consumption is 16 kg/person/year (Bogner 2012). However, it is expected that China's copper consumption will increase substantially mainly as a result of growing wealth, rather than just the growing population.

Technology – The introduction of new materials, for example in houses and vehicles, in new electronic communication equipment and in new 'green' energy technology, changes the desired physical and chemical properties of materials, which in turn creates demand for new mineral raw materials. Emerging technologies and new materials have created a rapidly growing demand for certain commodities such as indium and gallium used in light-emiting diode lamps; lithium, copper, neodymium and dysprosium used in electric cars; indium, cadmium and tellurium in photovoltaic thin-film and dysprosium and neodymium in magnets. Concurrently, the need for some traditional materials has been reduced. For example, light, strong materials such as aluminium and magnesium have reduced the amount of steel required to build car frames.

Critical minerals and vulnerability to supply restrictions

During the past decade mineral resource shortage has made headlines in the media, especially with regard to the REE. In response, a number of institutions have developed lists of mineral criticality on regional and national levels. For example, the European Union has defined 14 raw materials as critical to the EU (European Commission 2010). Typically, the studies have used a two-fold approach: (1) assessment of the supply risk and (2) assessment of the impact of an actual shortage. The term *critical minerals* is frequently used in this context. Critical minerals are those which are important to

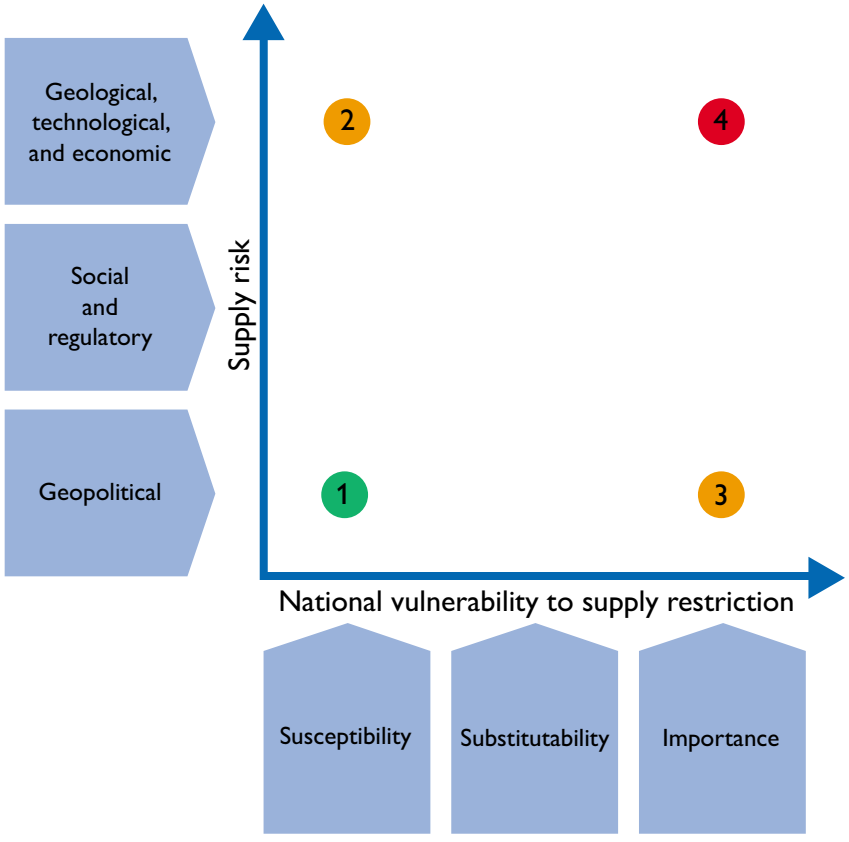

Fig. 1. Diagram of vulnerability to the supply risk and restriction (modified from Graedel *et al.* 2012). In the diagram element 1 has a low supply risk and even if a supply shortage occurs, this will not have a great impact on society; element 4 has a high supply risk and society is vulnerable to supply restictions; element 2 possesses a high supply risk but low vulnerability to supply restrictions; and for element 3 the opposite situation occurs, the supply risk is low, but in the event of a supply risk the national vulnerability is high.

society and subject to a specific availability or supply risk, e.g. at the corporate, national, regional or global industry level.

Scarcity is the potential outcome of criticality if a supply risk is not effectively mitigated. Scarcity can be a result of several factors such as political conflicts, embargos, cartels, natural disasters, sudden increases in demand, inadequate investment in new mines and processing facilities or resource depletion. Resource depletion causing significant shortages of mineral commodities has not yet been documented except in the case of cryolite, but it may pose a long-term threat.

Based on long- and medium-term supply risk Graedel *et al.* (2012) assessed the vulnerability to supply shortage and identified three general components, namely (1) geology, technology and economy; (2) social and regulatory factors and (3) geopolitical factors. Each of these were specified by six indicators, forming the 'supply risk axis'. The 'vulnerability to supply restrictions axis' is composed of another set of factors such as (1) importance, (2) substitutability and (3) susceptibility specified in eight indicators (see Figs 1, 2). Graedel *et al.* (2012) suggested that vulnerability should also include the environmental impact.

Forecasting and creating possibilities for adequate policies

The value chains for mineral raw materials include all stages of mineral exploration, mining and the processes transforming the minerals into intermediate goods applicable for manufacturing by industrial end users. However, most of the companies in the chain may be unaware of short- or long-term market constraints or opportunities. This prevents the industry itself from responding to sudden changes in demand. The exploration that targets new raw materials is therefore driven by commodity prices. Globally, 2556 companies spent 20.5 billion US$ on mineral exploration in 2012, of which 49% was spent on gold, 32% on base metals and the remaining 19% on all other commodities (Wilburn & Stanley 2013). This illustrates that the exploration sector is decoupled from the end user demand. Furthermore, there is a mismatch between the time scales of action in different parts of the value chain. Industrial demand for new raw materials and markets for raw materials fluctuate on short-time scales, whereas the time needed to adjust the supply is much longer; it typically takes more than ten years to open a new mine, and sometimes even substantially longer. Scrap supplies for recycling, *secondary raw materials*, are insufficient and usually too expensive to handle in order to bridge the gap between short-term demand and supply.

Individual governments and their institutions need updated assessment data on the national vulnerability to supply restrictions of mineral raw materials in order to develop and implement policies to avoid scarcity of particular critical minerals. For example, the general conditions for Europe may not necessarily be accurate and relevant for the Danish industrial and agricultural sectors. So far, only very limited data on vulnerability to supply restrictions are available for

Component		Importance		Substitutability				Susceptibility	
Indicator		National economic importance	Percentage of population utilising	Substitute performance	Substitute availability	Environmental impact ratio	Net import reliance ratio	Global innovation index	Net import reliance
Score	**87.5** (75–100)	See equation in SI	Score for percentage of population utilising	Poor	Supply risk score of substitute	See equation in SI	See equation in SI	See equation in SI	See equation in SI
	62.5 (50–75)			Adequate					
	37.5 (25–50)			Good					
	12.5 (0–25)			Exemplary					

Fig. 2. Components of the valuation methodology for the vulnerability to supply restriction, detailing the X-axis in Fig. 1 (from Graedel *et al.* 2012). Supporting Information (SI) is detailed in: *http://pubs.acs.org/doi/suppl/10.1021/es203534z/suppl_file/es203534z_si_001.pdf*

public and private stakeholders in Denmark. In 2013, the Geological Survey of Denmark and Greenland (GEUS) established the Center for Minerals and Materials (MiMa) to identify and study the most important raw material value chains. The Danish government subsequently decided to strengthen the knowledge about criticality, vulnerability and scarcity of raw materials and have requested MiMa to carry out a three-year research programme to complete a *vulnerability analysis* for Denmark. MiMa is currently identifying an adequate approach for this programme. Danish industry is characterised by an advanced downstream sector that depends on many imported components in end-product assemblages, while manufacturing of upstream products based on primary raw materials is of lesser importance. However, regardless of where the Danish manufacturing activities belong in the value chains, they are all based on mineral raw materials, some of which may be classified as critical minerals.

It is important to examine and map the extent to which Denmark is subject to supply restrictions and to understand the implications of such vulnerability. Danish consumers may not be aware of a product's requirements with regard to raw materials, and thus remain unaware of a potential supply problem attached to the product. Statistically, Denmark monitors export and import of all goods in compliance with international categories for goods and industries, but there is a need for more knowledge about the amount and types of processed raw materials in these goods and components used by Danish industry. MiMa and its partners will investigate these issues further and disseminate results, analyses and forecasts.

Conclusions

Denmark, like all other countries, depends on mineral raw materials – domestic and imported – to sustain and develop society and is thus vulnerable to mineral raw materials scarcity. However, most consumers and companies in the downstream parts of the value chains as well as decision makers in the administration and industry are relatively unaware of this. It is the aim of the Center for Minerals and Materials, MiMa, to build knowledge and disseminate information for the Danish society about mineral resource supply risks and vulnerability to supply restrictions.

References

Bogner, S. 2012: The commodity megatrend. Resource Investor (*www.resourceinvestor.com/2012/05/09*/the-commodity-megatrend).

European Commission 2010: Critical raw materials for the EU. Report of the ad-hoc working group on defining critical raw materials, 84 pp. Brussels: European Commission.

Graedel, T.E. *et al*. 2012: Methodology of metal criticallity determination. Environmental Science & Technology **46**, 1063–1070.

Malthus, T.R. 1798: An Essay on the Principle of Population, 388 pp. London: J. Johnson.

National Research Council 2008: Minerals, critical minerals, and the U.S. economy. Washington, DC: The National Academies Press.

Rosenau-Tornow, D., Buchholz, P., Riemann, A. & Wagner, M. 2009: Assessing the long-term supply risks for mineral raw materials – a combined evaluation of past and future trends. Resources Policy **34**, 161–175.

UNDP 2010: Human development report 2010 – 20th anniversary edition. The real wealth of nations: pathways to human development, 238 pp. Published for the United Nations Development Programme. Basingstoke: Palgrave MacMillan.

Wilburn, D.R. & Stanley, K.A. 2013: Exploration review. Annual review 2012. Mining engineering, May 2013, 22–42.

Authors' addresses

P.K., R.J.C. & K.H., *Geological Survey of Denmark and Greenland, Øster Voldgade 10, DK-1350 Copenhagen K, Denmark;* E-mail: *pka@geus.dk*

N.F., *Department of Geosciences and Natural Resource Management, Øster Voldgade 10, DK-1350 Copenhagen, K, Denmark.*

De Nationale Geologiske Undersøgelser for Danmark og Grønland (GEUS)

Geological Survey of Denmark and Greenland
Øster Voldgade 10, DK-1350 Copenhagen K
Denmark

The series *Geological Survey of Denmark and Greenland Bulletin* started in 2003 and replaced the two former bulletin series of the Survey, viz. *Geology of Greenland Survey Bulletin* and *Geology of Denmark Survey Bulletin*. Some of the twenty-one volumes published since 1997 in those two series are listed on the facing page. The present series, together with *Geological Survey of Denmark and Greenland Map Series*, now form the peer-reviewed scientific series of the Survey.

Geological Survey of Denmark and Greenland Bulletin

1	The Jurassic of Denmark and Greenland, 948 pp. (28 articles), 2003. *Edited by* J.R. Ineson & F. Surlyk.	500.00
2	Fish otoliths from the Paleocene of Denmark, 94 pp., 2003. *By* W. Schwarzhans.	100.00
3	Late Quaternary environmental changes recorded in the Danish marine molluscan faunas, 268 pp., 2004. *By* K.S. Petersen.	200.00
4	Review of Survey activities 2003, 100 pp. (24 articles), 2004. *Edited by* M. Sønderholm & A.K. Higgins.	180.00
5	The Jurassic of North-East Greenland, 112 pp. (7 articles), 2004. *Edited by* L. Stemmerik & S. Stouge.	160.00
6	East Greenland Caledonides: stratigraphy, structure and geochronology, 93 pp. (6 articles), 2004. *Edited by* A.K. Higgins & F. Kalsbeek.	160.00
7	Review of Survey activities 2004, 80 pp. (19 articles), 2005. *Edited by* M. Sønderholm & A.K. Higgins.	180.00
8	Structural analysis of the Rubjerg Knude Glaciotectonic Complex, Vendsyssel, northern Denmark, 192 pp., 2005. *By* S.A.S. Pedersen.	300.00
9	Scientific results from the deepened Lopra-1 borehole, Faroe Islands, 156 pp. (11 articles), 2006. *Edited by* J.A. Chalmers & R. Waagstein.	240.00
10	Review of Survey activities 2005, 68 pp. (15 articles), 2006. *Edited by* M. Sønderholm & A.K. Higgins.	180.00
11	Precambrian crustal evolution and Cretaceous–Palaeogene faulting in West Greenland, 204 pp. (12 articles), 2006. *Edited by* A.A. Garde & F. Kalsbeek.	240.00
12	Lithostratigraphy of the Palaeogene – Lower Neogene succession of the Danish North Sea, 77 pp., 2007. *By* P. Schiøler, J. Andsbjerg, O.R. Clausen, G. Dam, K. Dybkjær, L. Hamberg, C. Heilmann-Clausen, E.P. Johannessen, L.E. Kristensen, I. Prince & J.A. Rasmussen.	240.00
13	Review of Survey activities 2006, 76 pp. (17 articles), 2007. *Edited by* M. Sønderholm & A.K. Higgins.	180.00
14	Quaternary glaciation history and glaciology of Jakobshavn Isbræ and the Disko Bugt region, West Greenland: a review, 78 pp., 2007. *By* A. Weidick & O. Bennike.	200.00
15	Review of Survey activities 2007, 96 pp. (22 articles), 2008. *Edited by* O. Bennike & A.K. Higgins.	200.00
16	Evaluation of the quality, thermal maturity and distribution of potential source rocks in the Danish part of the Norwegian–Danish Basin, 66 pp., 2008. *By* H.I. Petersen, L.H. Nielsen, J.A. Bojesen-Koefoed, A. Mathiesen, L. Kristensen & F. Dalhoff.	200.00
17	Review of Survey activities 2008, 84 pp. (19 articles), 2009. *Edited by* O. Bennike, A.A. Garde & W.S. Watt.	200.00
18	Greenland from Archaean to Quaternary. Descriptive text to the 1995 Geological map of Greenland, 1:2 500 000. 2nd edition, 126 pp., 2009. *By* N. Henriksen, A.K. Higgins, F. Kalsbeek & T.C.R. Pulvertaft.	280.00
19	Lithostratigraphy of the Cretaceous–Paleocene Nuussuaq Group, Nuussuaq Basin, West Greenland, 171 pp., 2009. *By* G. Dam, G.K. Pedersen, M. Sønderholm, H.H. Midtgaard, L.M. Larsen, H. Nøhr-Hansen & A.K. Pedersen.	300.00
20	Review of Survey activities 2009, 106 pp. (23 articles), 2010. *Edited by* O. Bennike, A.A. Garde & W.S. Watt.	220.00
21	Exploration history and place names of northern East Greenland, 368 pp., 2010. *By* A.K. Higgins.	200.00
22	Lithostratigraphy of the Upper Oligocene – Miocene succession of Denmark, 92 pp., 2010. *By* E.S. Rasmussen, K. Dybkjær & S. Piasecki.	240.00
23	Review of Survey activities 2010, 84 pp. (19 articles), 2011. *Edited by* O. Bennike, A.A. Garde & W.S. Watt.	200.00
24	The East Greenland rifted volcanic margin, 96 pp., 2011. *By* C.K. Brooks.	200.00

25	Upper Cretaceous chalk facies and depositional history recorded in the Mona-1 core, Mona Ridge, Danish North Sea. 2011. *By* K. Anderskouv & F. Surlyk.	200.00
26	Review of Survey activities 2011, 88 pp. (21 articles), 2012. *Edited by* O. Bennike, A.A. Garde & W.S. Watt.	200.00
27	Neoglacial and historical glacier changes around Kangersuneq fjord in southern West Greenland, 68 pp., 2012. *By* A. Weidick, O. Bennike, M. Citterio & N. Nørgaard-Pedersen.	200.00
28	Review of Survey activities 2012, 76 pp. (17 articles), 2013. *Edited by* O. Bennike, A.A. Garde & W.S. Watt.	200.00
29	Tectono-magmatic evolution of the younger Gardar southern rift, South Greenland, 124 pp., 2013. *By* B.G.J. Upton.	240.00
30	Stratigraphic landscape analysis, thermochronology and the episodic development of elevated, passive continental margins, 150 pp., 2013. *By* P.F. Green, K. Lidmar-Bergström, P. Japsen, J.M. Bonow & J.A. Chalmers.	250.00

Geological Survey of Denmark and Greenland Map Series

1	Explanatory notes to the Geological map of Greenland, 1:500 000, Humboldt Gletscher, Sheet 6, 48 pp. + map, 2004. *By* P.R. Dawes.	280.00
2	Explanatory notes to the Geological map of Greenland, 1:500 000, Thule, Sheet 5 (1991), 97 pp. + map, 2006. *By* P.R. Dawes.	300.00
3	Explanatory notes to the Geological map of Greenland, 1:100 000, Ussuit 67 V.2 Nord, 40 pp. + map, 2007. *By* J.A.M. van Gool & M. Marker.	280.00
4	Descriptive text to the Geological map of Greenland, 1:500 000, Dove Bugt, Sheet 10, 32 pp. + map, 2009. *By* N. Henriksen & A.K. Higgins.	240.00
5	Descriptive text to the Geological map of Greenland, 1:100 000, Kangaatsiaq 68 V.1 Syd and Ikamiut 68 V.1 Nord, 41 pp. + 2 maps, 2010. *By* A.A. Garde & J.A. Hollis.	280.00

Geology of Greenland Survey Bulletin (173–191; discontinued)

173	Cambrian shelf stratigraphy of North Greenland, 120 pp., 1997. By J.R. Ineson & J.S. Peel	250.00
174	The Proterozoic Thule Supergorup, Greenland and Canada: history, lithostratigraphy and development, 150 pp., 1997. *By* P.R. Dawes	300.00
175	Stratigraphy of the Neill Klinter Group; a Lower – lower Middle Jurassic tidal embayment succession, Jameson Land, East Greenland, 80 pp., 1998. *By* G. Dam & F. Surlyk.	250.00
176	Review of Greenland activities 1996, 112 pp. (18 articles), 1997. *Edited by* A.K. Higgins & J.R. Ineson.	200.00
177	Accretion and evolution of an Archaean high-grade grey gneiss – amphibolite complex: the Fiskefjord area, southern West Greenland, 115 pp., 1997. *By* A.A. Garde.	200.00
178	Lithostratigraphy, sedimentary evolution and sequence stratigraphy of the Upper Proterozoic Lyell Land Group (Eleonore Bay Supergroup) of East and North-East Greenland, 60 pp., 1997. *By* H. Tirsgaard & M. Sønderholm.	200.00
179	The Citronen Fjord massive sulphide deposit, Peary Land, North Greenland: discovery, stratigraphy, mineralization and structural setting, 40 pp., 1998. *By* F.W. van der Stijl & G.Z. Mosher.	200.00
180	Review of Greenland activities 1997, 176 pp. (26 articles), 1998. *Edited by* A.K. Higgins & W.S. Watt.	200.00
181	Precambrian geology of the Disko Bugt region, West Greenland, 179 pp. (15 articles), 1999. *Edited by* F. Kalsbeek.	240.00
182	Vertebrate remains from Upper Silurian – Lower Devonian beds of Hall Land, North Greenland, 80 pp., 1999. *By* H. Blom.	120.00
183	Review of Greenland activities 1998, 81 pp. (10 articles), 1999. *Edited by* A.K. Higgins & W.S. Watt.	200.00
184	Collected research papers: palaeontology, geochronology, geochemistry, 62 pp. (6 articles), 1999.	150.00
185	Greenland from Archaean to Quaternary. Descriptive text to the Geological map of Greenland, 1:2 500 000, 93 pp., 2000. *By* N. Henriksen, A.K. Higgins, F. Kalsbeek & T.C.R. Pulvertaft.	225.00
186	Review of Greenland activities 1999, 105 pp. (13 articles), 2000. *Edited by* P.R. Dawes & A.K. Higgins.	225.00
187	Palynology and deposition in the Wandel Sea Basin, eastern North Greenland, 101 pp. (6 articles), 2000. *Edited by* L. Stemmerik.	160.00

188	The structure of the Cretaceous–Palaeogene sedimentary-volcanic area of Svartenhuk Halvø, central West Greenland, 40 pp., 2000. *By* J. Gutzon Larsen & T.C.R. Pulvertaft.	130.00
189	Review of Greenland activities 2000, 131 pp. (17 articles), 2001. *Edited by* A.K. Higgins & K. Secher.	160.00
190	The Ilímaussaq alkaline complex, South Greenland: status of mineralogical research with new results, 167 pp. (19 articles), 2001. *Edited by* H. Sørensen.	160.00
191	Review of Greenland activities 2001, 161 pp. (20 articles), 2002. *Edited by* A.K. Higgins, K. Secher & M. Sønderholm.	200.00

Geology of Denmark Survey Bulletin (36–37; discontinued)

36	Petroleum potential and depositional environments of Middle Jurassic coals and non-marine deposits, Danish Central Graben, with special reference to the Søgne Basin, 78 pp., 1998. *By* H.I. Petersen, J. Andsbjerg, J.A. Bojesen-Koefoed, H.P. Nytoft & P. Rosenberg.	250.00
37	The Selandian (Paleocene) mollusc fauna from Copenhagen, Denmark: the Poul Harder 1920 collection, 85 pp., 2001. *By* K.I. Schnetler.	150.00

Prices are in Danish kroner exclusive of local taxes, postage and handling

Note that information on the publications of the former Geological Survey of Denmark and the former Geological Survey of Greenland (amalgamated in 1995 to form the present Geological Survey of Denmark and Greenland) can be found on *www.geus.dk*